REPORT DOCUMENTATION PAGE

Form Approved OMB No. 0704-0188

1. AGENCY USE ONLY (Leave blank)	2. REPORT DATE	3. REPORT TYPE AND DATES COVERED
	5 December 1994	Final Report

4. TITLE AND SUBTITLE

The Investigation of the Influence of Parameter $M\infty / \sqrt{Re}$ on the Aerodynamic Characteristics of a Body of Revolution with the Contour Generatrix Break at Hypersonic Velocities

5. FUNDING NUMBERS

F6170894W0179

6. AUTHOR(S)

Dr. V I Plyashechnik

7. PERFORMING ORGANIZATION NAME(S) AND ADDRESS(ES)

Central Aerodynamics Institute
Zhykovsky St
Moscow 140160
Russia

8. PERFORMING ORGANIZATION REPORT NUMBER

N/A

9. SPONSORING/MONITORING AGENCY NAME(S) AND ADDRESS(ES)

EOARD
PSC 802 BOX 14
FPO 09499-0200

10. SPONSORING/MONITORING AGENCY REPORT NUMBER

SPC 94-4009

11. SUPPLEMENTARY NOTES

12a. DISTRIBUTION/AVAILABILITY STATEMENT

Approved for public release; distribution is unlimited.

12b. DISTRIBUTION CODE

A

13. ABSTRACT (Maximum 200 words)

This report contains the results of testing a body of revolution featuring the contour generatrix break in the wind tunnel T-121 of TsAGI.

14. SUBJECT TERMS

Nil

15. NUMBER OF PAGES

166

16. PRICE CODE

N/A

17. SECURITY CLASSIFICATION OF REPORT	18. SECURITY CLASSIFICATION OF THIS PAGE	19. SECURITY CLASSIFICATION OF ABSTRACT	20. LIMITATION OF ABSTRACT
UNCLASSIFIED	UNCLASSIFIED	UNCLASSIFIED	UL

PROJECT SPC - 94 - 4009

THE INVESTIGATION OF THE INFLUENCE OF PARAMETER $M_\infty/\sqrt{Re}$ ON THE AERODYNAMIC CHARACTERISTICS OF A BODY OF REVOLUTION WITH THE CONTOUR GENERATRIX BREAK AT HYPERSONIC VELOCITIES

(Final report)

Project Supervisor **Dr. V.Plyashechnic**

Please keep with file.

1994

CONTENTS

	page
Introduction	3
Abstract	5
Description of test program and conditions	6
Test tesults	12
Conclusions	24
Resume	25

INTRODUCTION

The aerodynamic configuration of numerous hypersonic vehicles is often formed using conical and cylindrical surfaces. The junction of these surfaces, i.e., the contour generatrix break, is, as a rule, either on the hypersonic vehicle forebody (for example, the transition of a nose part to a cylindrical body) or on its afterbody (for example, the transition of a cylindrical body part to a conical aft "skirt").

The influence of the contour generatrix break on aerodynamic characteristics of a vehicle at hypersonic velocities, all other conditions being equal, depends basically on Mach and Reynolds numbers and is attributed to different flow behavior over the break point. It effects mostly the position of the vehicle center of pressure and free-stream drag in the region of a zero angle of attack.

When aerodynamic characteristics of hypersonic vehicle models are tested in wind tunnels it is often impossible to attain a complete correspodence of wind tunnel flow conditions to flows over a full-scale vehicle in real flights. It concerns basically the Reynolds number, i.e., the Mach number in wind tunnel tests corresponds generally to a full-scale value, while the Reynolds number is inconsistent with real conditions and chosen from the capabilities of a particular wind tunnel. The inconsistency of this kind between wind tunnel test conditions and real flights leads often to a disagreement of wind tunnel test results and flight data. Some tests of slender bodies carried out earlier at TsAGI give grounds to suggest that sometimes it is reasonable to apply complex similarity parameter $M_\infty/\sqrt{Re}$ for tests of hypersonic vehicle models at hyperso-

nic velocities when it is impossible to simulate simultaneously real flow conditions in terms of Mach amd Reynolds numbers.

The experimental investigations under Contract SPC-94-4009 were conducted precisely to evaluate the influence of the complex parameter $M_\infty/\sqrt{Re}$ on aerodynamic characteristics of a body of revolution of the type of " an ogive- a cylinder- a truncated cone".

ABSTRACT

This report contains the results of testing a body of revolution featuring the contour generatrix break in the wind tunnel T-121 of TsAGI.

The test model is a body of revolution having an ogive nose, a central cylindrical body and an aft conical "skirt" with a generatrix angle of $\theta_{SK}=6.5^0$.

The tests of the aerodynamic characteristics of the model (balance tests) were performed using an external three-component strain-gage balance at zero sideslip angle and angles of attack ranging from -4^0 to 10^0 for flow conditions corresponding to Mach numbers $M_\infty \approx 4.0$, 5.0, 6.0, 7.0, 8.0, and 9.0. The Reynolds numbers, Re_x, based on the free-stream flow parameters and the reference linear dimension x=0.172 characterizing the distance from the model nose to the generatrix break point were varied in possible ranges at all Mach numbers being tested. Eventually, the Reynolds numbers, Re_x, were varied from $Re_x=0.9\times10^6$ ($M_\infty=4.96$) to $Re_x=8.6\times10^6$ ($M_\infty=4.06$) with the complex parameter $M_\infty/\sqrt{Re_x}$ varying from 1.38×10^{-3} to 8.15×10^{-3}.

The tests of flow spectra over the model (optical tests) were carried out at $M_\infty \approx 4.0$, 5.0, 6.0, 7.0, and 8.0, at zero sideslip angle and zero angle of attack and at Reynolds numbers, Rex, varying from $Re_x=0.9\times10^6$ ($M_\infty=4.96$) to $Re_x=8.2\times10^6$ ($M_\infty=4.06$).

DESCRIPTION OF TEST PROGRAM AND CONDITIONS

The tests were carried out in May, 1994 in the wind tunnel T-121 of TsAGI.

T-121 is an intermittent wind tunnel with compressed air as a test gas stored in gas tanks. The wind tunnel T-121 is equipped with an ejector system and intended for various tests (see the 1st progress report) in the range of $M_\infty \approx 4.0 \div 9.0$. The required Mach number in the test section was attained by using an adequate contoured nozzle made integral with the test section. Two-dimensional nozzles and 0.2×0.2m test section were used in flow conditions corresponding to $M_\infty \approx 4.0$, 5.0, and 6.0, while axisymmetric nozzles and test section 0.2m in diameter were applied for $M_\infty \approx 7.0$, 8.0, and 9.0.

The required Reynolds number was achieved by providing for an adequate pressure P_0 in the plenum chamber using a fixed nozzle.

For all Mach and Reynolds numbers realized in the test section, air entering the test section was preheated by an electric heater which was capable to provide for the stagnation flow temperature T_0 up to 1000K.

Two types of models were designed and manufactured to investigate the influence of the parameter $M_\infty/\sqrt{Re}$ on aerodynamic characteristics of a body of revolution with the contour generatrix break in the wind tunnel T-121. These models made it possible to conduct tests with different versions of the nose, the central body and the aft conical "skirt". The detailed description of all the model versions is given in the 1st progress report where the test program for several model versions suggested at that time is presented.

But because of the unfavorable financial and economical

situation that had arisen by the time of the tests it was possible to perform rather detailed investigations of aerodynamic characteristics for only one model version. The version shown in Fig.1 was chosen for tests. As illustrated in this figure, the model had a slightly blunt ogive nose with the aspect ratio λ_n of 2 gages, a central cylindrical body (λ_c=4.65) and aft conical "skirt" (λ_{sk}=1.16) with the generatrix angle of $\theta_{sk}=6.5^0$. Thus, the total model aspect ratio λ_m was 7.81 gages.

All three main model components were made separately of a special aluminium-magnesium alloy and joined using thread connections.

In the test section, the model was placed on the sting. Fig. 2 shows the model arrangement in the wind tunnel T-121.

The loads acting on the model in the tests were measured in the body-fixed coordinate system using the three-component strain-gage balance beyond the action of the flow on the test section wall (Fig.2). The main balance characteristics are summarized in Table 1.

Table 1

Maximum loads to be measured			Measurement errors		
X [кg]	Y [кg]	M_Z [кг×cm]	$б_x$	$б_y$	$б_{mz}$
14.0	±14.0	± 0.6	0.0020	0.0024	0.000751

The base pressure was measured using a pressure tap placed under the strain-gage balance fairing rather than immediately on the model base section. As follows from the multi-year experience of balance tests in the wind tunnel T-121, this

technique of measuring the base pressure did not essentially influence the base pressure value, but such an approach made it possible to simplify the model afterbody design and manufacturing and, more importantly, to facilitate, the model assembly and reassembly in the test section during the tests.

To estimate aerodynamic coefficients C_X, C_y and m_Z, the aerodynamic forces X and Y were related to the free-stream dynamic pressure q and the model base area S_b=0.000835m, and the aerodynamic moment M_Z, in addition, to the model length L_Z=0.2016m. In this case, the coefficients m_Z were calculated with respect to the conditional mass center in the model nose.

The longitudinal force coefficient C_X was calculated by applying a correction for the base pressure, i.e., the model base pressure P_b was reduced to the free-stream static flow pressure P_∞.

During the test data processing, the corrections for the sting deflection under the aerodynamic load were applied to angles of attack α measured from the model axis.

Table 2 presents the balance model test program in the wind tunnel T-121 with the indication of averaged main flow parameters attained in the tests.

The following notations are used in Table 2:

M_∞ - free-stream Mach number;
P_0 - total pressure in plenum chamber;
q_∞ - free-stream dynamic pressure;
P_∞ - free-stream static pressure;
T_0 - free-stream stagnation temperature;
Re_X - Reynolds number based on the free-stream flow parameters and the reference linear dimension x=0.172m characterizing the distance from the model nose to the contour generatrix break, i.e., to the transition of a cylindrical surface to a conical one.

Table 2

Run #	M_∞ number	P_0 [psia]	q_∞ [kg/cm^2]	P_∞ [kg/cm^2]	T_0 [K]	$Re_x \times 10^{-6}$	$(M/\sqrt{Re_x}) \times 10^3$
1	4.00	1.47	0.1085	0.00970	293	1.16	3.71
2	4.01	1.84	0.1350	0.01198	-"-	1.45	3.33
3	4.02	2.31	0.1675	0.01480	-"-	1.81	2.98
4	4.03	2.97	0.2133	0.01885	-"-	2.34	2.63
5	4.03	3.98	0.2870	0.02511	-"-	3.13	2.28
6	4.04	4.97	0.3545	0.03105	-"-	3.91	2.04
7	4.05	7.95	0.5630	0.04904	-"-	6.27	1.62
8	4.06	10.93	0.7687	0.06644	-"-	8.60	1.38
9	4.96	2.90	0.1005	0.00575	403	0.90	5.23
10	4.97	4.45	0.1505	0.00870	-"-	1.38	4.23
11	4.98	5.90	0.1985	0.01145	-"-	1.82	3.69
12	5.00	10.78	0.3568	0.02040	408	3.23	2.78
13	5.00	15.40	0.5075	0.02900	413	4.52	2.35
14	5.02	25.95	0.8455	0.04795	-"-	7.60	1.82
15	6.00	6.85	0.1095	0.00435	513	0.98	6.06
16	6.05	13.20	0.2025	0.00785	-"-	1.85	4.45
17	6.08	20.95	0.3160	0.01225	-"-	2.99	3.52
18	6.96	24.10	0.2050	0.00605	623	1.69	5.35
19	7.03	32.40	0.2635	0.00760	-"-	2.27	4.67
20	7.05	39.85	0.3190	0.00920	633	2.74	4.25
21	7.07	63.90	0.5070	0.01445	-"-	4.39	3.37
22	7.07	95.85	0.7615	0.02170	643	6.26	2.83
23	7.97	31.75	0.1480	0.00333	703	1.28	7.04
24	8.00	51.90	0.2385	0.00532	723	2.00	5.66
25	8.03	96.05	0.4340	0.00960	773	3.30	4.42
26	8.96	46.95	0.1290	0.00229	-"-	1.21	8.15
27	9.04	95.70	0.2535	0.00442	823	2.23	6.05

During the balance tests in all conditions stated in Table 2, the model sideslip angle β was taken to be equal to zero, while the angle of attack α was varied from -4^0 to 10^0 with the variation step $\Delta\alpha$ of 1^0 in the range $=-4^0 \div 6^0$ and 2^0 when $\alpha>6^0$.

For the optical tests, the model was in the test section at zero angles of attack and sideslip angles all the time. When one or another nozzle was mounted, only one run was performed with the plenum chamber pressure varying discretely. As a required flow condition was attained, the region near the model contour generatrix break was photographed three times in the scale 1:1 through optical windows in the test section walls (window diameter is 150mm) using aerial photographic films. The model flow spectra were obtained by the direct shadow technique on the ИАБ-451 device. Unfortunately, it was impossible to combine the balance and optical tests, since for the balance tests the external strain-gage balance were mounted on the test section wall precisely at the location of one of the optical windows.

The main flow parameters obtained during the optical tests are summarized in Table 3. It is seen that the optical tests were not conducted at $M_\infty \approx 9.0$ which was primarily caused the fact that the flow densities in that test condition were extremely small and, hence, it seemed to be questionable to obtain model flow spectrum patterns of high quality.

The variation ranges of the Mach and Reynolds numbers realised during the balance and optical tests are presented in Figs.3 and 4 in the form of plot for more comfortable assimilating.

It should be also noted that 9 special methodical runs were undertaken immediately before the main series of the model tests aimed at obtaining the aerodynamic characteristics and model generatrix break flow spectra. These runs were done to evaluate the flow quality at the current time at all Mach numbers and pressures in the plenum chamber assumed for the

main test series of a chosen model version.

Table 3

Run #	M_∞ number	P_0 [psia]	$Re_X \times 10^{-6}$	$(M_\infty/\sqrt{Re_X}) \times 10^3$
28	4.00	1.48	1.16	3.71
	4.01	1.85	1.45	3.33
	4.02	2.33	1.81	2.98
	4.03	3.00	2.34	2.63
	4.03	3.98	3.13	2.28
	4.04	4.98	3.91	2.04
	4.05	8.01	6.27	1.62
	4.06	10.25	8.20	1.42
29	4.96	2.92	0.90	5.23
	4.97	4.45	1.38	4.23
	4.98	5.95	1.82	3.69
	4.99	8.52	2.63	3.08
	5.00	10.82	3.23	2.78
	5.00	15.44	4.52	2.35
	5.01	21.45	6.31	1.99
	5.02	26.00	7.60	1.82
30	6.00	6.88	0.98	6.06
	6.02	9.55	1.37	5.14
	6.03	11.04	1.56	4.83
	6.05	13.26	1.85	4.45
	6.06	14.95	2.15	4.13
	6.08	20.95	2.99	3.52
31	6.96	24.15	1.69	5.35
	7.03	32.40	2.27	4.67
	7.05	40.03	2.74	4.25
	7.07	63.85	4.39	3.37
	7.07	78.04	5.09	3.13
	7.07	95.93	6.26	2.83
32	7.97	31.80	1.28	7.04
	8.00	52.05	2.00	5.66
	8.02	76.05	2.95	4.67
	8.03	96.00	3.30	4.42

TEST RESULTS

The balance test results for a model of a body of revolution of the type of "an ogive-a cylinder- a truncated cone" obtained in the wind tunnel T-121 of TsAGI at $M_\infty \approx 4.0 \div 9.0$, $Re_x = (0.9 \div 8.6) \times 10^6$. $\alpha = -4^0 \div 10^0$, $\beta = 0$ are presented in Figs. 5÷112 in the form of plots C_x, C_{xa}, C_{pb}, C_y, C_{ya}, K, m_z, $C_d = f(\alpha)$ and $m_z = f(C_y)$.

The optical test results for the model at $M_\infty \approx 4.0 \div 8.0$, $Re_x = (0.9 \div 8.2) \times 10^6$, $\alpha = 0$, $\beta = 0$ are given in the photos of flow spectra over the contour generatrix break areas in Figs. 127÷÷142.

Unfortunately, we have to state that the quality of the photos taken leaves, to put it mildly, much to be desired especially when the flow density is small ($M_\infty \approx 6.0$, 7.0, and 8.0). The reason is that by the time of conducting optical tests we had at our disposal an aerial photo film with overdue application time only and its development even by using special agents did not provide the desired quality. Nevertheless, the photos obtained are, however, a great help in the analysis of the balance test results.

Special emphasis will be placed on the influence of variations of different kind in the flow behaviour over the model on its moment characteristics and the pressure center position at small angles of attack. But first, we consider briefly the plots C_{x0}, C_y^α, $m_z^\alpha = f(Re_x)$ characterizing the aerodynamic characteristics of the model at angles of attack close to zero for all flow conditions of interest (Figs.113 ÷115).

From these curves it is obvious that as a whole the longitudinal forse coefficients in the range of Mach and Reynolds numbers under study are close to each other in the vicinity of $\alpha = 0$. At $M_\infty \approx 6.0$ the values of the coefficient C_{x0} are somewhat greater, and at $M_\infty \approx 9.0$ they are somewhat smaller.

The highest lifting properties of the model characterized by C_y^α at angles of attack close to zero are exhibited at $M_\infty \approx$

$\approx$5.0, while the lowes ones at $M_\infty \approx 4.0$. Closer values of C_y^α are obtained at close Reynolds numbers, Re_x in flow conditions corresponding to $M_\infty \approx 6.0$, 7.0, 8.0 and 9.0. As for the lifting properties of the model near $\alpha=0$ it should be also noted that at $M_\infty \approx 4.0$, 5.0 and 6.0, C_y^α tends to decrease as Re_x increases (it is especiablynoted at $M_\infty \approx 4.0$ and 5.0). Conversely the lifting properties of the model slightly increase at $M_\infty \approx 7.0$, 8.0 and 9.0 as Re_x rises.

At $M_\infty \approx 4.0$ in the range of Reynolds numbers in question the values of the derivative m_z^α being the smallest in their absolute values are also obtained. The derivative m_z^α characterizes the moment characteristics of the model in the pitching plane at angles of attack close to zero. As is the case with C_y^α, the greatest values of $|m_z^\alpha|$ take place at $M_\infty \approx 5.0$ for Reynolds numbers under study. As the Mach number increases from $M_\infty \approx 5.0$ to $M \approx 9.0$, the values of $|m_z^\alpha|$ decrease gradually. Note that beginning with certain values of the Re_x at $M_\infty \approx 4.0$ and 5.0, the values of $|m_z^\alpha|$ decrease rather intensively, while at $M_\infty \approx 6.0$, 7.0, 8.0 and 9.0, the values of $|m_z^\alpha|$ increase monotonically as Re_x rises.

Now turn to the matter concerning variations of the pressure center psition characterized by $m_z{}^{Cy}$ at $\alpha=0$. It is obvious from the dependeces $m_z{}^{Cy}=f(Re_x)$ shown in Fig.116, that the greatest pressure center displacement due to varied Reynolds numbers takes place at $M_\infty \approx 4.0$ and 5.0. The pressure center displacement is especially great at $M_\infty \approx 4.0$ when it displays forward to the model nose for a distance of almost 15% of the body length L_m as Re_x rises from $Re_x=1.16\times10^6$ to $Re_x=8.60\times10^6$. At $M_\infty \approx 5.0$ the pressure center also displays forward as Re_x rises but this displacement is smoller than at $M_\infty \approx 4.0$ and amounts to approximately 5% of L_m. In flow conditions corresponding to $M_\infty \approx 6.0$, 7.0, 8.0 and 9.0 the increse in the Reynolds numbers, Re_x in the ranges of interest, causes the pressure center displacement backward from the model nose by a distance that does not exceed approximately 2% of the model length.

At the same time, the analysis of the dependences $C_d=f(\alpha)$ (Figs. 86÷112) characterising variations in the pressure center coefficient in terms of the angle of attack reveals somewhat different values of the pressure center position at $\alpha=0$ (see the dependence $C_{d0}=f(Re_x)$ in Fig.117).

Figs. 118÷123 compare the pressure center position values obtained by prosessing the dependences $m_z=f(C_y)$, i.e. the values of m_z^{Cy} and dependences $C_d=f(\alpha)$ consequently, the values of C_{d0}. It is obvious that when the values of m_z^{Cy} and C_{d0} differ, the more aft pressure center position corresponds to the results of processing the dependences $C_d=f(\alpha)$, while more forward position concerns results of the analysis of the dependences $m_z=f(C_y)$. In some flow conditions this difference is about 4÷5% of L_m.

The difference in the test data processing raizis,naturally, the question which of them are most reliable. To elucidate this point, consider the dependences $C_d=f(\alpha)$ in Figs. 86÷÷112 in more ditail.

It should be noted, first of all, that reduced values of the pressure center coefficient Cd are determined as follows:

$$C_d = \frac{m_z(\alpha_i) - m_z(\alpha=0)}{C_y(\alpha_i) - C_y(\alpha=0)} . \qquad (1)$$

The application of this approach instead of using the ratio $m_z(\alpha)/C_y(\alpha)$ is motivated by two reasons. At first, the calculation of this kind includes the presence of some nonzero coefficients C_y and m_z at $\alpha=0$ which are actually obtained during the test. Secondly, in this case the so-called "effect of small-value ratio" manifests itself to a considerably smaller extent at angles of attack close to zero. This effect implies that at small coefficients C_y and m_z, attained at these angles of attack, even small variations in their values can result in a rather essential variations in the ratio of these values.

Neglecting $C_y(\alpha=0)$ and $m_z(\alpha=0)$ leads often to the same result. As a consequence, the dependence $C_d=f(\alpha)$ acquires a considerably nonsymmetric form relative to the coordinate axis and, what is more important, the error probability increases in the test data analysis. It is impossible, of course, to state that the calculation of the pressure center coefficient using (1) allows the "effect of small-value ratio" to be avoided entirely, since the errors in measuring aerodynamic forces and moments acting on the model by a strain-gage balance at angles of attack close to zero are the greatest and so-called "maverisks" are characteristic of precisely this range of . Nevertheless, the calculation of C_d in this manner yields objectively more reliable results.

Now we proceed to the analysis of the test results beginning with plots $C_d=f(\alpha)$ obtained at $M_\infty\approx4.0$. It is seen from Figs. 86 ÷ 93 that the behaviour of the plot $C_d=f(\alpha)$ is essentially nonlinear at $Re_x<3.9\times10^6$. As the angle of attack increases from $\alpha=0$ to $\alpha\approx3^0\div4.5^0$, the pressure center displays rather appreciably forward to the model nose (up to 6 ÷ 8% of the model length L_m), and further increases in results in the pressure center movements backwards (by 3 ÷ 8% of L_m). As for flow conditions corresponding to $Re_x>6.27\times10^6$, there are no longer drastic variations in the pressure center position at small angles of attack. In these conditions, the pressure center displays gradually backwards from the model nose for a distance of 10 ÷ 12% of the body length as increases from 0 to 10^0. To appreciate the reasons of so distinct behaviours of the plots $C_d=f(\alpha)$ at different values of Re_x, consider the optical test results shown in Figs.127 ÷ 130.

It is well seen in these photos that at $Re_x<3.91\times10^6$ a boundary layer develops on the model surface which has a very great thickness in the region of the aft "skirt". As a result, the geometry of an actually streamlined liquid contour differs considerably from that of the model. The difference is, first of all, that the model contour generatrix break in the region

where the cylindrical body section transforms to the aft conical "skirt" ($\theta_{sk}=6.5^0$) is smoothed essentially by the boundary layer and there is no shock in the break zone. Most likely, the boundary layer in these conditions is laminar. It is well seen that as the Reynolds number, Re_x, rises from 1.16×10^6 to 3.91×10^6, the boundary layer thickness decreases gradually and, accordingly, the geometry of the streamlined liquid contour becomes more and more similar to the model geometry.

At $Re_x>6.27\times10^6$, when the boundary layer is most probably turbulent, a shock in the region of the aft "skirt" can be seen in the photos of the flow spectra (Fig.130). In this case, the boundary layer geometry follows almost completely the model geometry.

Thus, in the flow condition corresponding to $M_\infty\approx4.0$, the behaviour of the free-stream flow over the model at $Re_x<3.91\times10^6$ differs most considerably from that at $Re_x>6.27\times10^6$ especially in the region of the contour generatrix break. This is just the reason for different behaviour of the dependence $C_d=f(\alpha)$ at different Reynolds numbers, Re_x, which is revealed in the balance tests and mentioned above.

It should be only added that the appreciable nonlinearity in the behaviour of $C_d = f(\alpha)$ observed at $Re_x < 3.92\times10^6$ is explained by a high susceptibility of the liquid contour to the transformation when the angle of attack varies. Most likely, a flow with a shock in the region of the aft conical "skirt" forms both on the windward surface and on the leeward one as the angle of attack is reached when the absolute value of the pressure center coefficient is the smallest. Of course, it is only an assumption, since the photos of the flow spectra were taken only at zero angle of attack. But this assumption is confirmed indirectly even by the available photos. As stated above, the boundary layer thickness decreases at $\alpha=0$ as the Reynolds number, Re_x, increase from 1.16×10^6 to 3.29×10^6. Consequently, a shock in the contour generatrix break zone at $Re_x=3.19\times10^6$ must occur earlier than at lower values of Re_x as

the angle of attack changes. It is seen that the plots $C_d=f(\alpha)$ in Figs.86 ÷ 93 are in conformity with this assumption. A minimum value of $|C_d|$ at $Re_x=3.91\times10^6$ is attained for $\alpha\approx3^0$, while at $Re_x=1.16\times10^6$ for $\alpha\approx4.5^0$.

Similar phenomena are also observed at $M_\infty\approx5.0$. In this case, one of two above-considered model flow types is realized depending on Re_x, which is clearly seen in the analysis of the balance and optical test results presented in Figs.94 ÷ 99 and 131 ÷ 134, respectively.

At $Re_x<4.52\times10^6$, there is no shock in the contour generatrix break zone due to a boundary layer with a great displacement thickness which develops on the model surface. As for the flow conditions when $Re_x>6.31\times10^6$, they are characterized by a developed shock upstream of the aft conical "skirt". The behaviour of the dependences $C_d=f(\alpha)$ is identical and features a nonlinear region at $Re_x<4.52\times10^6$ with minimum values of $|C_d|$ in the range $\alpha\approx2^0\div3^0$.

At $M_\infty\approx6.0$ and 7.0, only such a flow over the model forms in the ranges of Re_x under study that has no shock upstream of the aft conical "skirt". It follows from the photos of the flow spectra in Figs. 135 ÷ 140 that the contour generatrix break zone is smoothed by a boundary layer with a great displacement thickness. The nonlinearity degree of the dependences $C_d=f(\alpha)$ in the range of small angles of attack becomes greater as the number Re_x increases (Figs.100 ÷ 107). The smallest values of $|C_d|$ are exhibited in the range of $\alpha\approx2.0^0\div2.5^0$ at $M\approx6.0$ and in the range $\alpha\approx2.0^0$ at $M_\infty\approx7.0$. The sole exception to this regularity concerns the results of the run 15 ($M_\infty=6.00$, $Re_x=0.98\times10^6$) for which the nonlinearity of the dependence $C_d=f(\alpha)$ is almost absent at angles of attack close to zero. Nevertheless, the pressure center position is likely to vary at $\alpha=0$ but this variation is small and comparable with the error in determining C_d.

At $M_\infty\approx8.0$, a laminar boundary layer of a great thickness develops on the model surface at all values of Re_x of interest

(Figs.141 and 142). When analyzing the dependences $C_d=f(\alpha)$ obtained at $M_\infty \approx 8.0$ (Figs. 108 ÷ 110), their noticeable nonsymmetry about the coordinate axis (zero angle of attack) attracts the attention. The degree of this nonsymmetry decreases as the number Re_x rises.

This is not, most likely, the consequence of incorrect measurements of aerodynamic loads acting on the model during the test. Probably, hysteresis of the aerodynamic characteristics takes place in this condition at small angles of attack, that is at $M_\infty \approx 8.0$, the direction of the model motion in terms of angles of attack exerts some influence on the aerodynamic characteristics of the model in the range of $\alpha=0$. Since the nonlinear behaviour of the dependence $C_d=f(\alpha)$ at small angles of attack is caused, as indicated above, by the boundary layer transformation, the hysteresis effect is quite possible in the case of a viscous boundary layer. At $M_\infty \approx 8.0$, the temperature inside the boundary layer is higher than in the flow conditions considered above which is followed by a decreased gas density and, what is more important, by an increased gas viscosity. In addition, hysteresis of the aerodynamic characteristics of the model in these conditions can be caused, to a large extent, by different states of the boundary layer on the windward and leeward model sides, i.e., to be more precise, by different positions of the laminar-turbulent boundary layer transition point. The influence of this kind is quite possible at Reynolds numbers under consideration ($Re_x = 1.28\times10^6$, 2.00×10^6, and 3.30×10^6).

Minimum values of $|Cd|$ on the nonlinear branch of the curve $C_d=f(\alpha)$ (the region of positive angles of attack) take place at $\alpha \approx 1.5^0 \div 2.0^0$.

At $M_\infty \approx 9.0$, the region of drastic variations in the behaviour of the dependence $C_d=f(\alpha)$ due to the liquid contour transformation gets narrow down to 1^0 (Figs.111 and 112). It is precisely the narrowing of the boundary layer transformation zone, as compared to $M_\infty \approx 8.0$, is likely to be responsible

for the fact that hysteresis of the aerodynamic characteristics of the model is not exhibited at $M_\infty \approx 9.0$ in spite of a higher temperature inside the boundary layer.

Thus, the analysis of the dependences $C_d = f(\alpha)$ supported by the optical test resalts shows that when a laminar boundary layer with a great displacement thickness forms on the model surface in the region of the aft conical "skirt", the behaviour of the dependences $C_d = f(\alpha)$ at small angles of attack is essentially nonlinear. In this case, the range of angles of attack, in which the pressure center position varies appreciably, decreaces as Mach and Reynolds numbers rise. This is well seen from the analysis of the plot $\alpha' = f(Re_x)$ in Fig.124 which characterizes the variation in the angle of attack α' at which the most forward pressure center position ($|C_d|_{min}$) is attained depending on the number Re_x at different Mach numbers.

Next, consider again the comparative plots in Figs 118÷123 showing the dependences $C_{d0} = f(Re_x)$ and $m_z^{Cy} = f(Re_x)$ and analyze them wiht taking account of the above dependences $\alpha' = f(Re_x)$. The analysis of this kind makes it possible to notice that when $\alpha' = 3.0^0 \div 4.5^0$ ($M_\infty \approx$ 4.0 and 5.0), the difference in values of C_{d0} and m_z^{Cy} either is not great or absent at all. But when $\alpha < 3.0^0$, the values of $|m_z^{Cy}|$ are always smaller then values of $|C_{d0}|$. In the present report, the value of m_z^{Cy} was obtained by a cubic approximation of the test values of C_y and m_z. It is probably that when the liquid contour transformation zone on the the boundary layer edge reduces to angles of attack $\alpha < 3.0^0$, such an approximation is insufficient in order to represent adequatly a complicated nature of variations in the flow over the model. As a consequence, the values of $|m_z^{Cy}|$ are underestimated as compared to these of $|C_{d0}|$. But when the variation step of the angle of attack is $\Delta\alpha = 1.0^0$, the the approximation of the test values for C_y and m_z by a higher - order curve at angles of attack close to zero is very cumbersome. Which would be possible for the tests with the varia-

tion step of the angle of attack $\Delta\alpha=0.5^0$.

Thus, the above considerations indicate that quantitatively the pressure center position values obtained as a result of the analysis and prosessing of the dependences $C_d=f(\alpha)$ represented more reliably those variations in the model flow behaviour which are characteristic for $\alpha=0$ in the flow conditions in question.

In view of this, consider again the plots $C_{d0}=f(Re_x)$ in Fig.117.

As mentioned above, the pressure center displays forward to the model nose for a distance of 15% of the model length L_m at $M_\infty\approx4.0$, as the Reynolds number increase from $Re_x=1.16\times10^6$ to $Re_x=8.60\times10^6$. Based on the optical test results, it is possible to state that for the most part this displacement is caursed by the trsnsition from the flow over the model of one tupe, when a laminar boundary layer, smoothing the generatrix break, develops on the model surface, to another flow tupe featuring a shock upstream of the aft conical "skirt". At $M_\infty\approx5.0$ the behaviour of the dependence $C_{d0}=f(Re_x)$ is similar and due to the same reasons. But in this case, the forward pressure center displacement is not so great and amounts to about 9% of L_m.

As we have shown,only such a type of a flow over the model forms at $M_\infty\geqslant6.0$ and $\alpha=0$ for Reynolds numbers under study when there is no shock upstream of the aft conical "skirt". At $M_\infty\approx6.0\div9.0$, the pressure center position variation due to variations in the number Re_x is not so considerable as at $M_\infty\approx4.0$ and 5.0. Moreover, in these flow conditions, the pressure center displays backwards from the model nose rather forward as Re_x rises, and greater is the Mach number the smaller is this displacement:

at $M_\infty\approx6.0$ $\Delta c_{d0}=0.060$;
at $M_\infty\approx7.0$ $\Delta c_{d0}=0.045$;
at $M_\infty\approx8.0$ $\Delta c_{d0}=0.035$;
at $M_\infty\approx9.0$ $\Delta c_{d0}=0.025$.

Thus, the plots in Fig.117 show that in the range of $M_\infty \approx$ $\approx 4.0 \div 9.0$ the behaviour and magnitude of the pressure center position variation at one and the same fixed value of M due to varations in the number Re_x can differ greatly from each other.

The same plots also indicate that it is rather difficult to determine the influence of the Mach number on the presure center position at a fixed value of the number Re_x. For example, the pressure center displays forward at $Re_x < 1.8 \times 10^6$ as the Mach number increaces, while at $Re_x > 4.0 \times 10^6$, the influence of the Mach number is exactly the opposite. As for $Re_x = 3.0 \times 10^6$, it is impossible to clear up the manner in which the Mach number influences the pressure center position.

In order to understand more clearly the degree and nature of the influence of Mach and Reynolds numbers on pressure center position of the model with the contour generatrix break at hypersonic velocities, we consider the dependence of the pressure center coefficient C_{d0} on the complex parameter $M_\infty/\sqrt{Re_x}$ given in Fig.125. The complex parameter used is in effect the ratio of the nondimensional laminar boundary layer thickness $1/\sqrt{Re_x}$ to the nondimensional tickness of the inviscid disturbed flow $1/M_\infty$(this is the plot slope at high Mach numbers).

Passing an averaging curve through a set of points corresponding to the test values of C_{d0} makes it possible to get a rather clear representation of the nature of the influence of the complex parameter $M_\infty/\sqrt{Re_x}$ on the pressure center position. It is well seen that the greatest absolute values of C_{d0} are characteristic for $M_\infty/\sqrt{Re_x} \approx (2.5 \div 3.5) \times 10^{-3}$. The increase or decrease of the parameter $M_\infty/\sqrt{Re_x}$ with respect to these values results in reduced values of $|C_{d0}|$. The previous analysis shows that a drastic decrease in values of $|C_{d0}|$ at $M_\infty/\sqrt{Re_x} < 2.3 \times 10^{-3}$ is caused by changing the model flow type . As mentioned above, in the transition to the model flow with a shock upstream of the aft "skirt", the boundary layer becomes nonlaminar to a large degree of probability. The values of

$|C_{d0}|$ at $M_\infty/\sqrt{Re_x}>3.5\times10^{-3}$ decrease much more smoothly. This portion of the curve $C_{d0}=f(M_\infty/\sqrt{Re_x})$ corresponds to flow conditions when a laminar boundary layer of a great displacement thickness develops on the model surface which makes the contour generatrix break smooth.

It is seen in Fig.125 that the difference of the test values of C_{d0} from the averaging curve $C_{d0}=f(M_\infty/\sqrt{Re_x})$ does not exceed 2.5% of the model length L_m. Bearing in mind that the variation in the number Re_x for most Mach numbers in question resulted in much greater variations in the pressure center position it is also reasonable to apply the complex parameter $M_\infty/\sqrt{Re_x}$ to estimate quantitatively the model pressure center position.

Close analysis of the data given in Fig.125 makes it possible to point out that the test values of C_{d0} obtained at $M_\infty\approx7.0$ coincide essentially wiht the averaging curve $C_{d0}=f(M/\sqrt{Re_x})$. The points obtained at $M_\infty\approx4.0\div6.0$ lie below this curve,while those for $M_\infty\approx8.0$ and 9.0 are above the curve. When analyzing Table 2 containing main flow parameter values it is seen that at $M_\infty\approx4.0\div6.0$ the values of T_0 are smoller then at $M_\infty\approx7.0$, while at $M_\infty\approx8.0$ and 9.0 they are greater. In other words, slightly increased values of $|C_{d0}|$ with respect to the averaging curve are obtained for a "colder" model and somewhat decreased values for a "hoter" model.

This finding makes it possible to suggest that a more correct correlation of the pressure center coefficient values with respect to the parameter $M_\infty/\sqrt{Re_x}$ dictates the model temperature to be taken account. Now we try to correct the test results obtained including the temperature factor.

Rough calculation estimates and some fragmentary data about the surface temperature of a nonhollow metal model with taking account of heat transfer inside the model allow the suggestion that this model had surface temperature T_w and temperature factor $t_w=T_w/T_0$ given in Table 4 for flow conditions under study and at the time when $\alpha=0$.

Table 4

Run number	M_∞ number	T_0 [K]	T_W [K]	t_W
1÷8	4	293	293	1.000
9÷11	5	403	323	0.801
12	5	408	325	0.797
13,14	5	413	327	0.792
15÷17	6	513	363	0.708
18,19	7	623	413	0.663
20,21	7	633	415	0.656
22	7	643	416	0.647
23	8	703	443	0.630
24	8	723	445	0.615
25,26	8,9	773	473	0.612
27	9	823	488	0.593

Plotting the test data of C_{d0} for flow conditions with a laminar boundary layer as functions of the parameter $M/\sqrt{Re_x}\times t_W$ makes it possible to conclude that their difference from the averaging curve is almost 1% of the model length L_m (Fig.126).

It is possible that the temperature factor should be taken into account by anothe way. To do this, it is necessary, however, to have, first exact data about the model surface temperature while testing and, second, experimental statistical data which exceed considerably the scope of the test carried out. As for the results of the present test series, they only demonstrate that the temperature factor exerts some influence on the pressure center position of a body of revolution having the contour generatrix break at hypersonic velocities and it should be taken into account in the analysis of wind tunnel test results.

CONCLUSIONS

From the analisis of the test results for a model of the type of "an ogive - a cylinder - a truncated cone" carried out under contract SPC-94-4009 in the wind Tunnel T-121 at $M \approx 4.0 \div 9.0$ and $Re_x = (0.90 \div 8.60) \times 10^6$ it may be inferred:

1. The application of the complex parameter $M_\infty / \sqrt{Re_x}$ yields a clear qualitative representation about the character of pressure center position variations in the vicinity of $\alpha = 0$ at hypersoniic velocities.

2. The difference of the test pressure center coefficient values C_{d0} from the averaging curve $C_{d0} = f(M_\infty / \sqrt{Re_x})$ passing through a set of test values of C_{d0} does not exceed 2.5% of the model length L_m.

3. The tests carried out indicate the influence of the temperature factor t_w on the model pressure center position at angles of attack close to zero.

4. The difference of the test pressure center coefficient values C_{d0} from the averaging curve $C_{d0} = f(M_\infty / \sqrt{Re_x} \times t_w)$ passing through a set of the test values of C_{d0} is about 1% of the model lenth L_m.

RESUME

The tests carried out show that more comprehensive and correct taking account of all factors influencing the pressure center position of a body of revolution with a contour generatrix break at hypersonic velocities necessitates conducting additional experimental investigations.

In the course of these tests it would be desirable to undertake the following activities:

1. To measure the model surface temperature while conducting balance tests.

2. To change angle of attack α in the range of no less than $\alpha = -5^0 \div 5^0$ with a step of no greater than $\Delta\alpha = 0.5^0$.

3. To conduct optical tests in the range of angles of attack $\alpha = -5^0 \div 5^0$ at the minimum.

In addition, it would be desirable to carry out the tests of model with somewhat other geometric parameters and to investigate aerodynamic characteristics of geometrically-similar models at hypersonic velocities in other wind tunnels.

TsAGI has every possibility for those experimental investigations. Hence, if AFMC is interested in them, the tests above considered can be accomplished under a new contract.

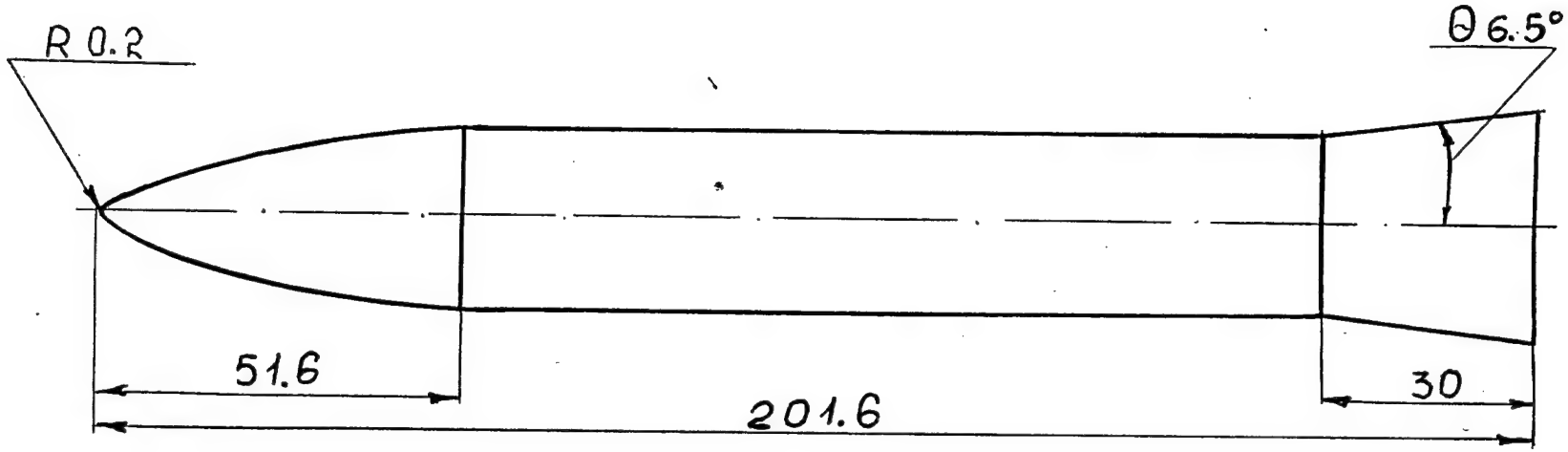

Fig. 1

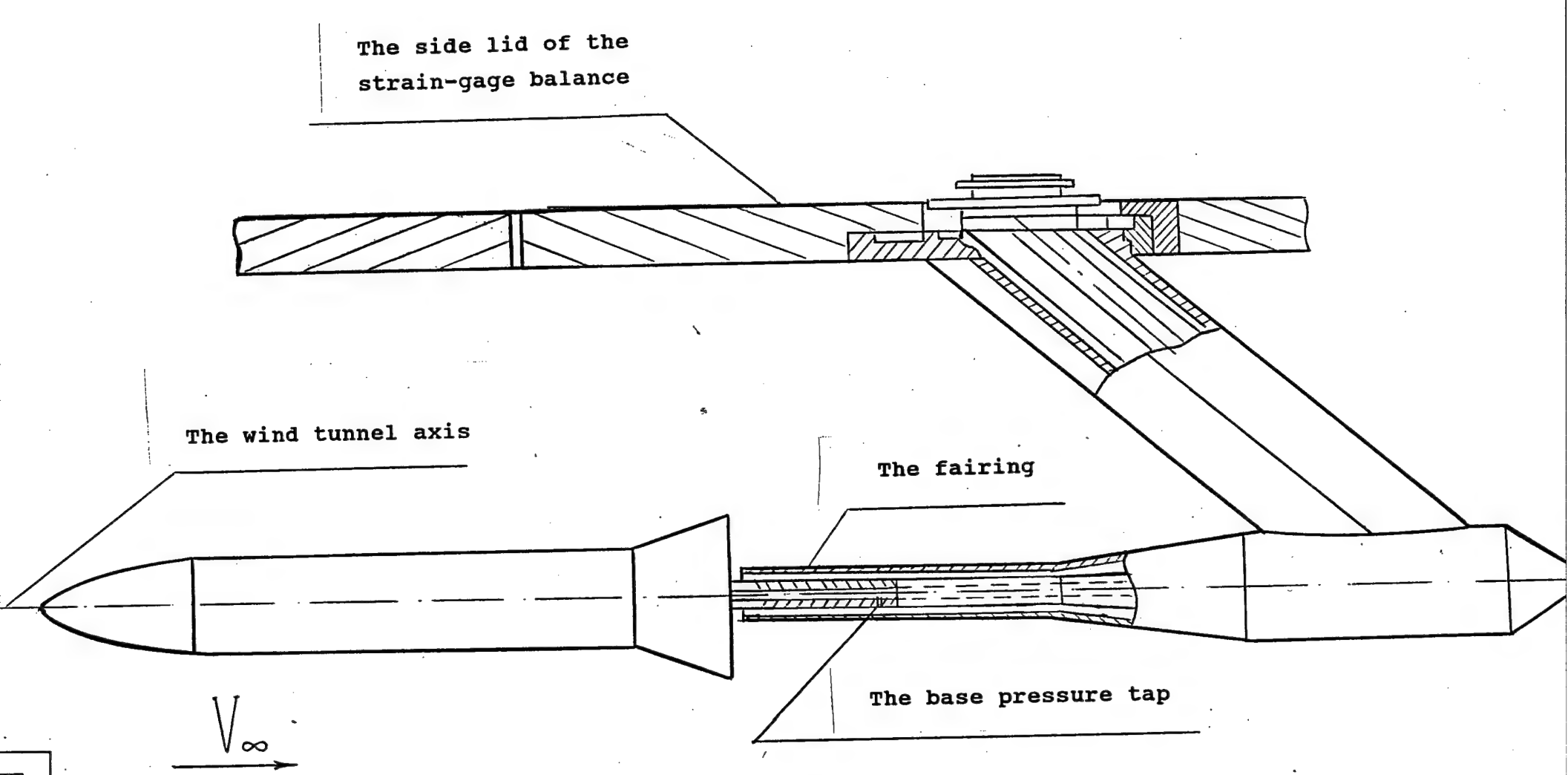
The side lid of the
strain-gage balance
The wind tunnel axis
The fairing
The base pressure tap
V_∞

Fig. 2

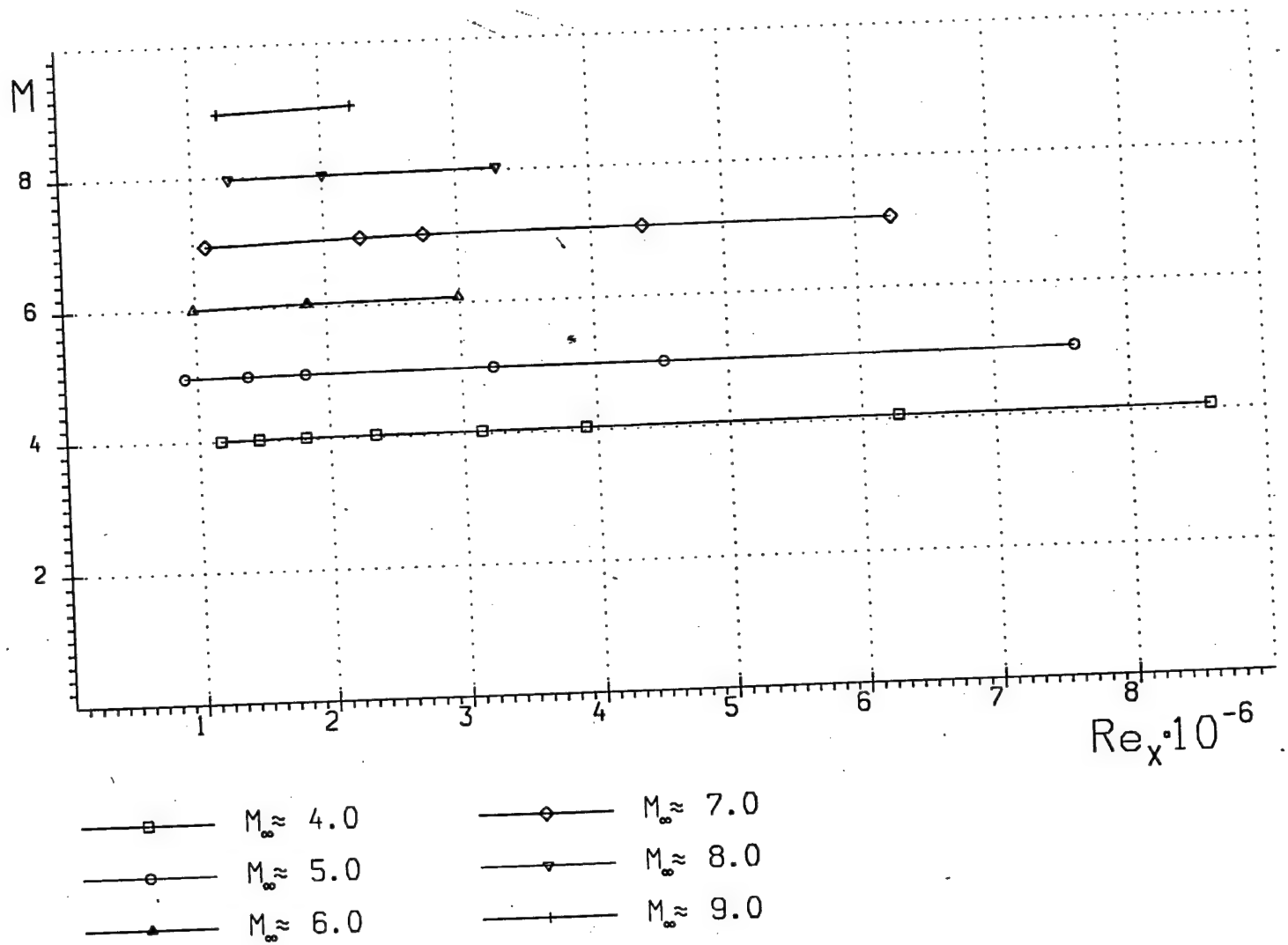
M
8
6
4
2
1
2
3
4
5
6
7
8
$Re_x \cdot 10^{-6}$
$M_\infty \approx$ 4.0
$M_\infty \approx$ 5.0
$M_\infty \approx$ 6.0
$M_\infty \approx$ 7.0
$M_\infty \approx$ 8.0
$M_\infty \approx$ 9.0

Fig. 2

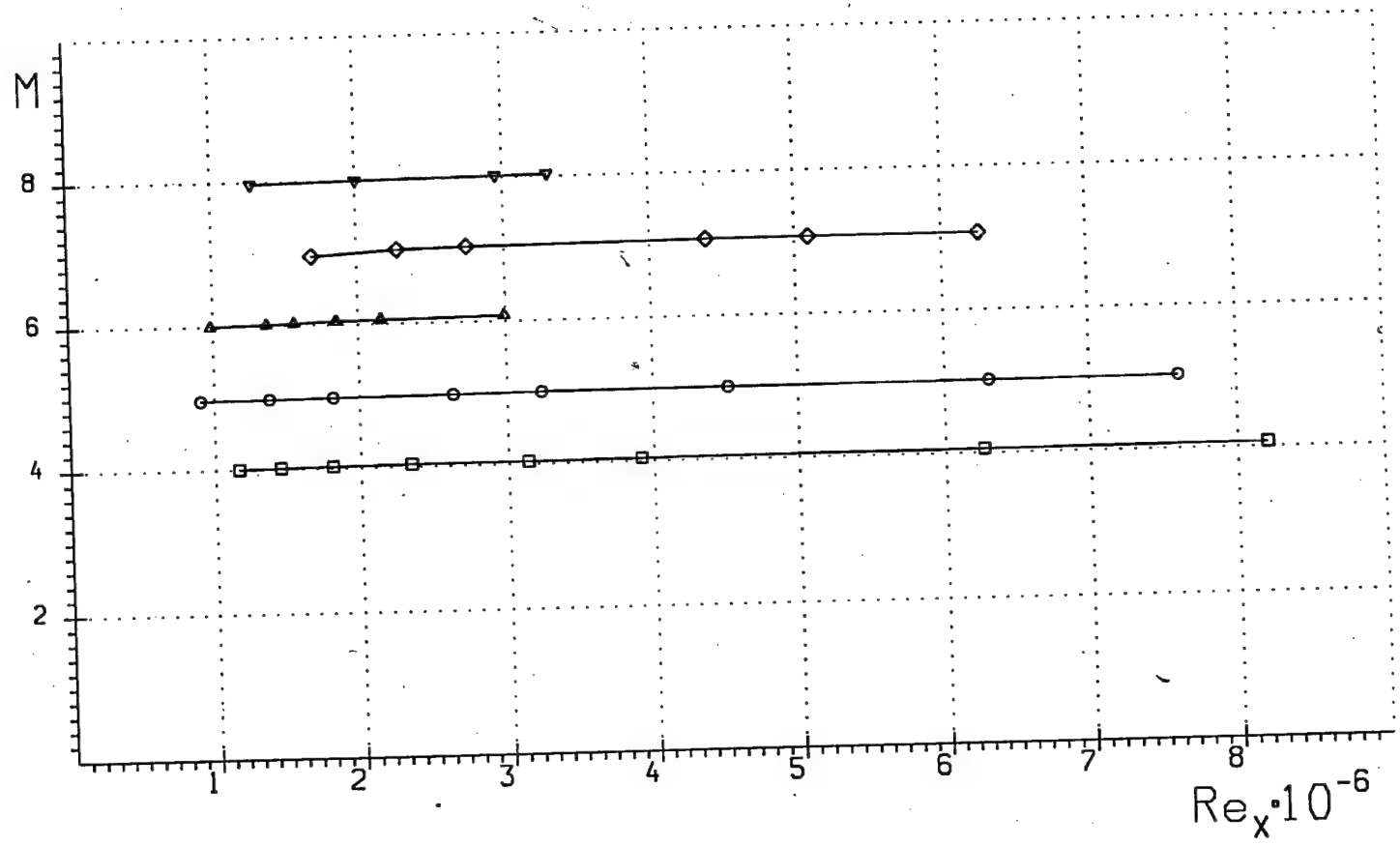
M
8
6
4
2
1
2
3
4
5
6
7
8
$Re_x \cdot 10^{-6}$
$M_\infty \approx 4.0$
$M_\infty \approx 5.0$
$M_\infty \approx 6.0$
$M_\infty \approx 7.0$
$M_\infty \approx 8.0$

Fig. 4

$M_\infty = 4.00$ $Re_x = 1.16 \cdot 10^6$

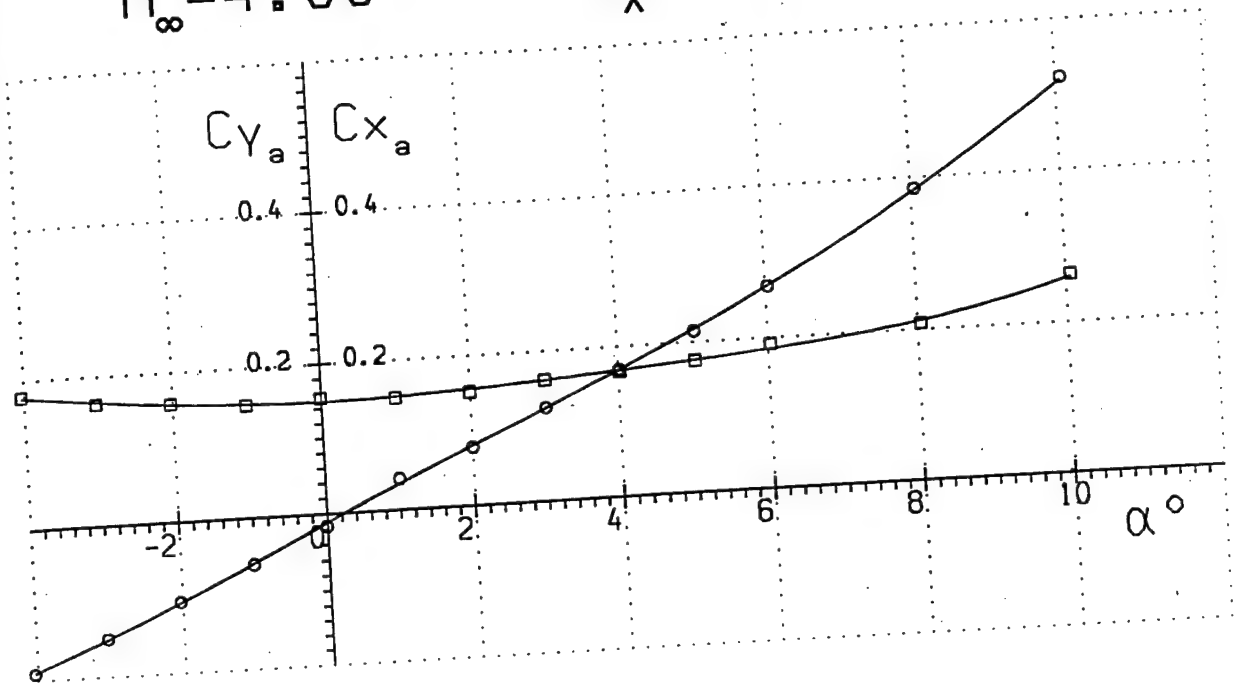

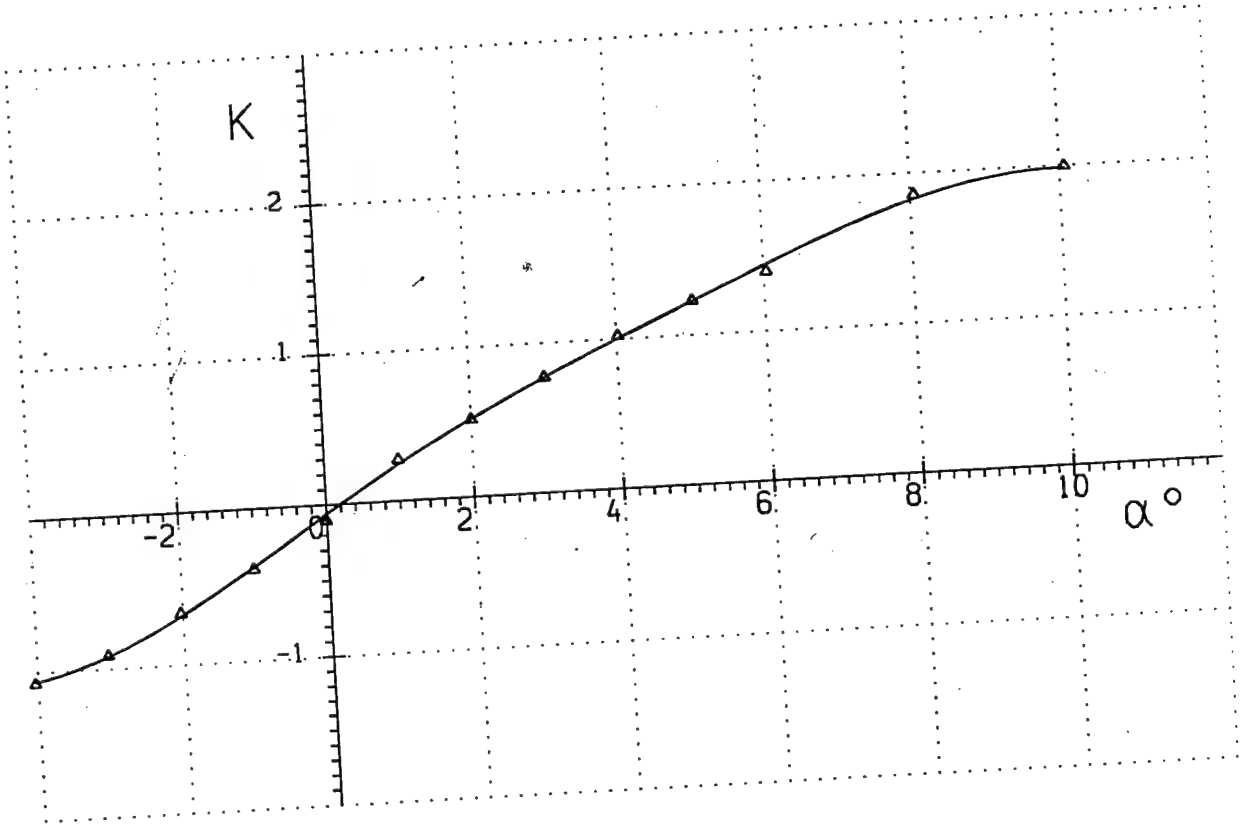

Cx_a

Cy_a

K

Run 1

Fig. 5

$M_\infty = 4.01$ $Re_x = 1.45 \cdot 10^6$

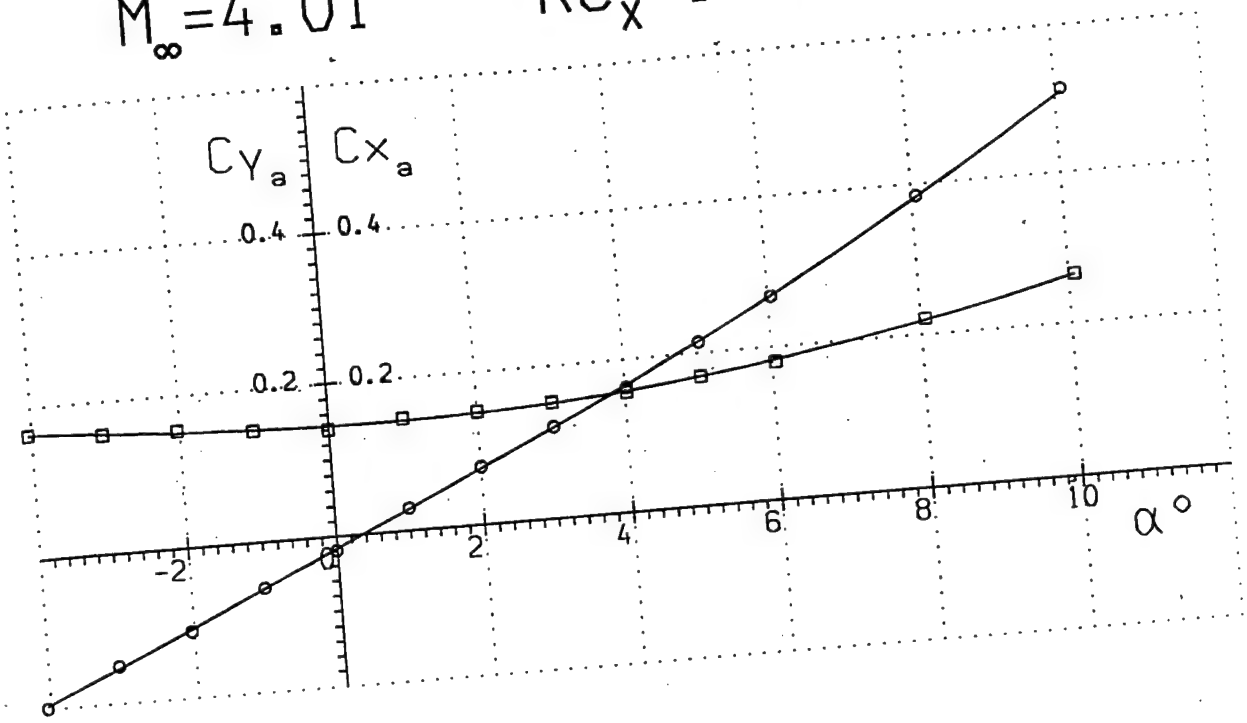

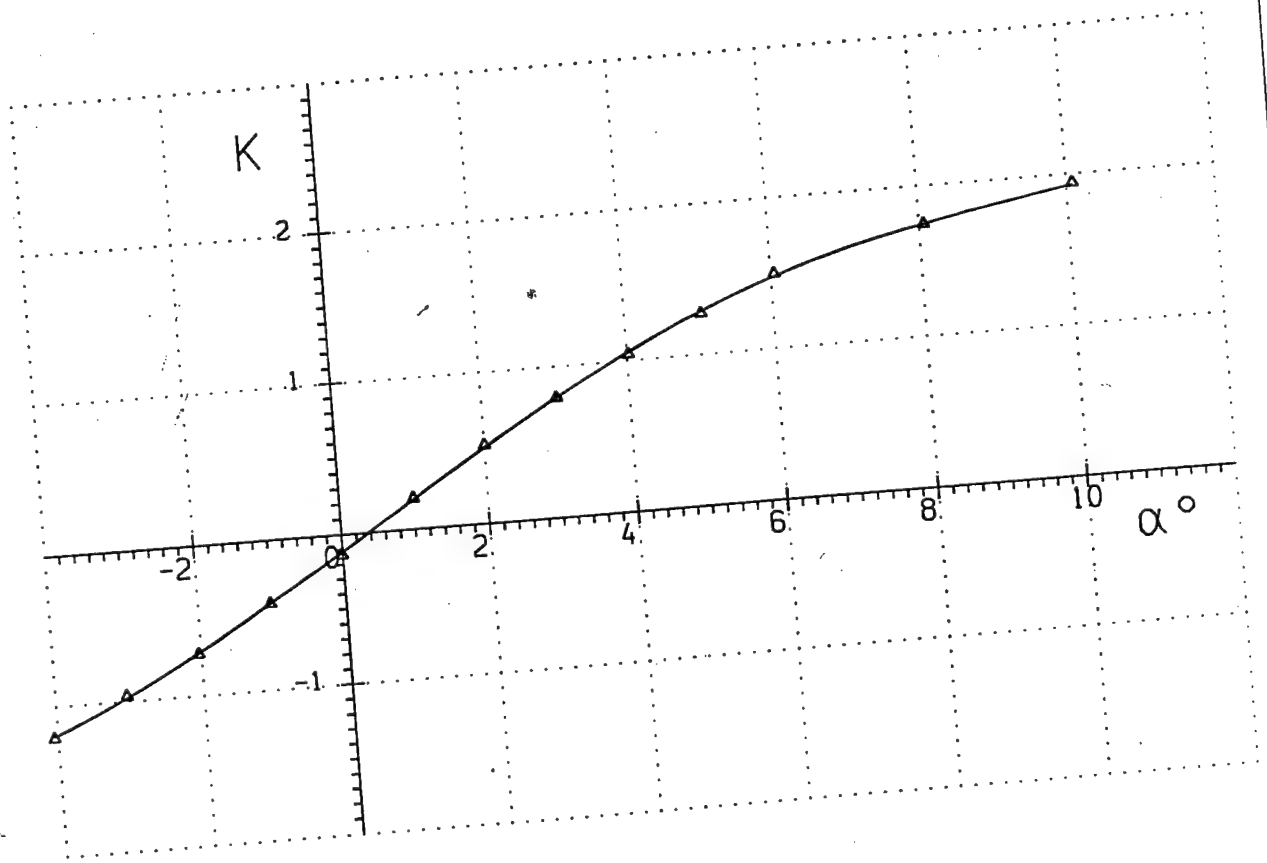

Cx_a

Cy_a

K

Run 2

Fig. 6

$M_\infty = 4.02$ $Re_x = 1.81 \cdot 10^6$

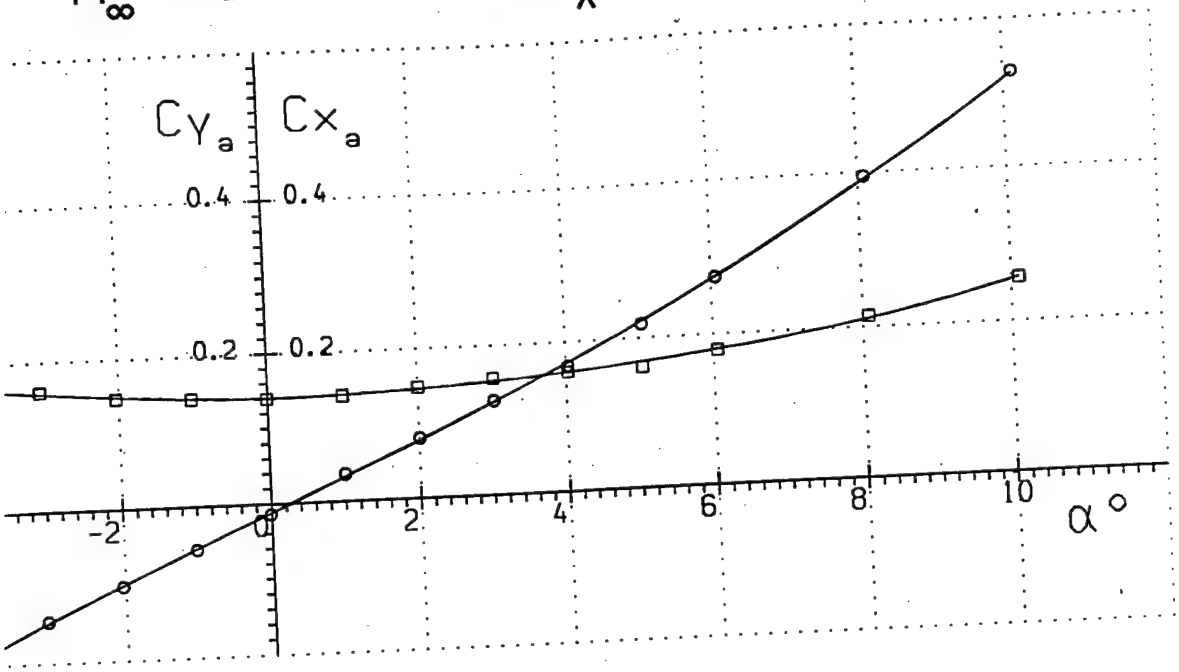

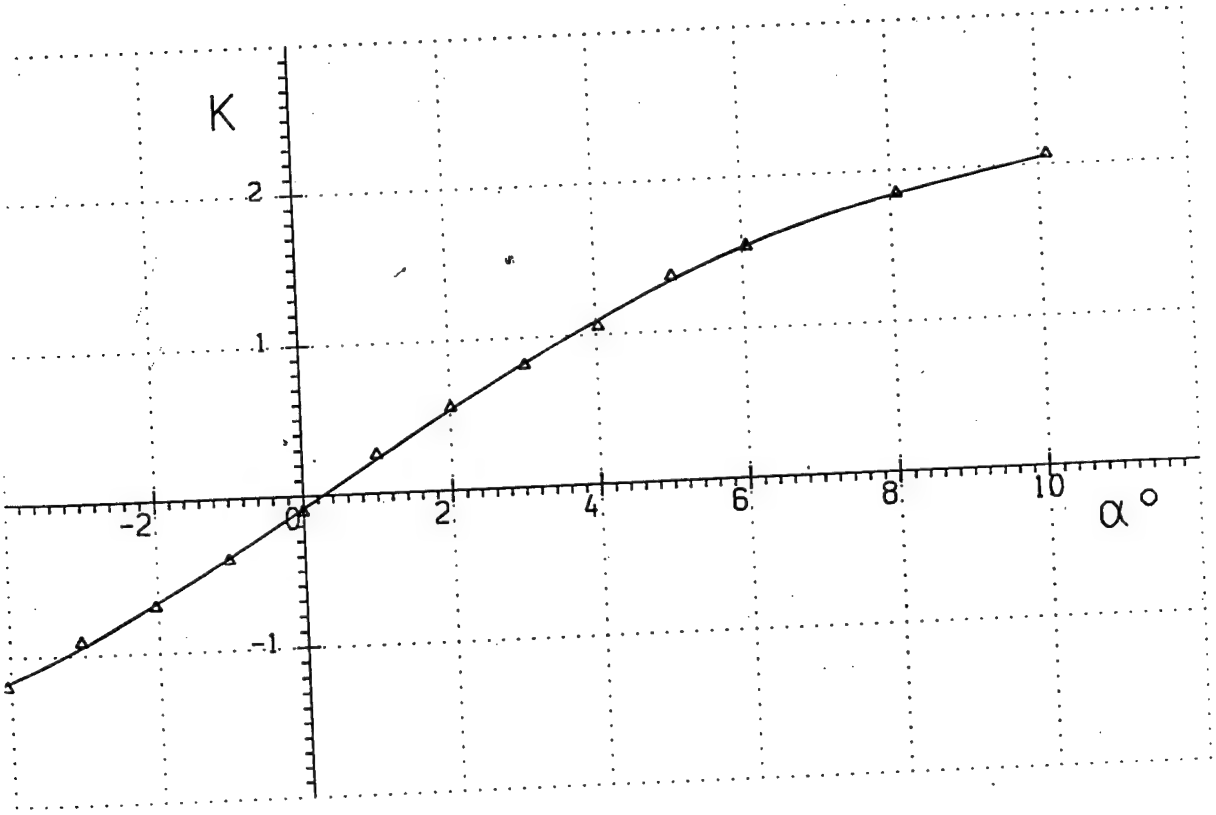

Cx_a

Cy_a

K

Run 3

$M_\infty = 4.03$ $Re_x = 2.34 \cdot 10^6$

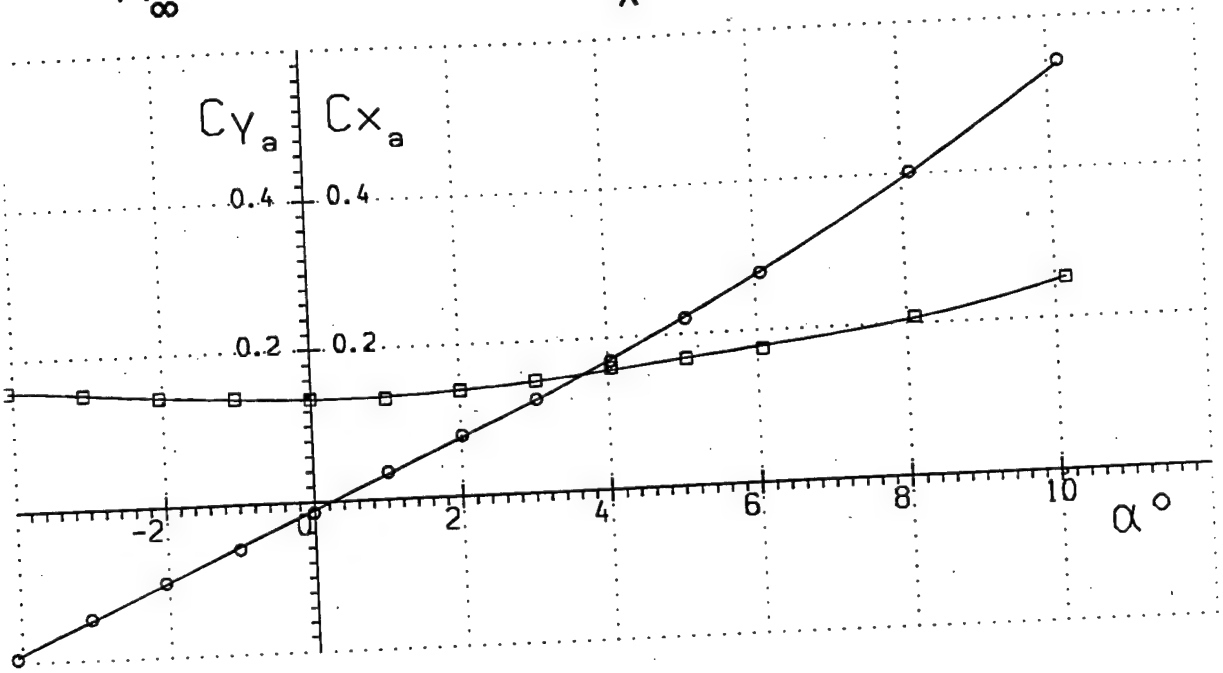

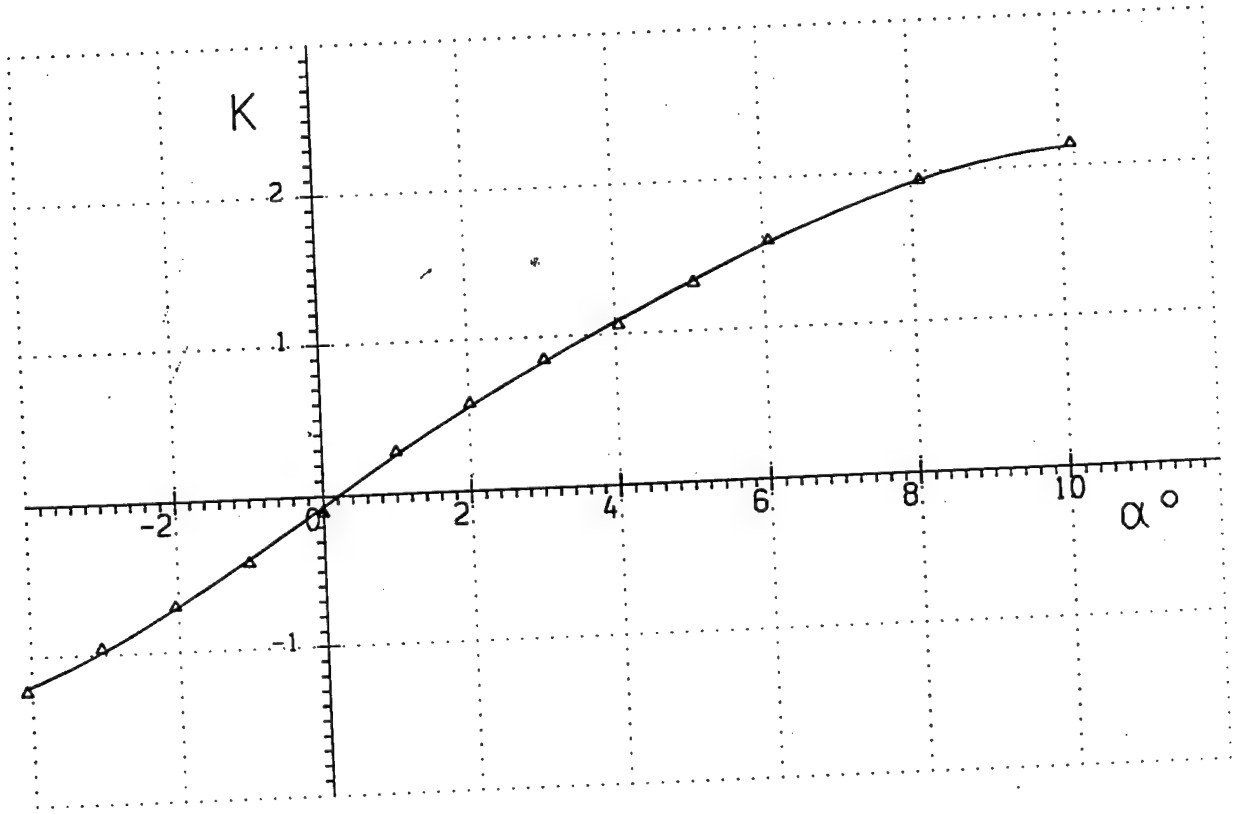

Cx_a

Cy_a

K

Run 4

Fig. 8

$M_\infty = 4.03$ $Re_x = 3.13 \cdot 10^6$

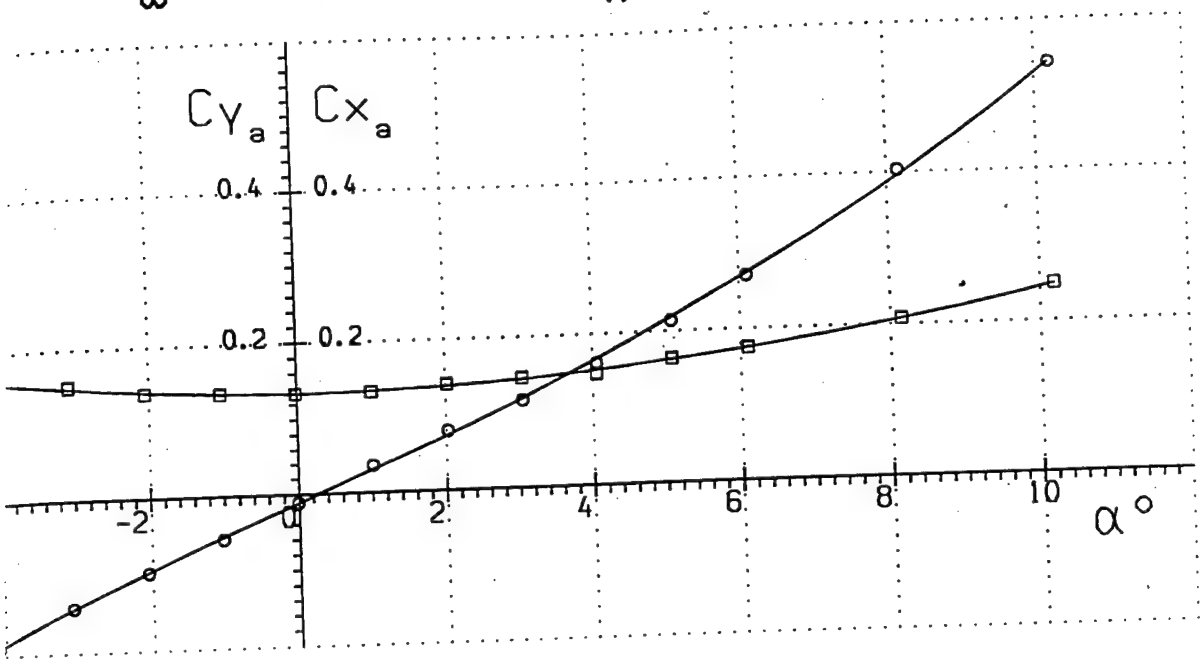

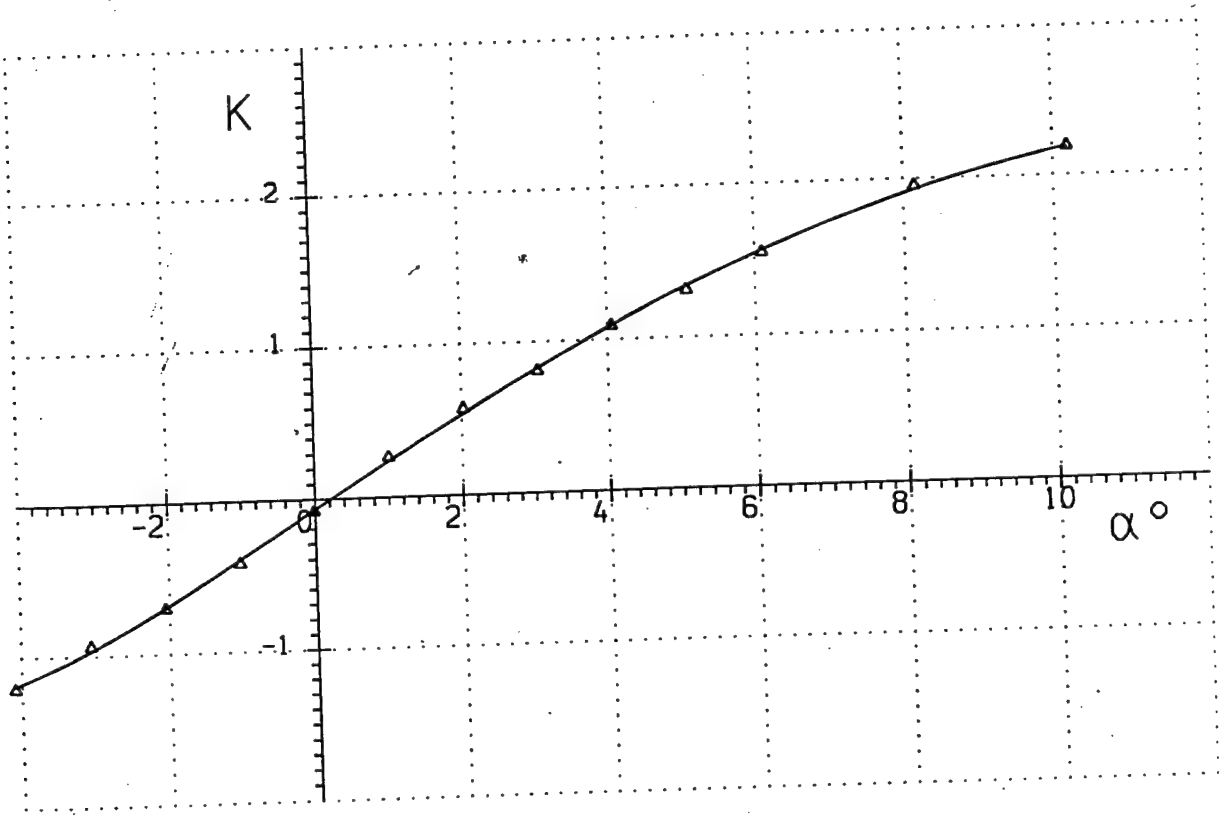

Cx_a
Cy_a
K

Run 5

Fig. 9

$M_\infty = 4.04$ $Re_x = 3.91 \cdot 10^6$

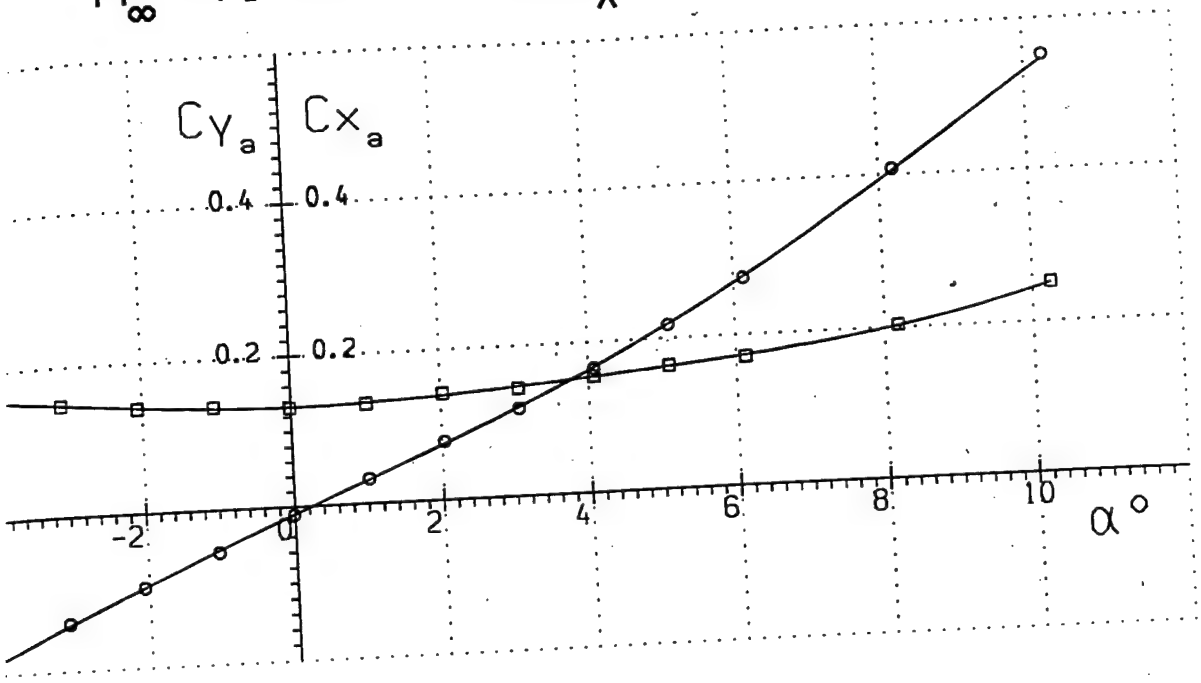

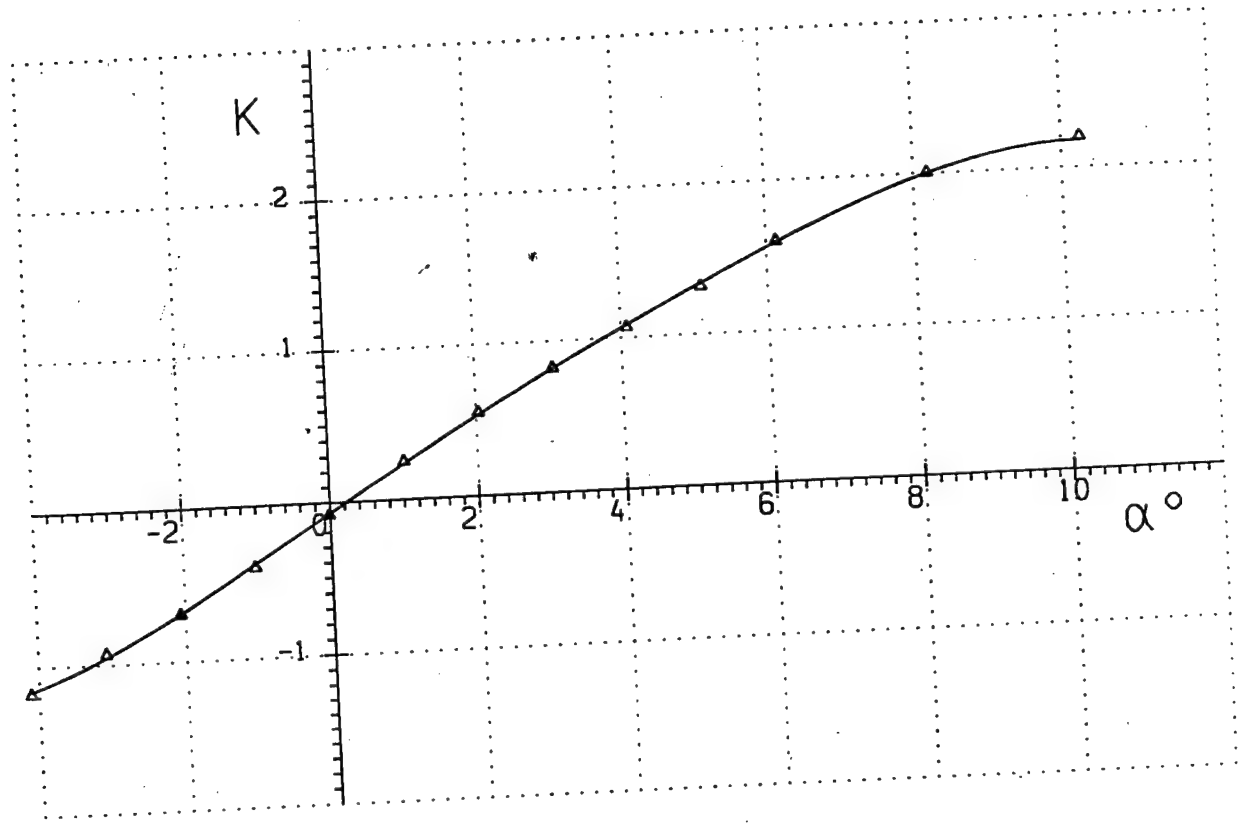

Cx_a
Cy_a
K

Run 6

Fig. 10

$M_\infty = 4.05$ $Re_x = 6.27 \cdot 10^6$

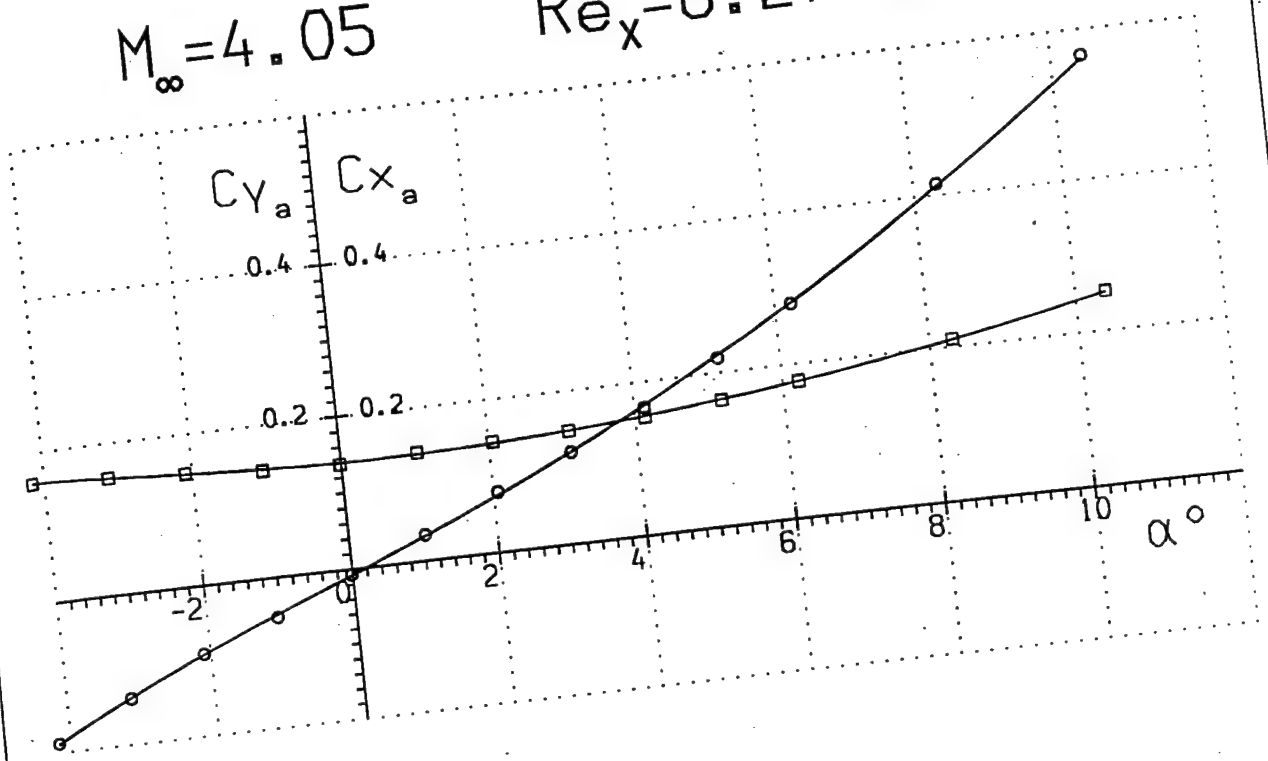

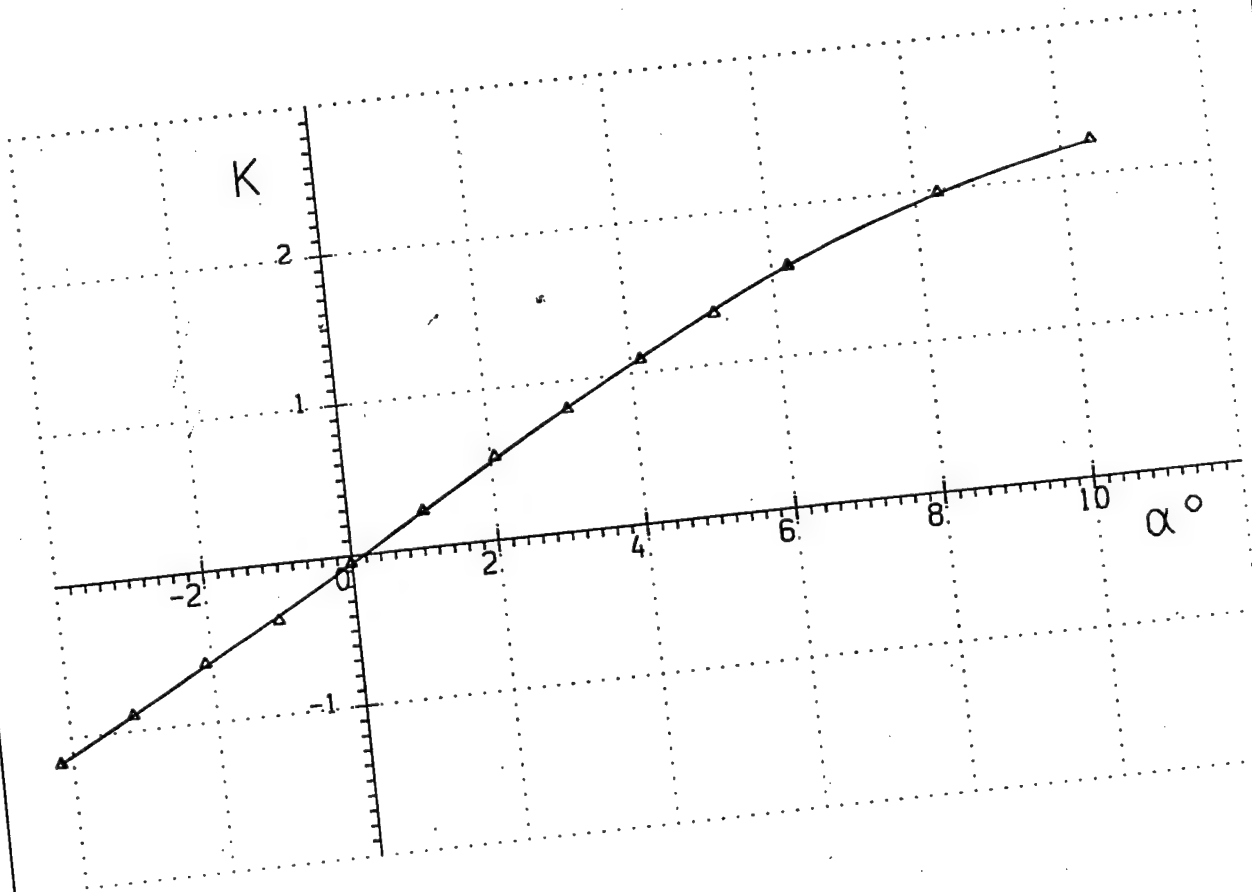

Cx_a
Cy_a
K

Run 7

Fig. 11

$M_\infty = 4.06$ $Re_x = 8.60 \cdot 10^6$

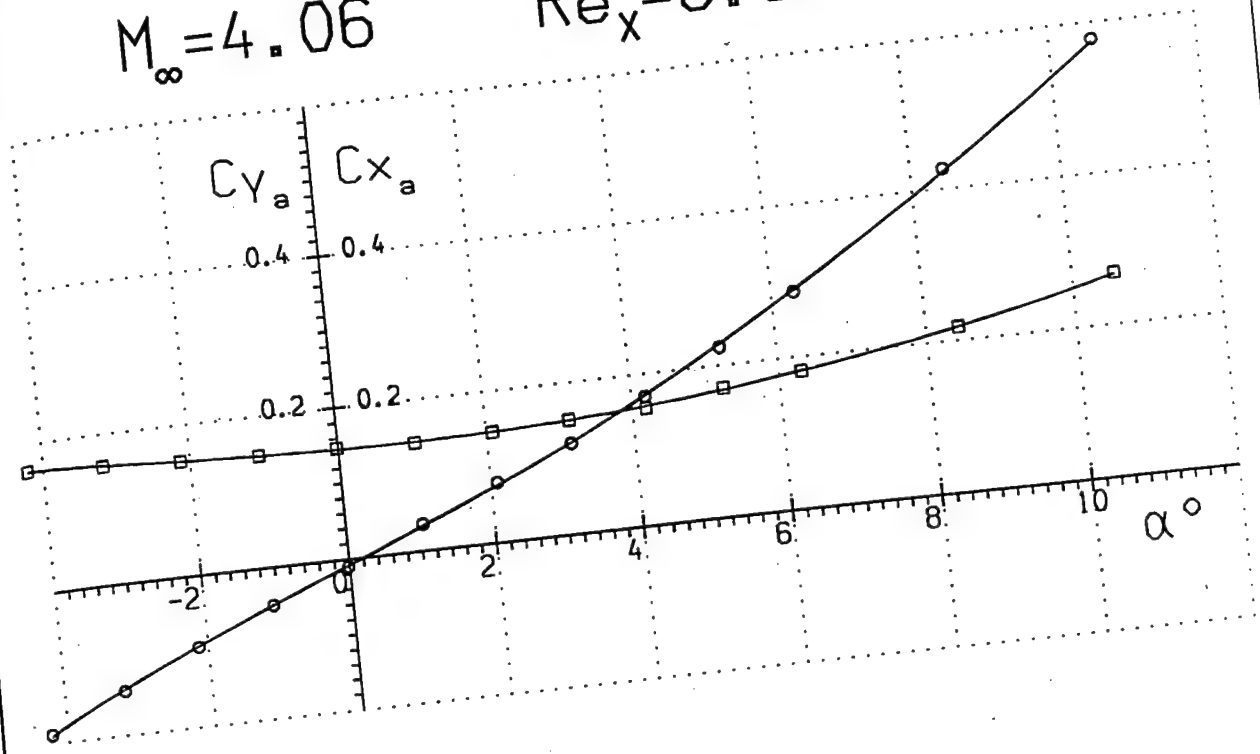

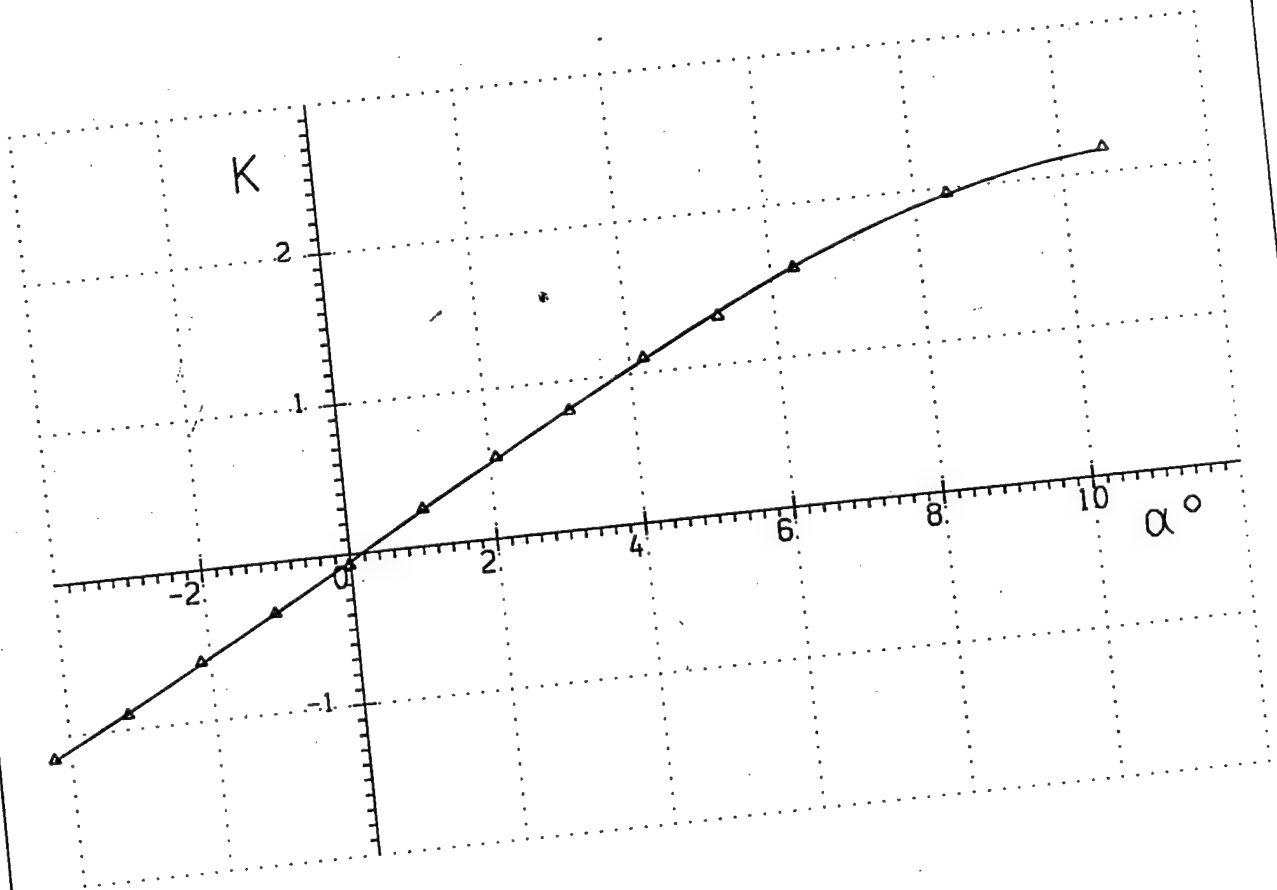

Cx_a

Cy_a

K

Run 8

Fig. 12

$M_\infty = 4.96$ $Re_x = .90 \cdot 10^6$

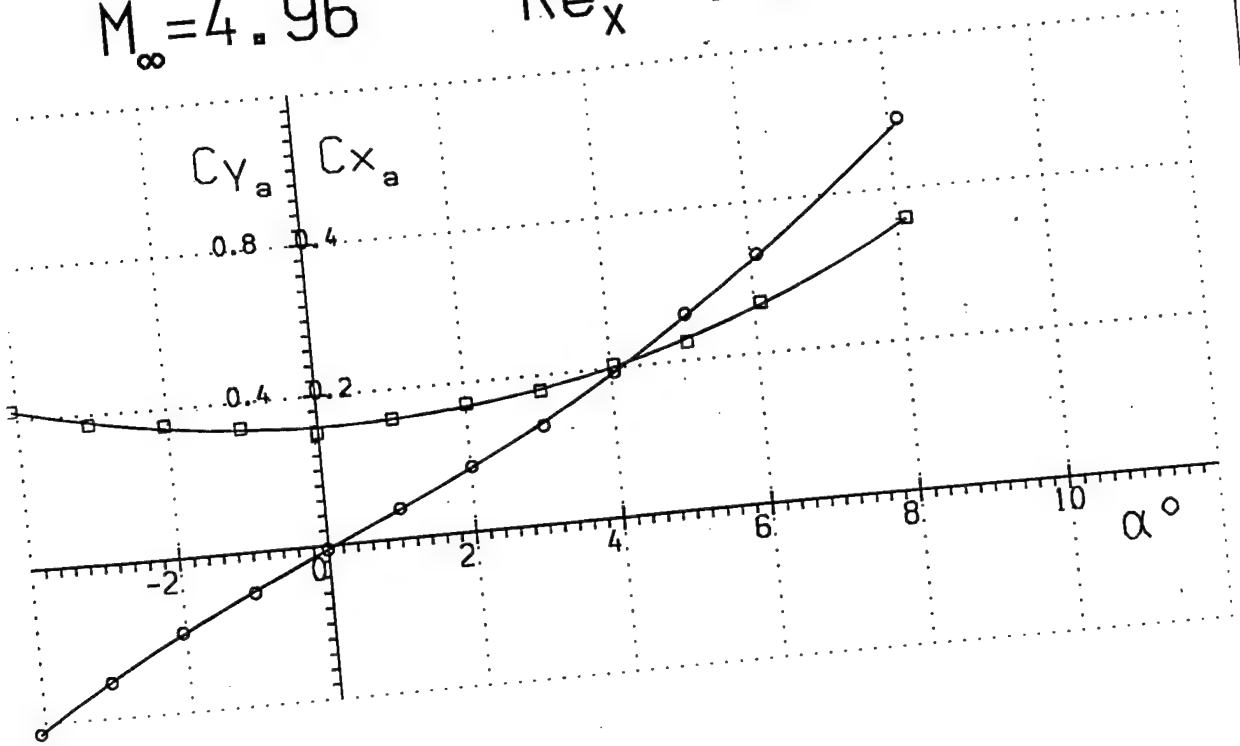

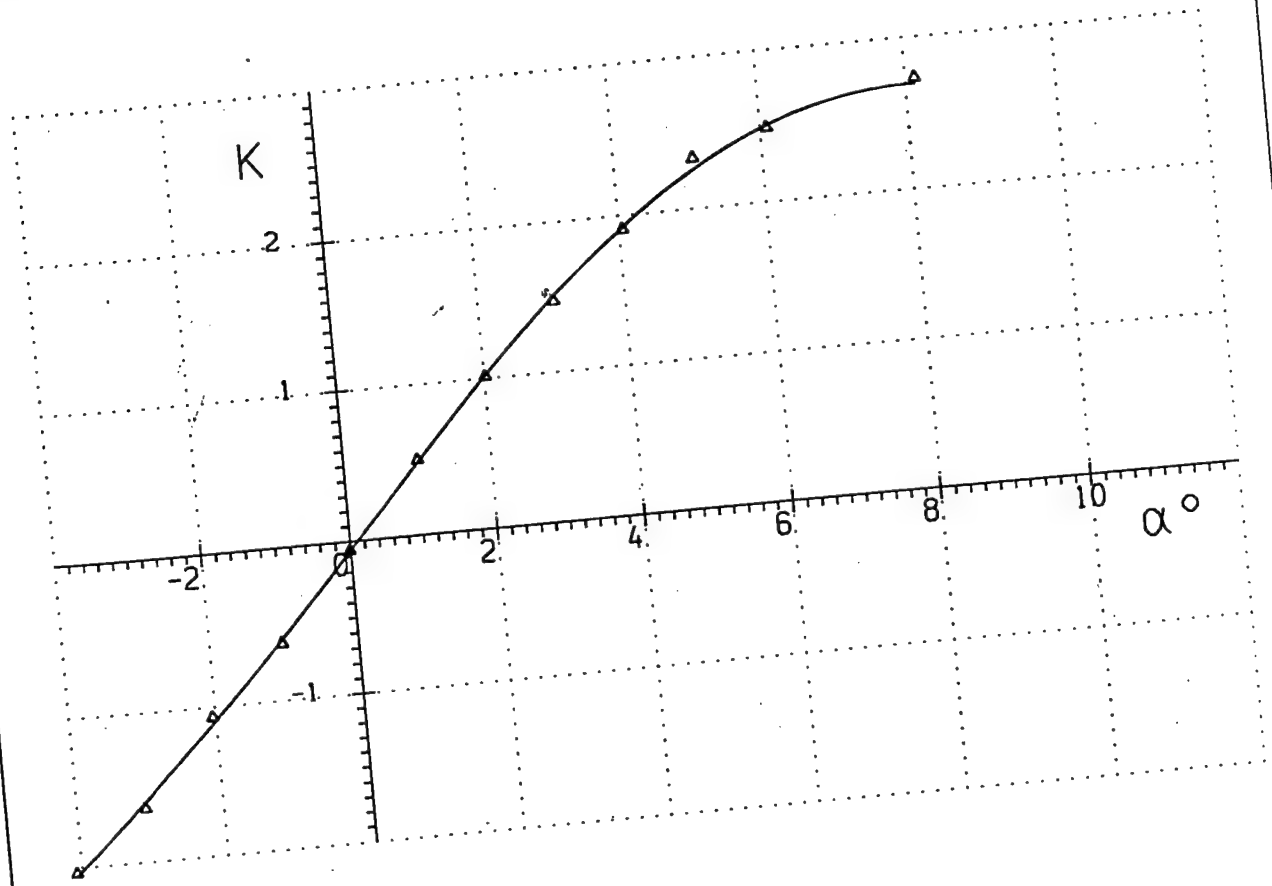

Cx_a

Cy_a

K

Run 9

Fig. 13

$M_\infty = 4.97$ $Re_x = 1.38 \cdot 10^6$

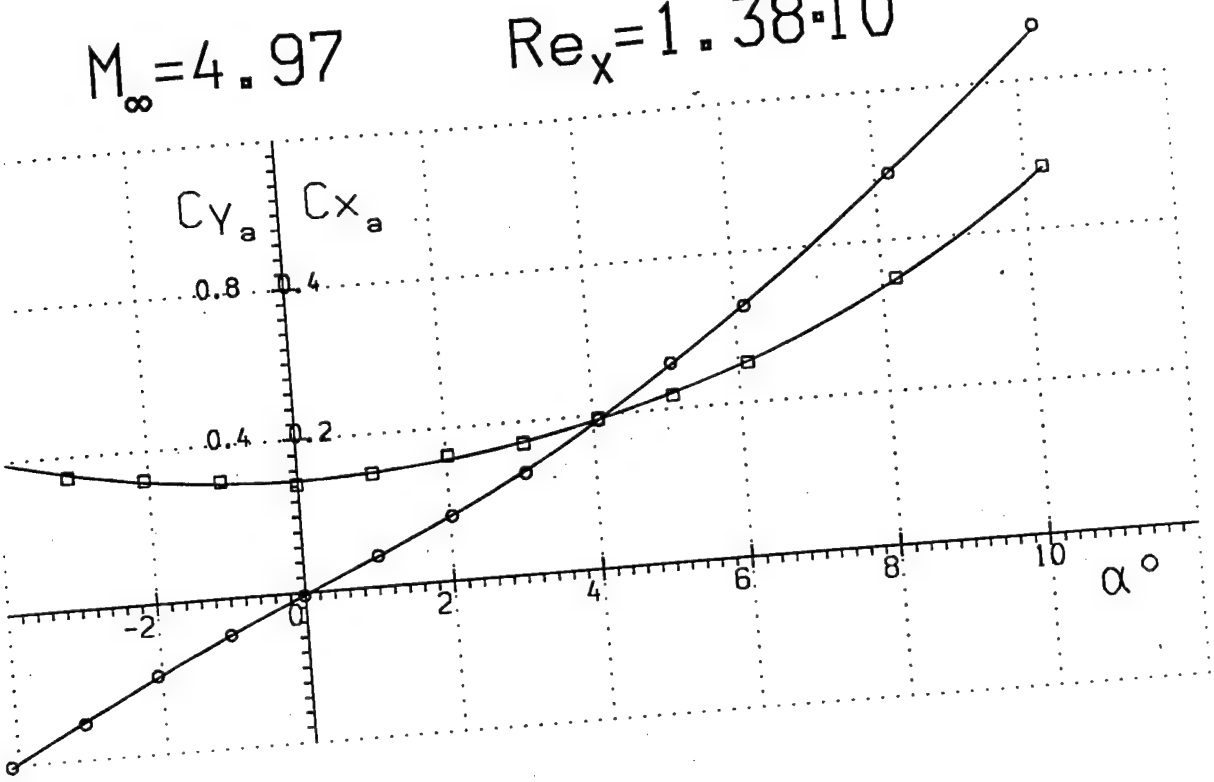

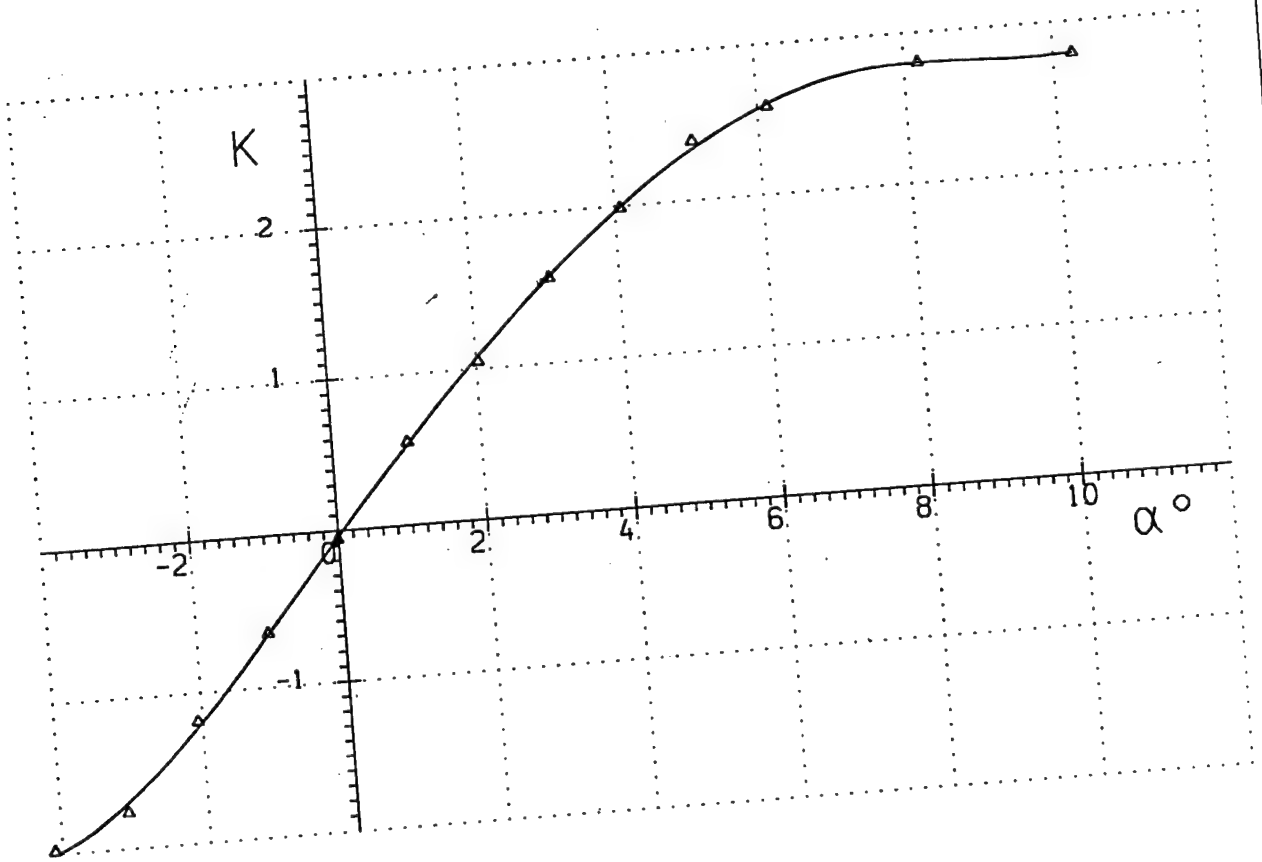

Cx_a
Cy_a
K

Run 10

Fig. 14

$M_\infty = 4.98$ $Re_x = 1.82 \cdot 10^6$

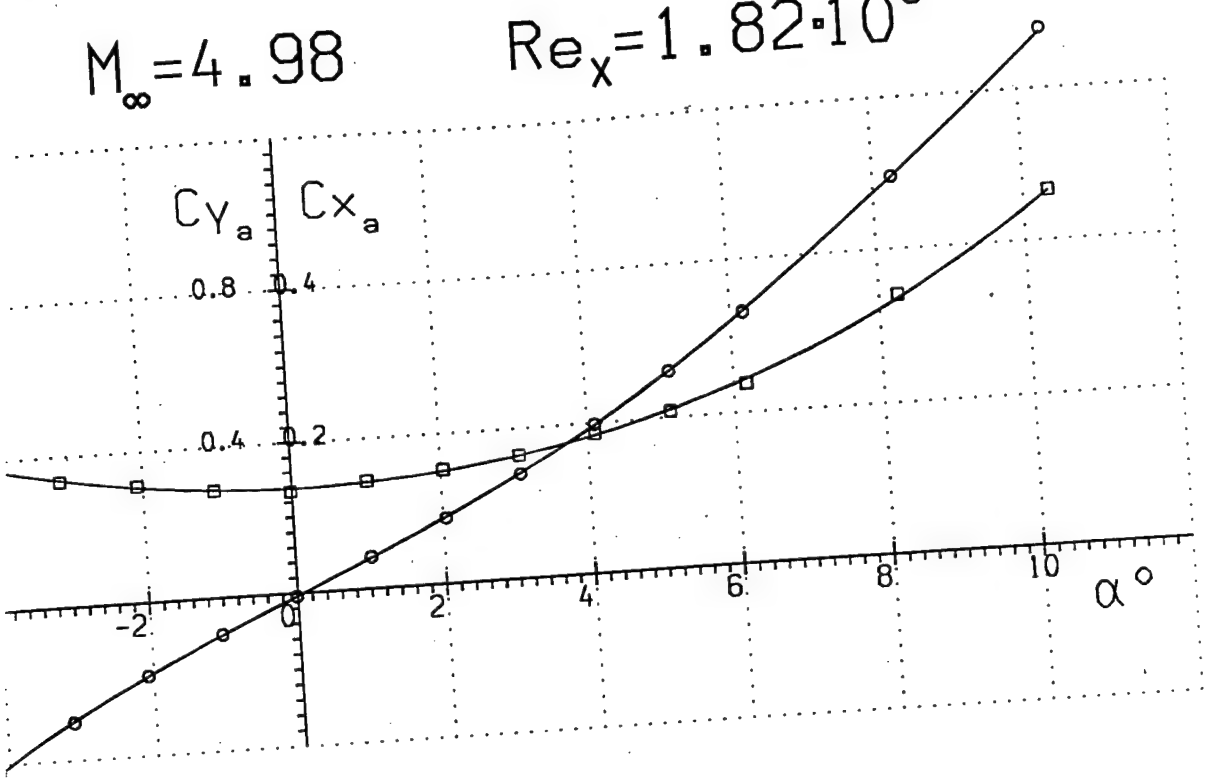

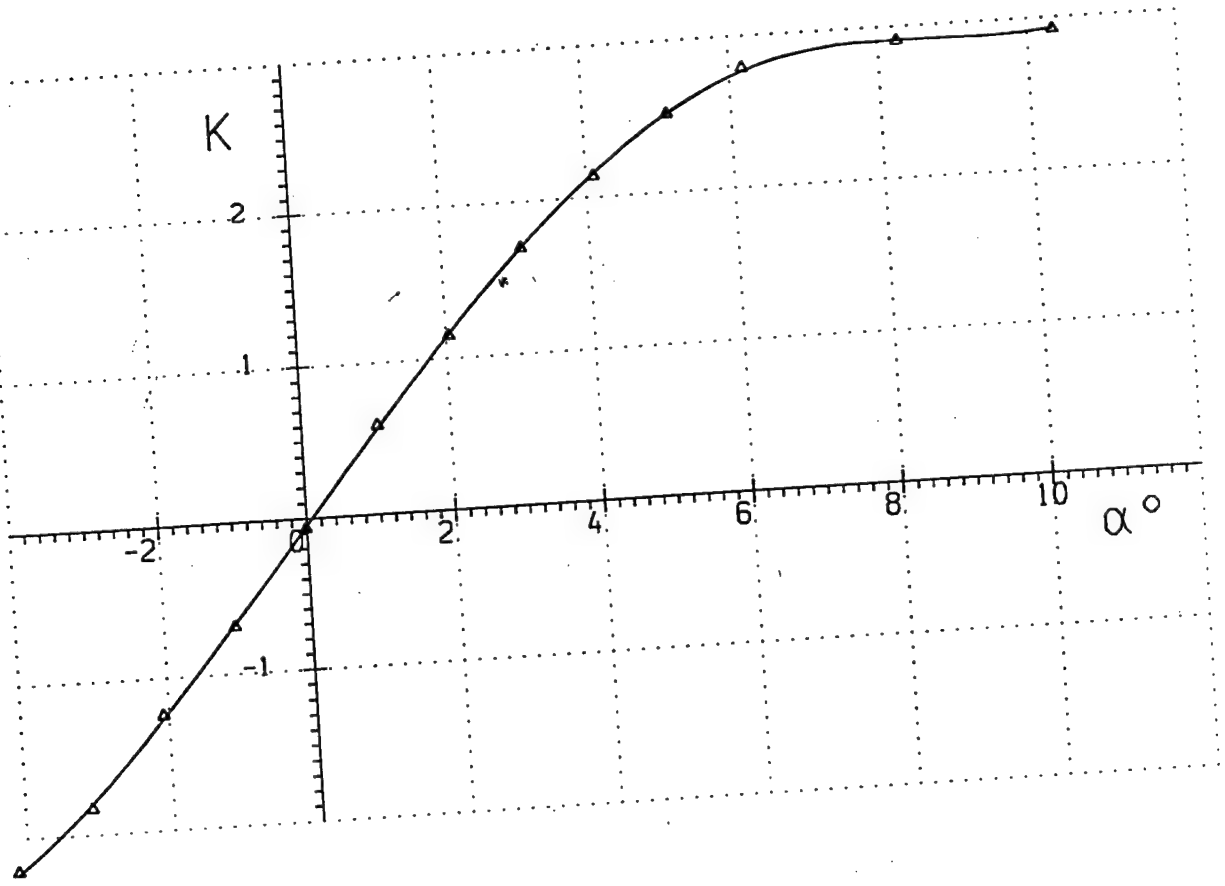

Cx_a
Cy_a
K

Run 11

Fig. 15

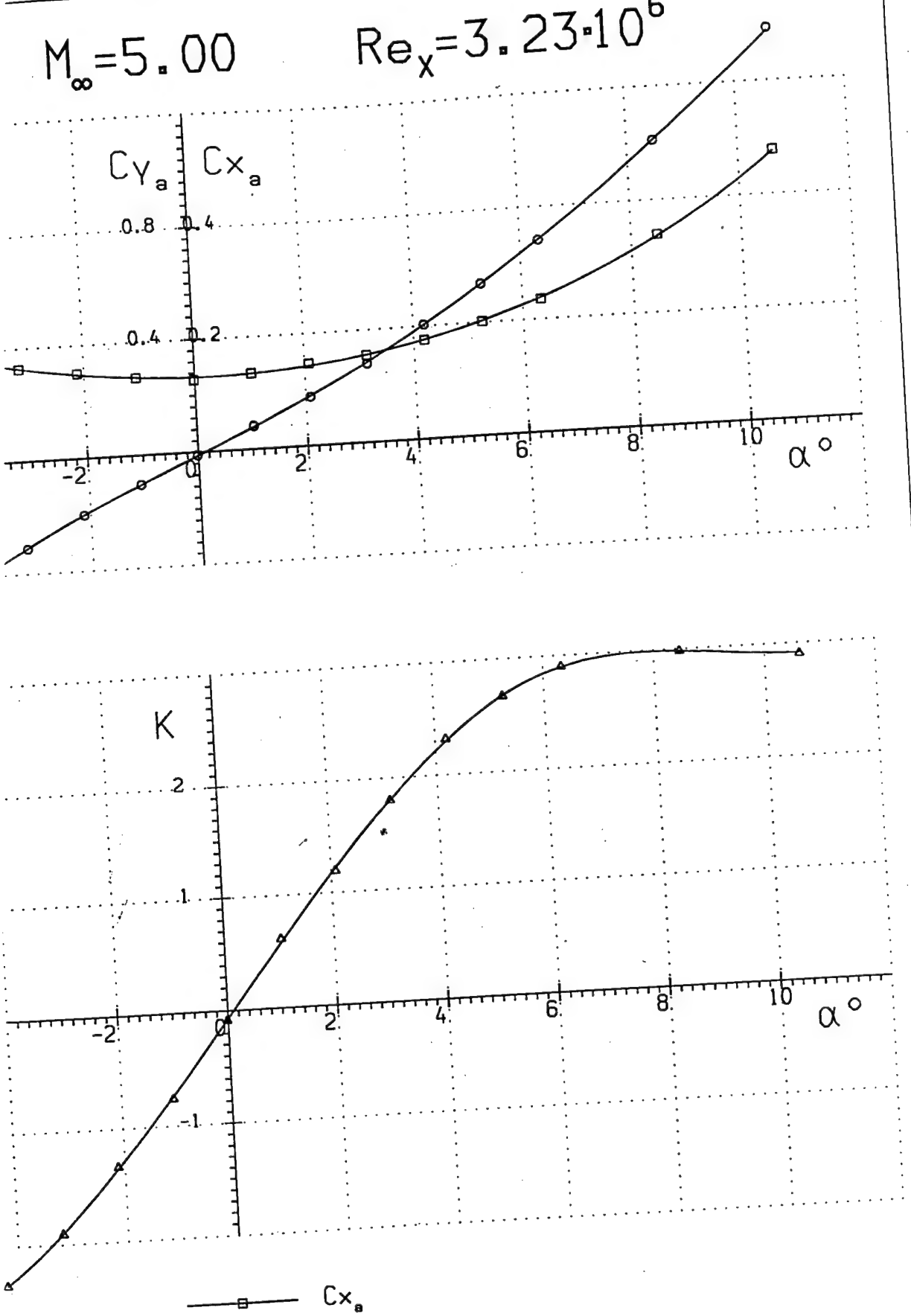
M_∞=5.00
Re_x=3.23·10^6
Cy_a
Cx_a
0.8
0.4
0.4
0.2
-2
0
2
4
6
8
10
α°
K
2
1
-1
Cx_a
Cy_a
K

Run 12

Fig. 16

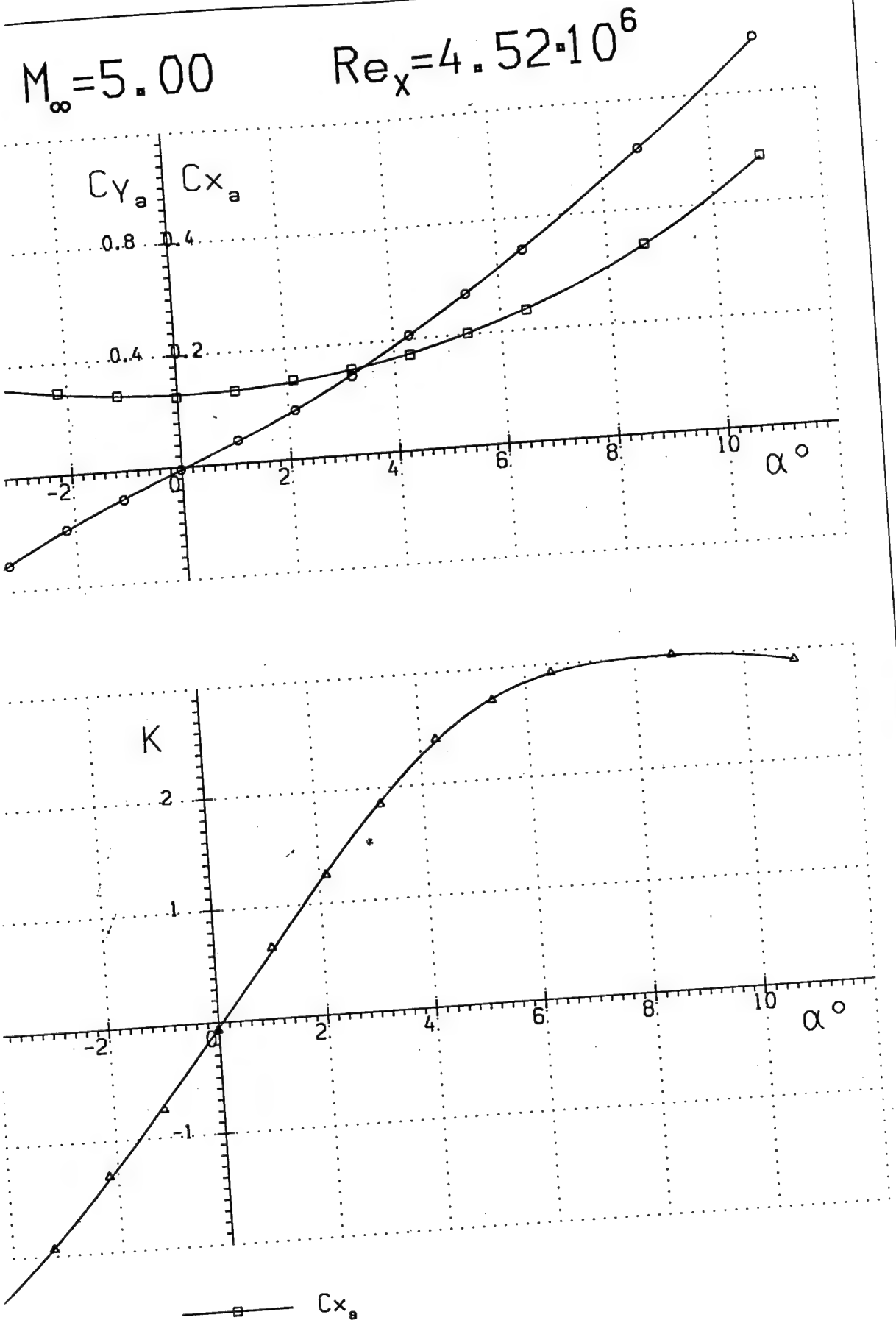
M_∞=5.00
Re_x=4.52·10^6
Cy_a
Cx_a
0.8
0.4
0.4
0.2
-2
0
2
4
6
8
10
α°
K
2
1
-1
Cx_a
Cy_a
K

Run 13

Fig. 17

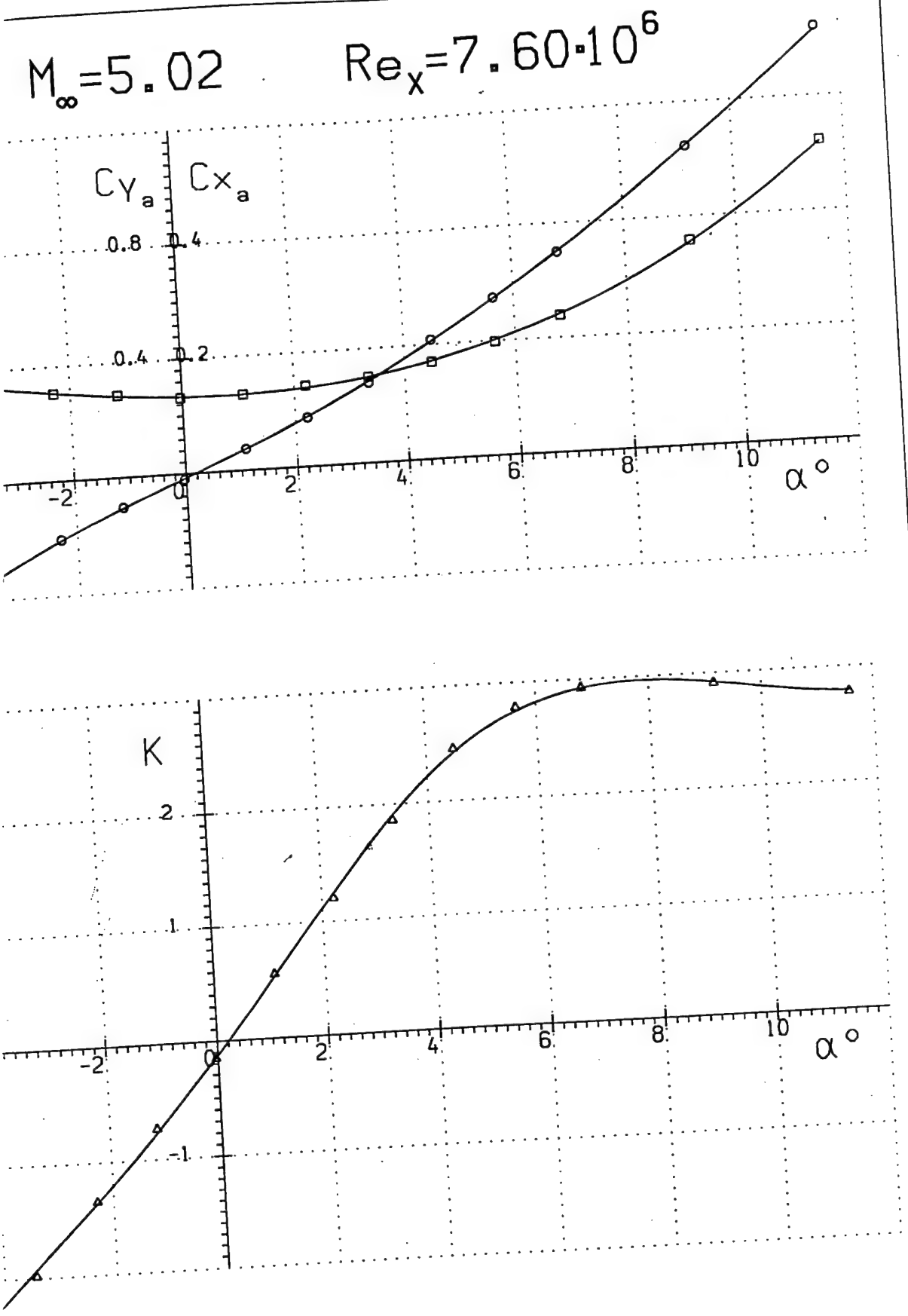
M_∞=5.02
Re_x=7.60·10^6
Cy_a
Cx_a
0.8
0.4
0.4
0.2
-2
0
2
4
6
8
10
α°
K
2
1
-1
-2
0
2
4
6
8
10
α°
Cx_a
Cy_a
K

Run 14

Fig. 18

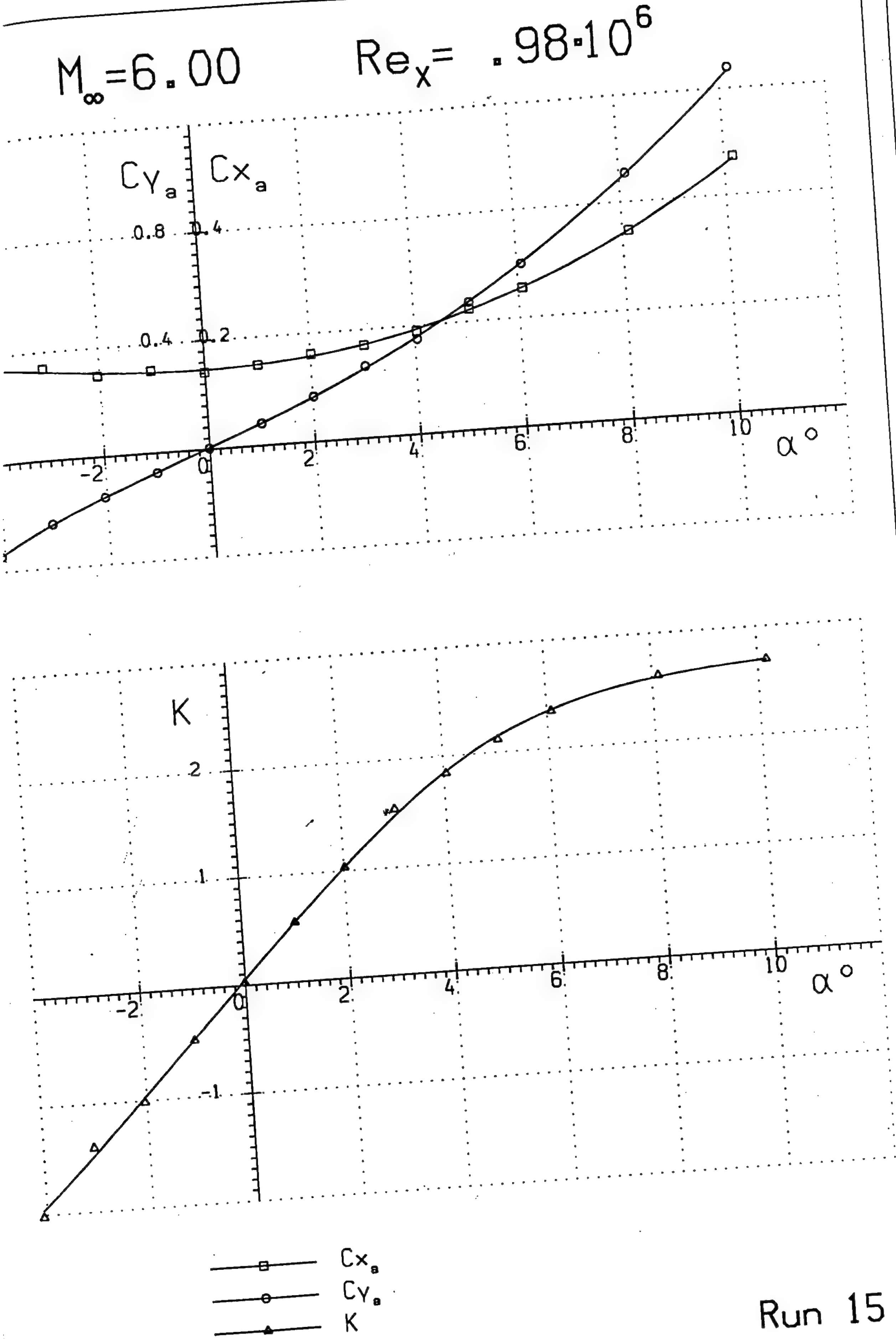

M∞=6.00
Rex= .98·10^6
Cya
Cxa
0.8
0.4
0.4
0.2
-2
0
2
4
6
8
10
α°
K
2
1
-1
-2
0
2
4
6
8
10
α°
Cxa
Cya
K

Run 15

Fig. 19

$M_\infty = 6.05$ $Re_x = 1.85 \cdot 10^6$

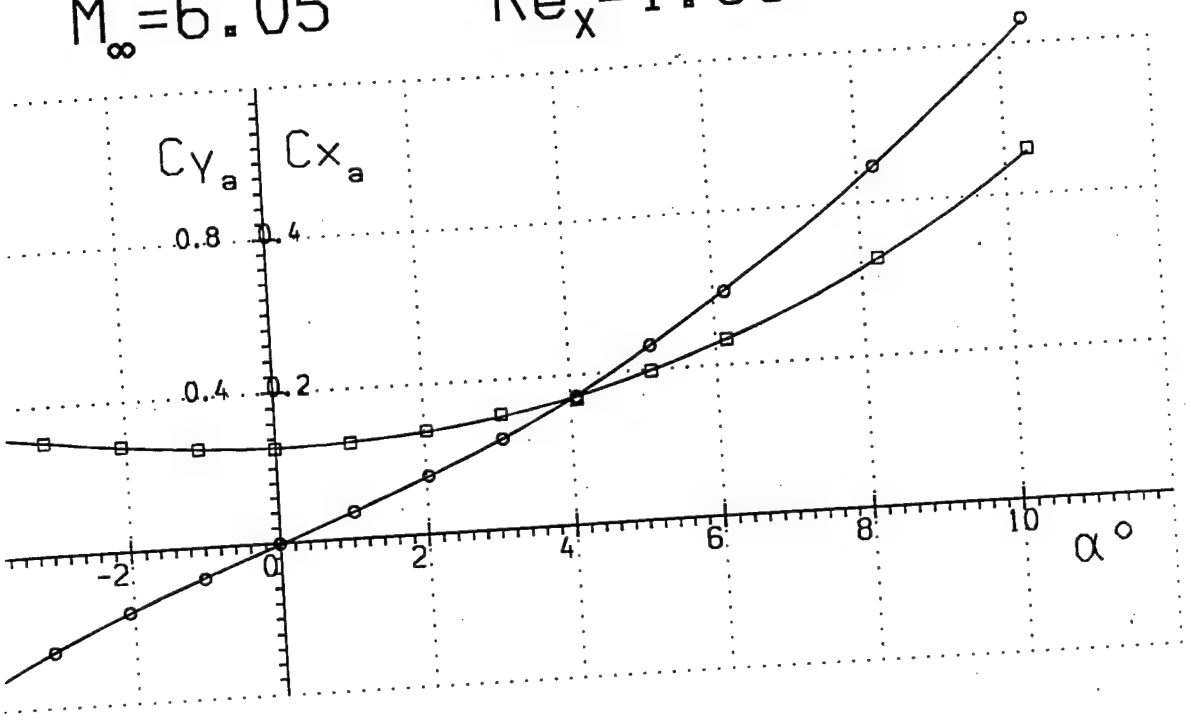

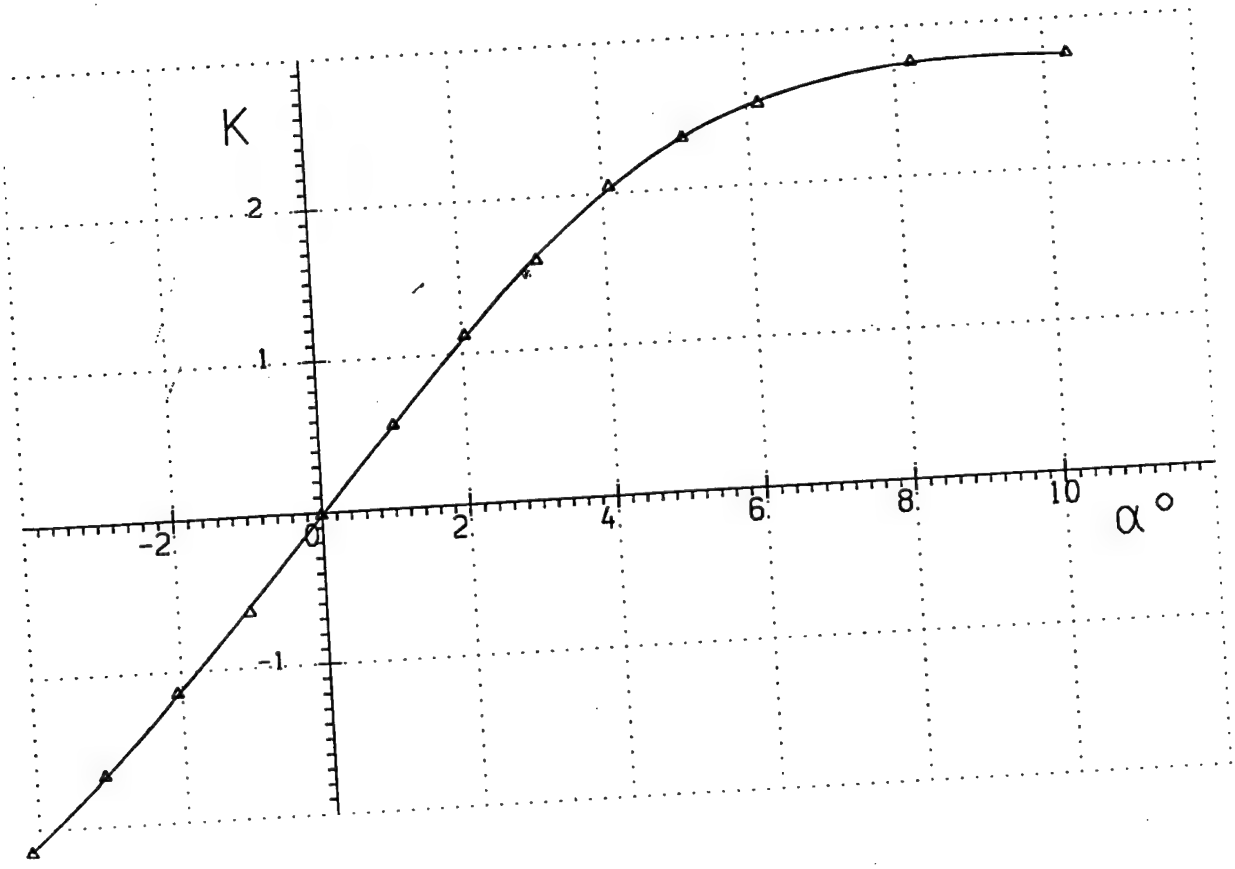

Cx_a

Cy_a

K

Run 16

Fig. 20

$M_\infty = 6.08$ $Re_x = 2.99 \cdot 10^6$

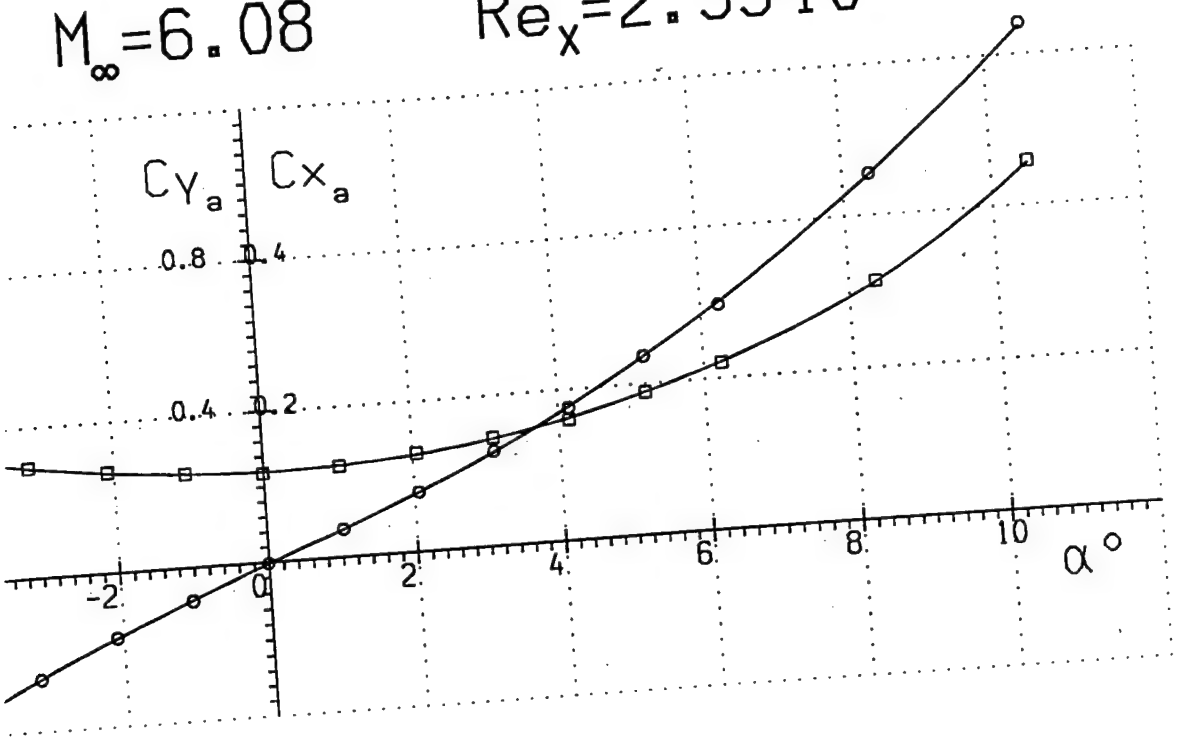

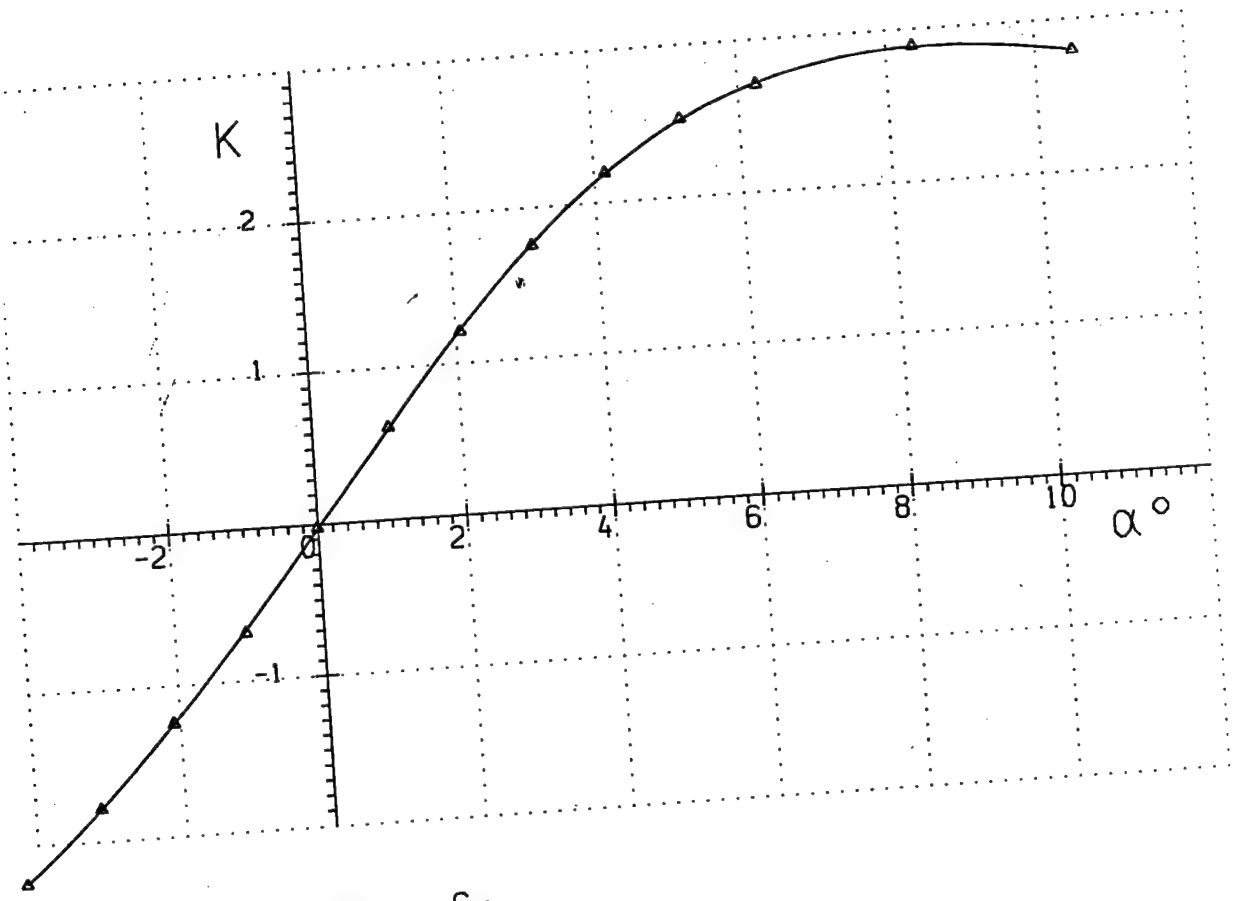

Cx_a
Cy_a
K

Run 17

Fig. 21

$M_\infty = 6.96$ $Re_x = 1.69 \cdot 10^6$

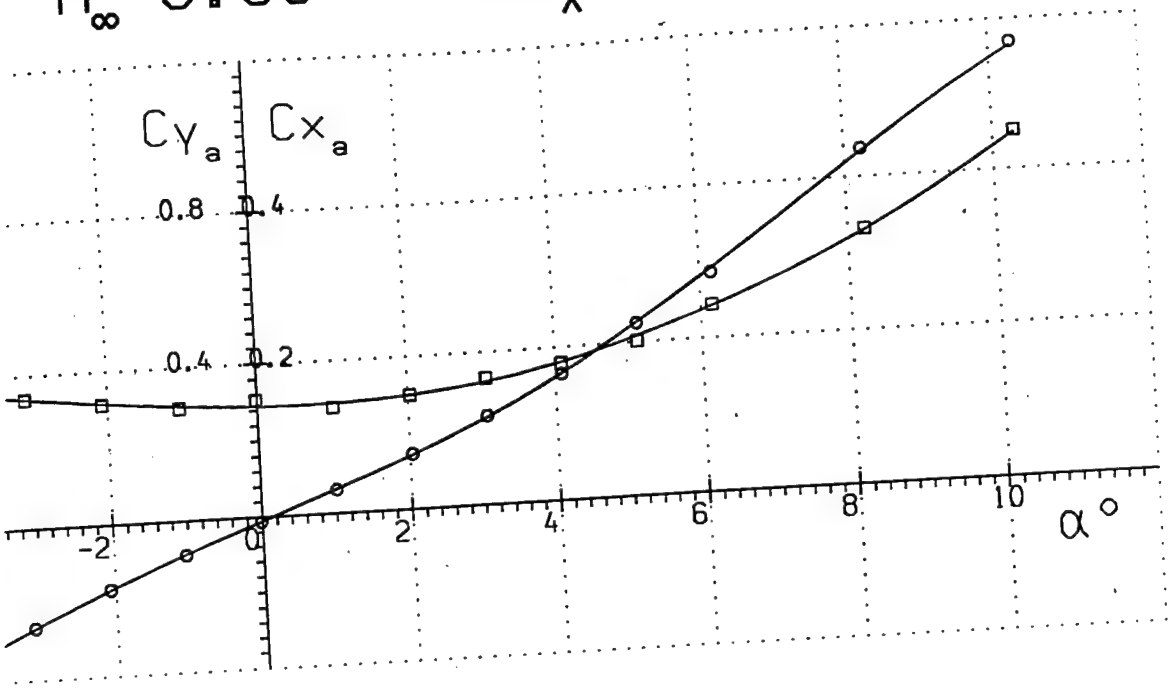

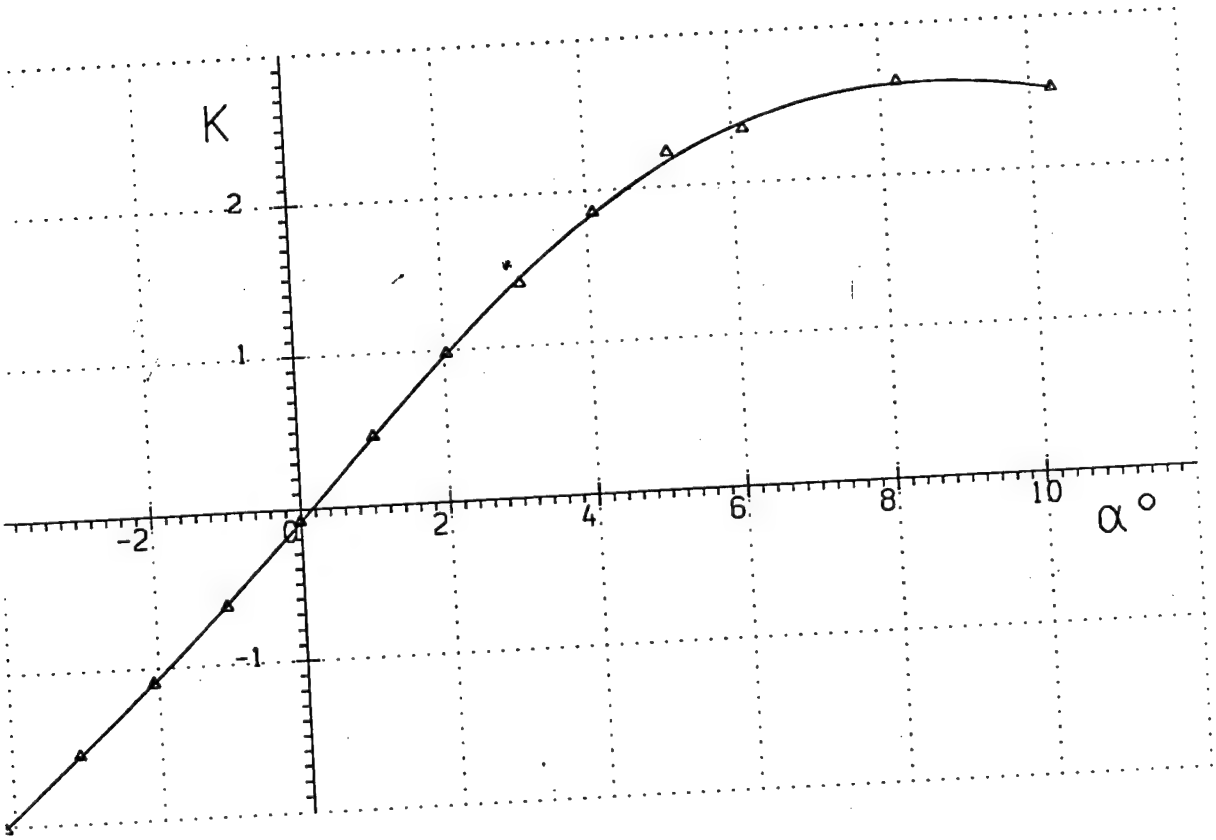

Cx_a

Cy_a

K

Run 18

Fig. 22

$M_\infty = 7.03$ $Re_x = 2.27 \cdot 10^6$

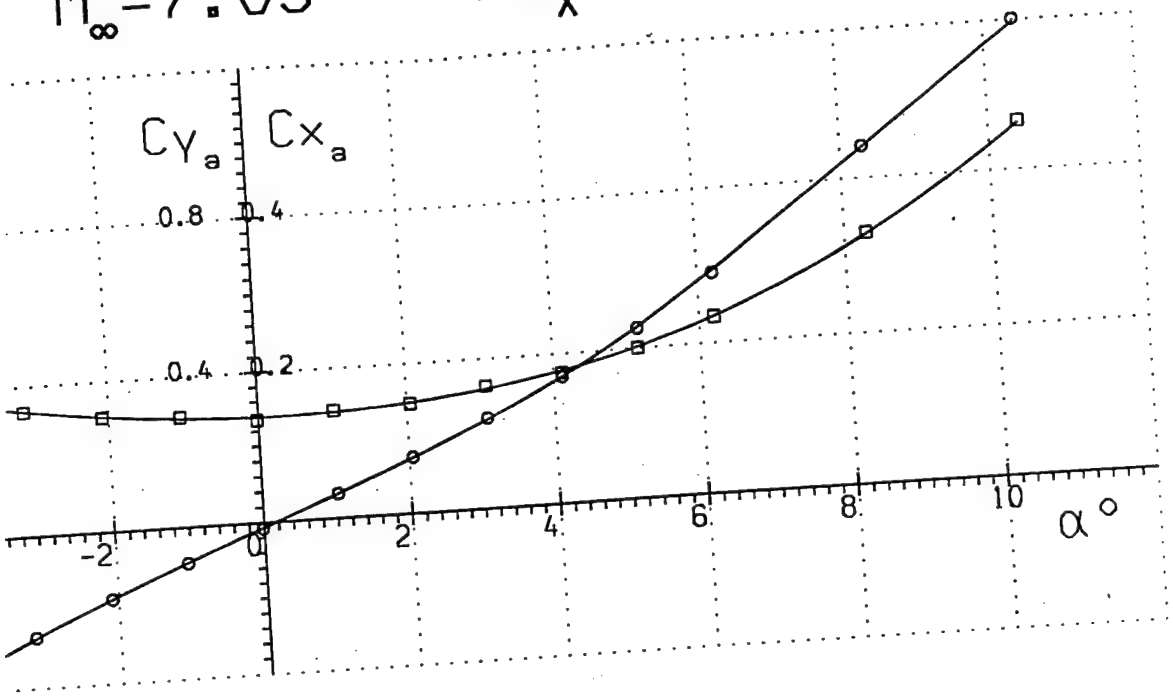

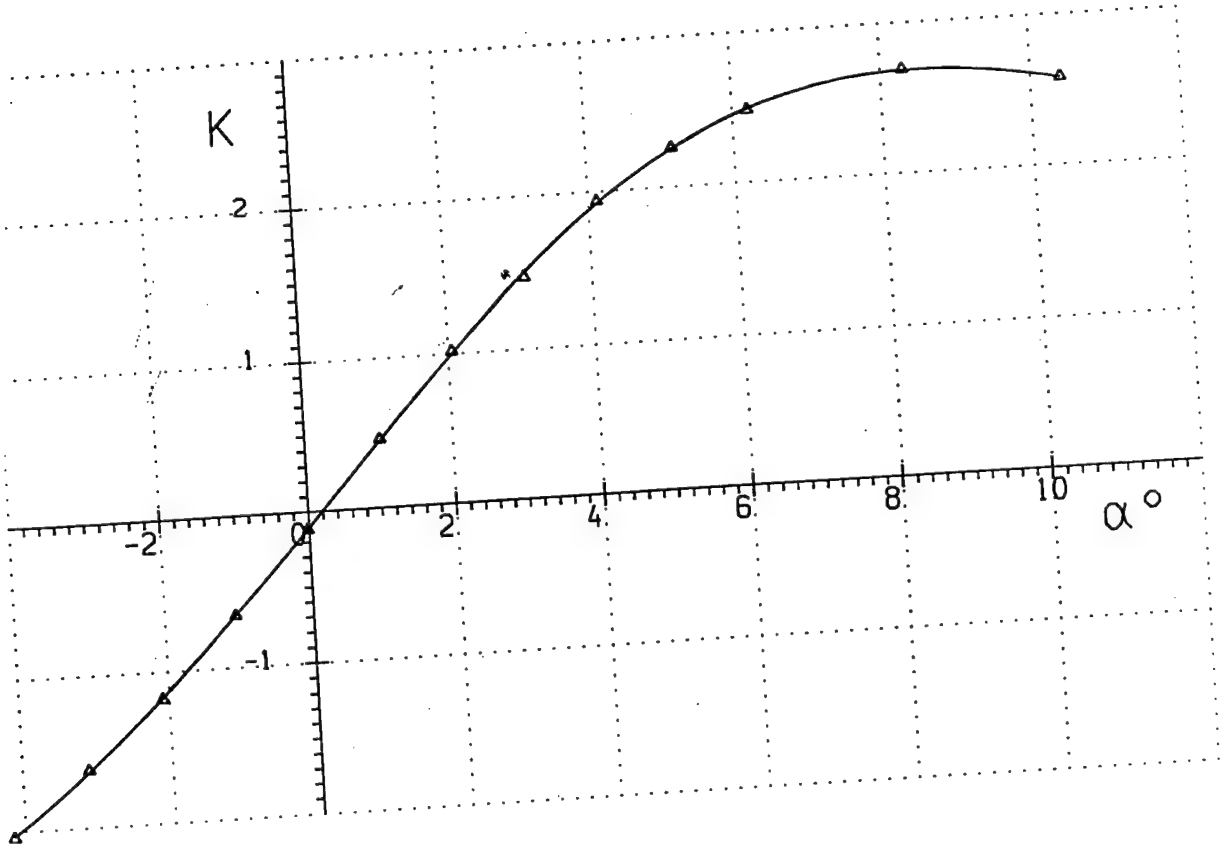

Cx_a
Cy_a
K

Run 19

Fig. 23

$M_\infty = 7.05$ $Re_x = 2.74 \cdot 10^6$

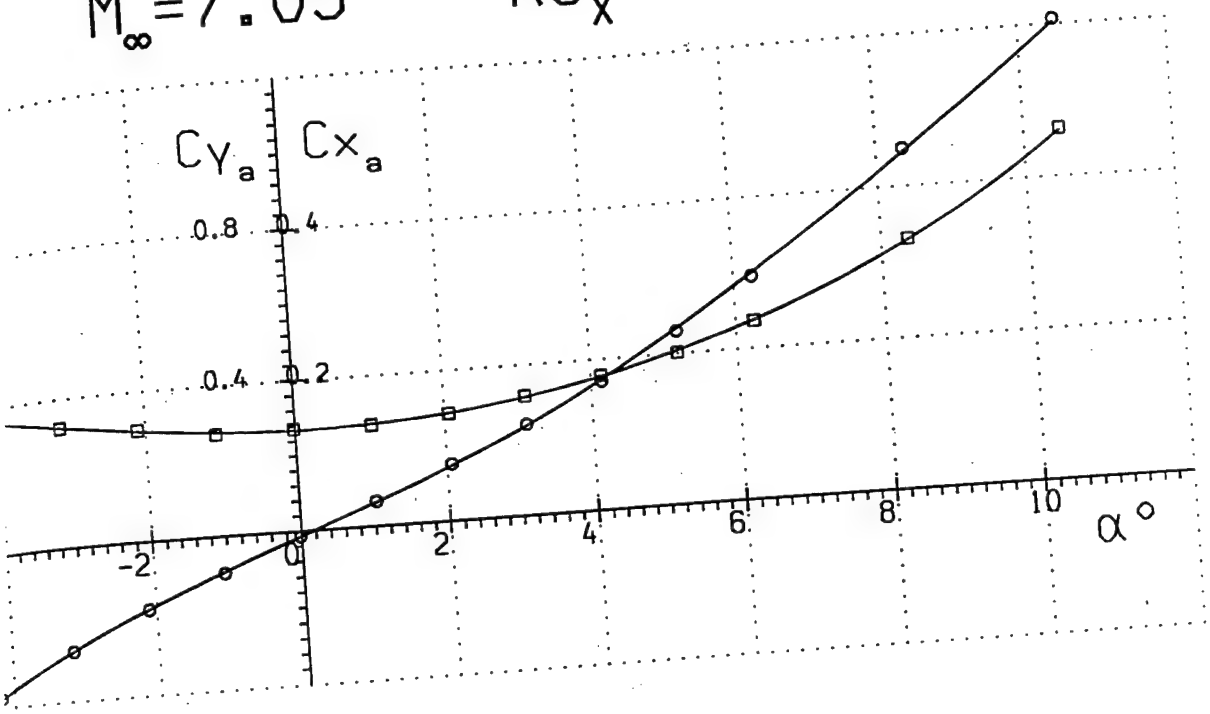

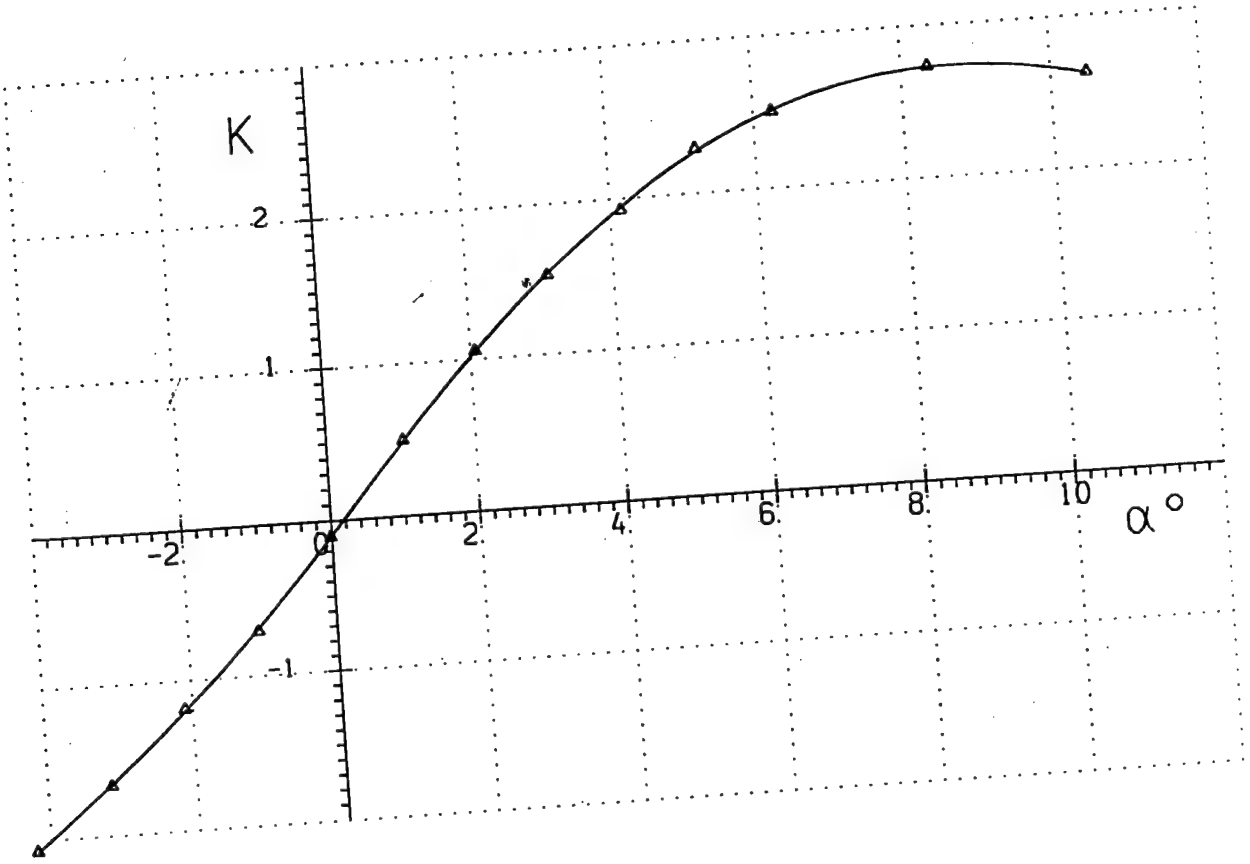

Cx_a

Cy_a

K

Run 20

Fig. 24

$M_\infty = 7.07$ $Re_x = 4.39 \cdot 10^6$

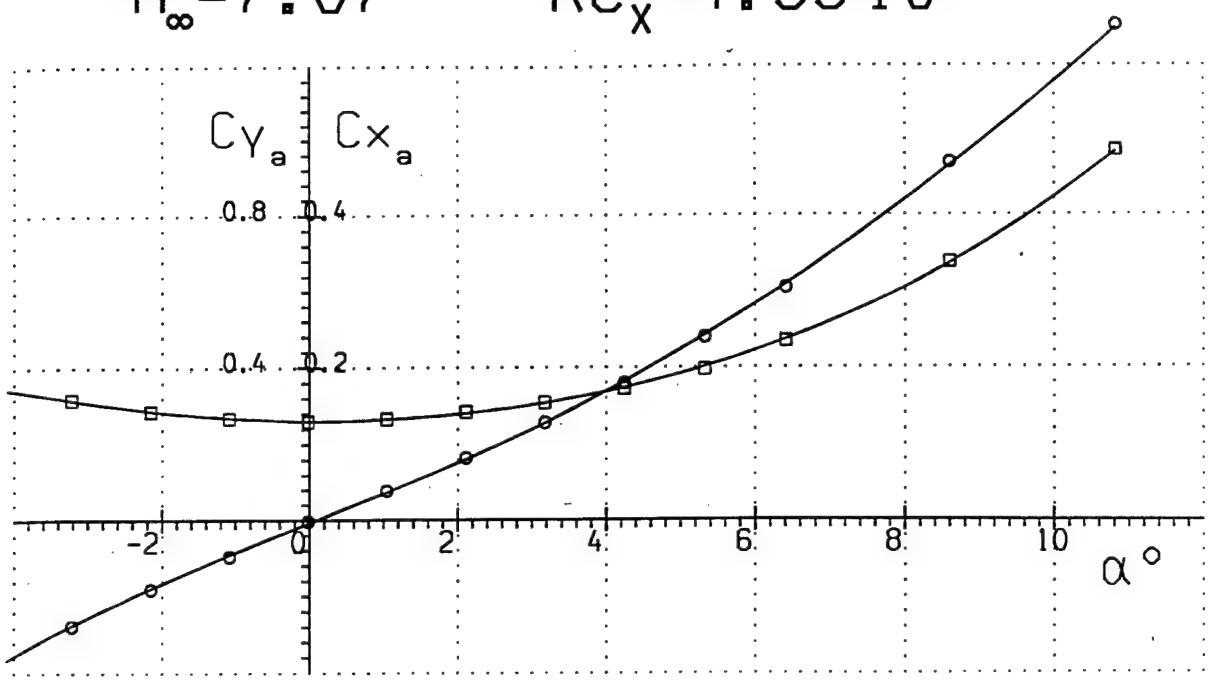

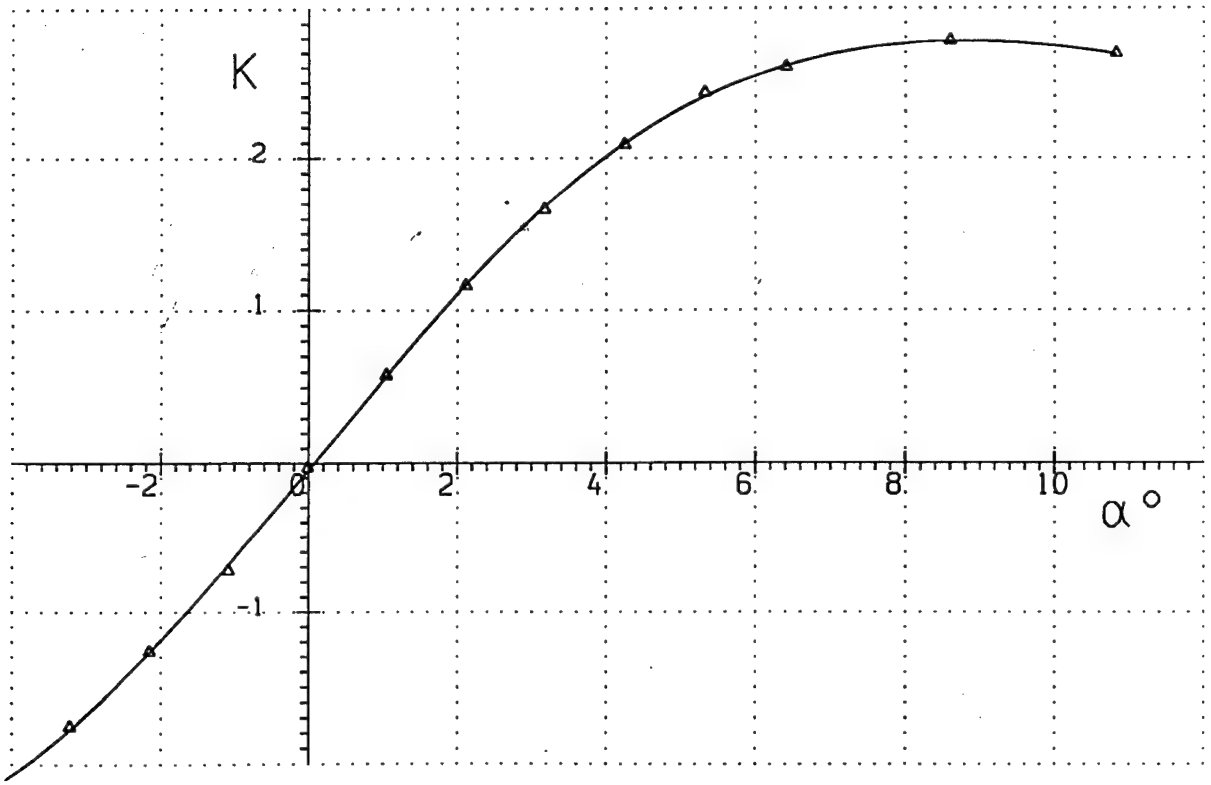

Cx_a
Cy_a
K

Run 21

Fig. 25

$M_\infty = 7.07$ $Re_x = 6.26 \cdot 10^6$

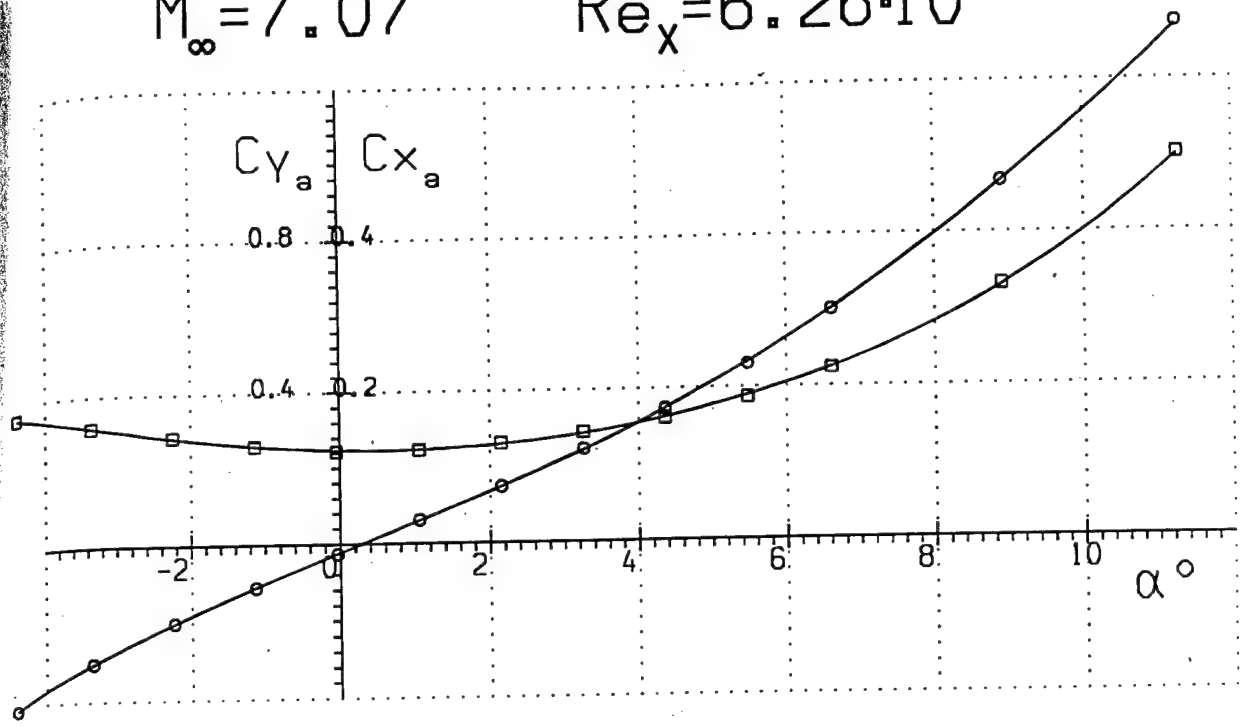

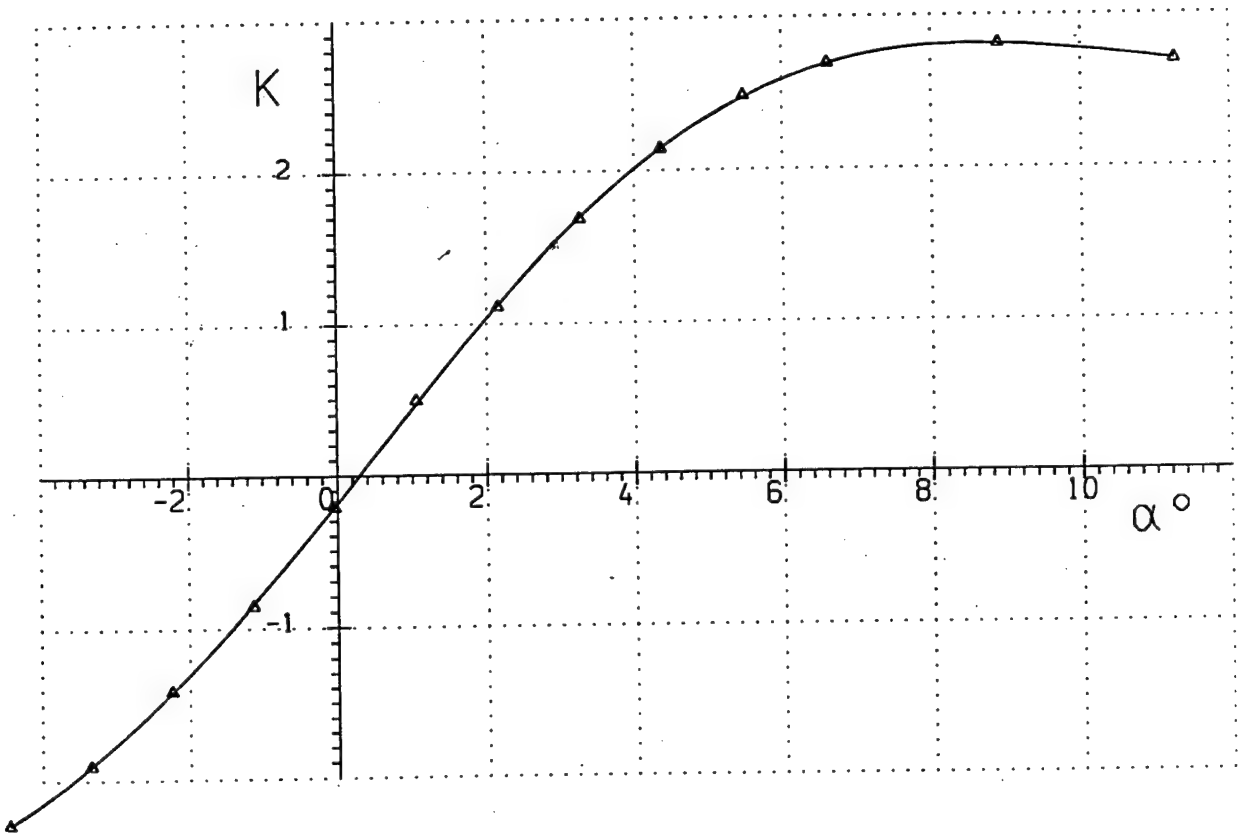

Cx_a

Cy_a

K

Run 22

Fig. 26

$M_\infty = 7.97$ $Re_x = 1.28 \cdot 10^6$

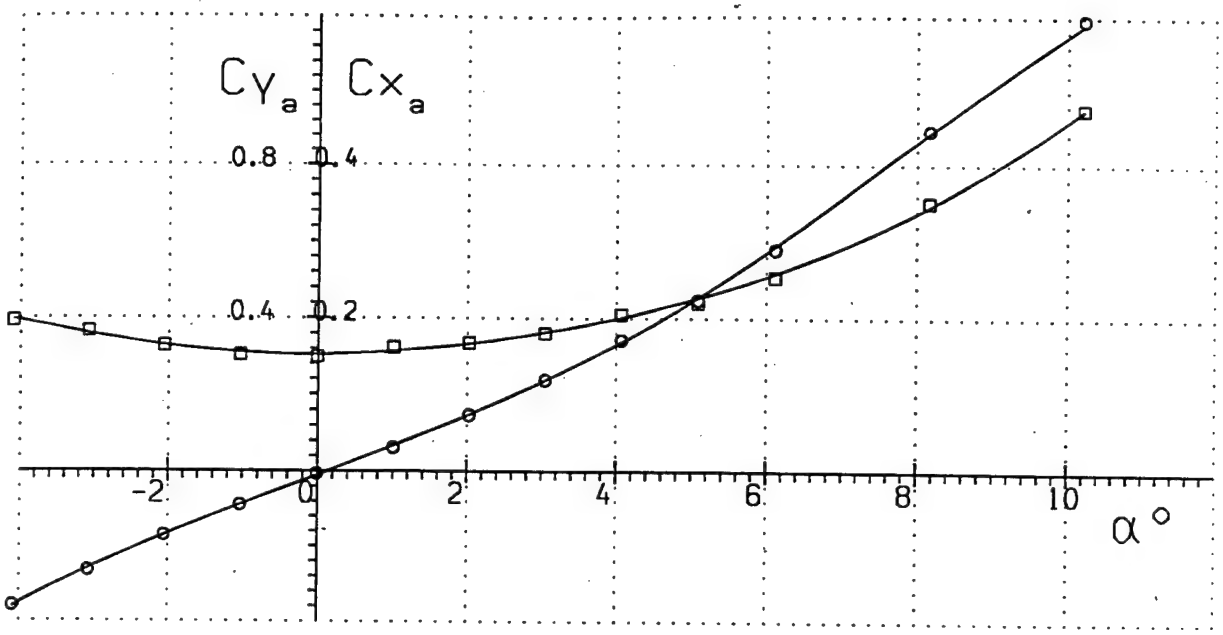

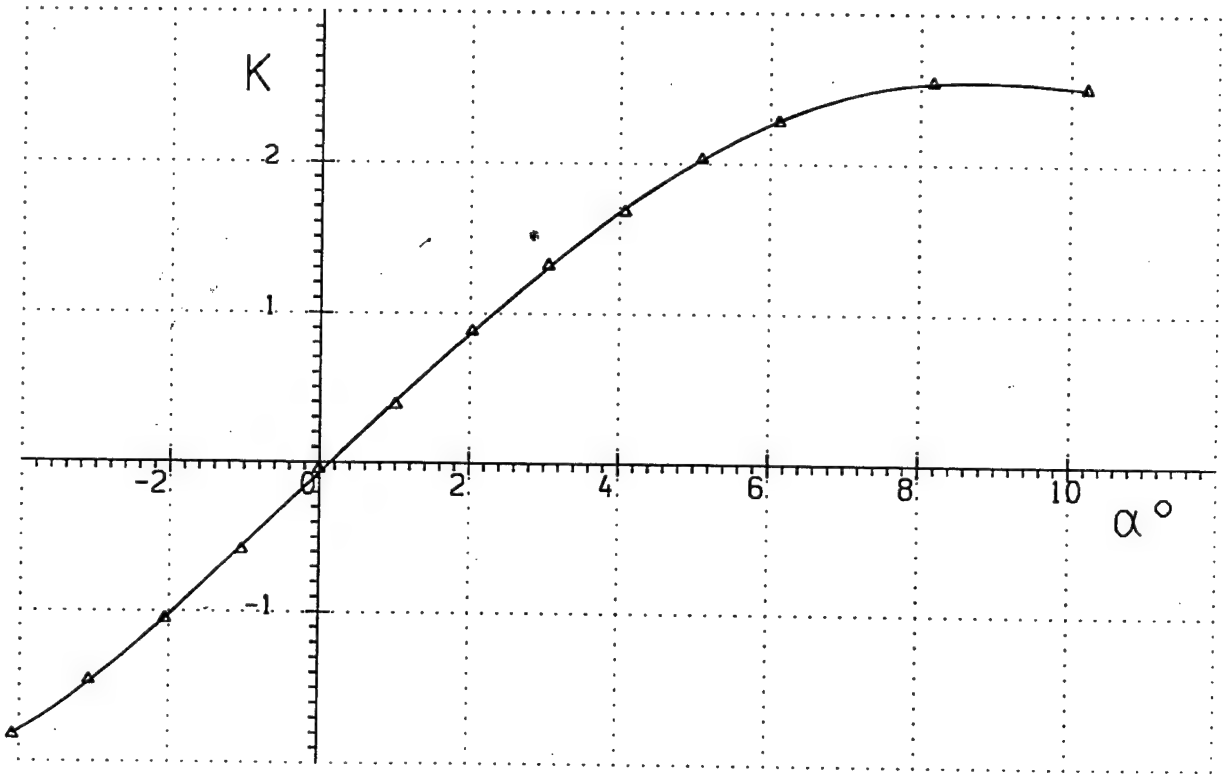

Cx_a
Cy_a
K

Run 23

Fig. 27

$M_\infty = 8.00$ $Re_x = 2.00 \cdot 10^6$

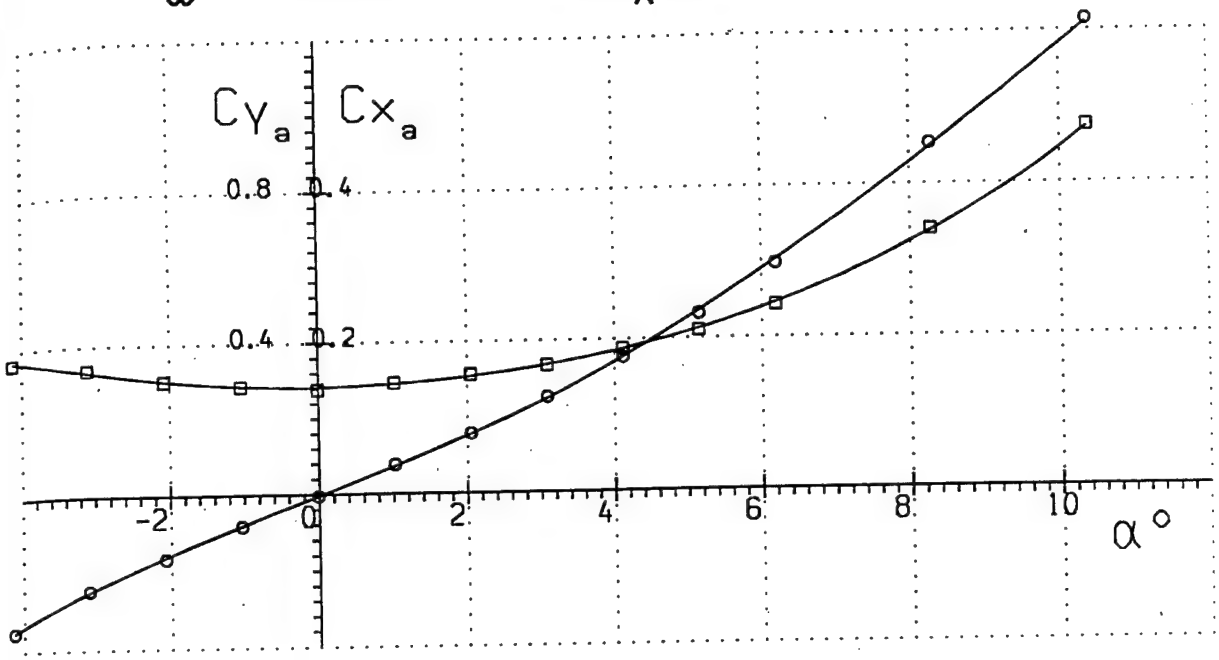

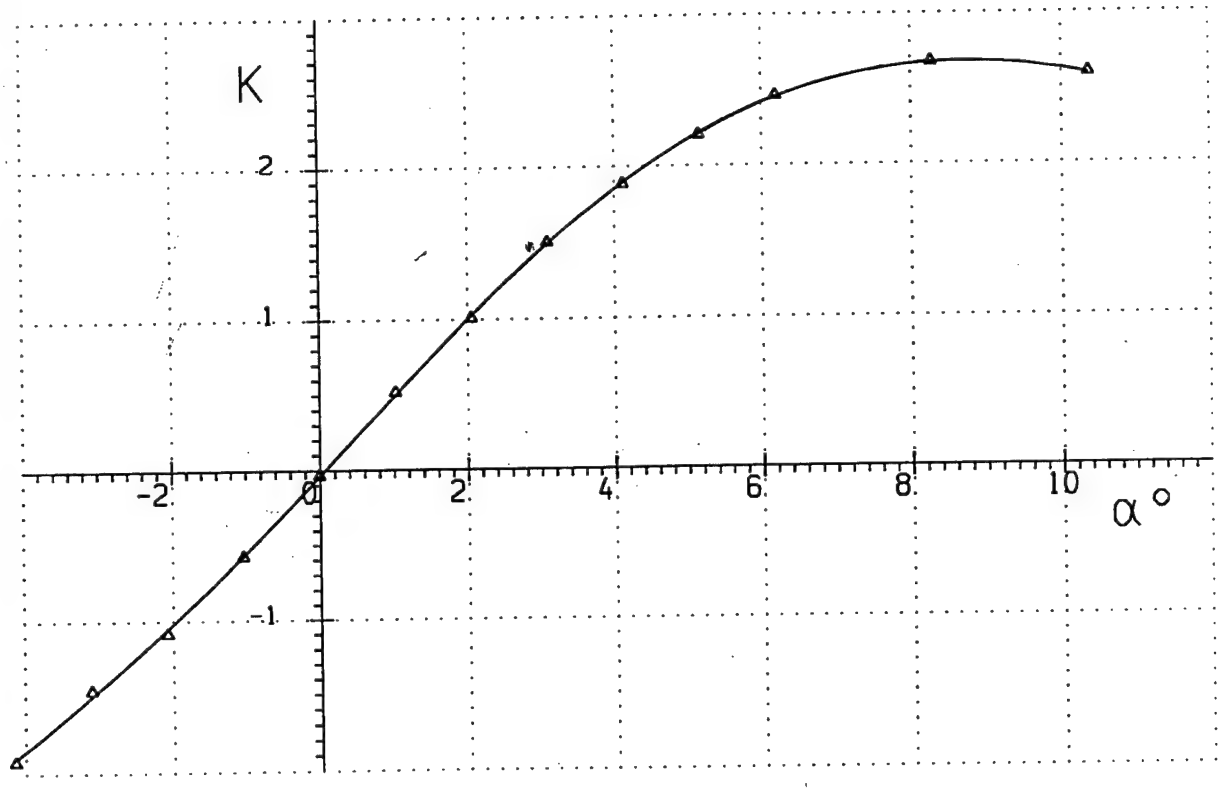

Cx_a
Cy_a
K

Run 24

Fig. 28

$M_\infty = 8.03$ Re_x 3.00

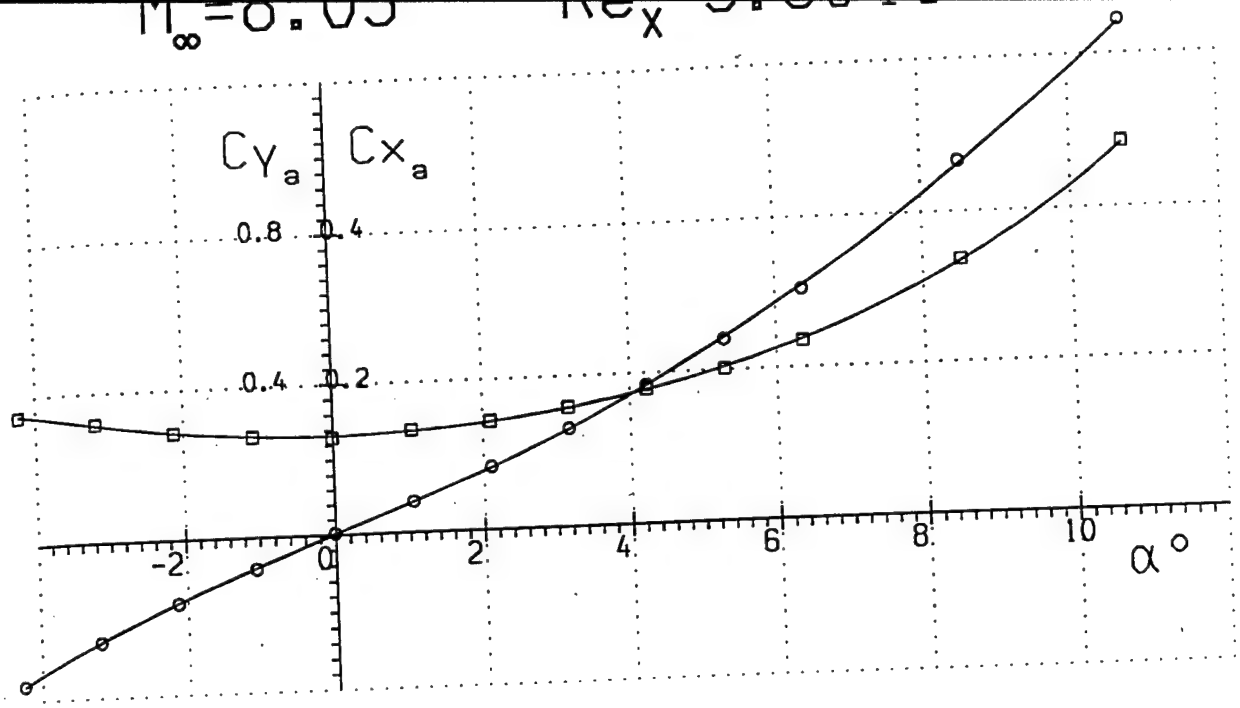

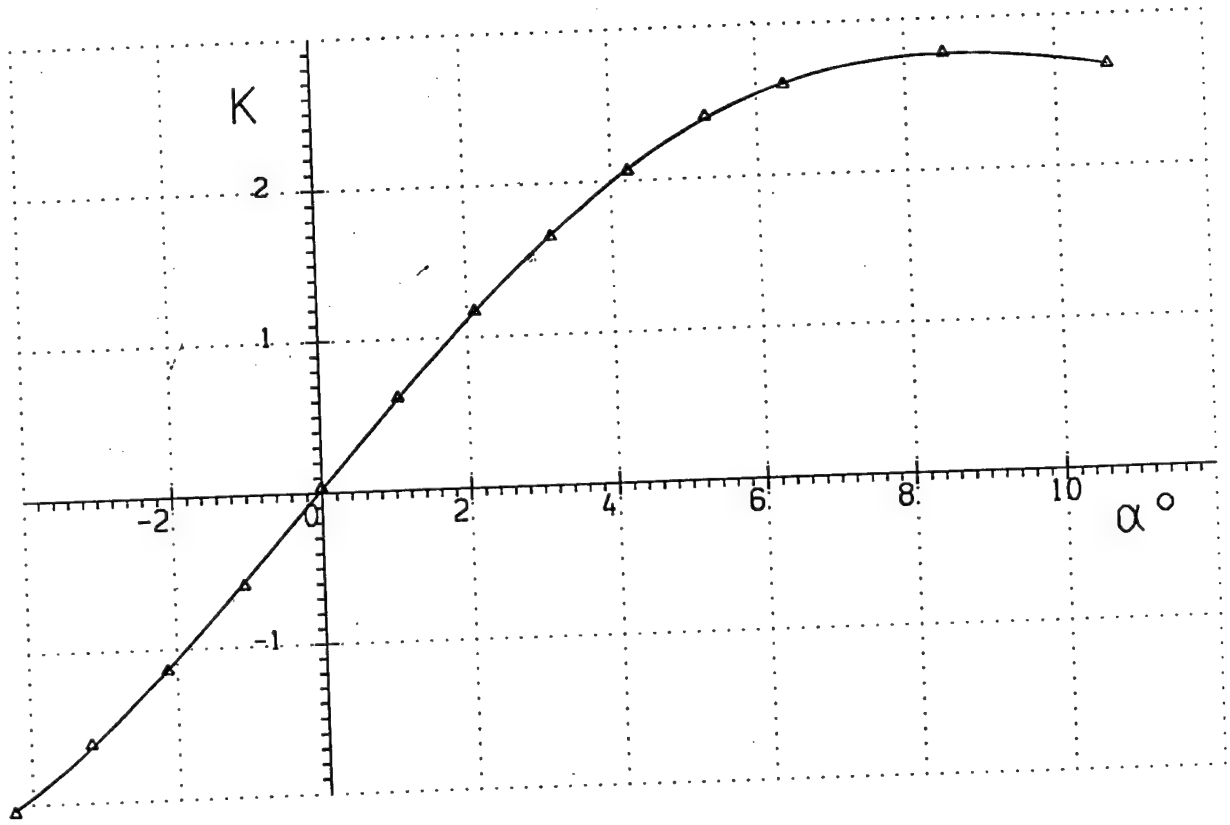

Cx_a
Cy_a
K

Run 25

Fig. 29

$M_\infty = 8.96$ $Re_x = 1.21 \cdot 10^6$

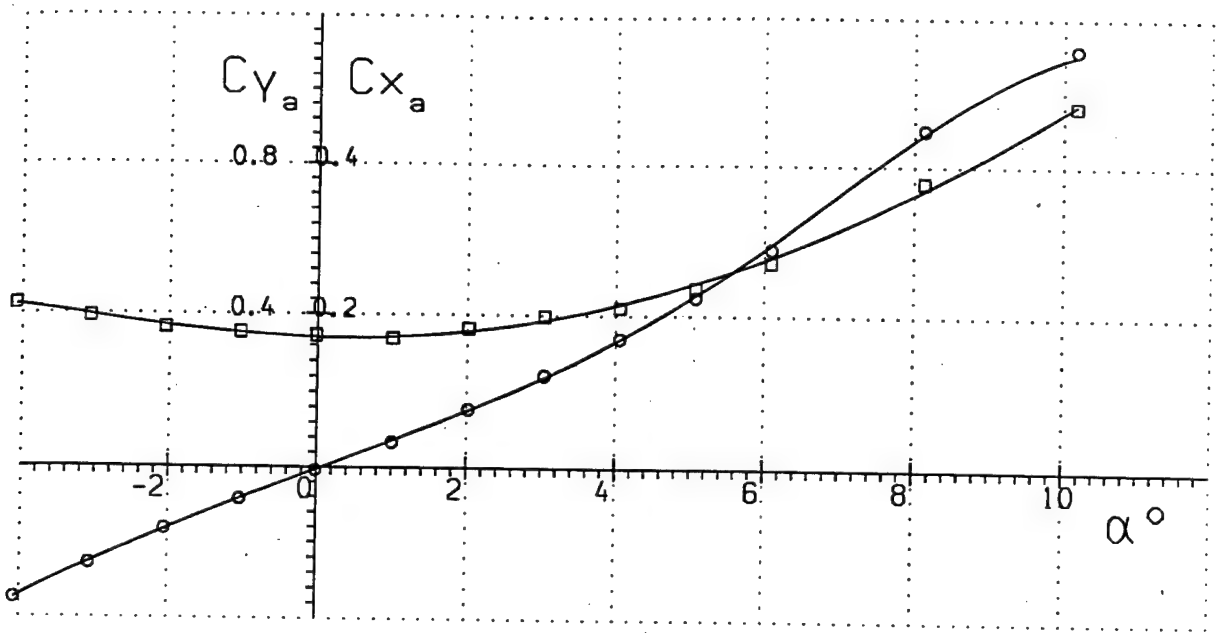

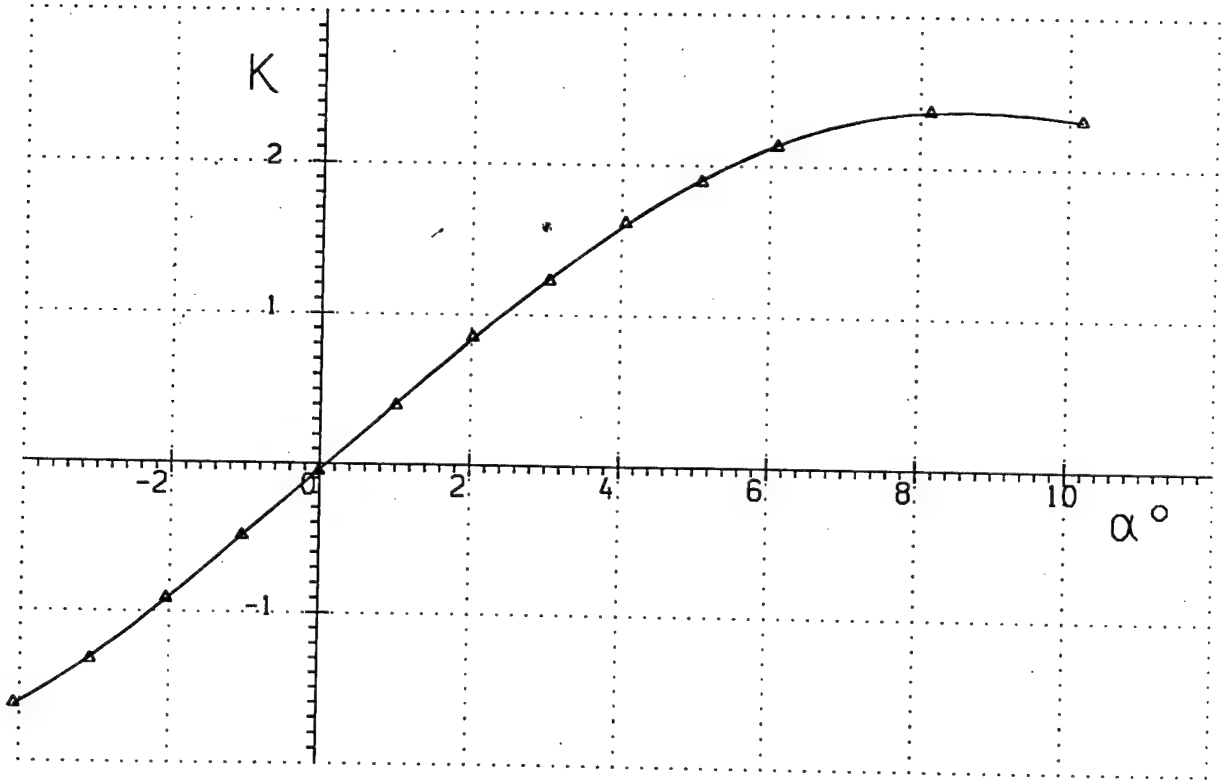

Cx_a
Cy_a
K

Run 26

Fig. 30

$M_\infty = 9.04$ $Re_x = 2.23 \cdot 10$

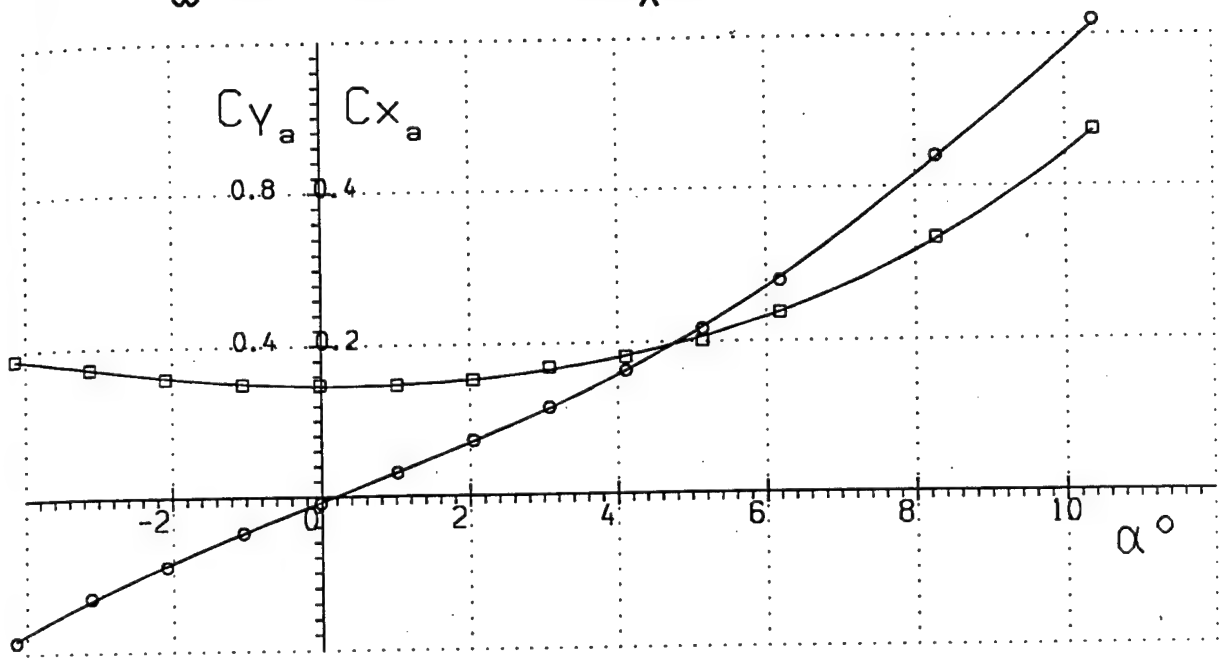

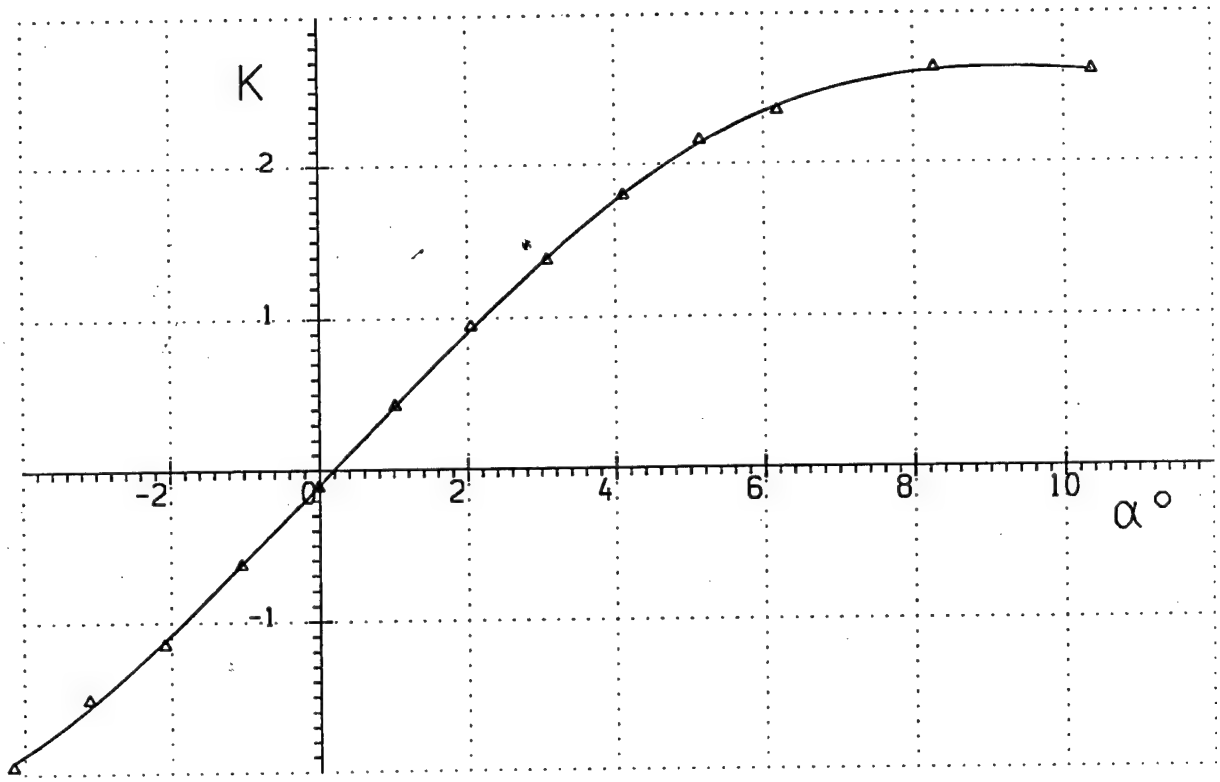

Cx_a

Cy_a

K

Run 27

Fig. 31

$M_\infty = 4.00$ $Re_x = 1.16 \cdot 10^6$

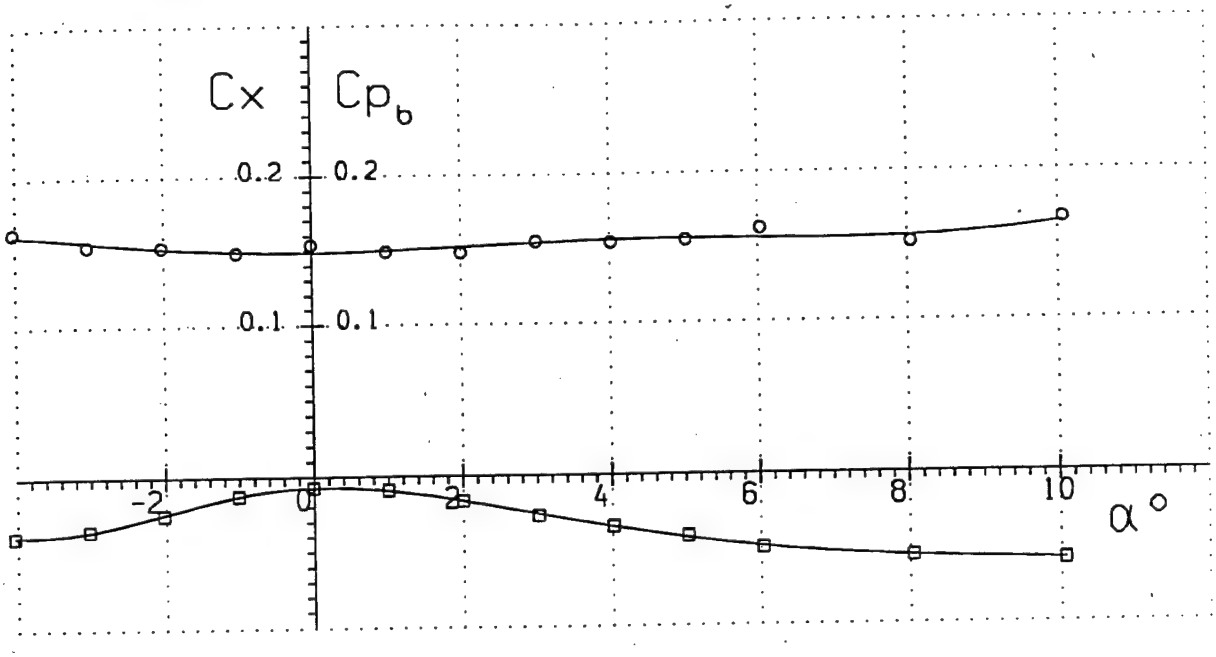

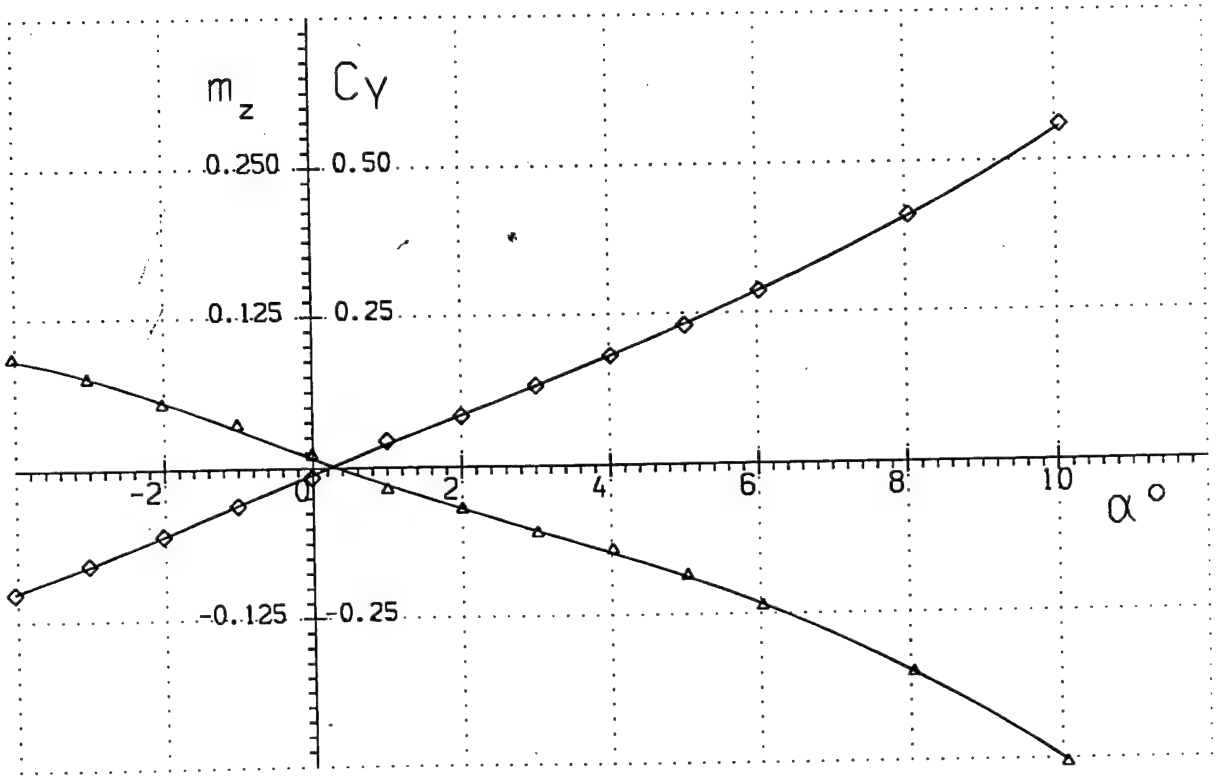

Cp_b
Cx
m_z
Cy

Run 1

Fig. 32

$M_\infty = 4.01$ $Re_x = 1.45 \cdot 10^6$

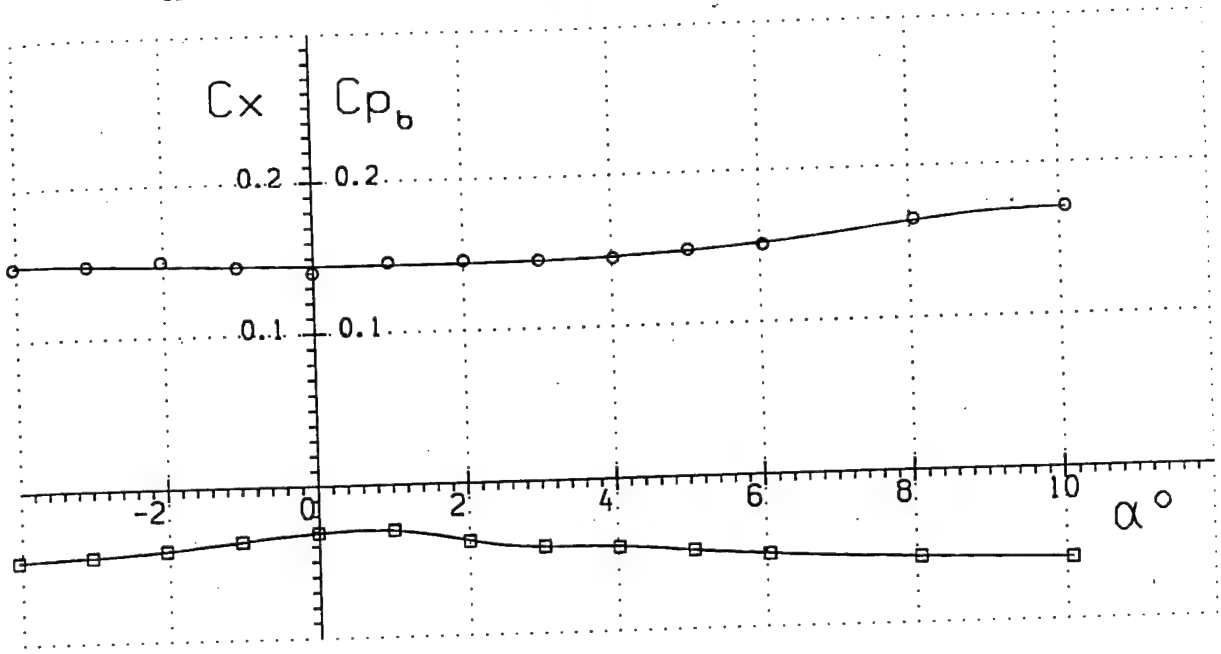

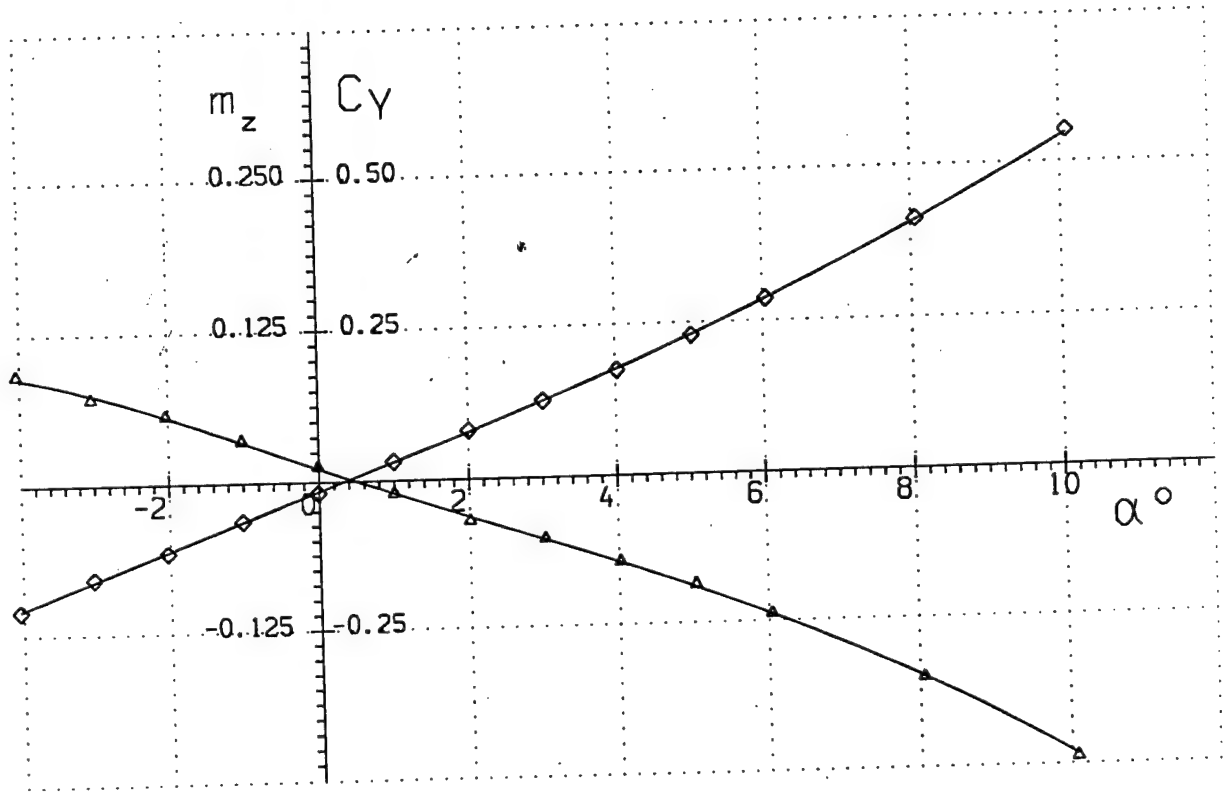

Cp_b
Cx
m_z
Cy

Run 2

Fig. 33

$M_\infty = 4.02$ $Re_x = 1.81 \cdot 10^6$

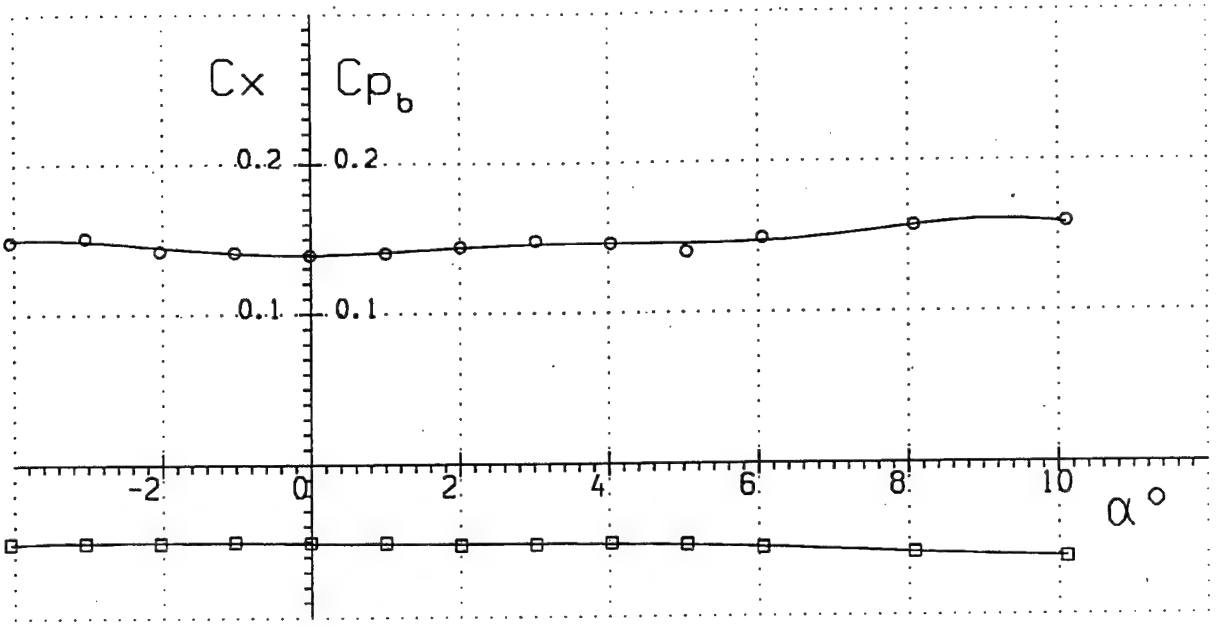

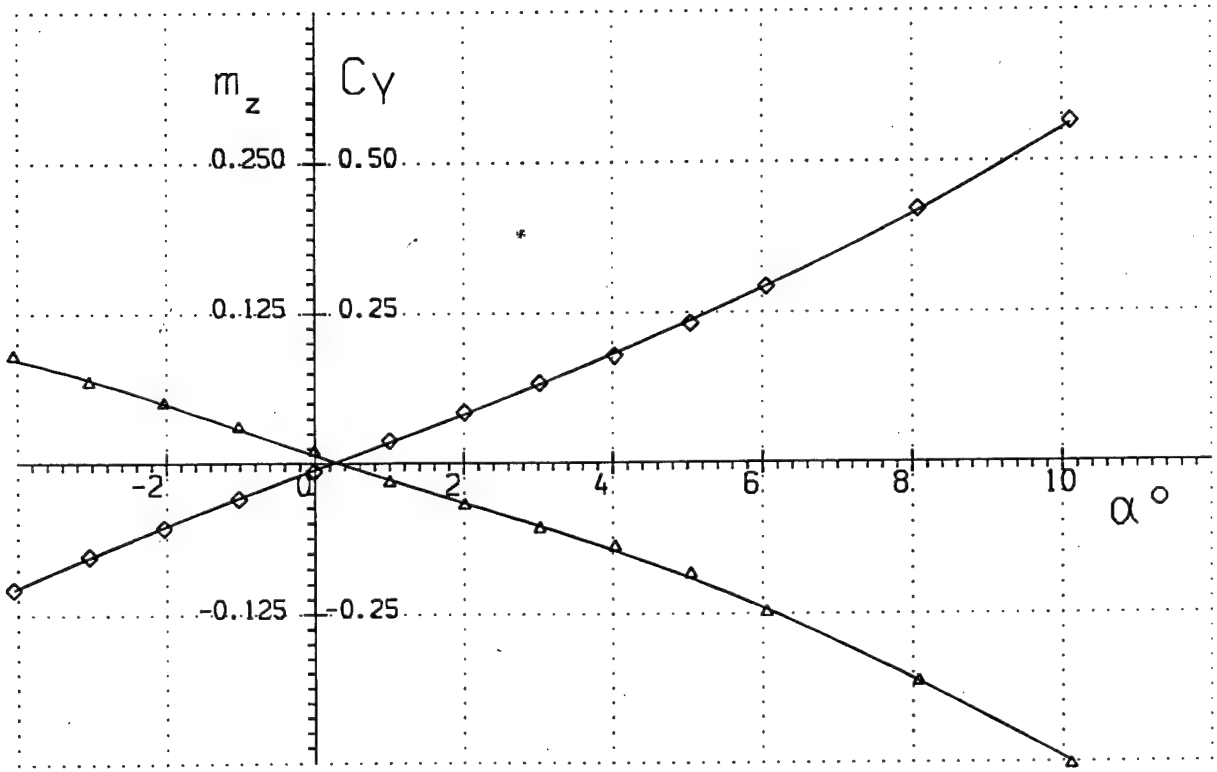

Cp_b
Cx
m_z
Cy

Run 3

Fig. 34

$M_\infty = 4.03$ $Re_x = 2.34 \cdot 10^{}$

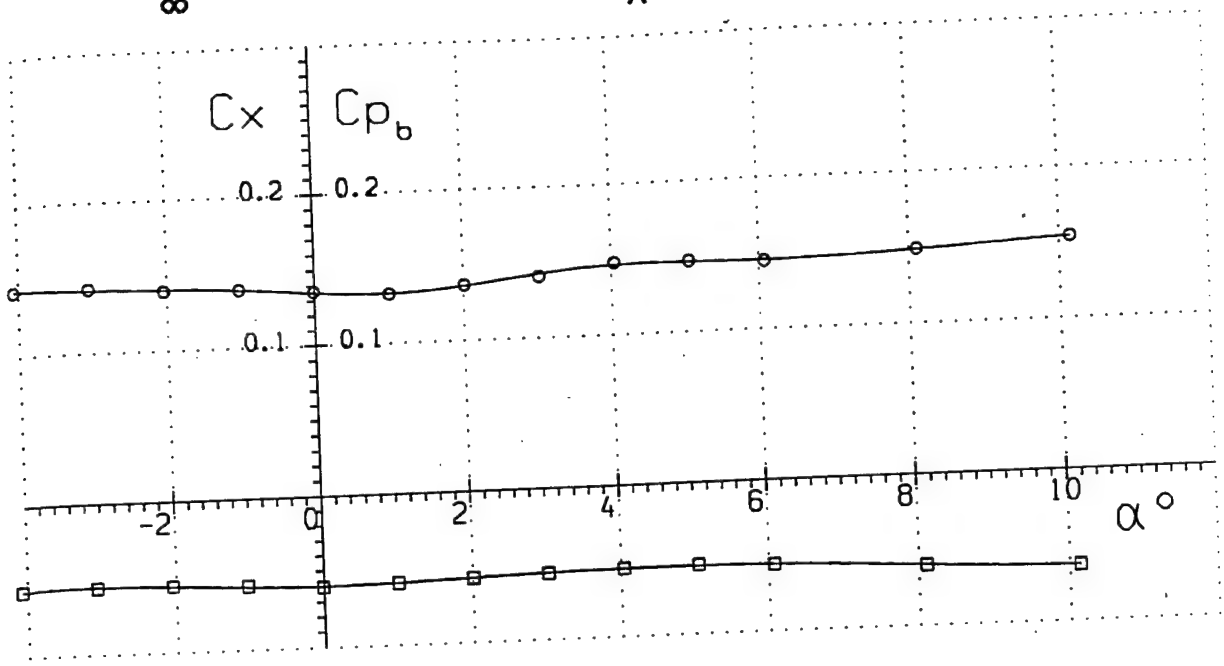

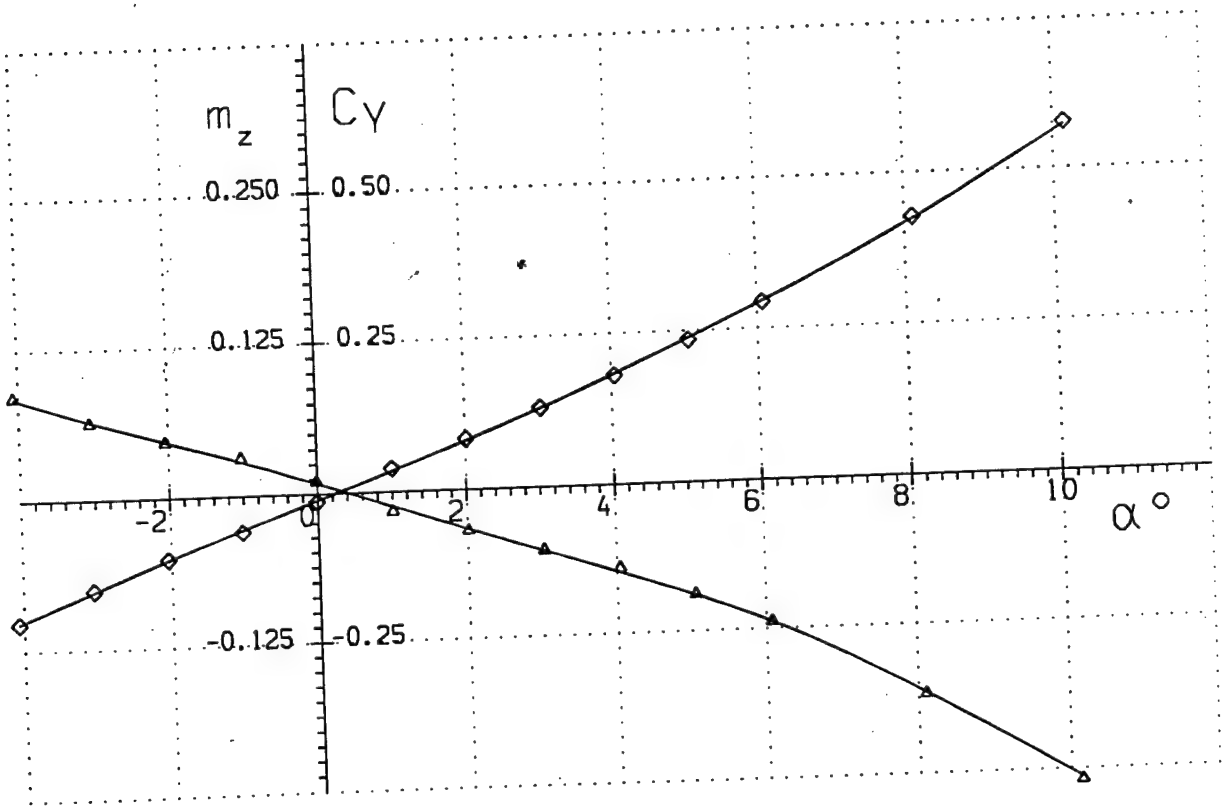

Cp_b
Cx
m_z
Cy

Run 4

Fig. 35

$M_\infty = 4.03$ $Re_x = 3.13 \cdot 10^6$

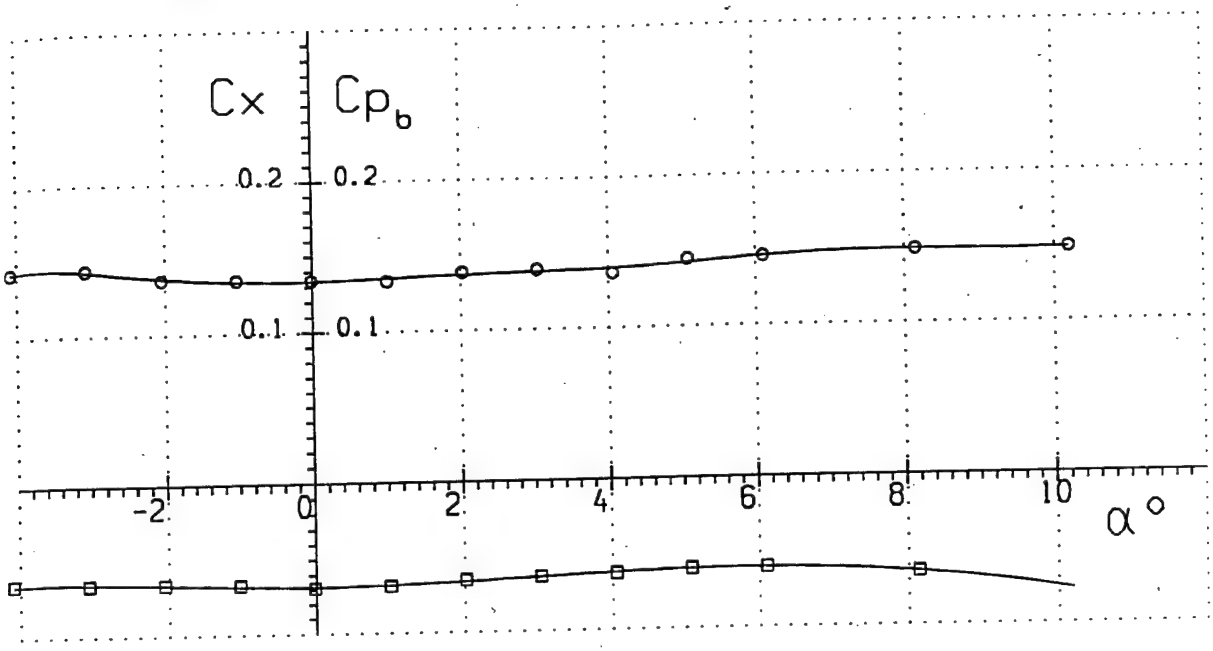

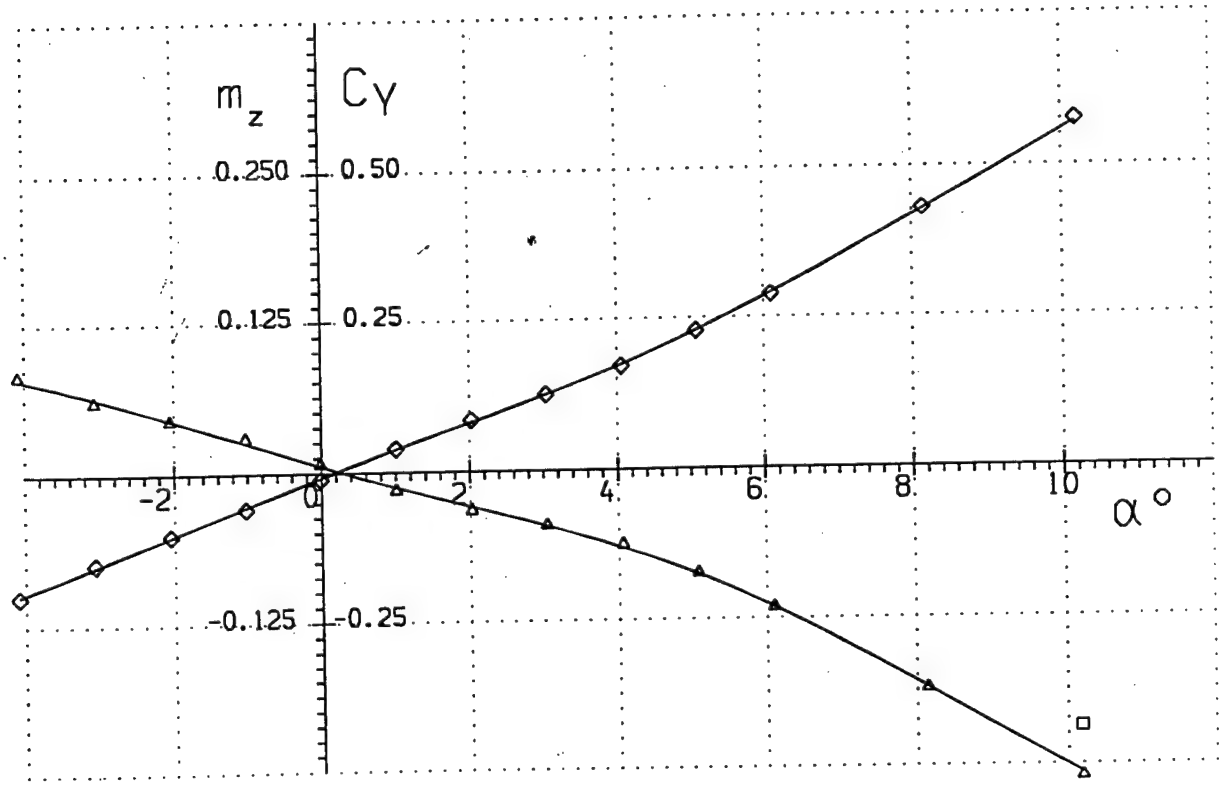

Cp_b
Cx
m_z
Cy

Run 5

Fig. 36

$M_\infty = 4.04$ $Re_x = 3.91 \cdot 10^6$

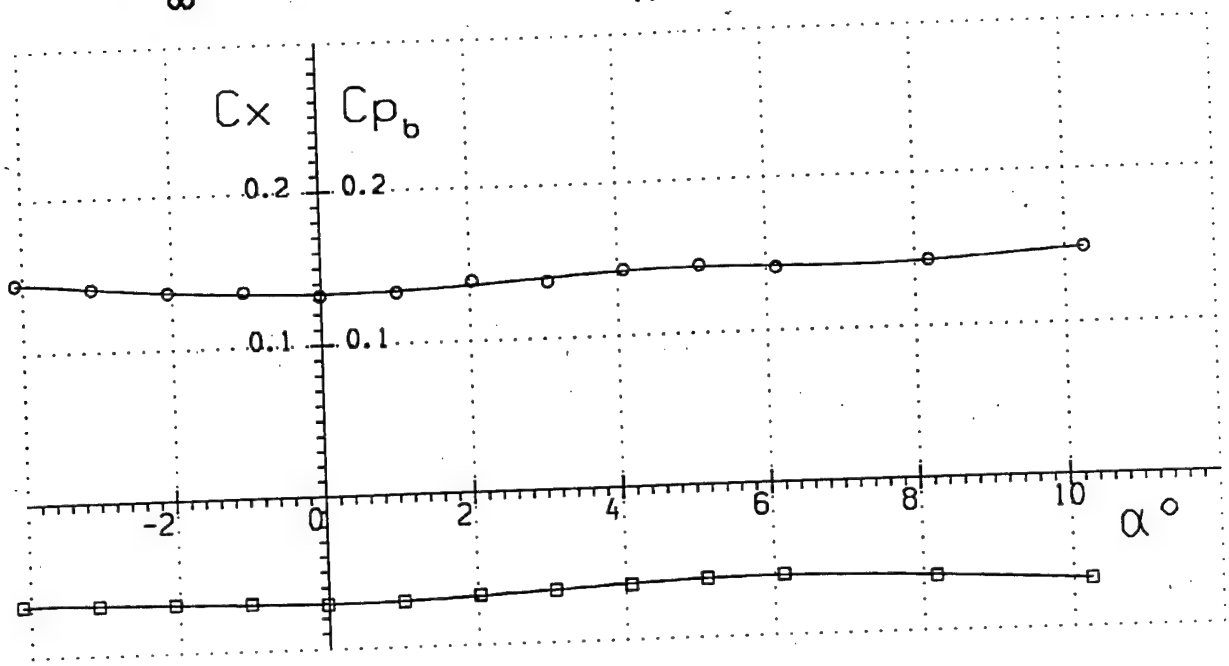

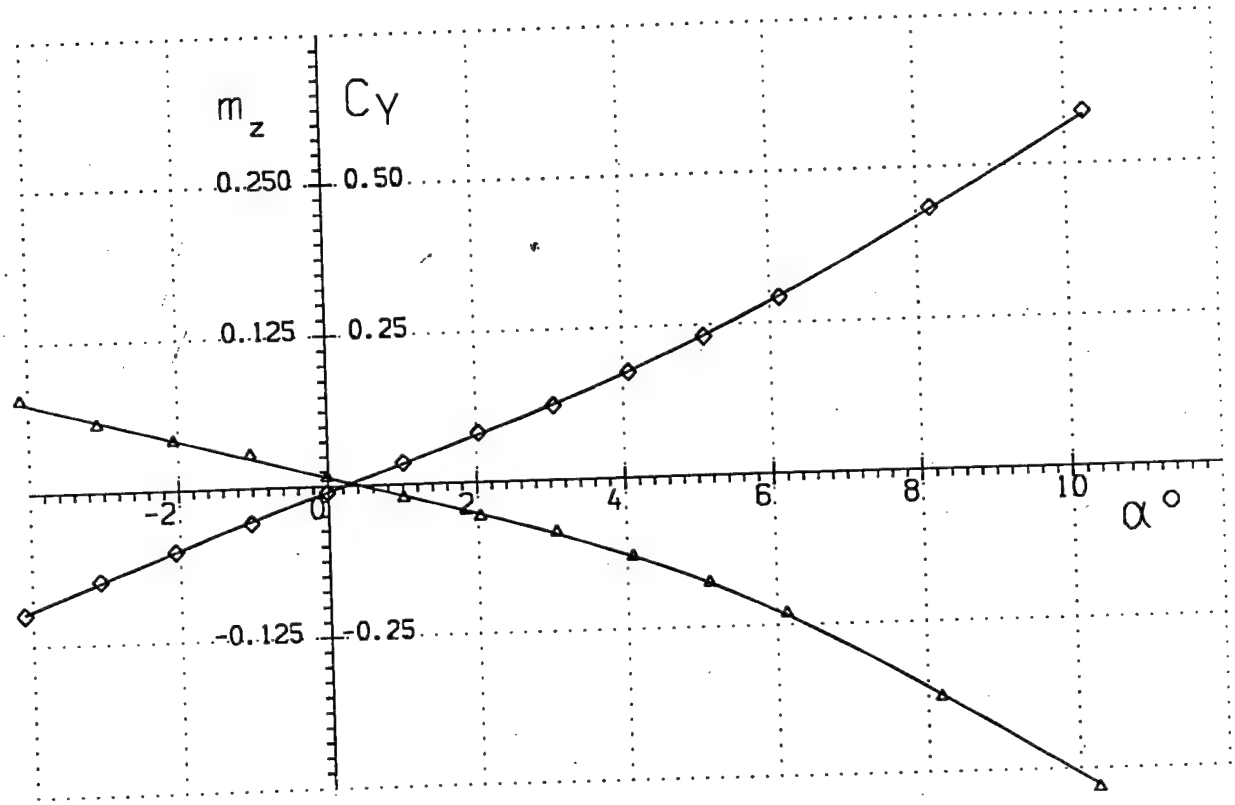

Cp_b
Cx
m_z
Cy

Run 6

Fig. 37

$M_\infty = 4.05$ $Re_x = 6.27 \cdot 10^6$

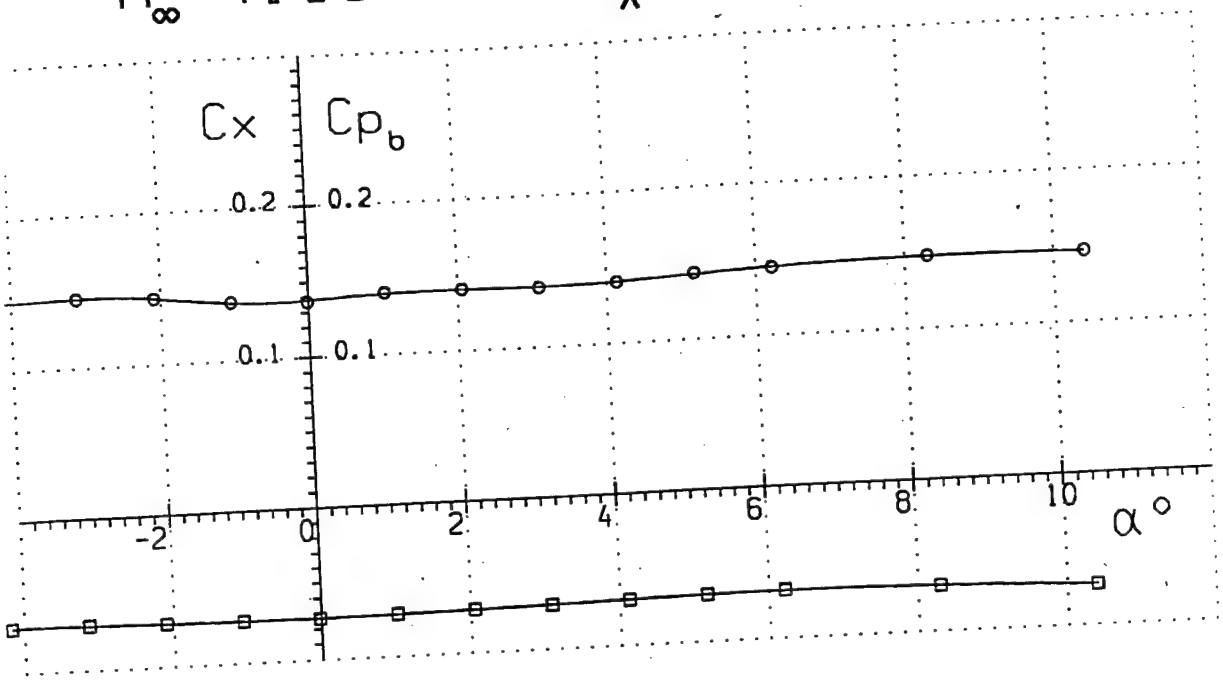

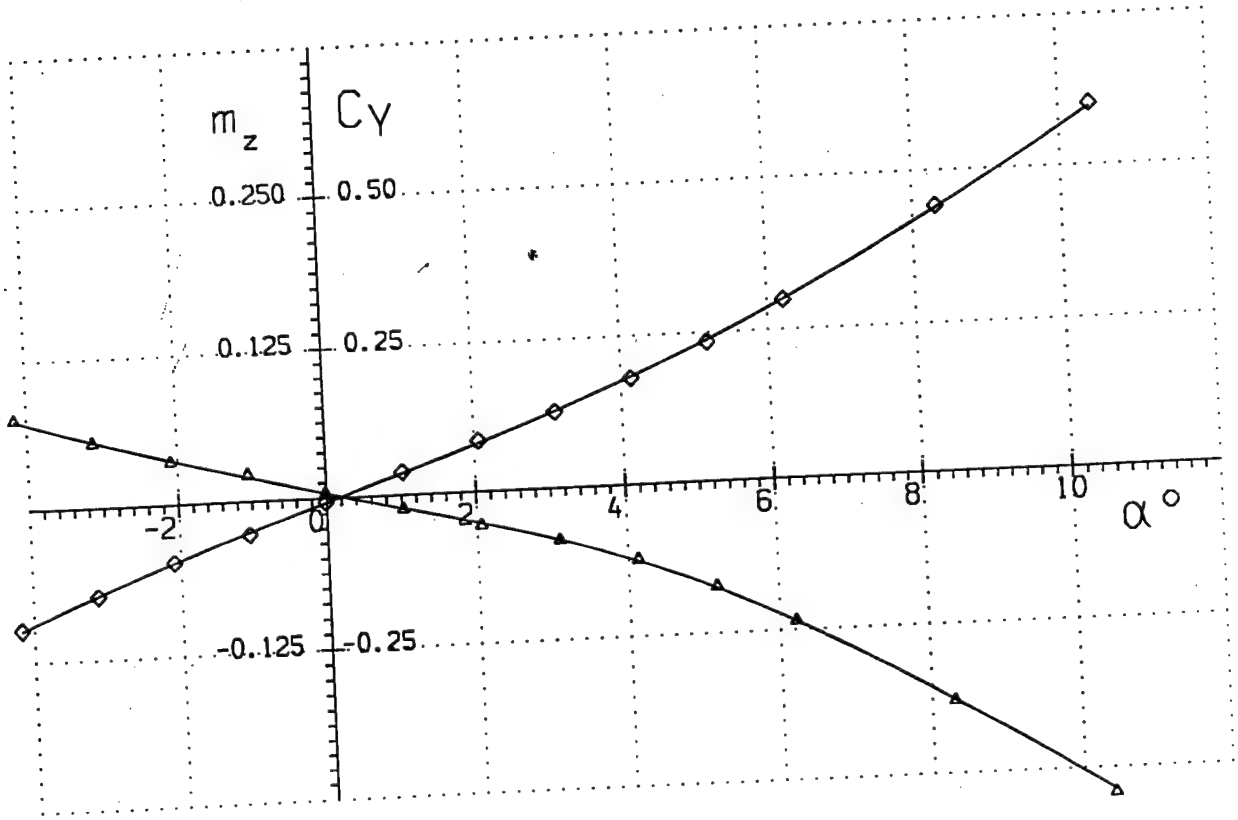

Cp_b
Cx
m_z
Cy

Run 7

Fig. 38

$M_\infty = 4.06$ $Re_x = 8.60 \cdot 10^6$

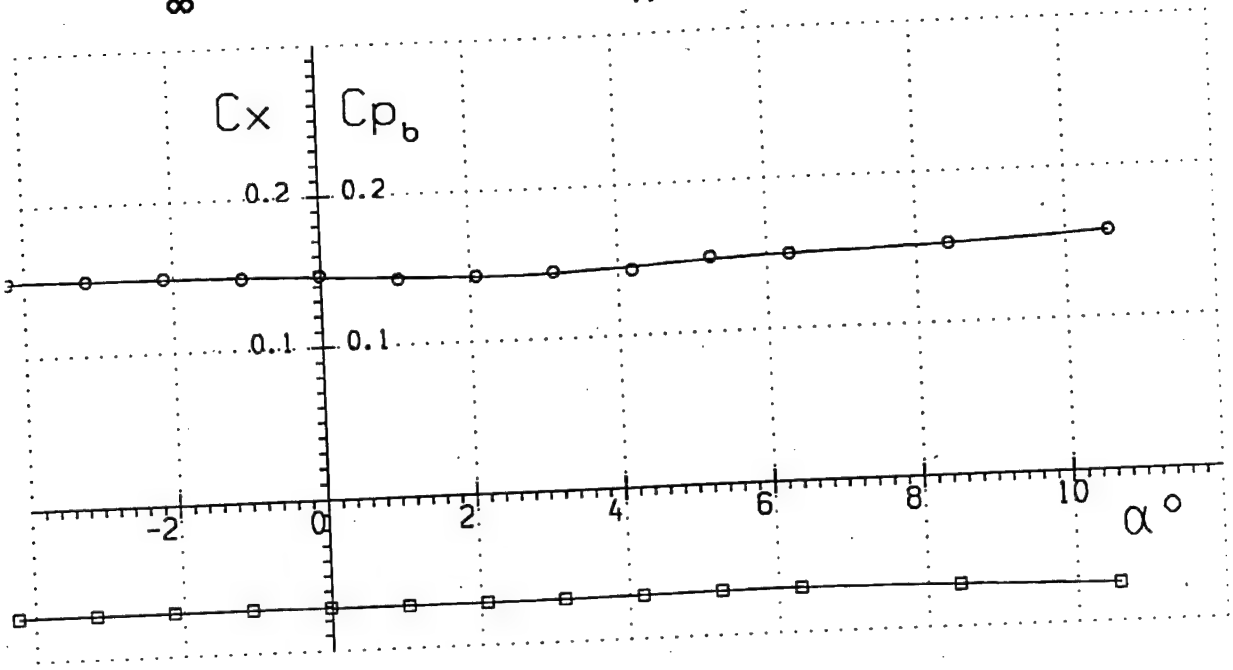

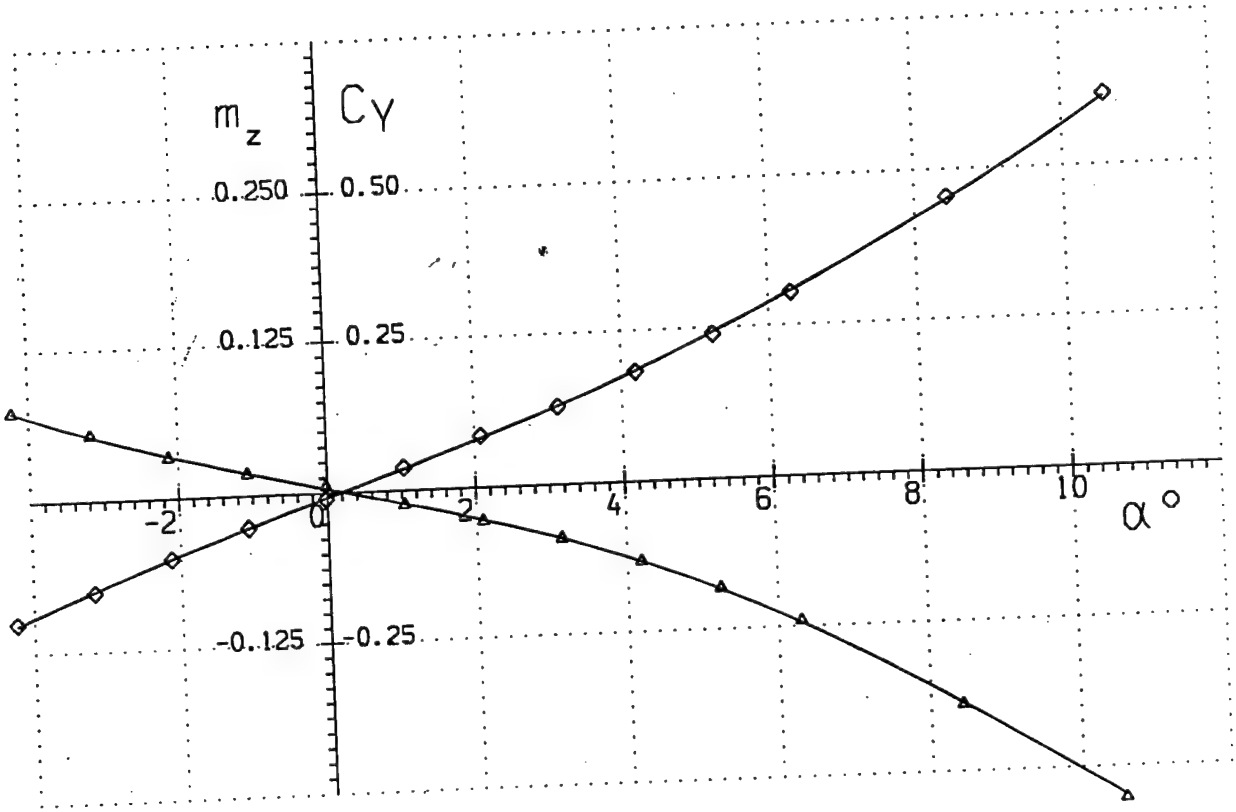

Cp_b
Cx
m_z
Cy

Run 8

Fig. 39

$M_\infty = 4.96$ $Re_x = .90 \cdot 10^6$

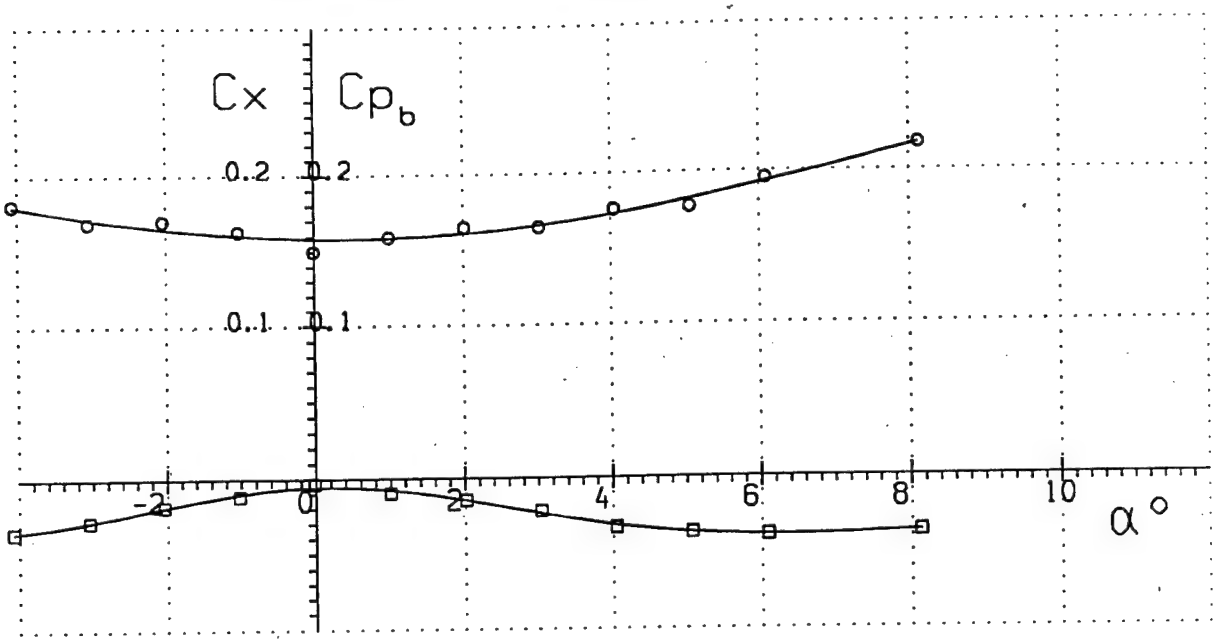

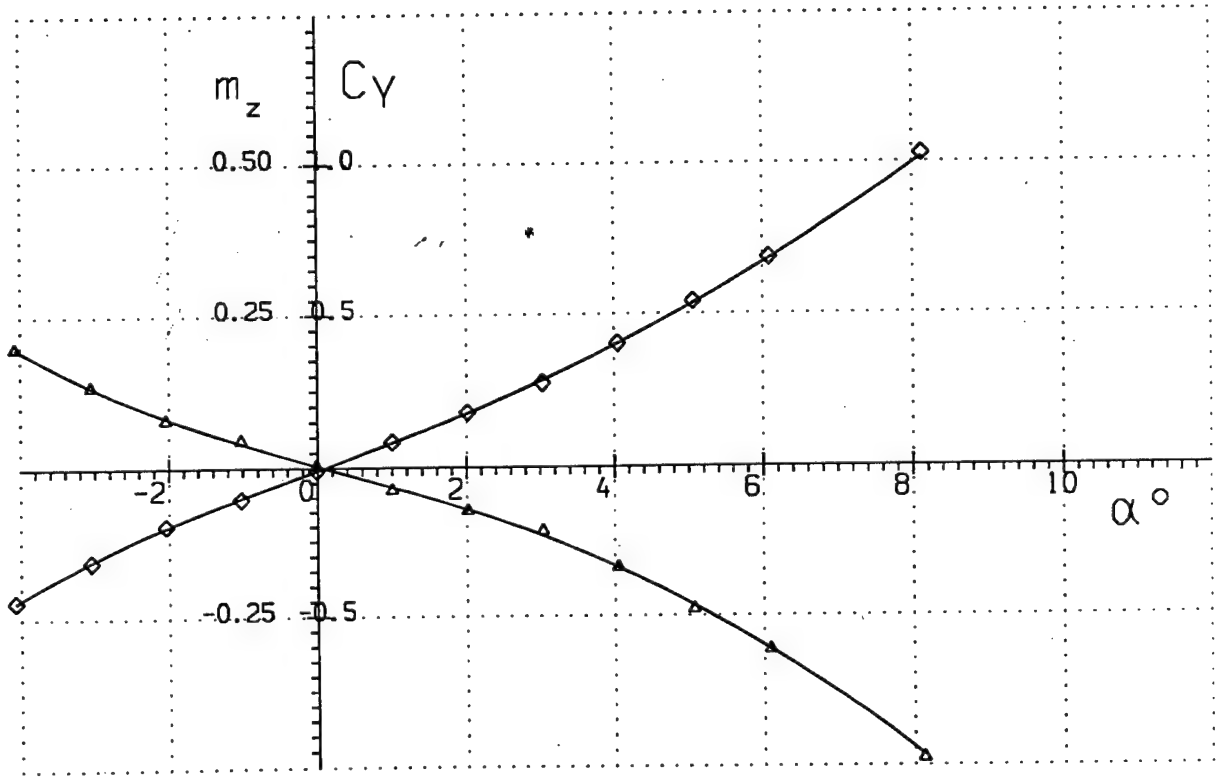

Cp_b
Cx
m_z
Cy

Run 9

Fig. 40

$M_\infty = 4.97$ $Re_x = 1.38 \cdot 10^6$

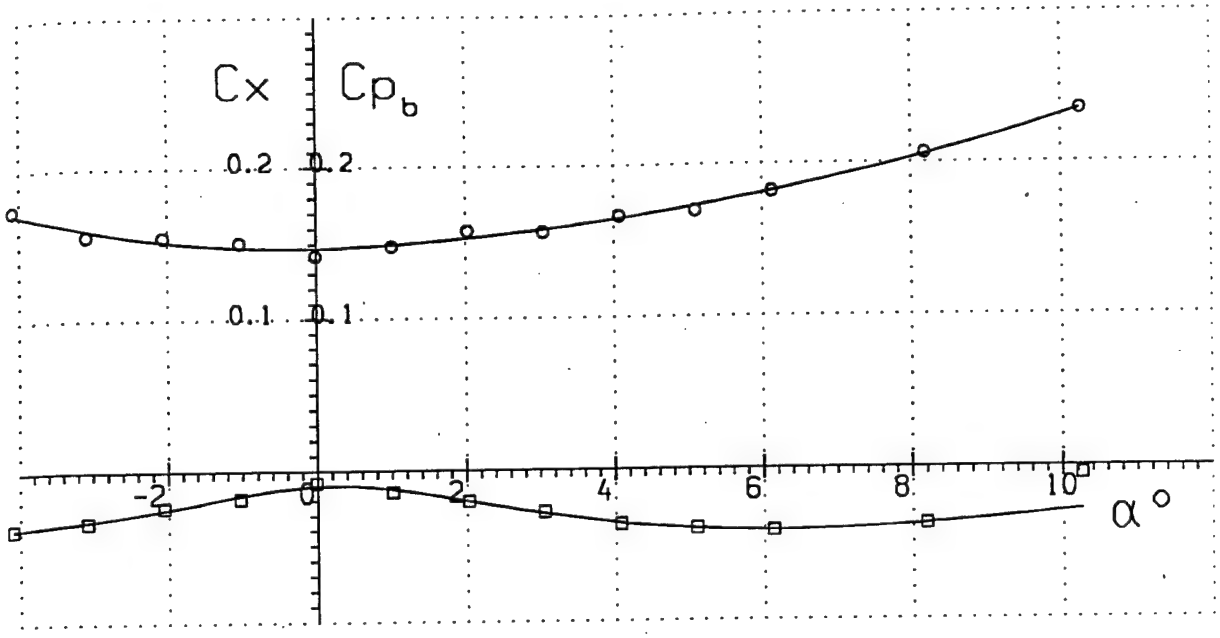

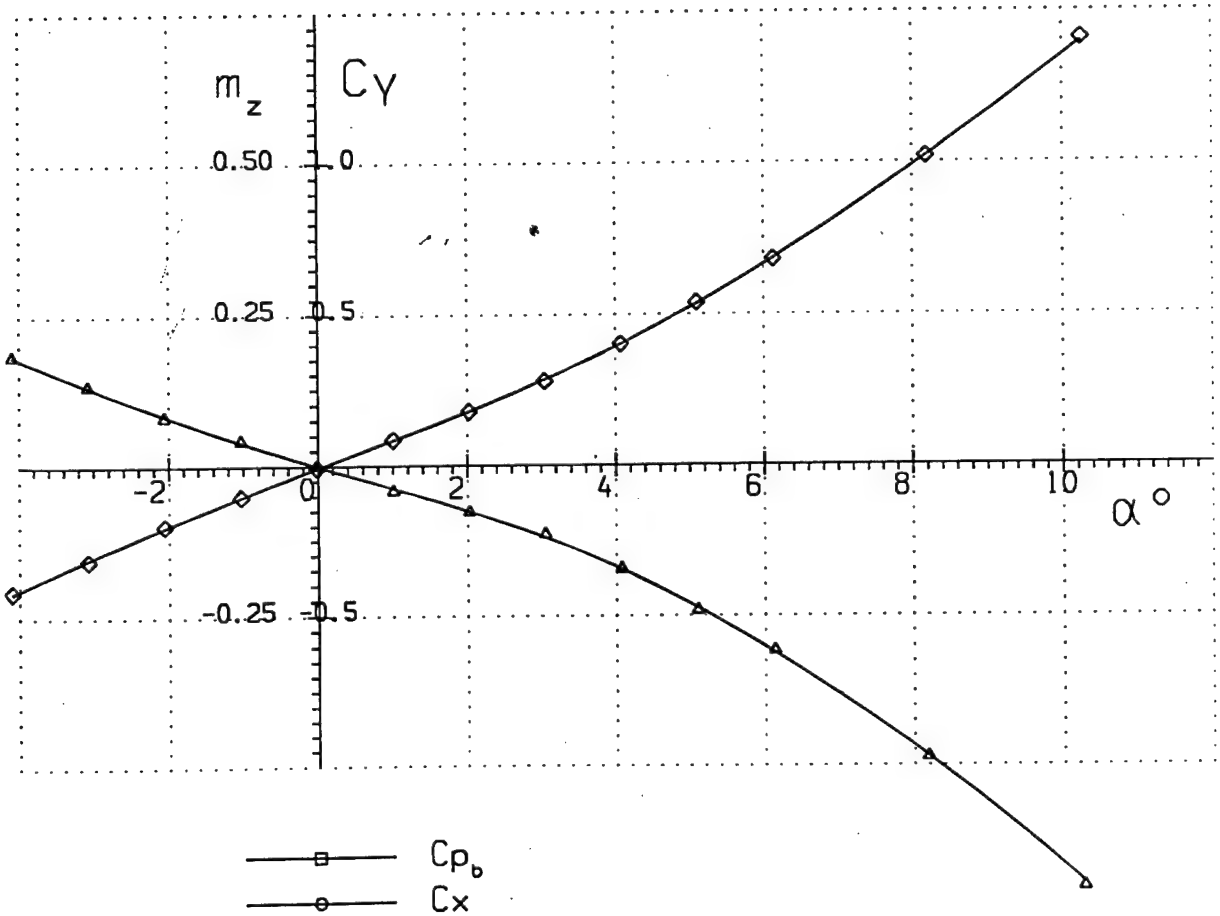

Cp_b
Cx
m_z
Cy

Run 10

Fig. 41

$M_\infty = 4.98$ $Re_x = 1.82 \cdot 10^6$

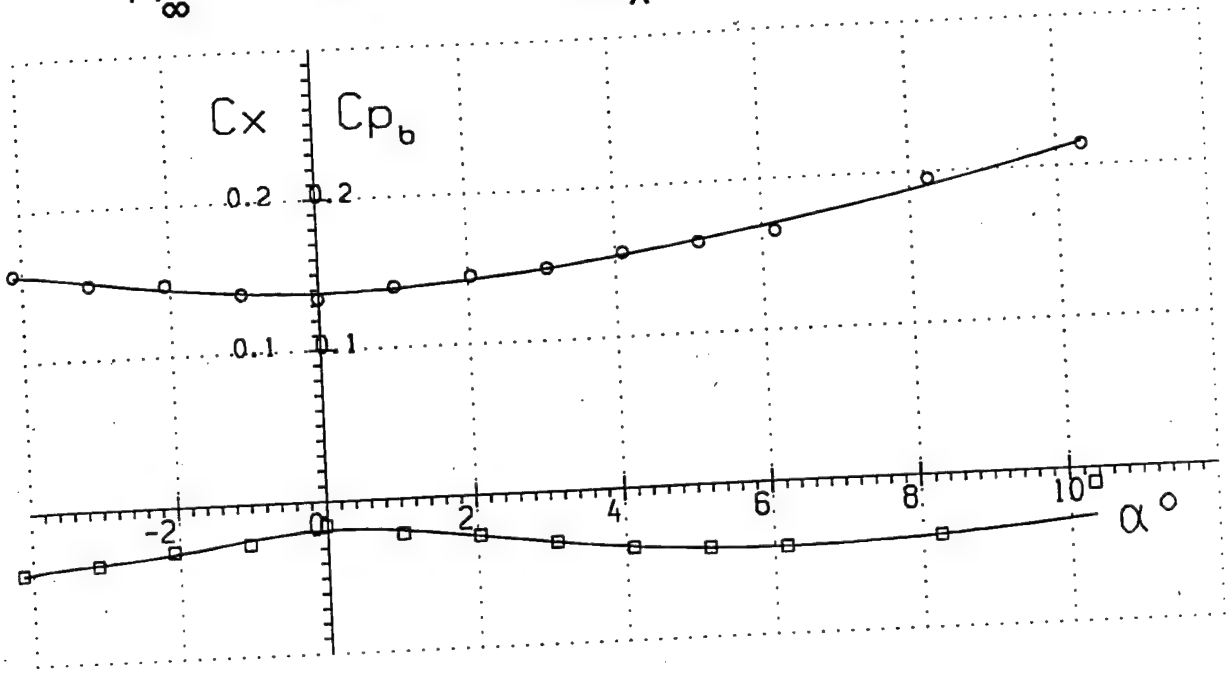

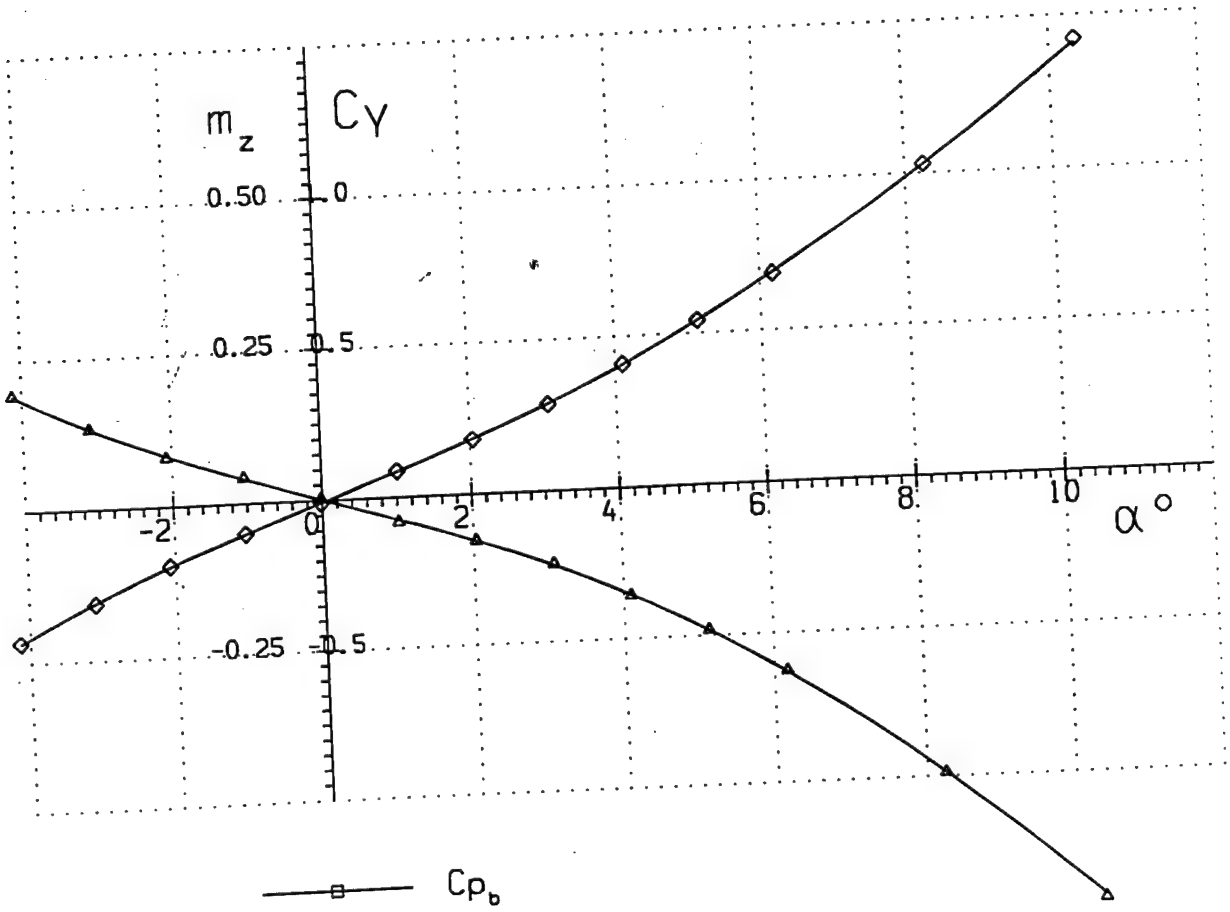

Cp_b
Cx
m_z
Cy

Run 11

Fig. 42

$M_\infty = 5.00$ $Re_x = 3.23 \cdot 10^6$

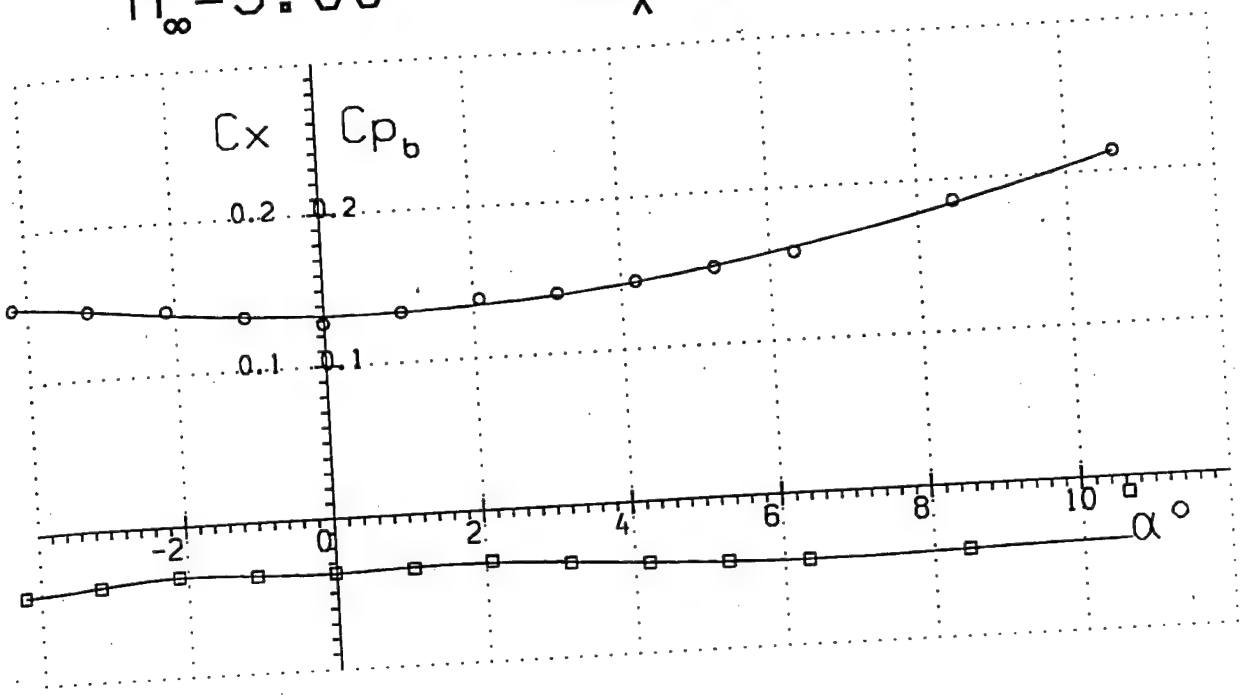

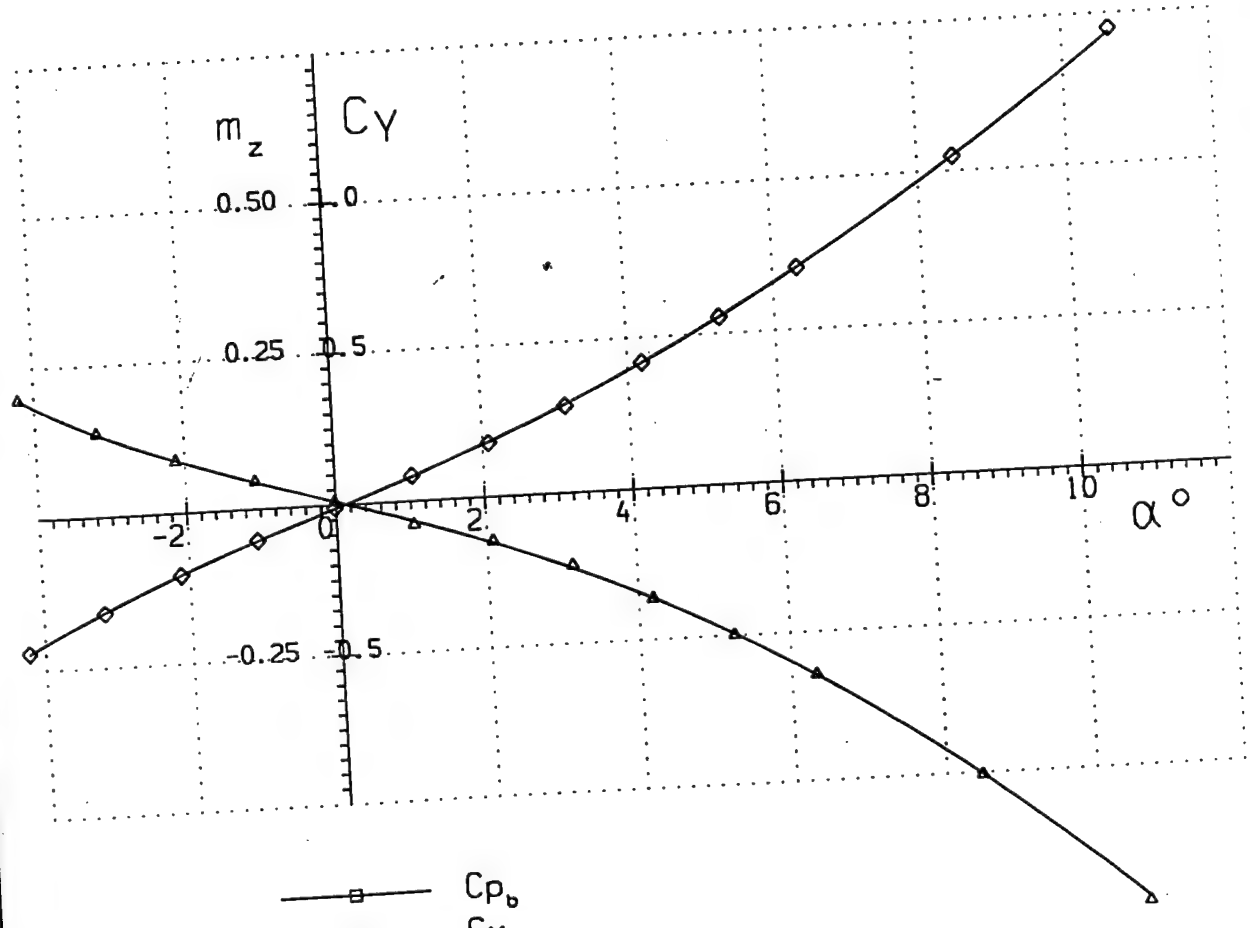

Cp_b
Cx
m_z
Cy

Run 12

Fig. 43

$M_\infty = 5.00$ $Re_x = 4.52 \cdot 10^6$

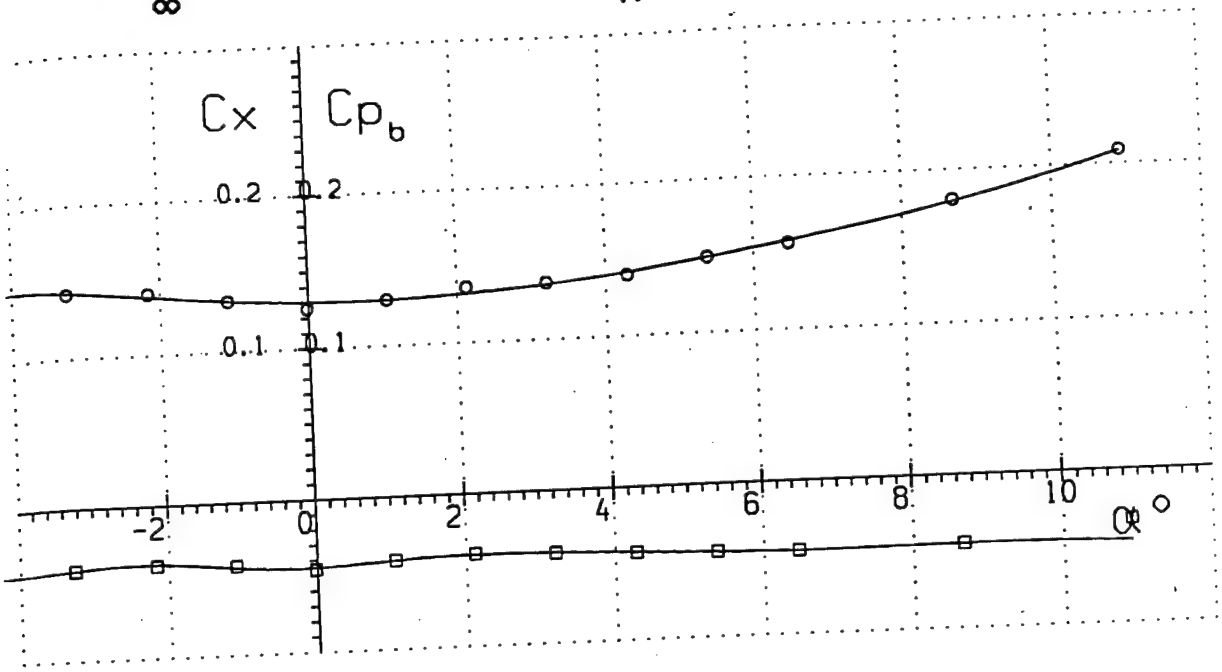

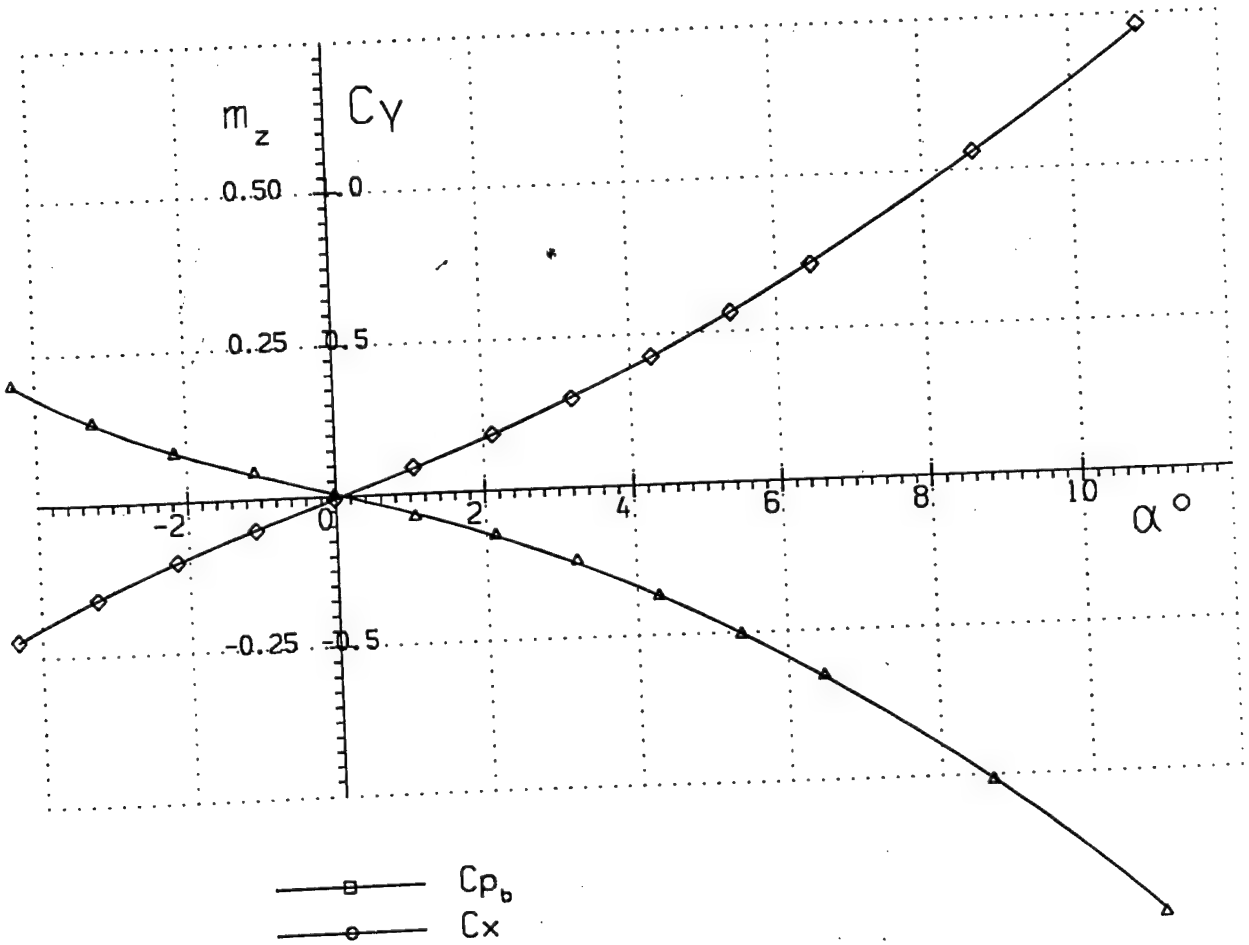

Cp_b
Cx
m_z
Cy

Run 13

Fig. 44

$M_\infty = 5.02$ $Re_x = 7.60 \cdot 10^6$

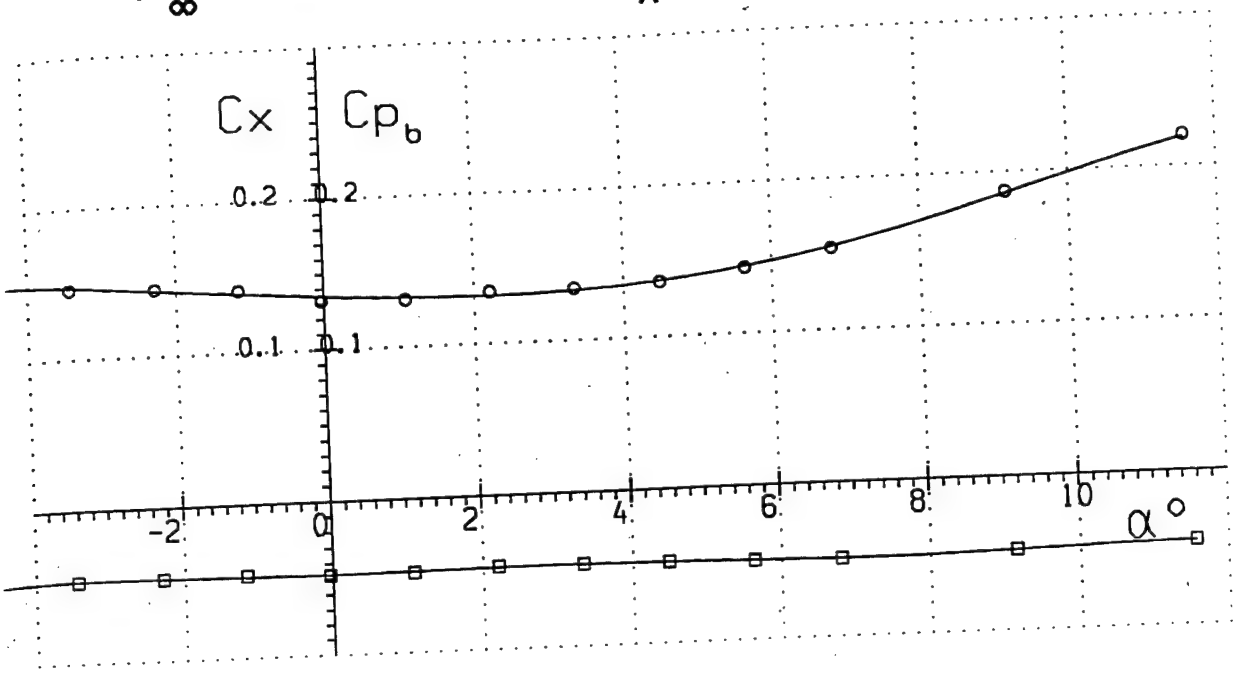

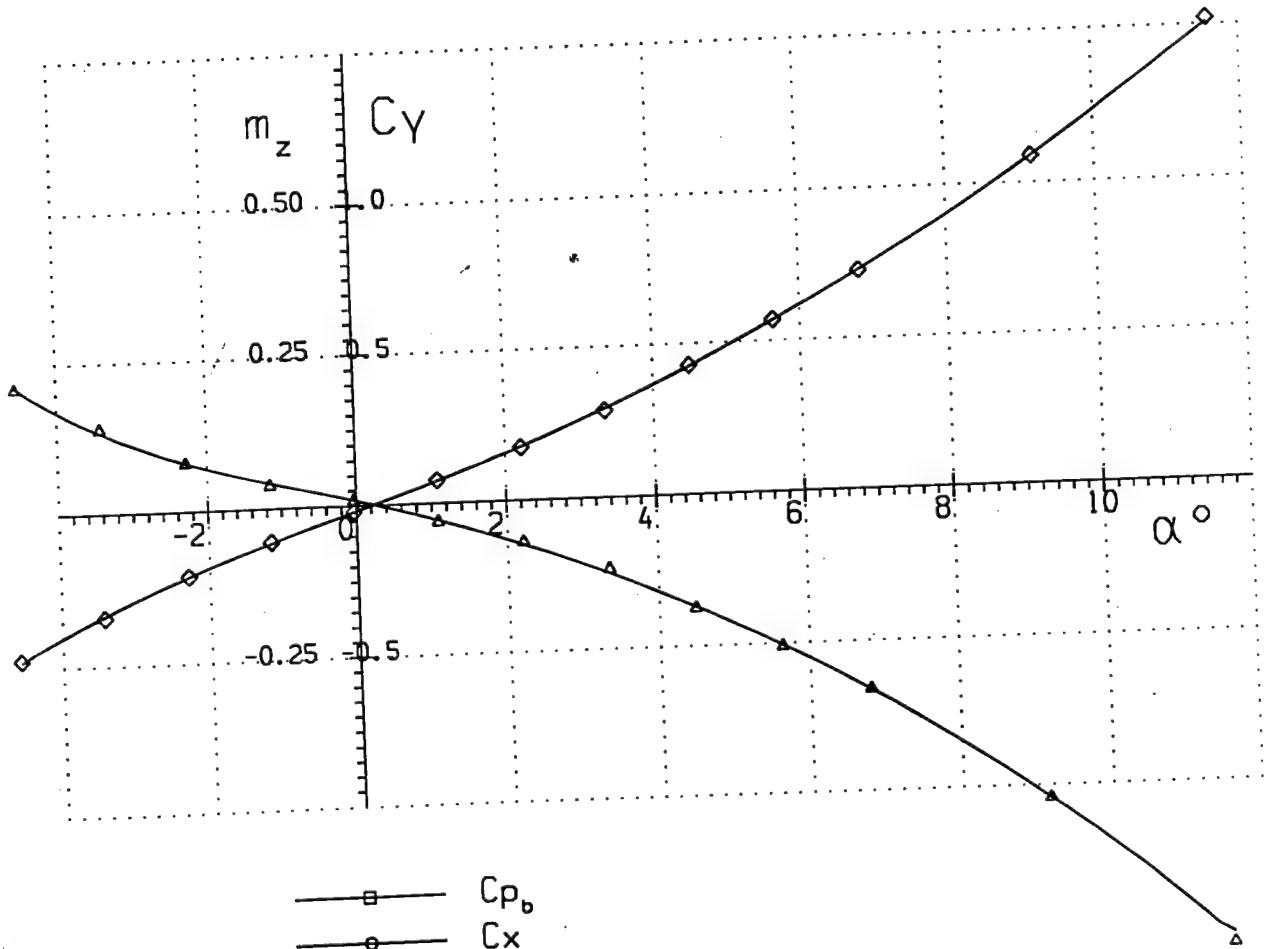

Cp_b
Cx
m_z
Cy

Run 14

Fig. 45

$M_\infty = 6.00$ $Re_x = .98 \cdot 10^6$

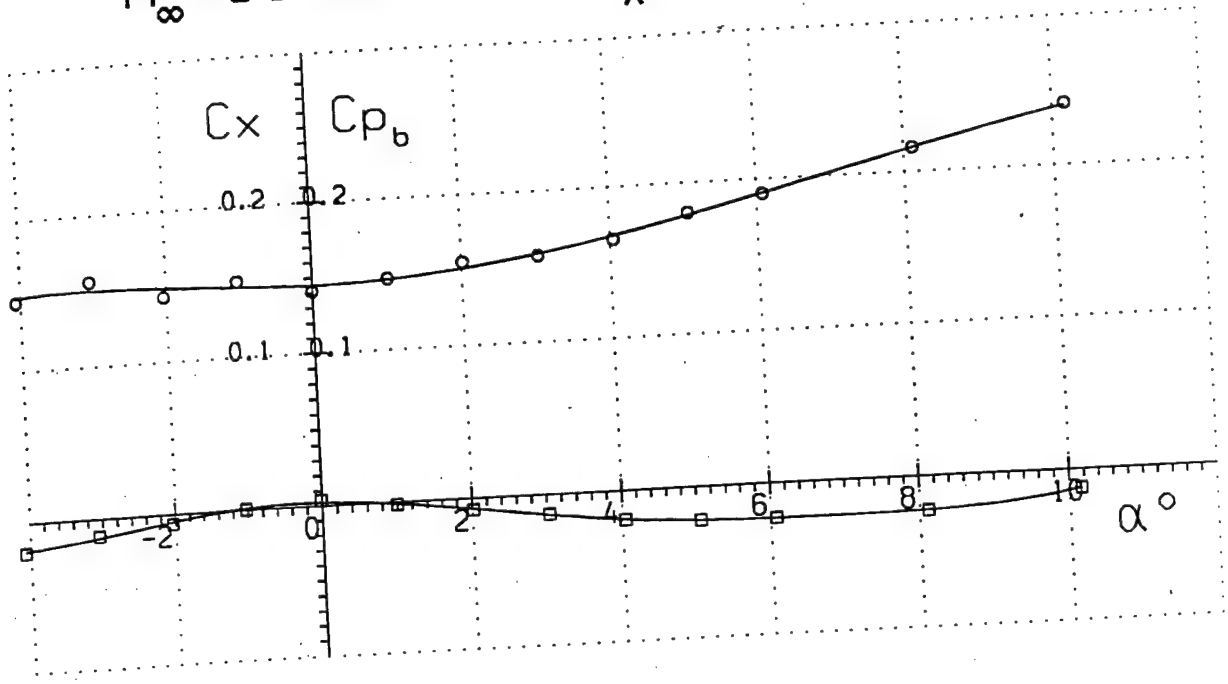

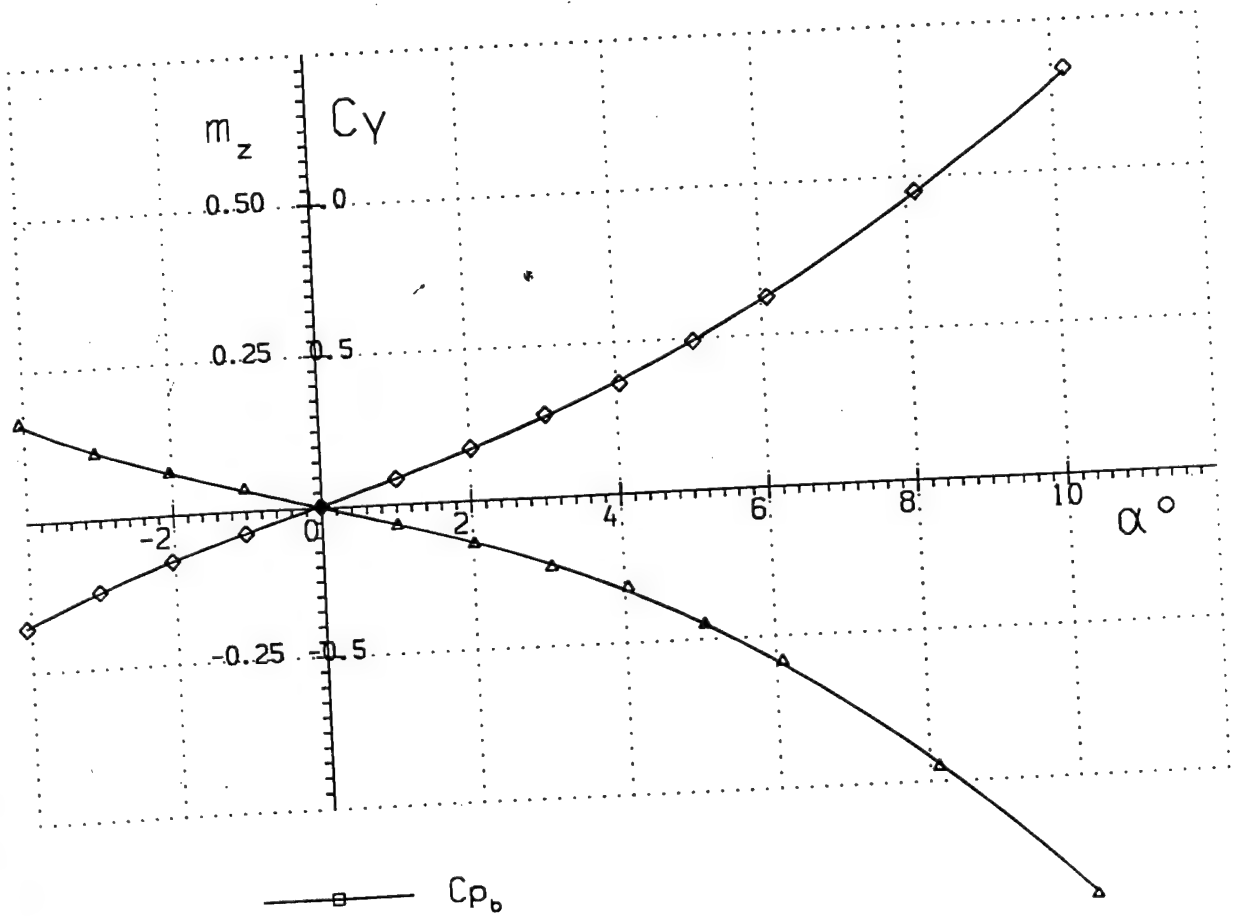

Run 15

Fig. 46

$M_\infty = 6.05$ $Re_x = 1.85 \cdot 10^6$

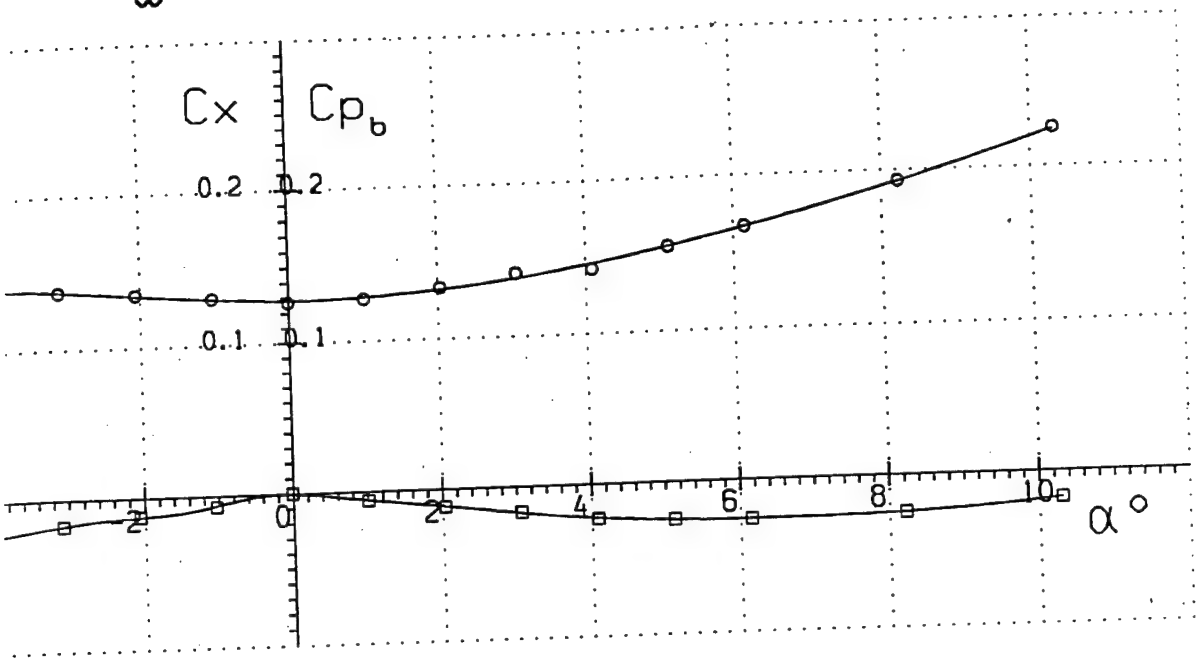

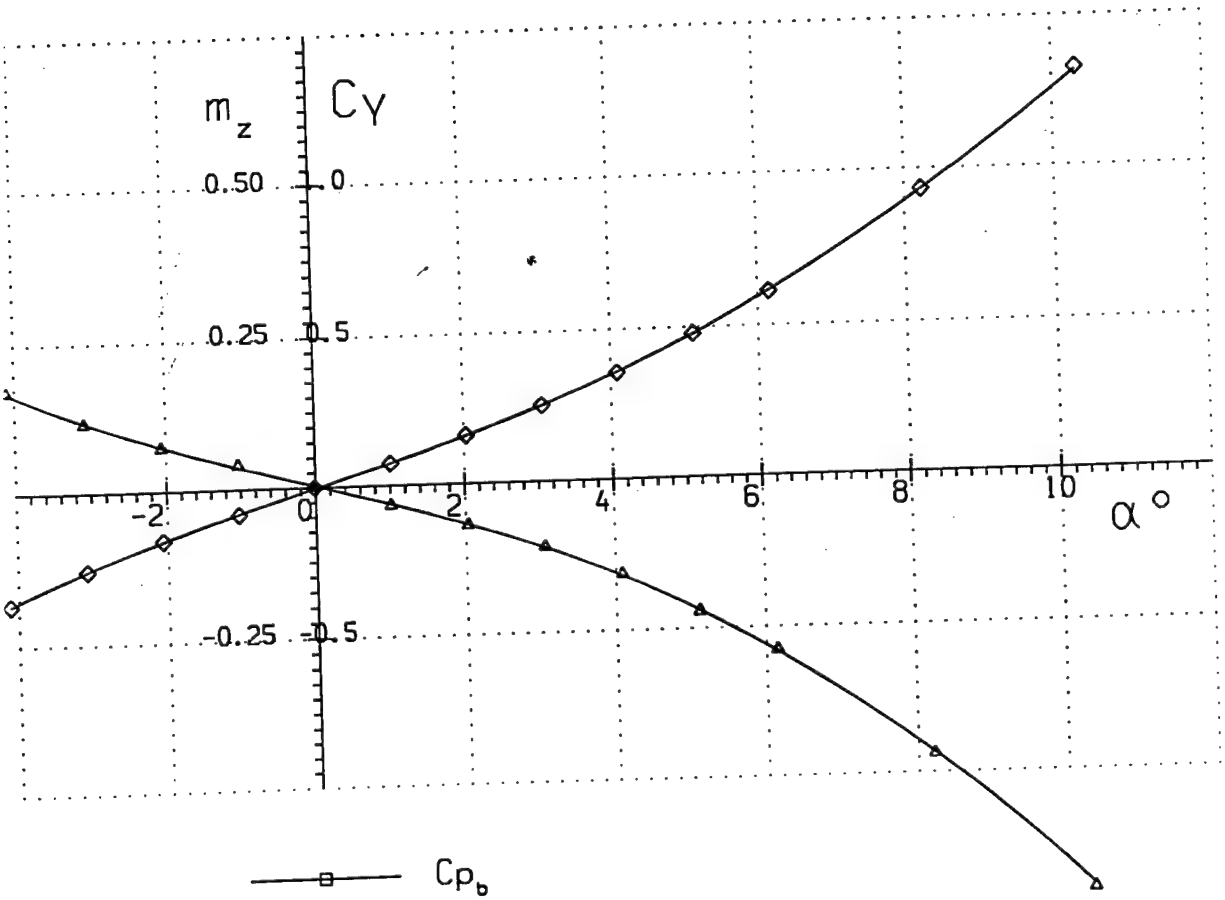

Cp_b
Cx
m_z
Cy

Run 16

Fig. 47

$M_\infty = 6.08$ $Re_x = 2.99 \cdot 10^6$

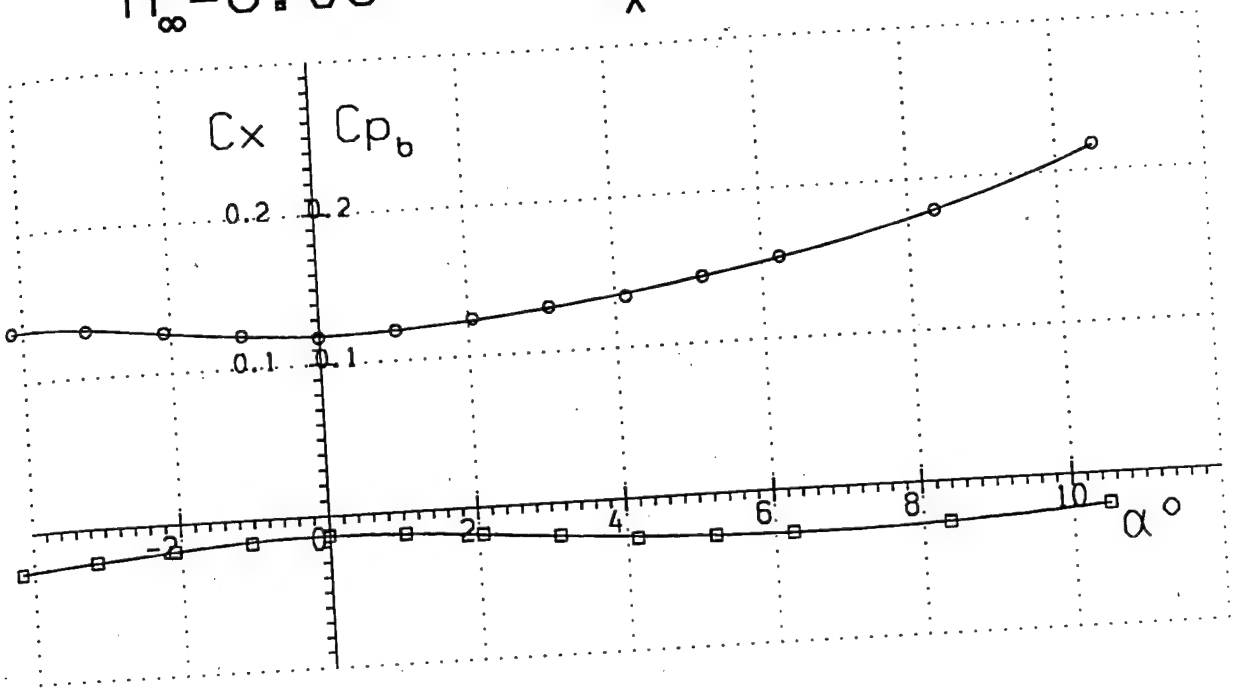

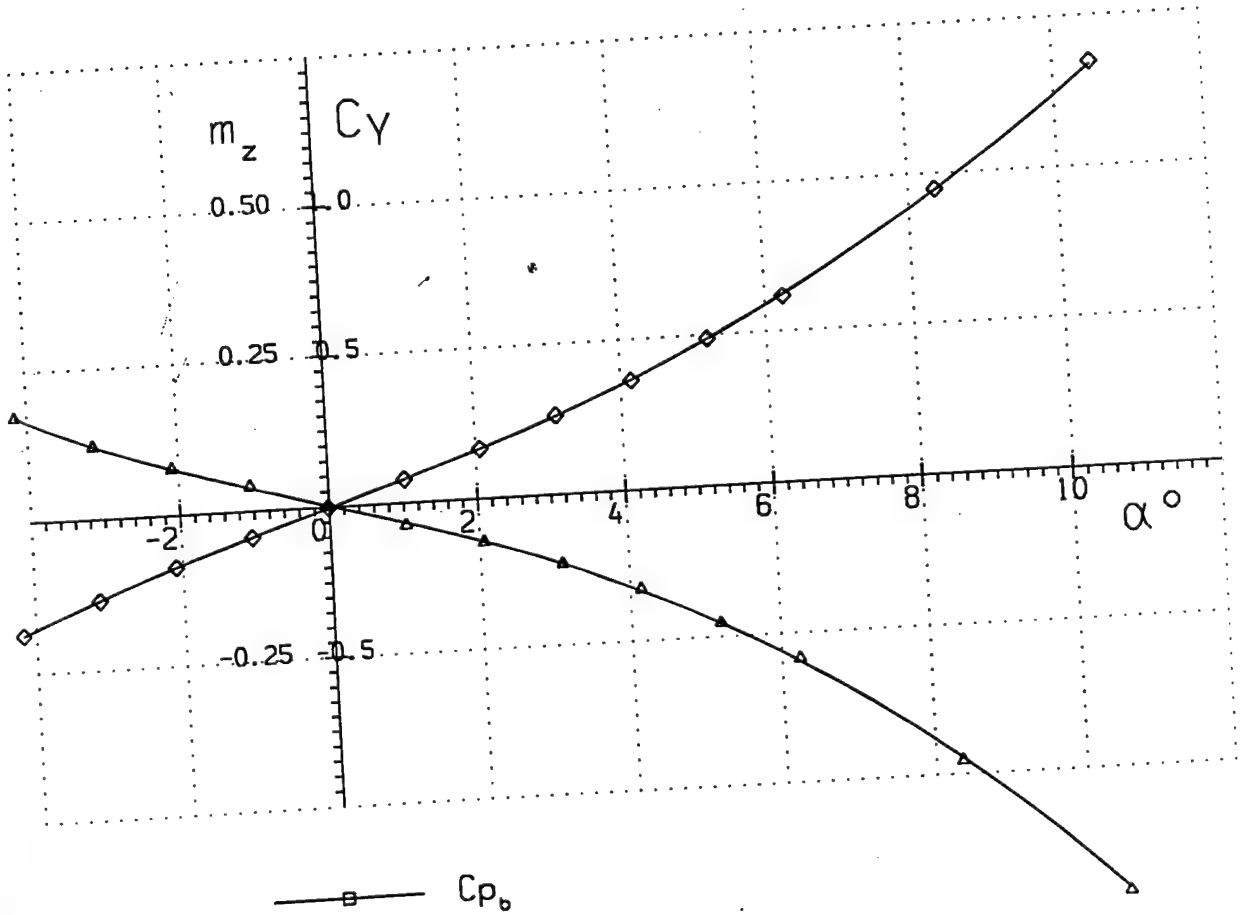

Cp_b
Cx
m_z
Cy

Run 17

Fig. 48

$M_\infty = 6.96$ $Re_x = 1.69 \cdot 10^6$

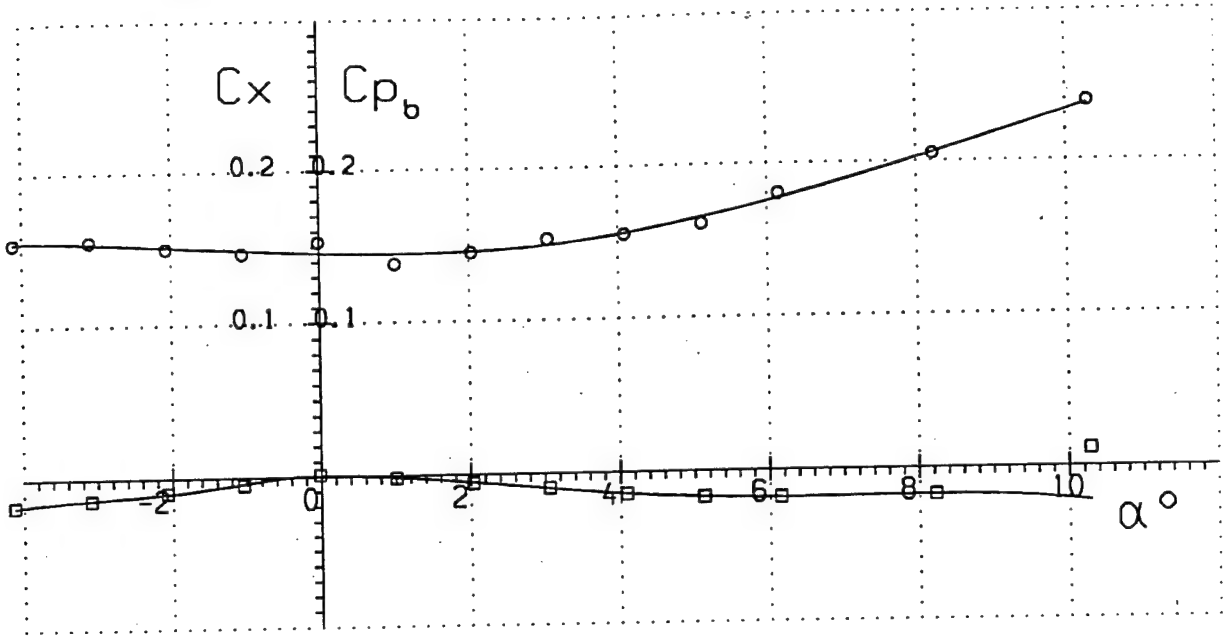

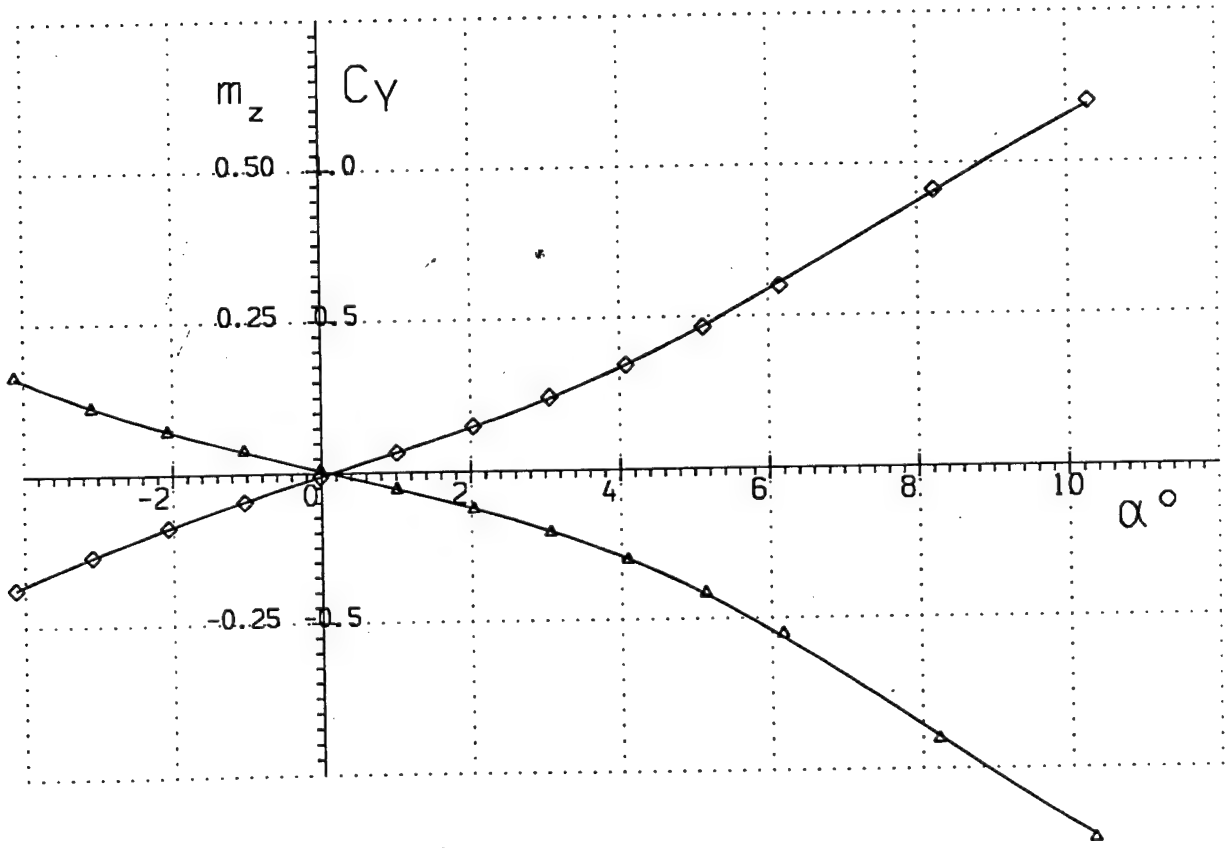

Cp_b
Cx
m_z
Cy

Run 18

Fig. 49

$M_\infty = 7.03$ $Re_x = 2.27 \cdot 10^6$

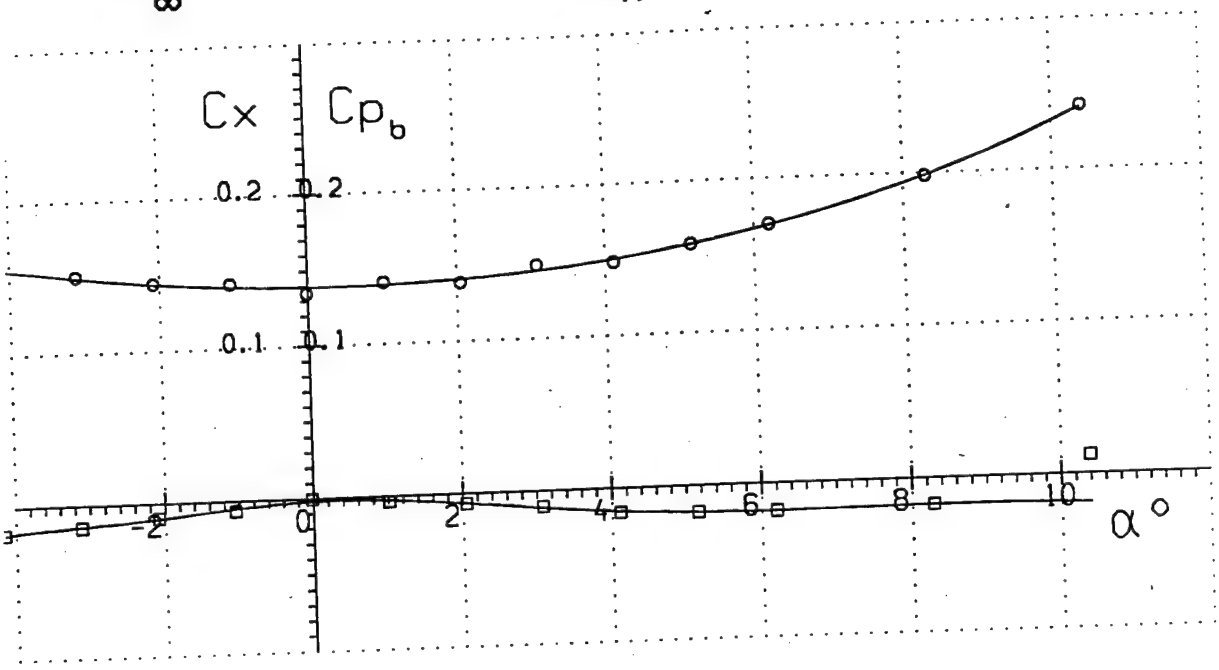

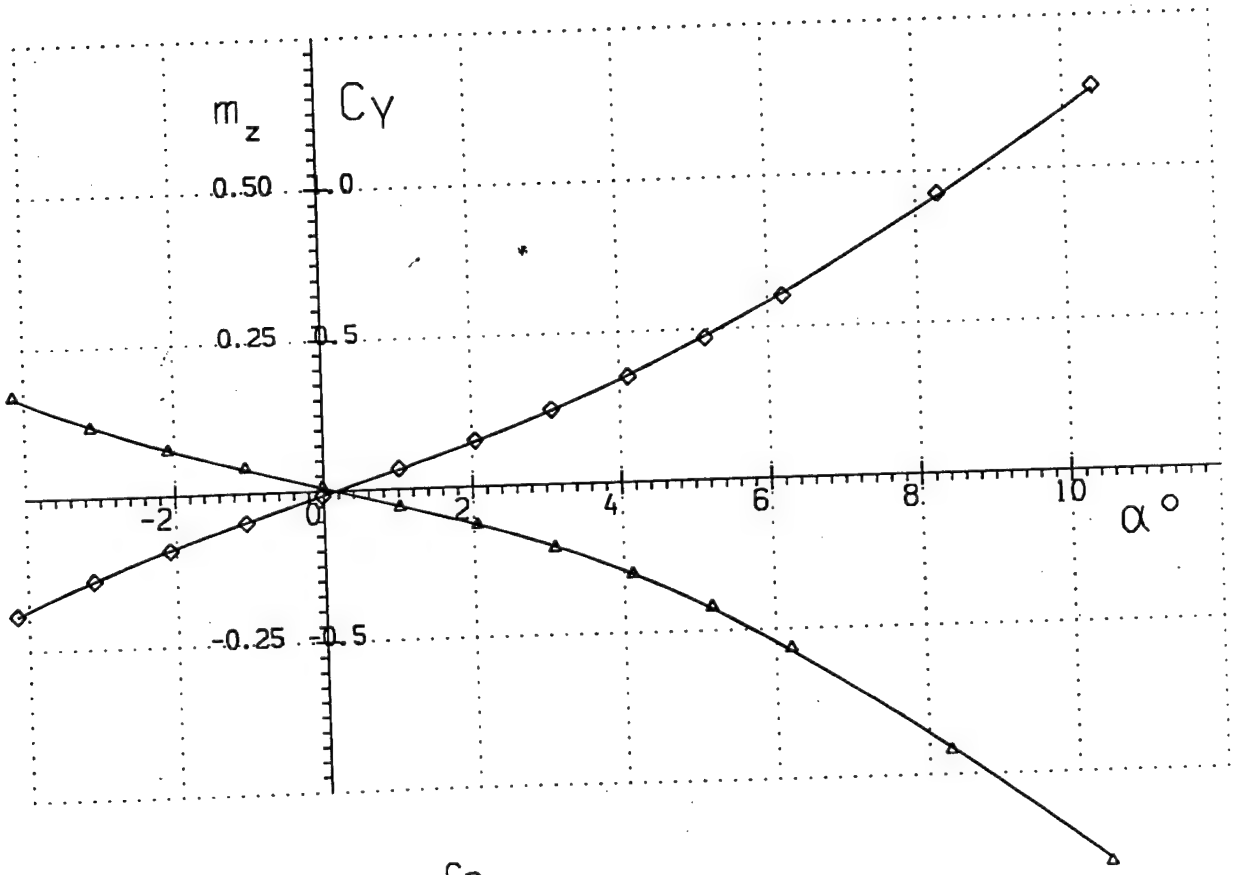

Cp_b
Cx
m_z
Cy

Run 19

Fig. 50

$M_\infty = 7.05$ $Re_x = 2.74 \cdot 10^6$

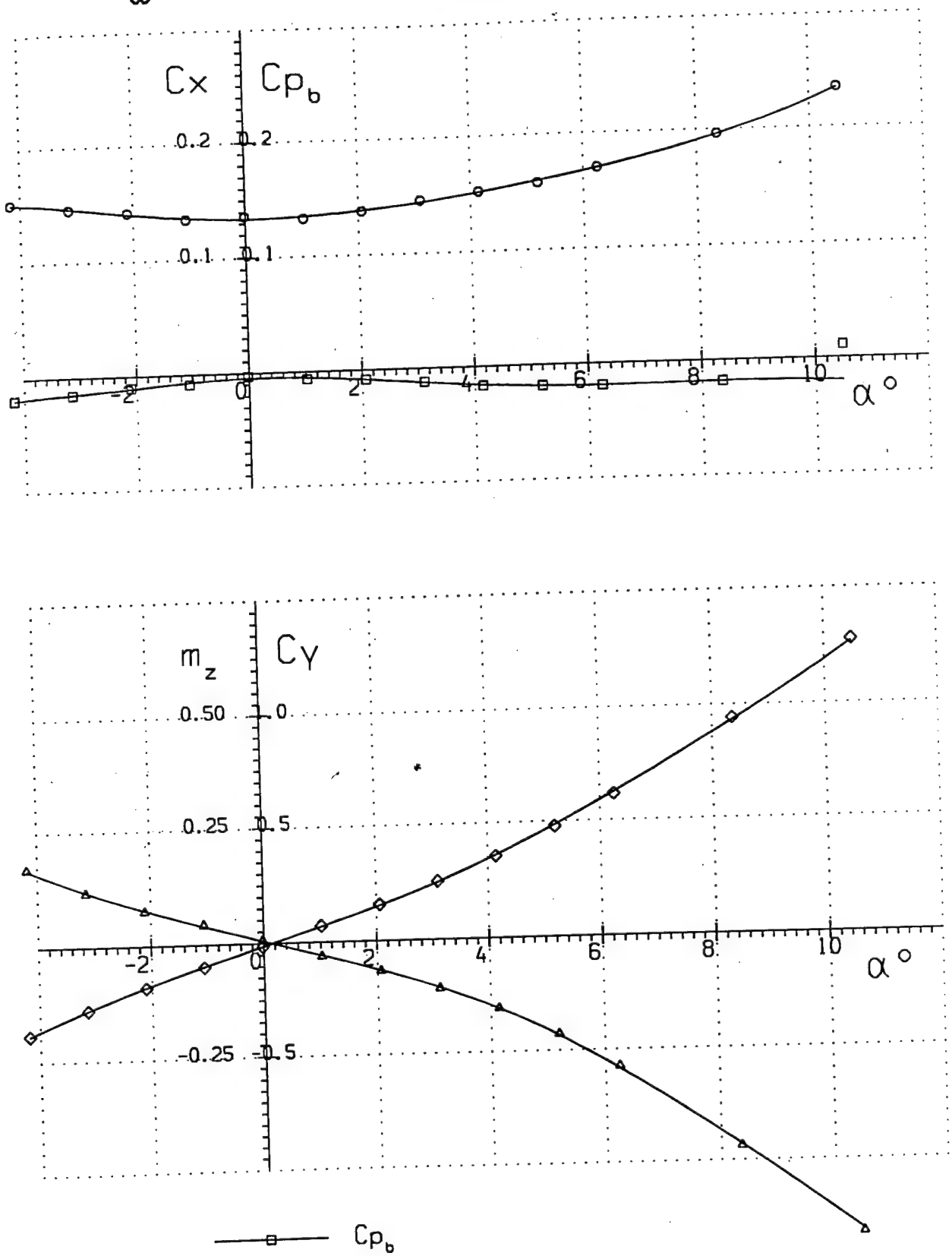

Cp_b
Cx
m_z
Cy

Run 20

Fig. 51

$M_\infty = 7.07$ $Re_x = 4.39 \cdot 10^6$

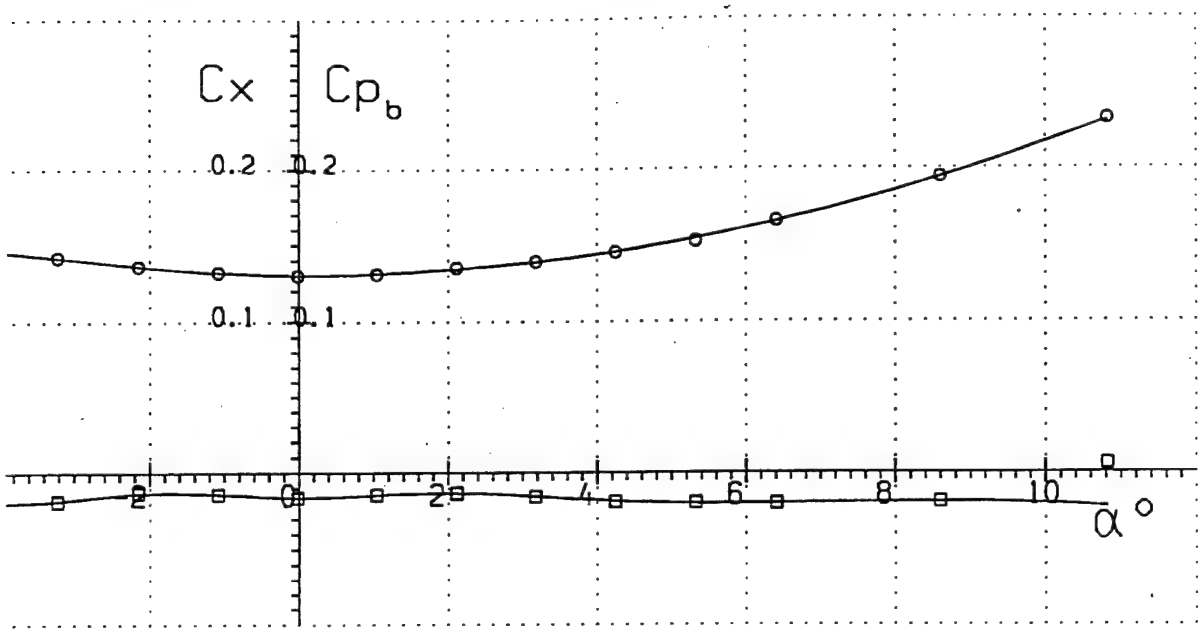

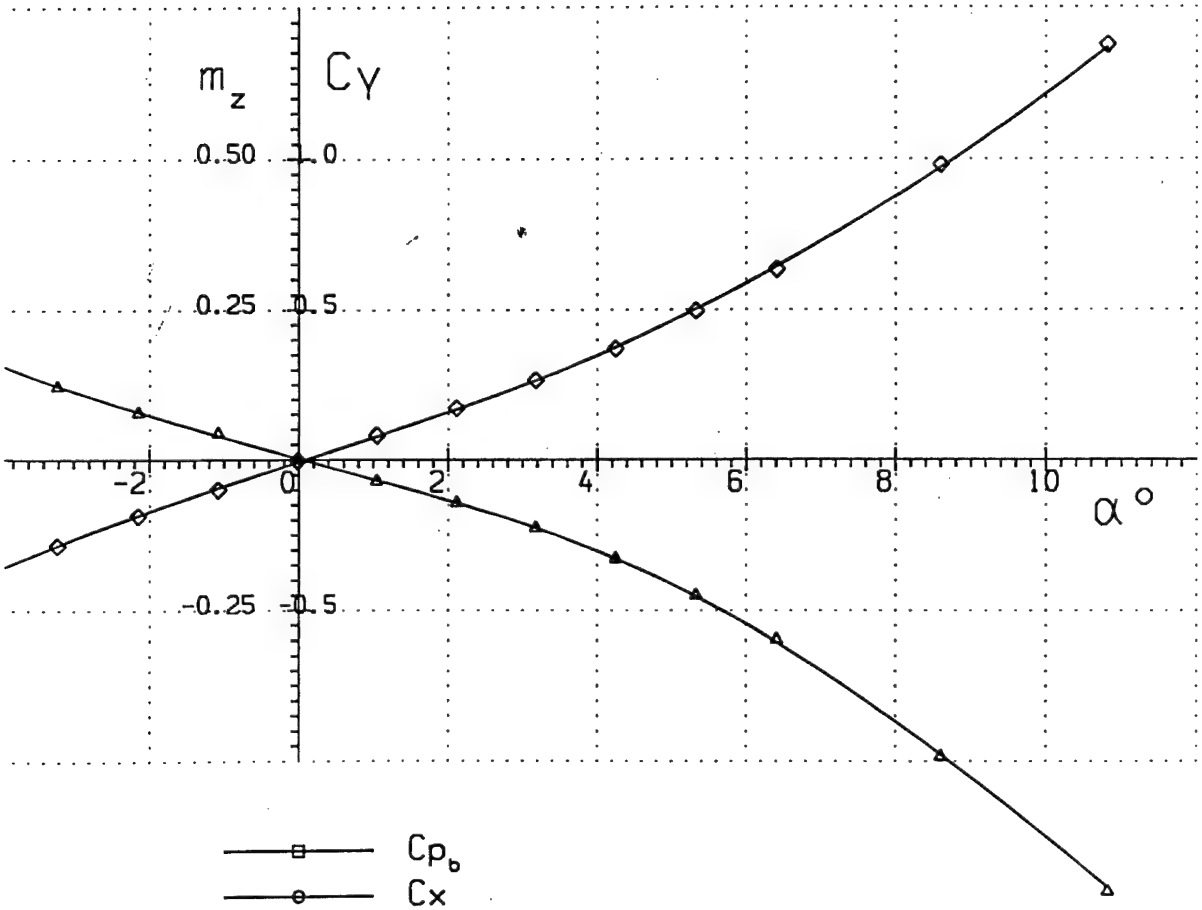

Cp_b
Cx
m_z
Cy

Run 21

Fig. 52

$M_\infty = 7.07$ $Re_x = 6.26 \cdot 10^6$

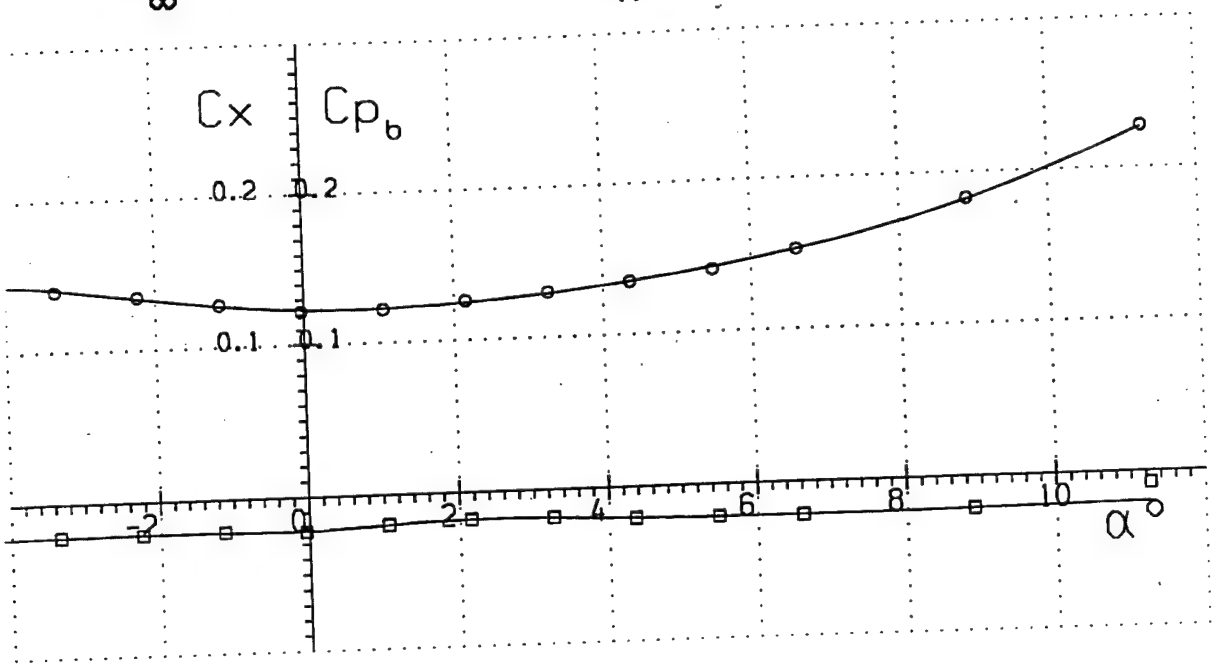

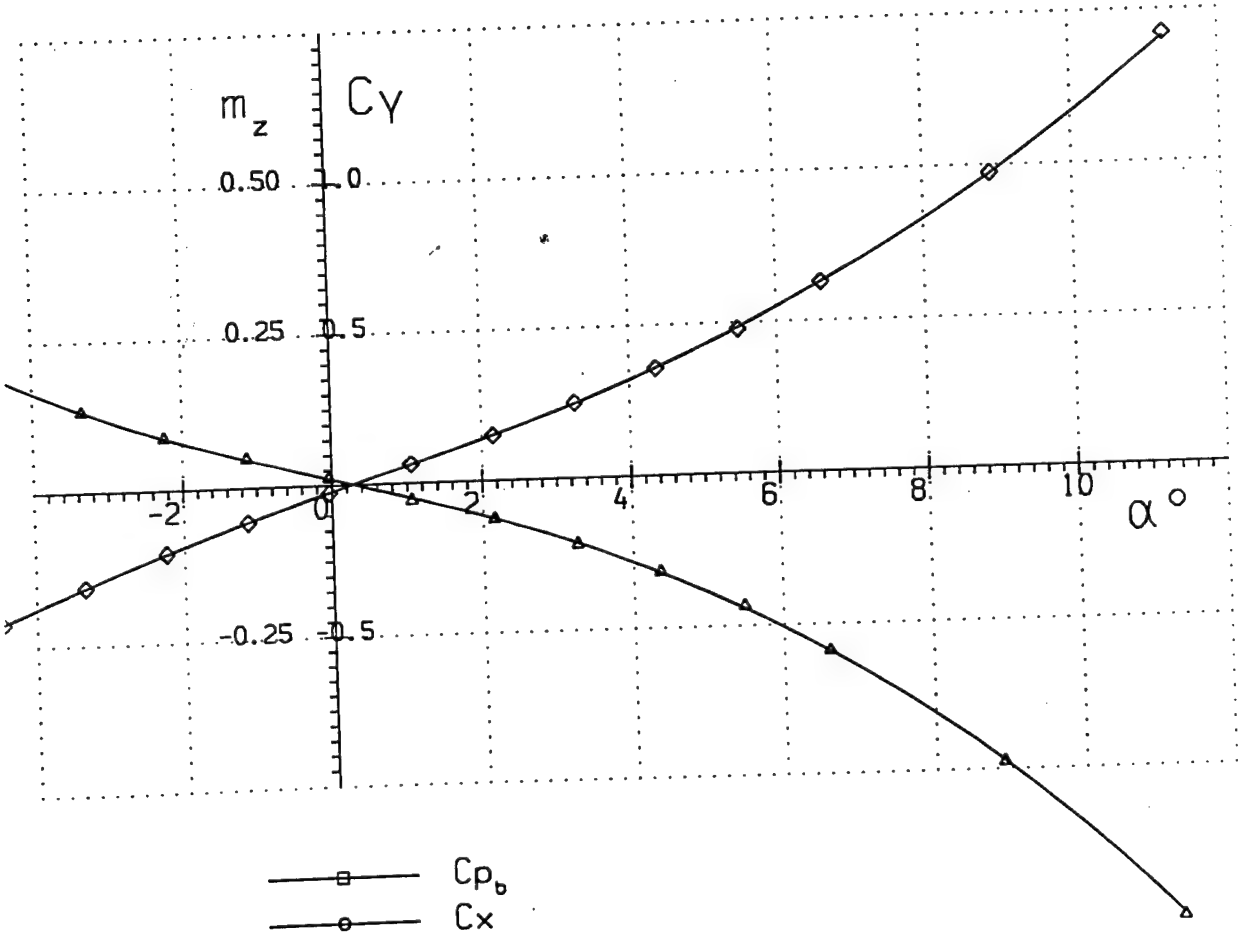

Cp_b
Cx
m_z
Cy

Run 22

Fig. 53

$M_\infty = 7.97$ $Re_x = 1.28 \cdot 10^6$

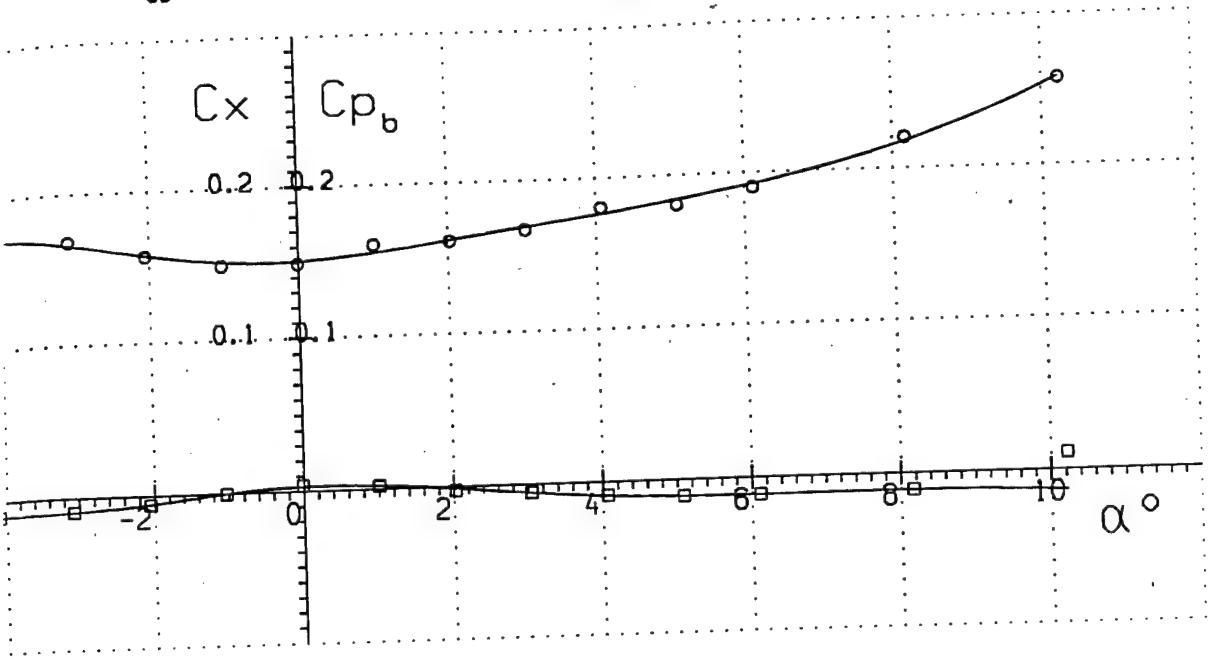

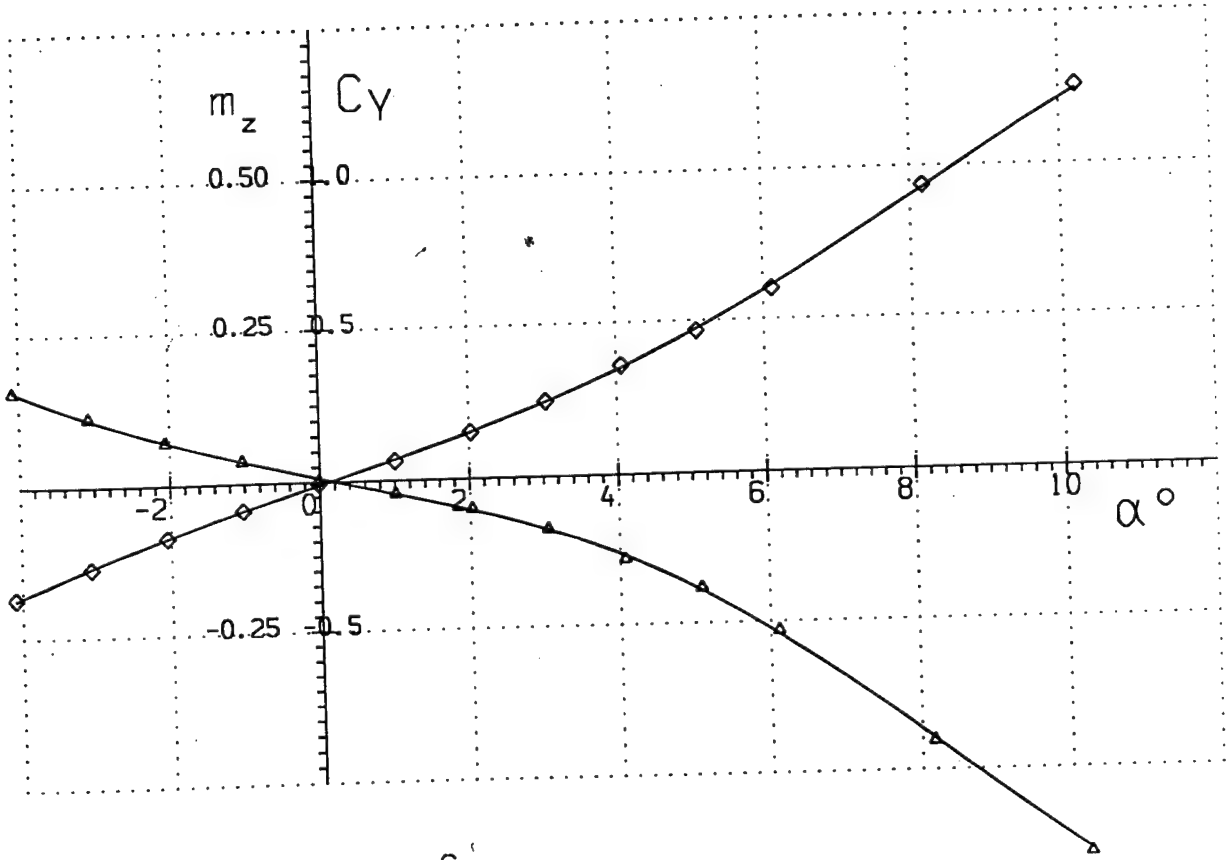

Cp_b
Cx
m_z
Cy

Run 23

Fig. 54

$M_\infty = 8.00$ $Re_x = 2.00 \cdot 10^6$

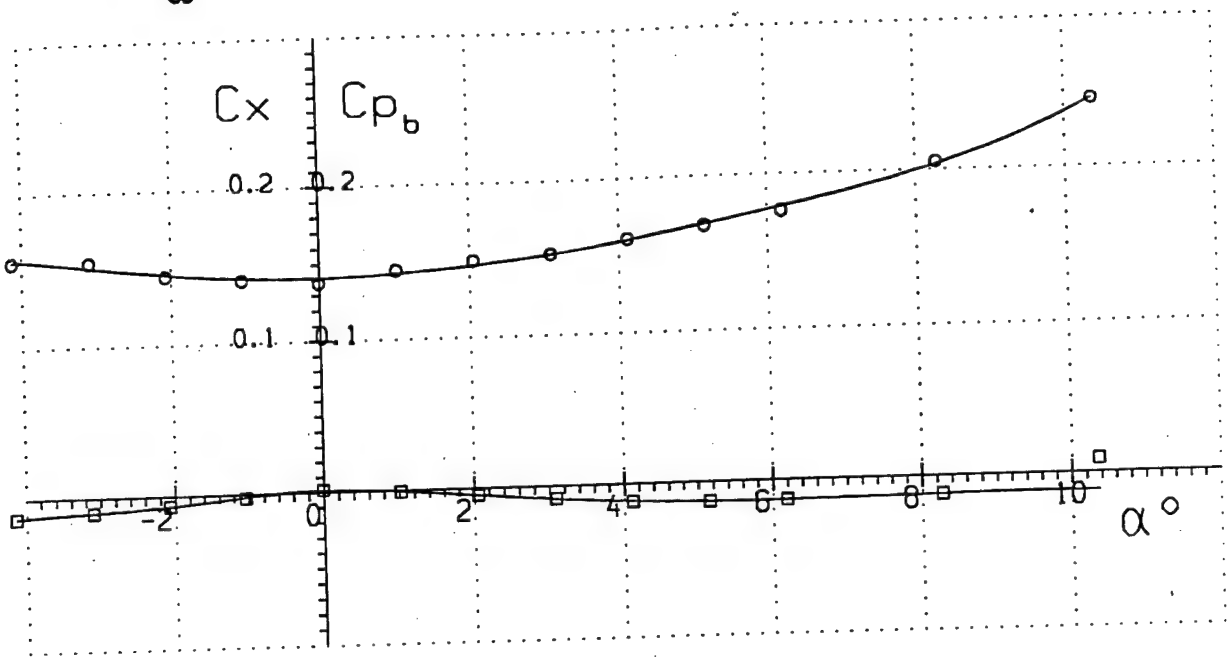

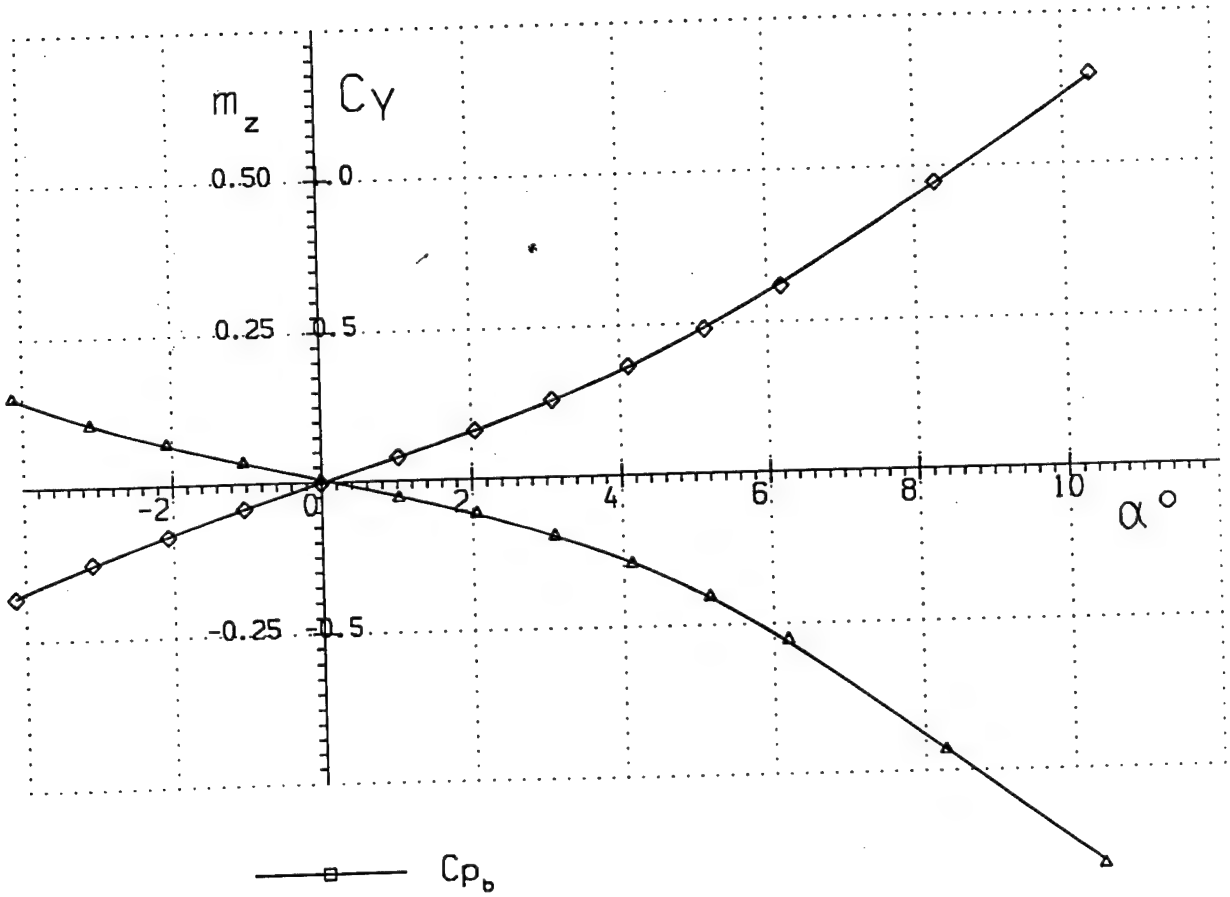

Cp_b
Cx
m_z
Cy

Run 24

Fig. 55

$M_\infty = 8.03$ $Re_x = 3.30 \cdot 10^6$

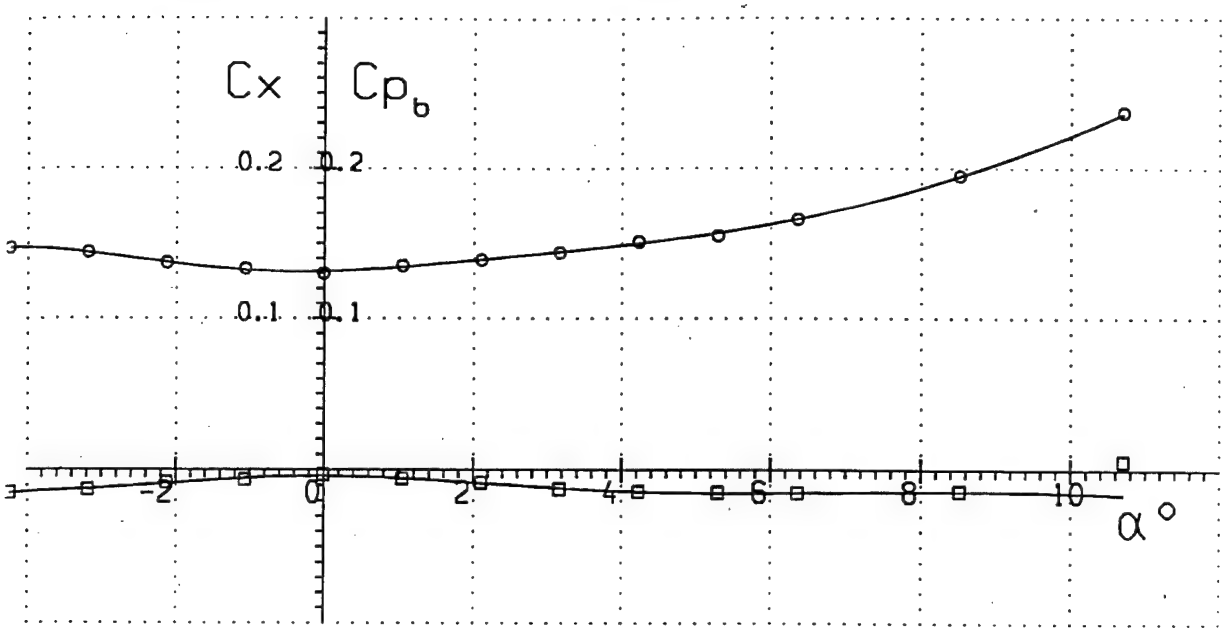

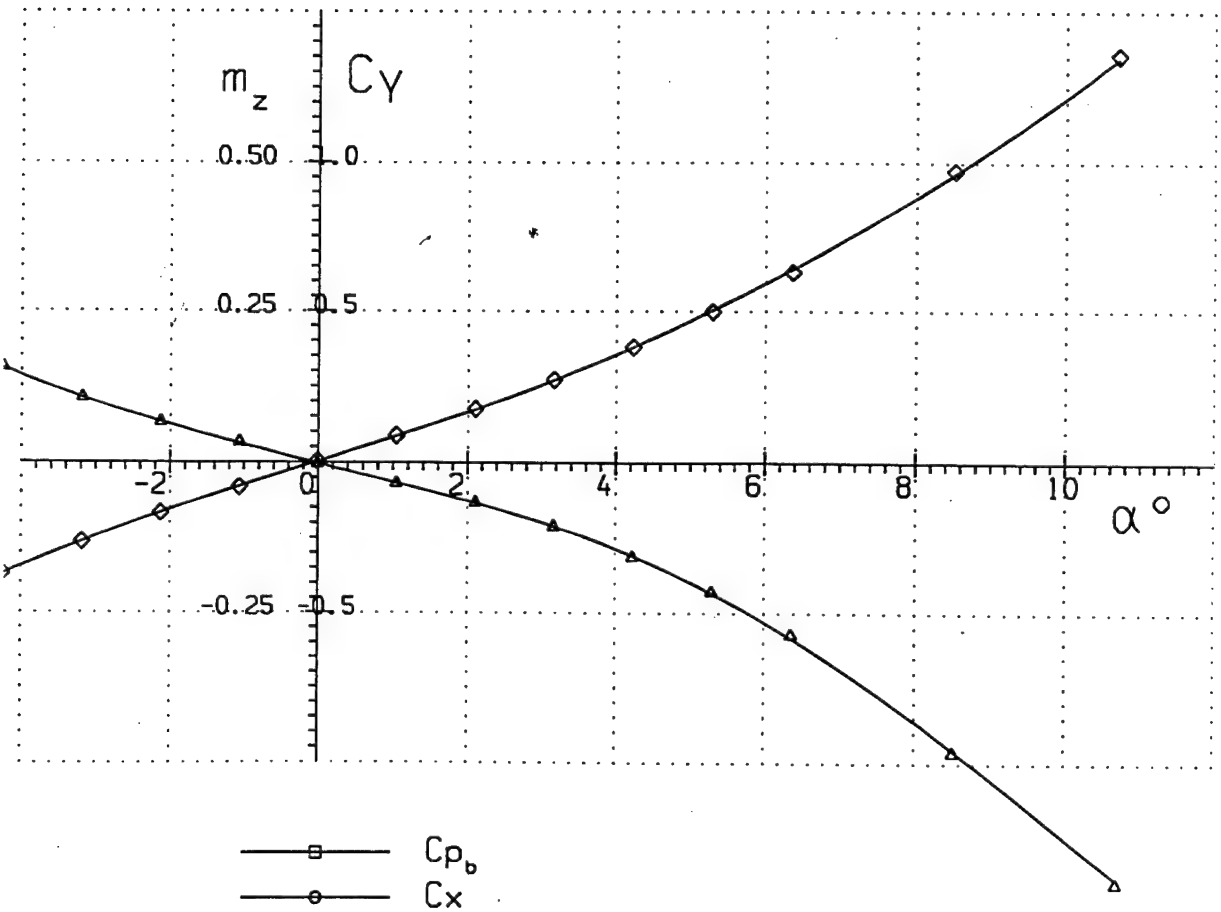

Cp_b
Cx
m_z
Cy

Run 25

Fig. 56

$M_\infty = 8.96$ $Re_x = 1.21 \cdot 10^6$

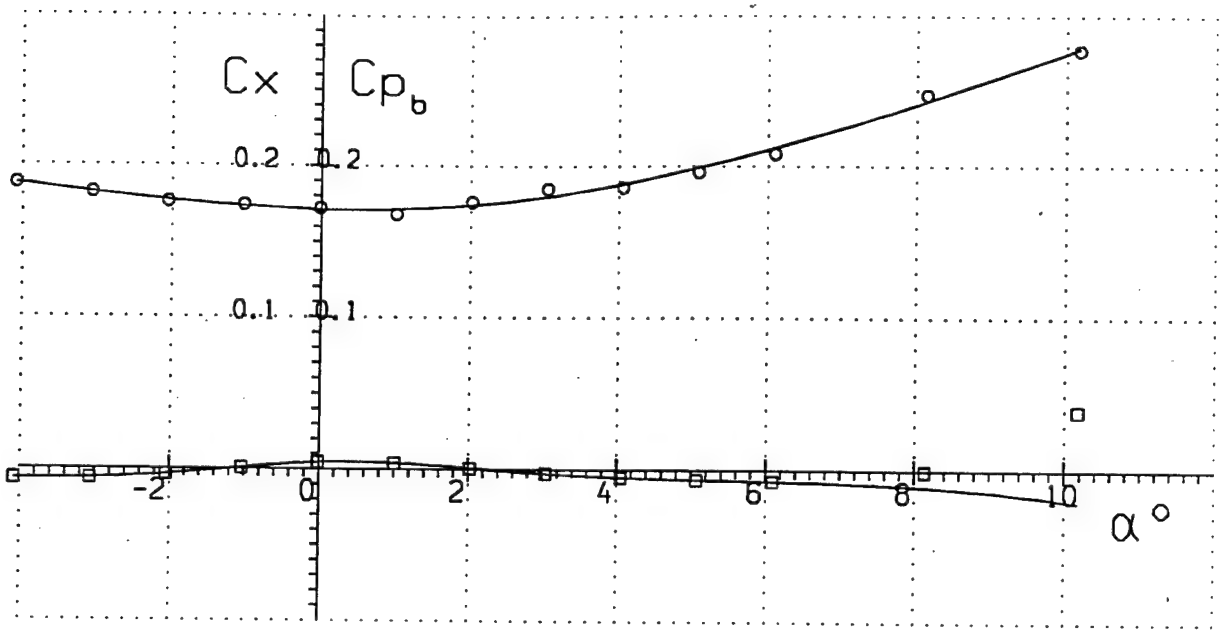

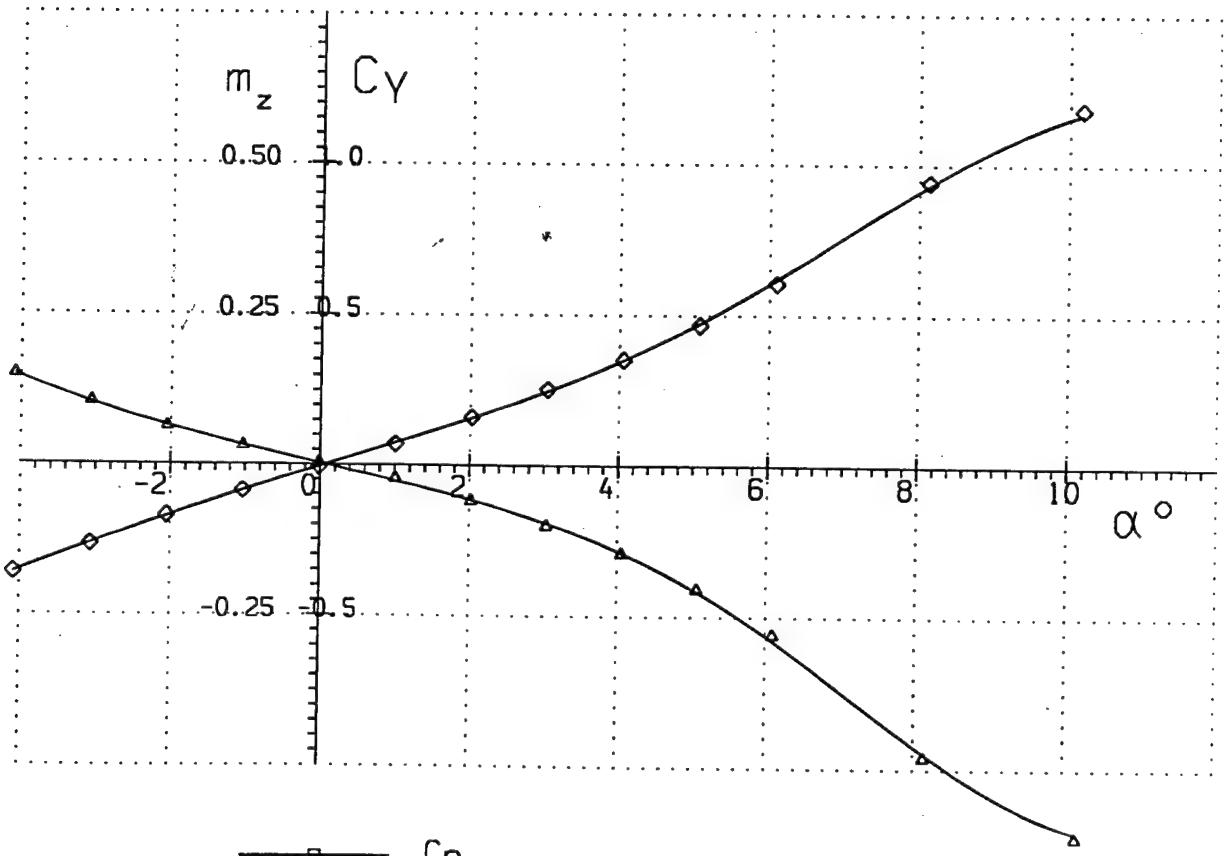

Cp_b
Cx
m_z
Cy

Run 26

Fig. 57

$M_\infty = 9.04$ $Re_x = 2.23 \cdot 10^6$

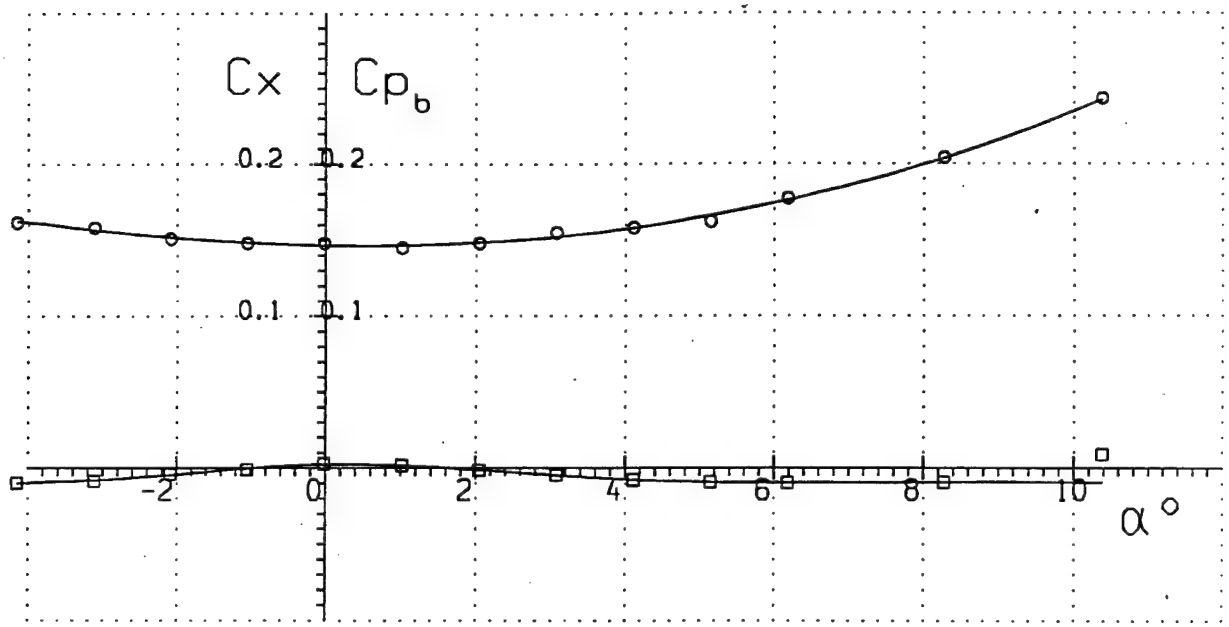

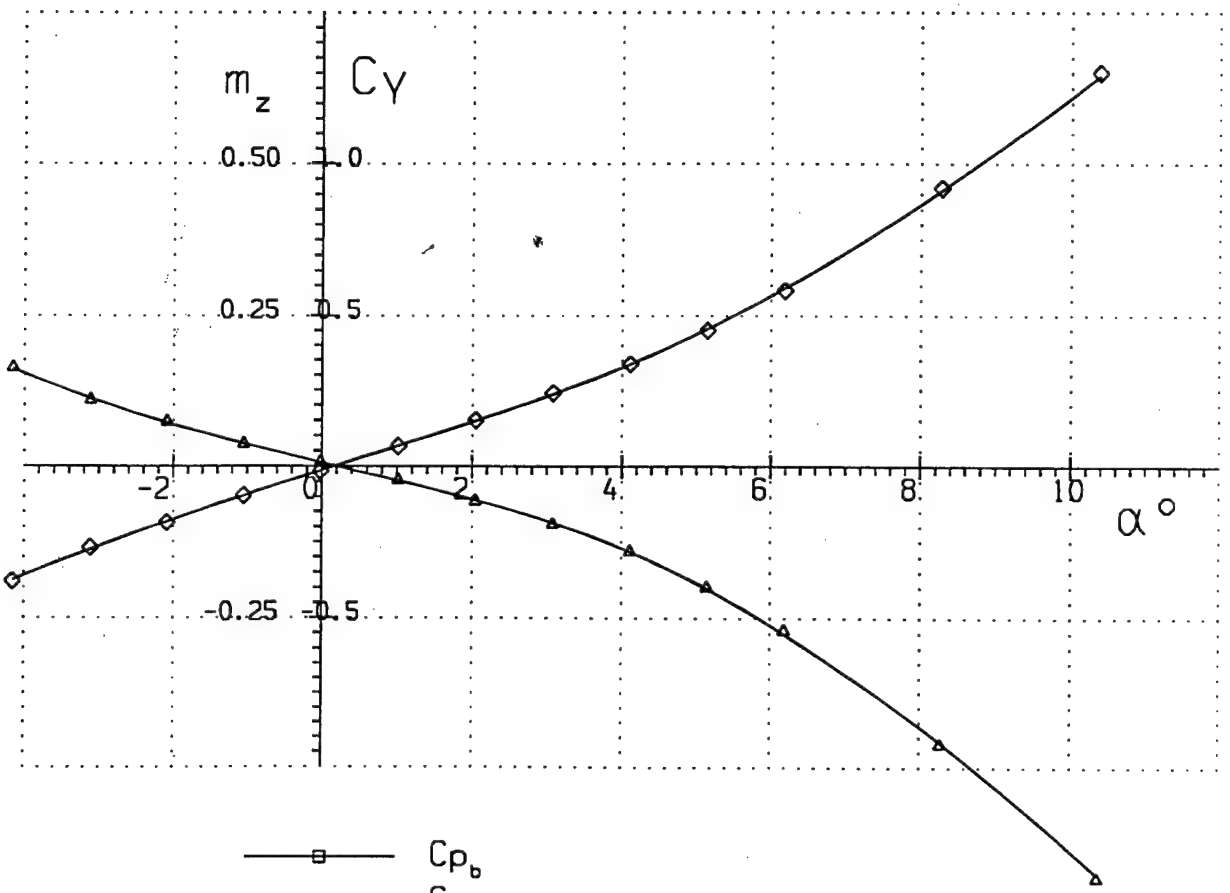

Cp_b
Cx
m_z
Cy

Run 27

Fig. 58

$M_\infty = 4.00$ $Re_x = 1.16 \cdot 10^6$

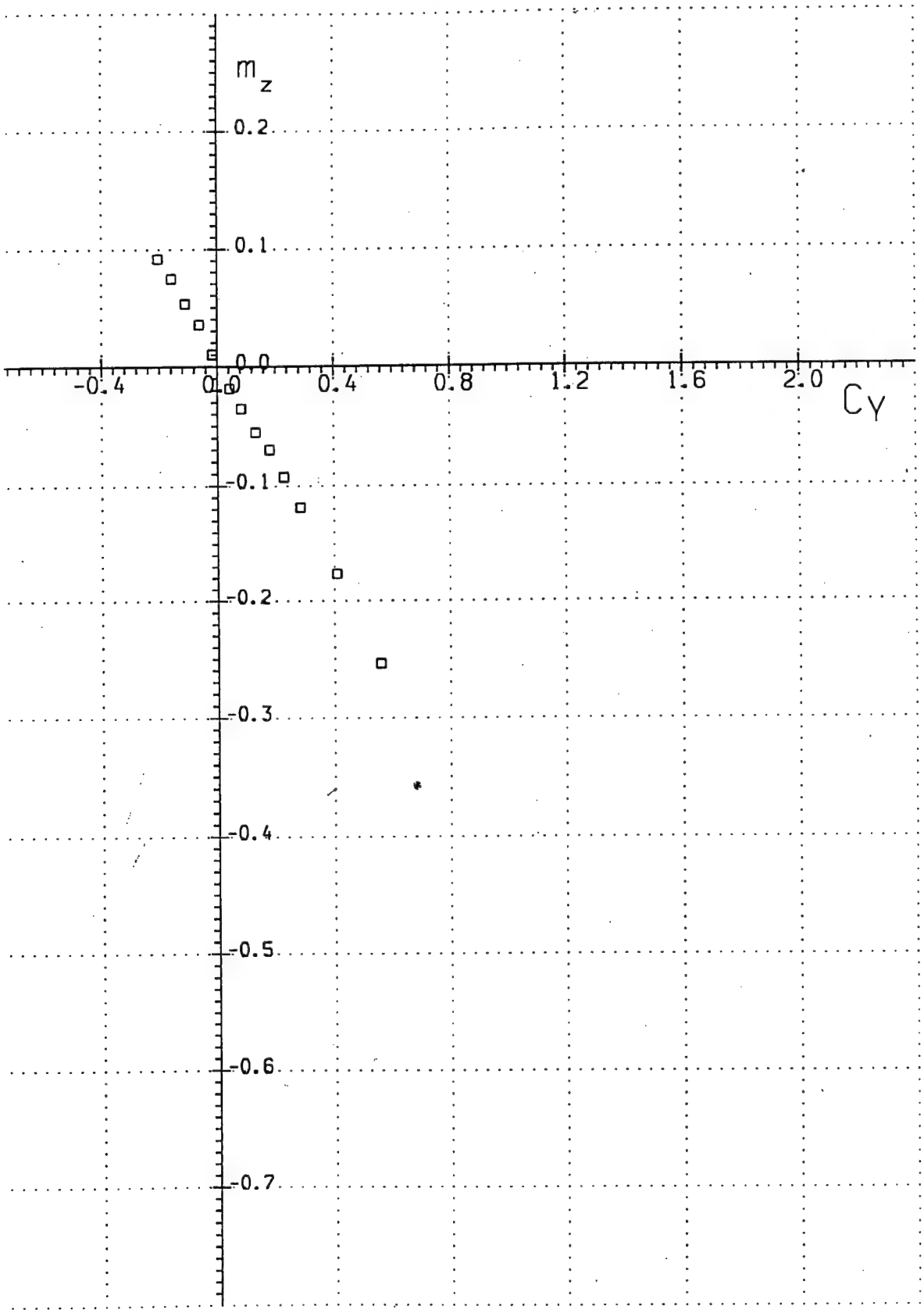

Run 1

Fig. 59

$M_\infty = 4.01$ $Re_x = 1.45 \cdot 10^6$

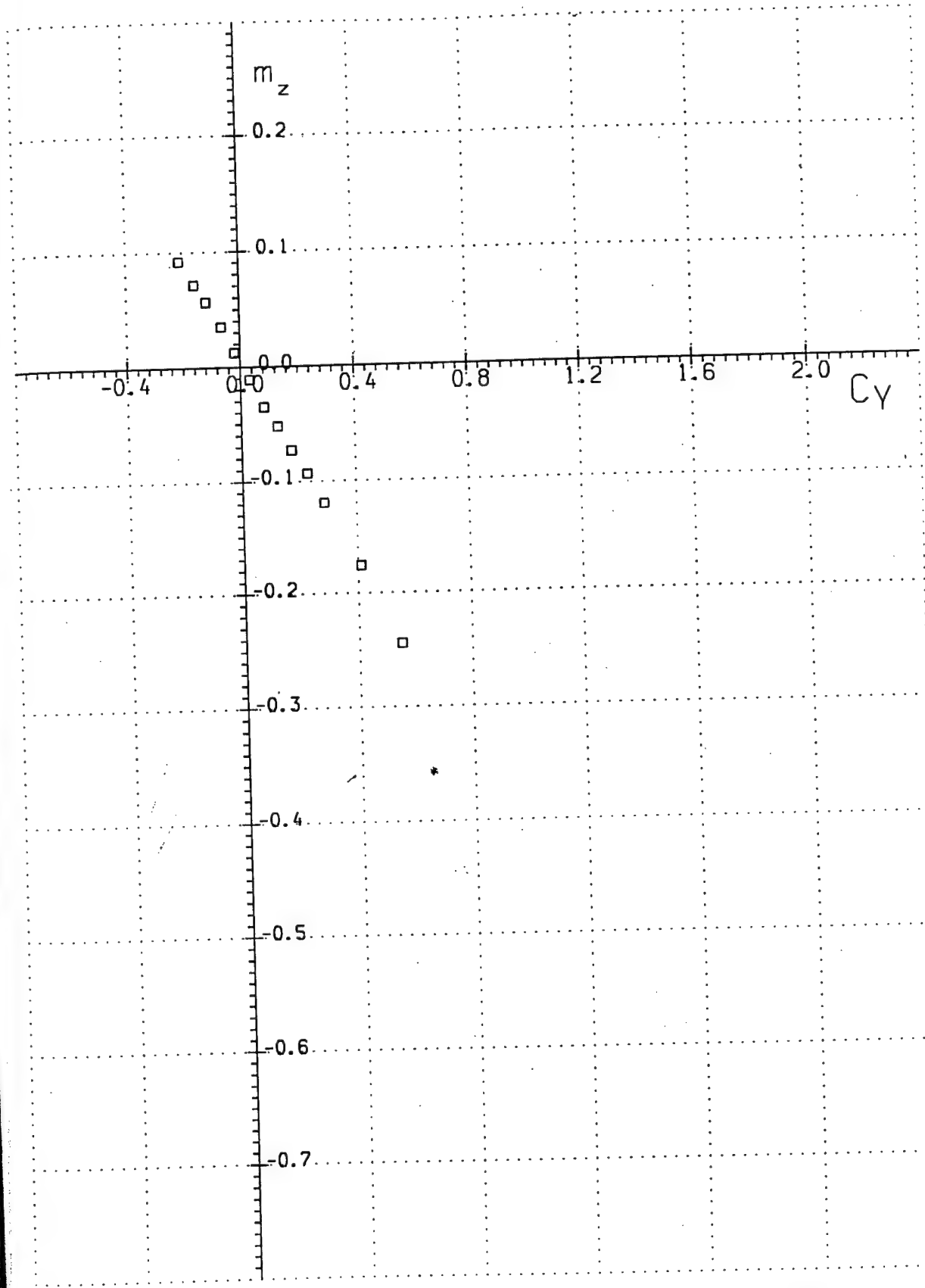

Run 2

Fig. 60

$M_\infty = 4.02$ $Re_x = 1.81 \cdot 10^6$

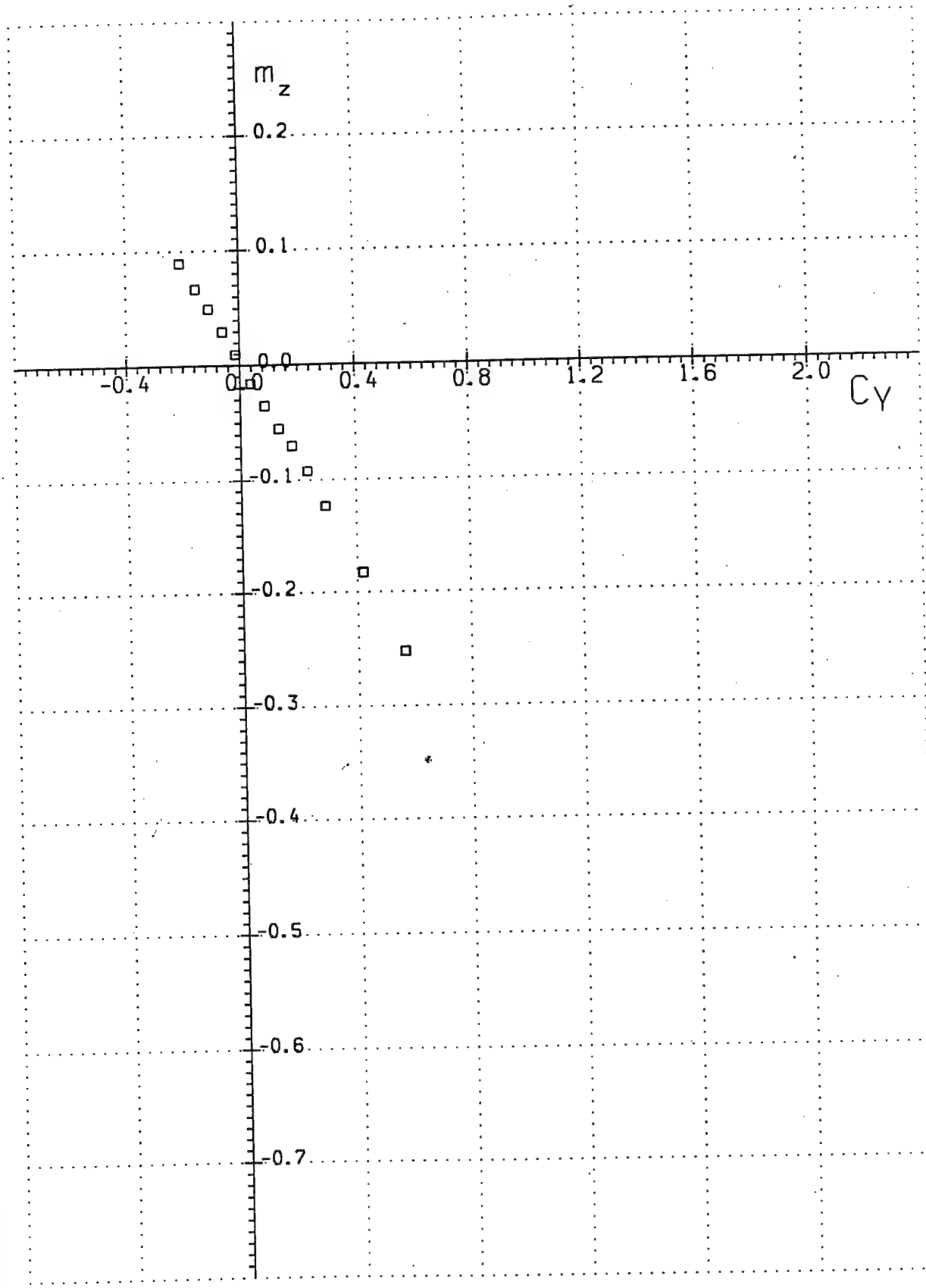

Run 3

Fig. 61

$M_\infty = 4.03$ $Re_x = 2.34 \cdot 10^6$

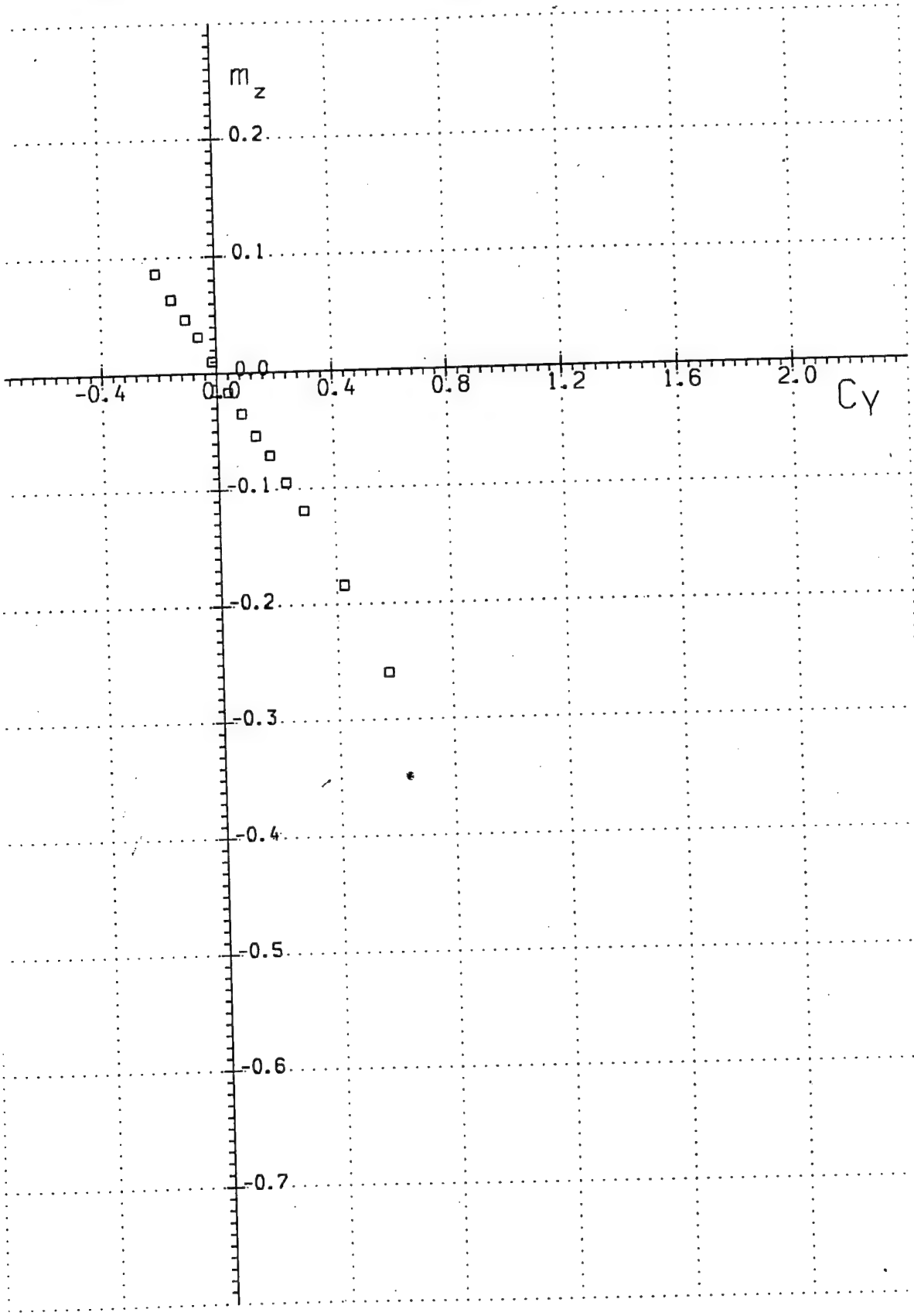

Run 4

Fig. 62

$M_\infty = 4.03$ $Re_x = 3.13 \cdot 10^6$

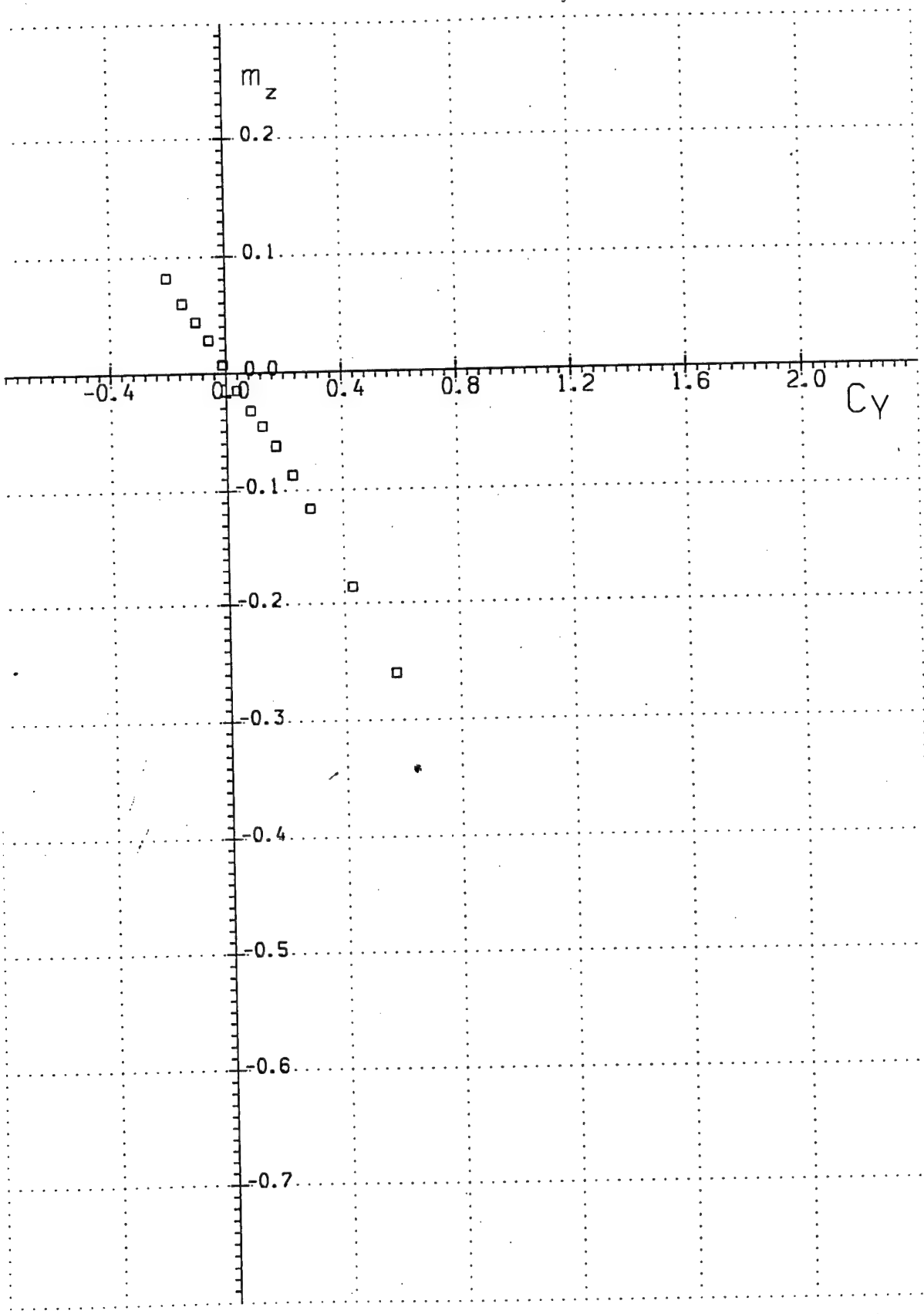

Run 5

Fig. 63

$M_\infty = 4.04$ $Re_x = 3.91 \cdot 10^6$

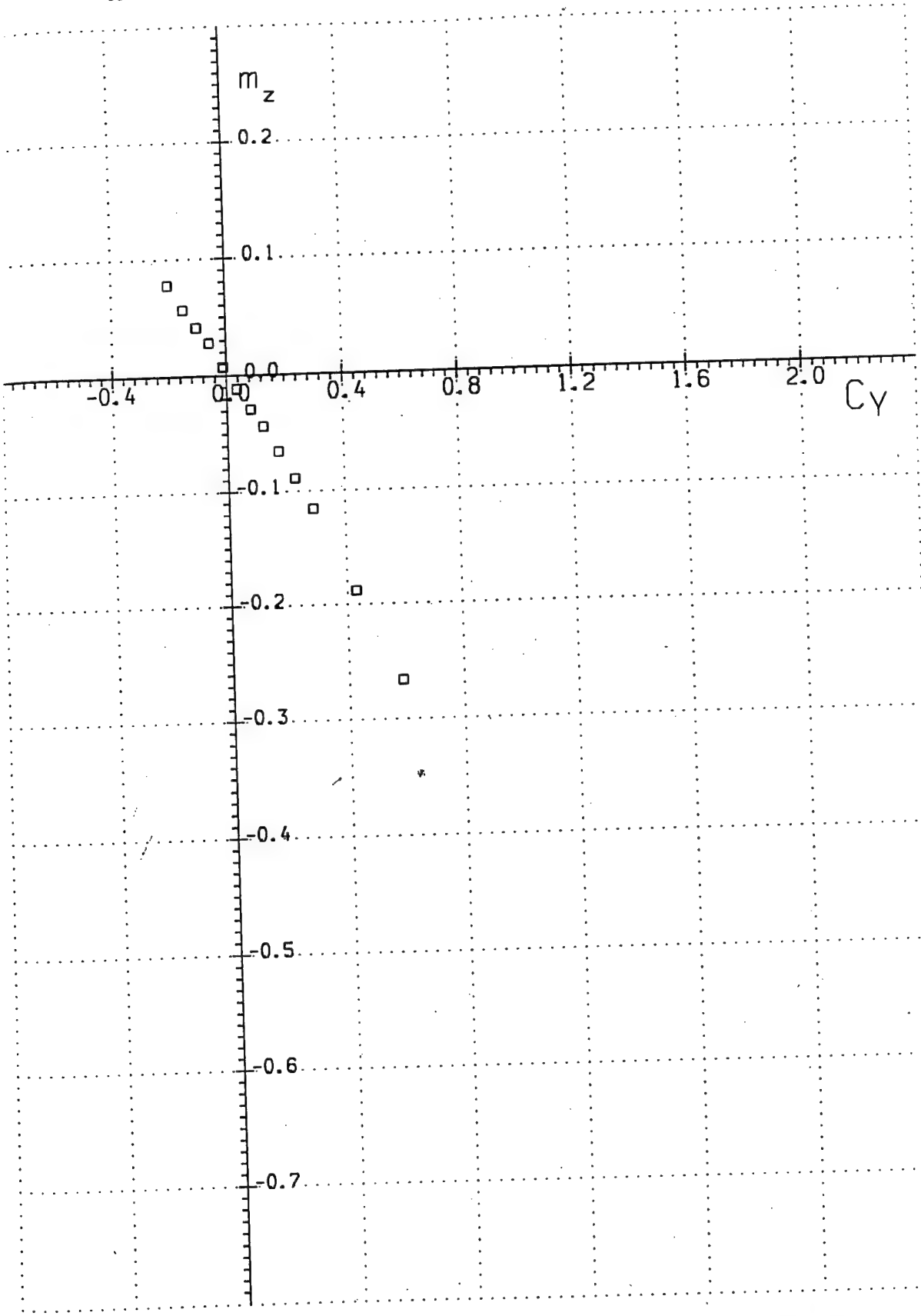

Run 6

Fig. 64

$M_\infty = 4.05$ $Re_x = 6.27 \cdot 10^6$

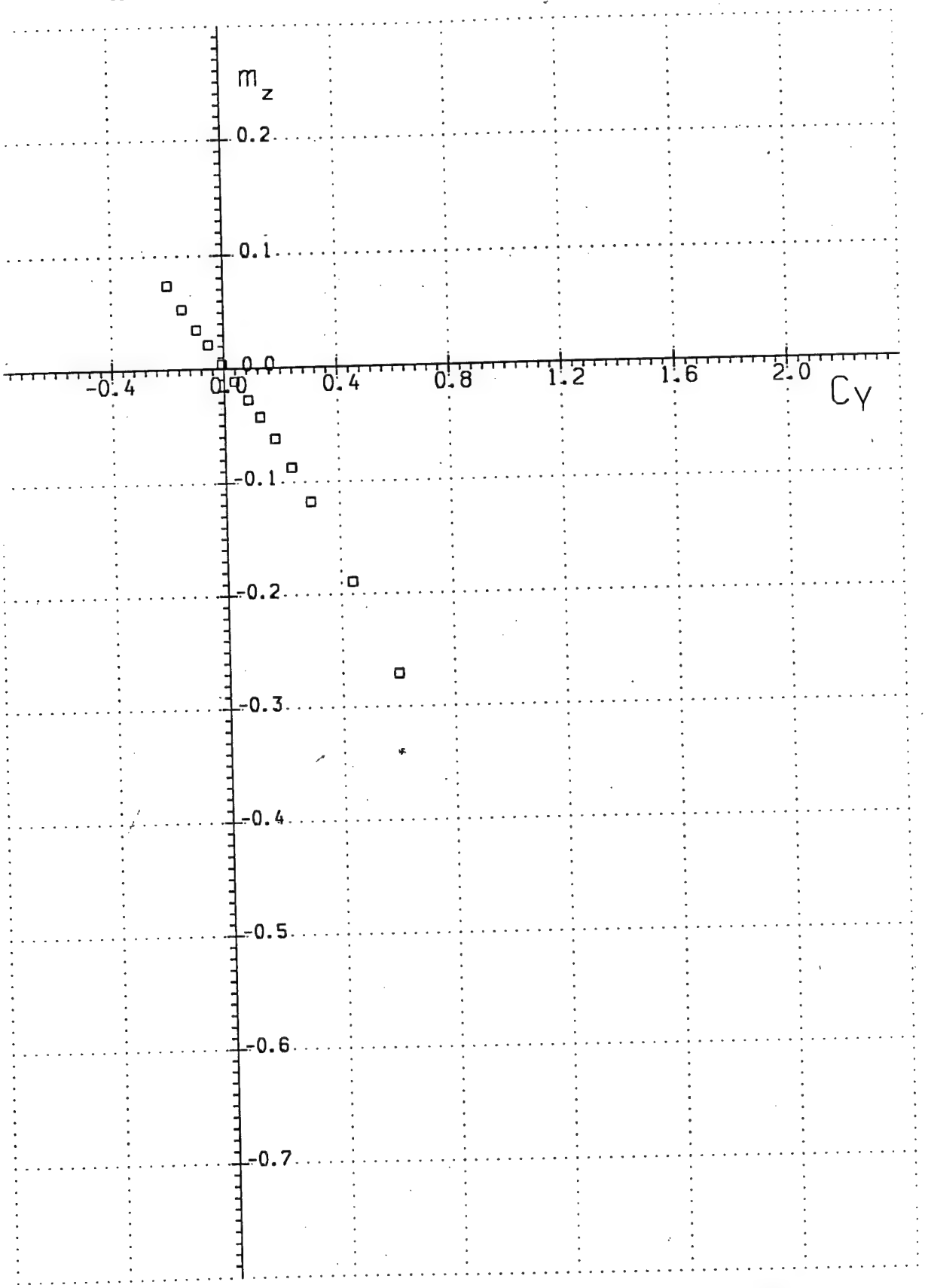

Run 7

Fig. 65

$M_\infty = 4.06$ $Re_x = 8.60 \cdot 10^6$

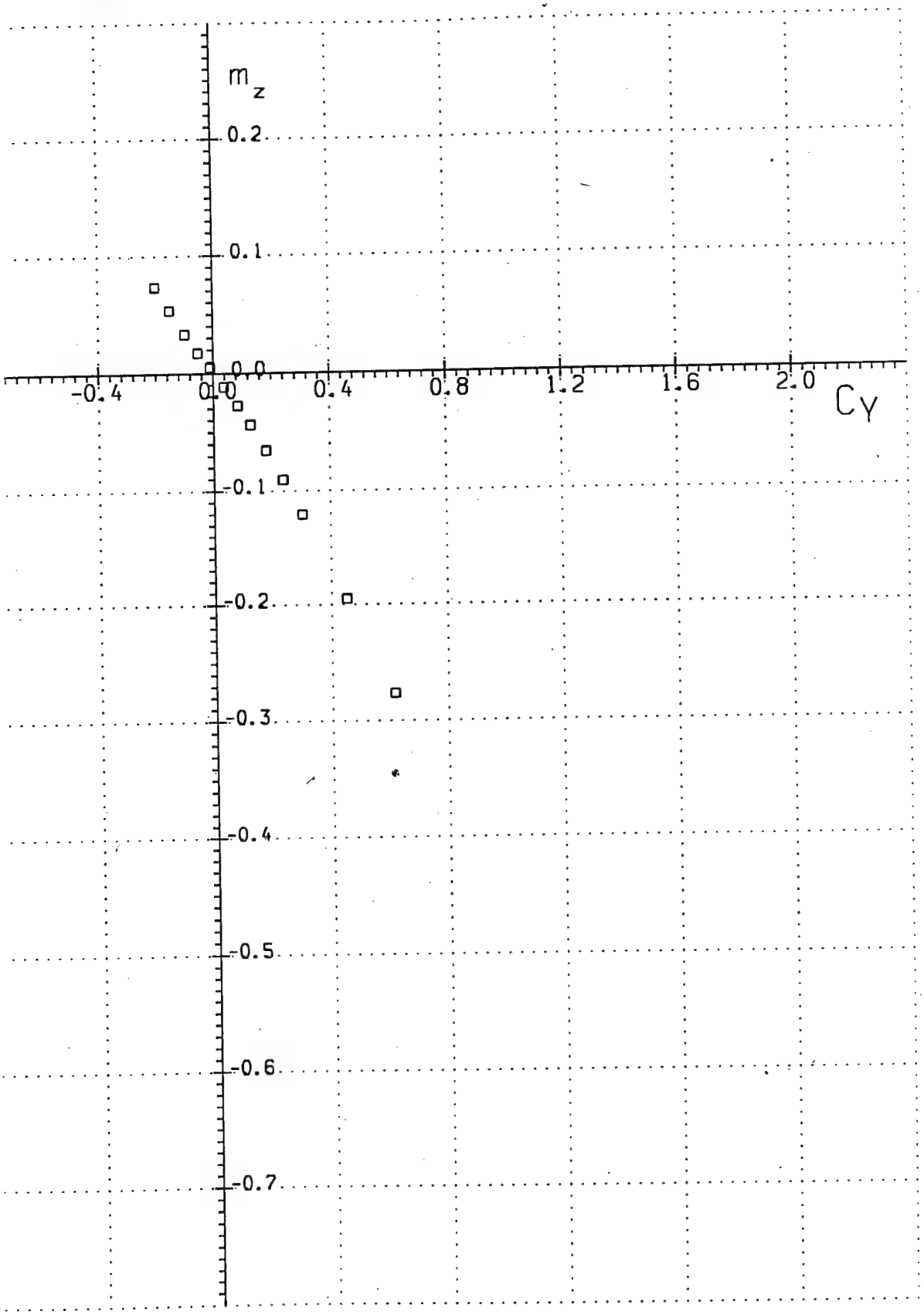

Run 8

Fig. 66

$M_\infty = 4.96$ $Re_x = .90 \cdot 10^6$

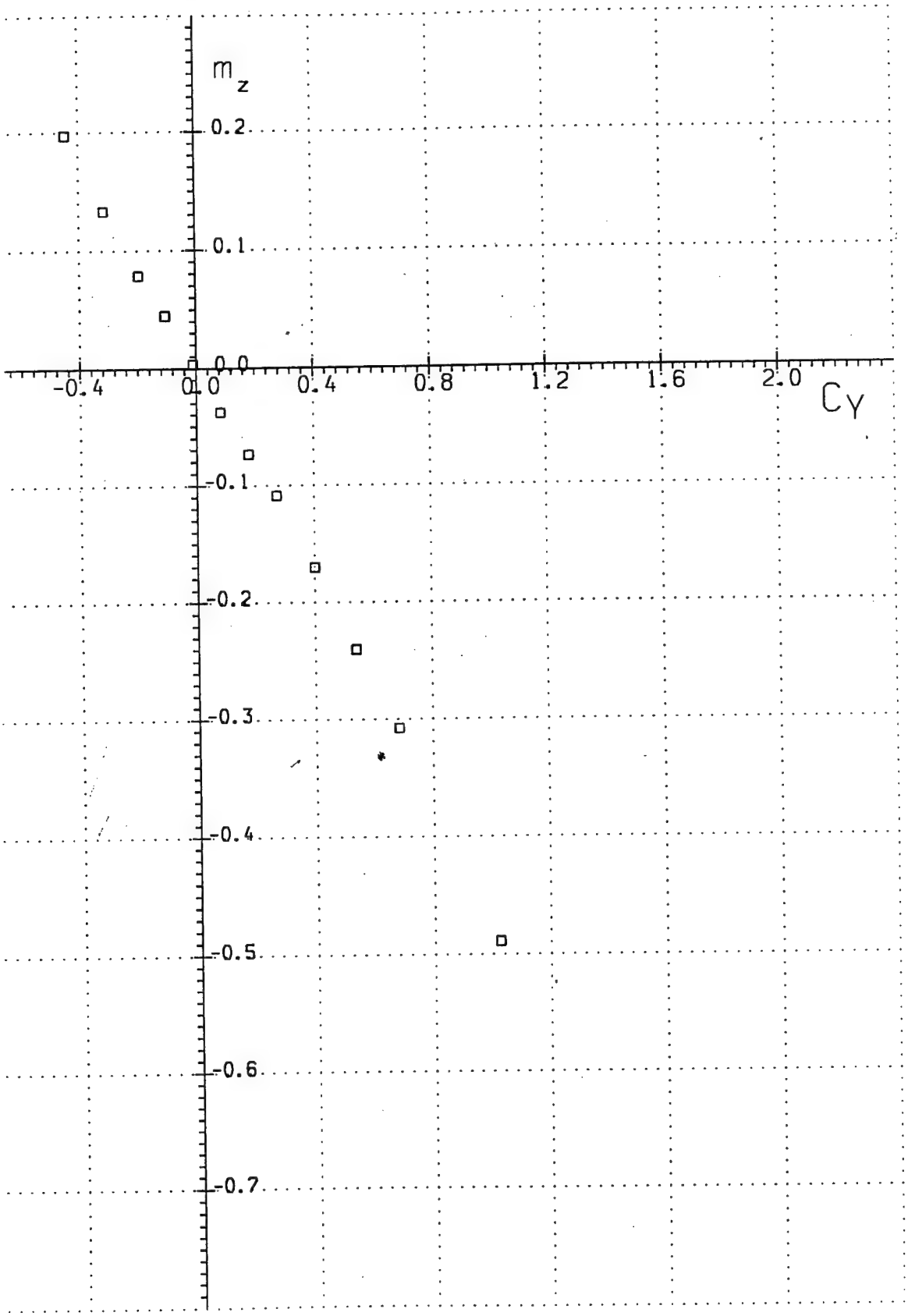

Run 9

Fig. 67

$M_\infty = 4.97$ $Re_x = 1.38 \cdot 10^6$

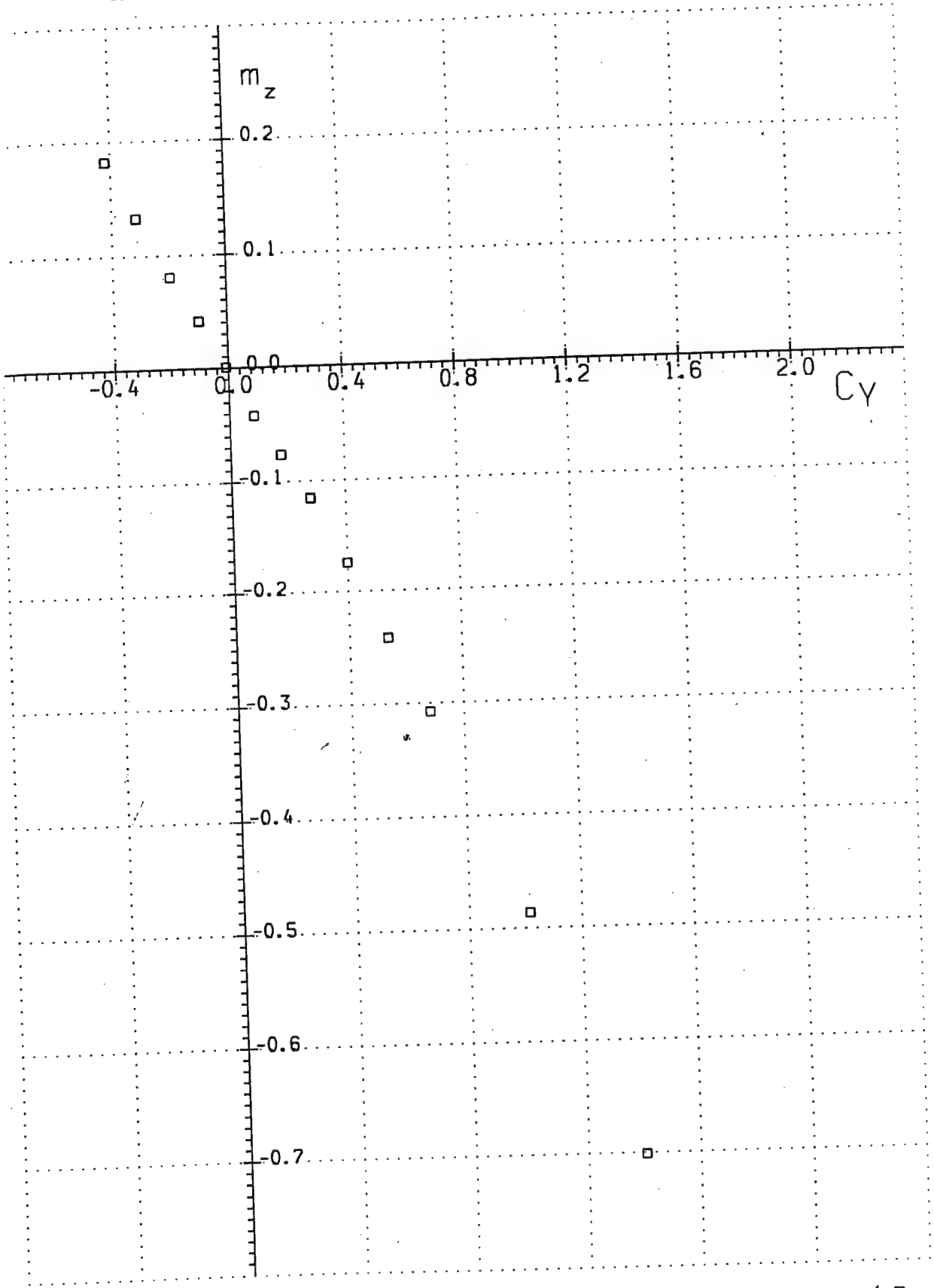

Run 10

Fig. 68

$M_\infty = 4.98$ $Re_x = 1.82 \cdot 10^6$

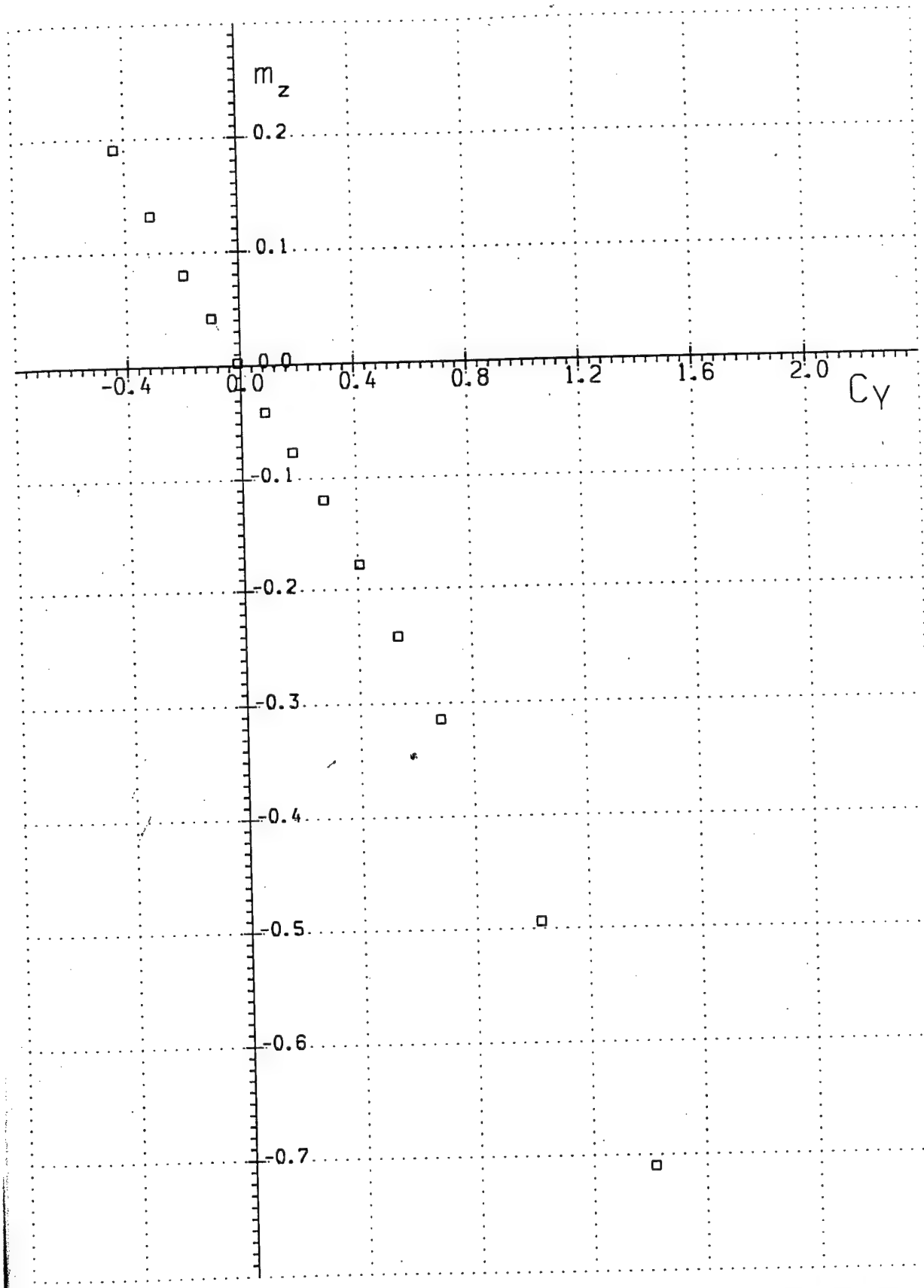

Run 11

Fig. 69

$M_\infty = 5.00$ $Re_x = 3.23 \cdot 10^6$

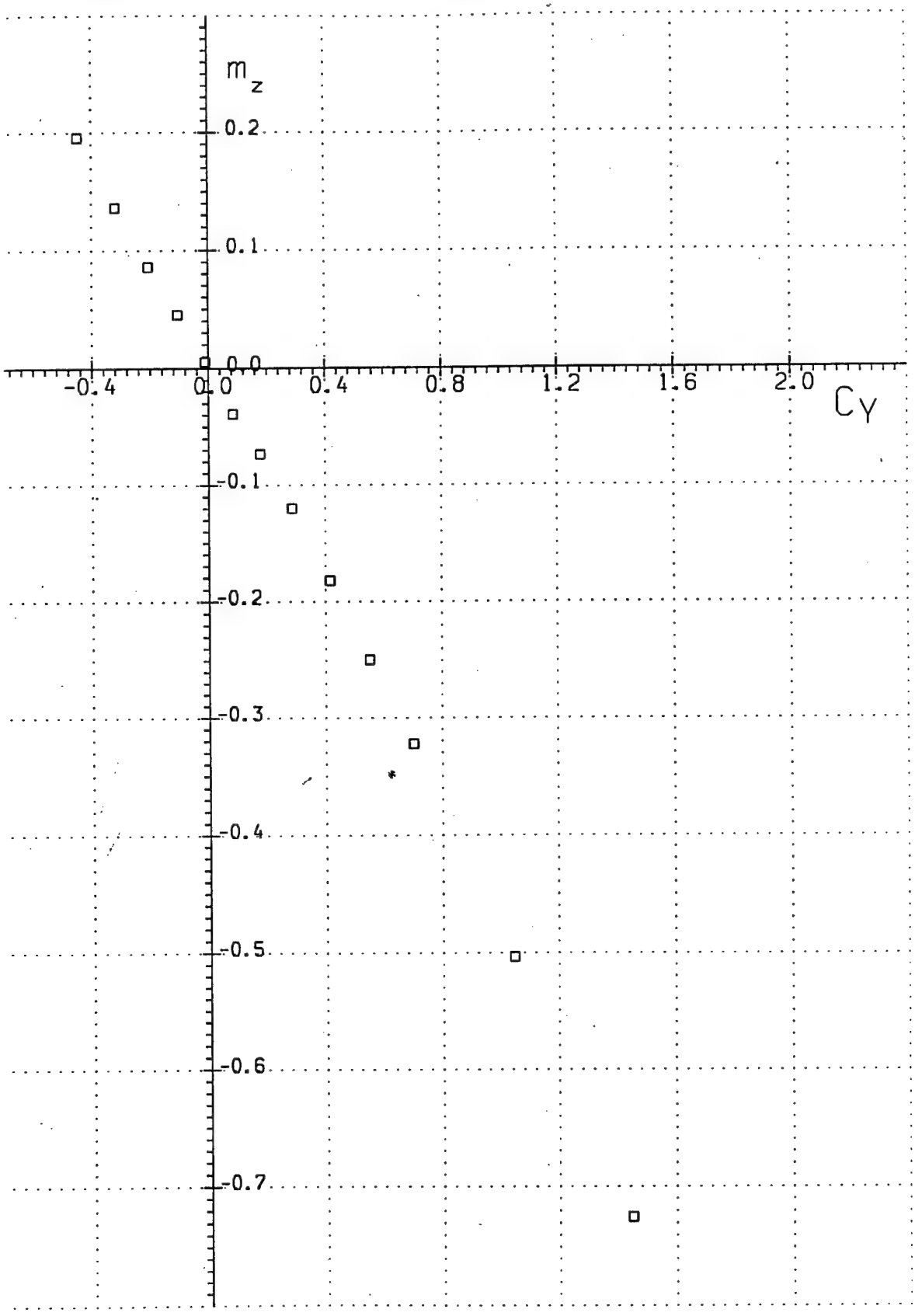

Run 12

Fig. 70

$M_\infty = 5.00$ $Re_x = 4.52 \cdot 10^6$

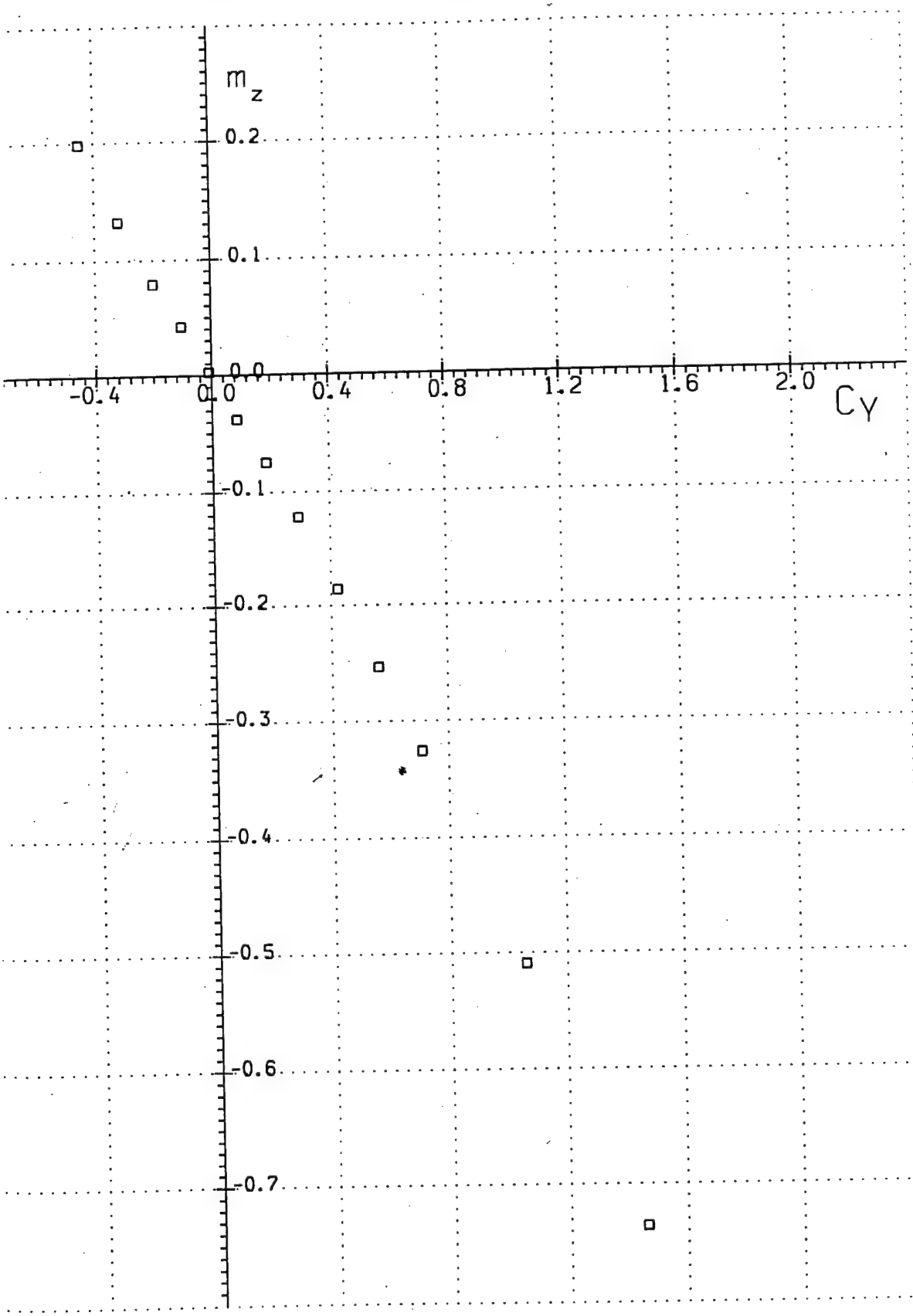

Run 13

Fig. 71

$M_\infty = 5.02$ $Re_x = 7.60 \cdot 10^6$

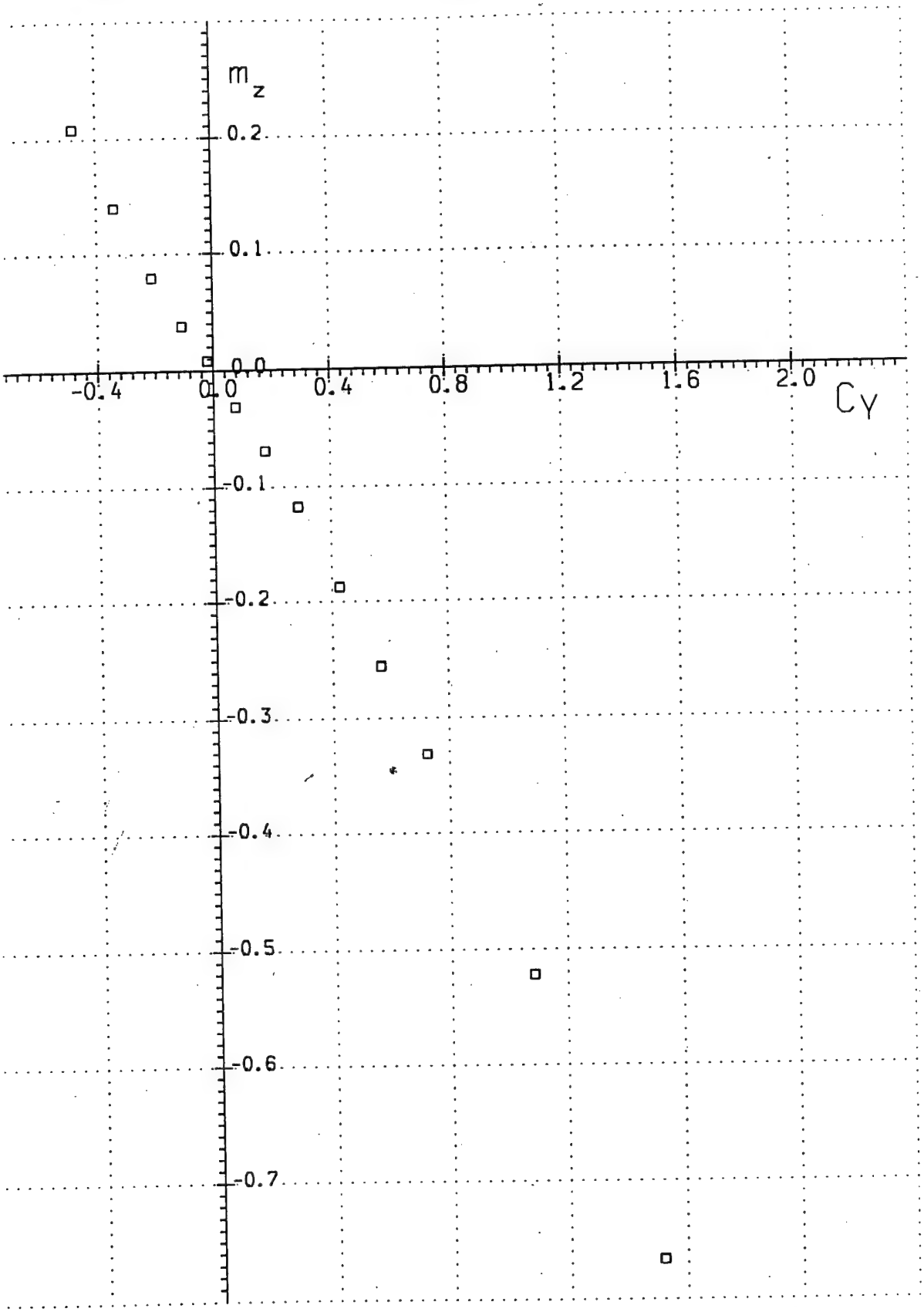

Run 14

Fig. 72

$M_\infty = 6.00$ $Re_x = .98 \cdot 10^6$

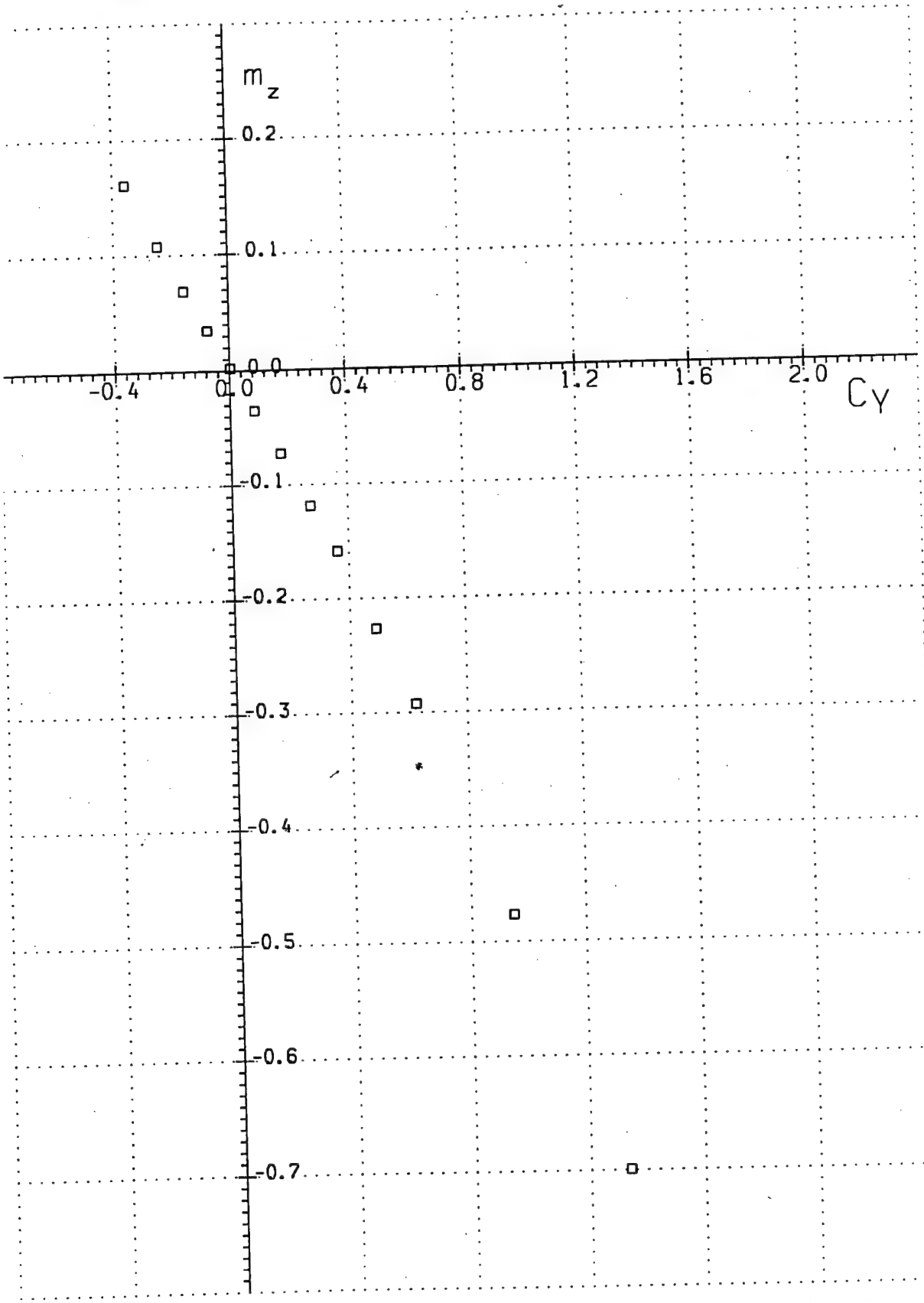

Run 15

Fig. 73

$M_\infty = 6.05$ $Re_x = 1.85 \cdot 10^6$

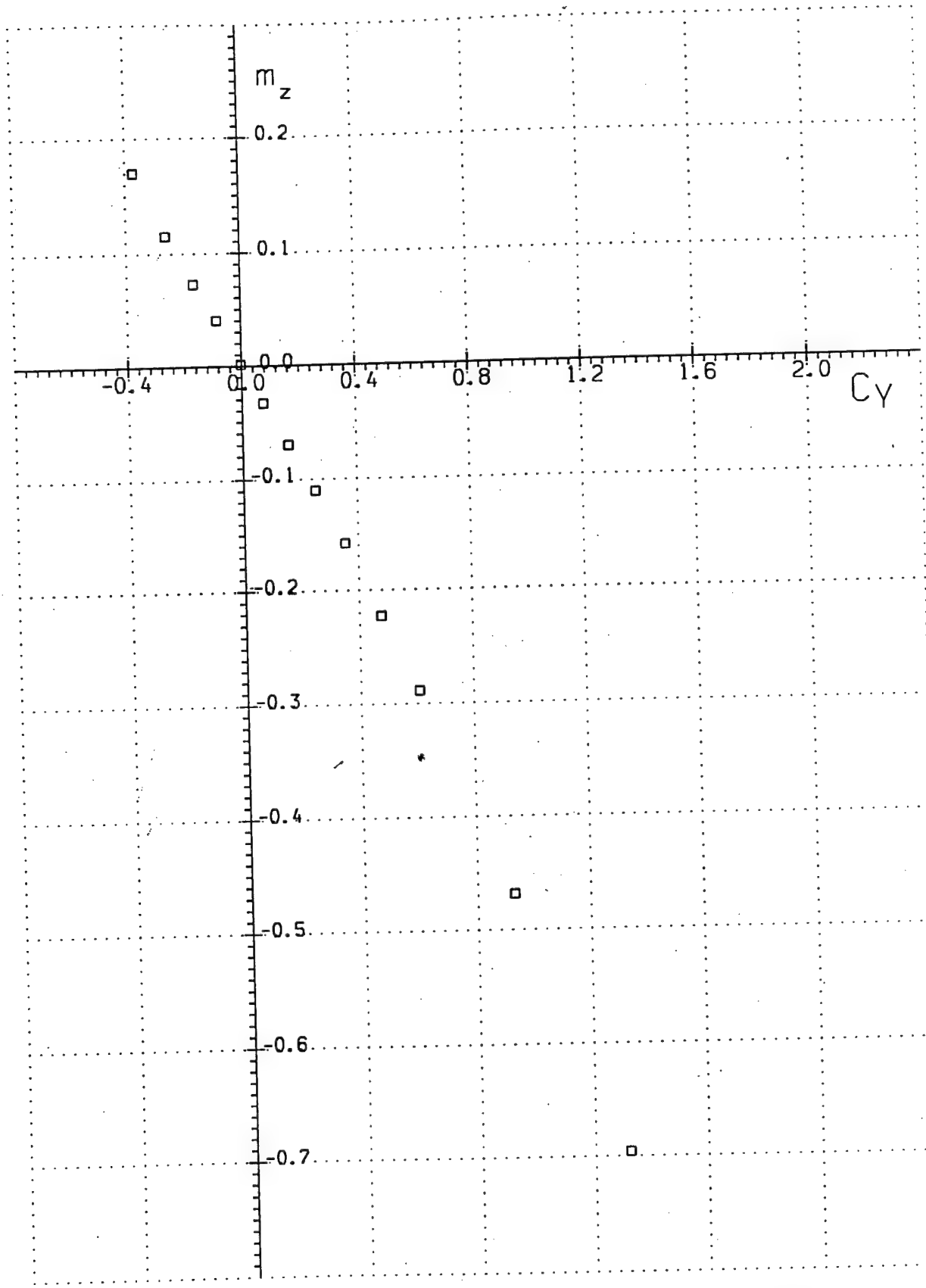

Run 16

Fig. 74

$M_\infty = 6.08$ $Re_x = 2.99 \cdot 10^6$

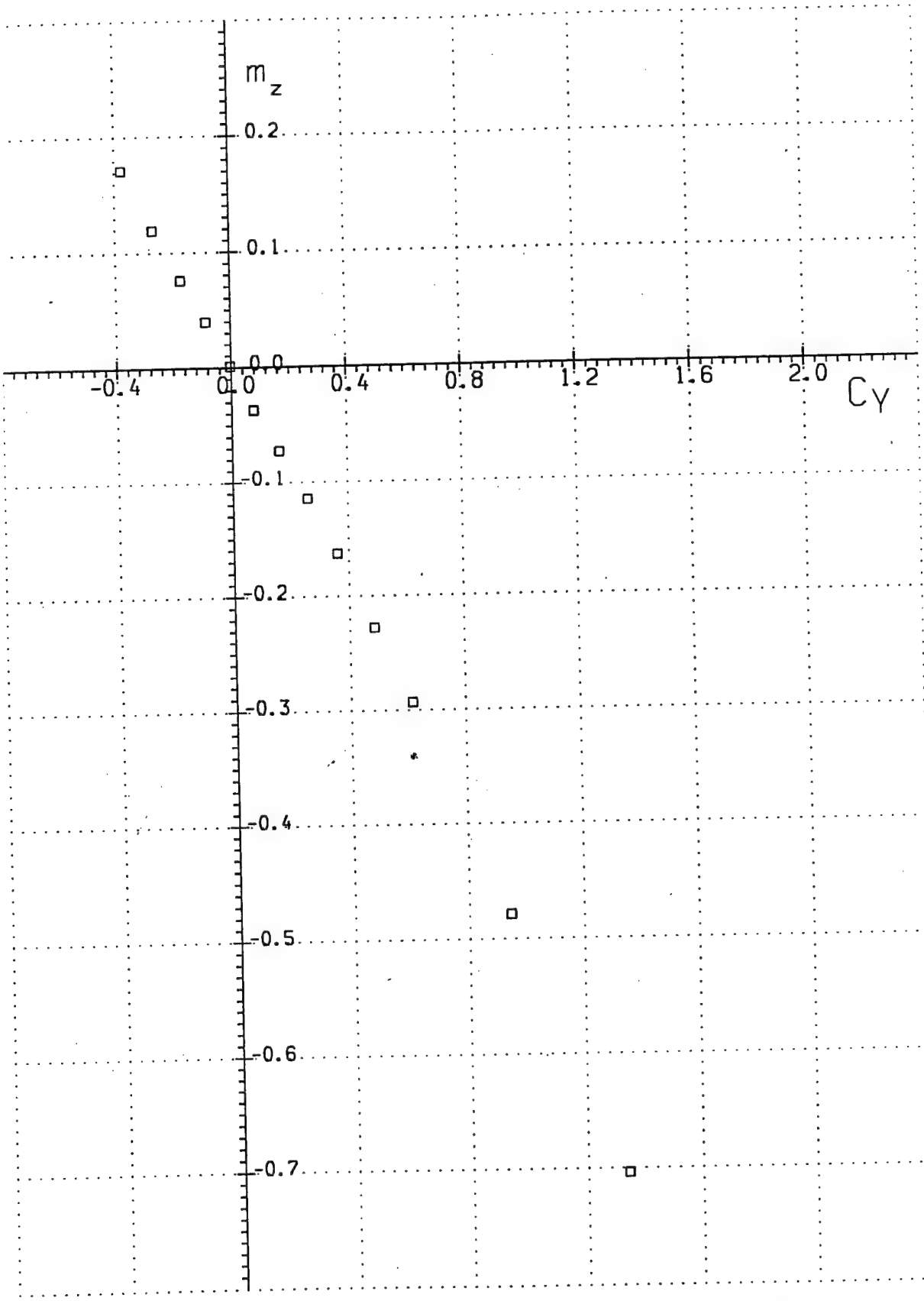

Run 17

Fig. 75

$M_\infty = 6.96$ $Re_x = 1.69 \cdot 10^6$

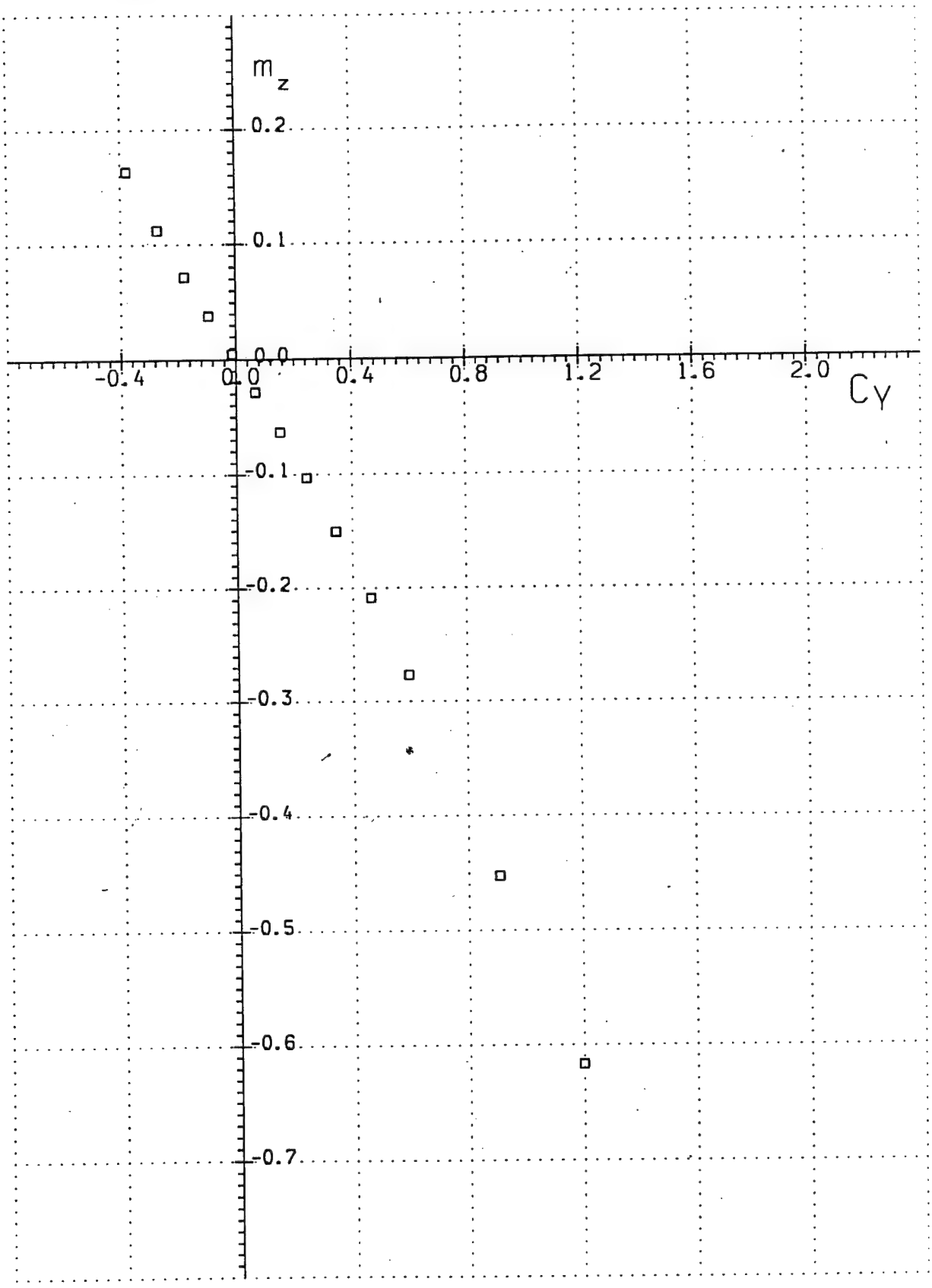

Run 18

Fig. 76

$M_\infty = 7.03$ $Re_x = 2.27 \cdot 10^6$

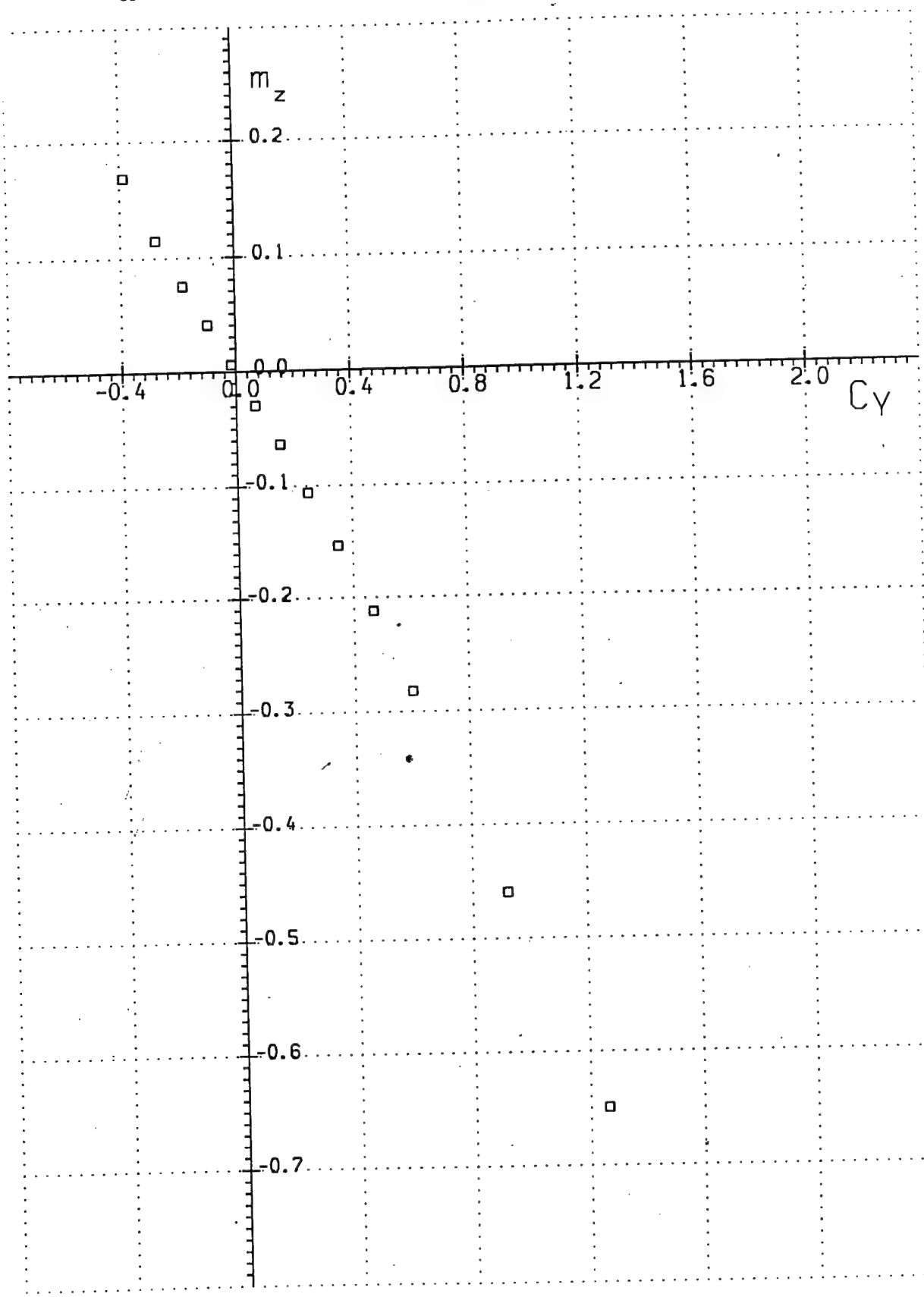

Run 19

Fig. 77

$M_\infty = 7.05$ $Re_x = 2.74 \cdot 10^6$

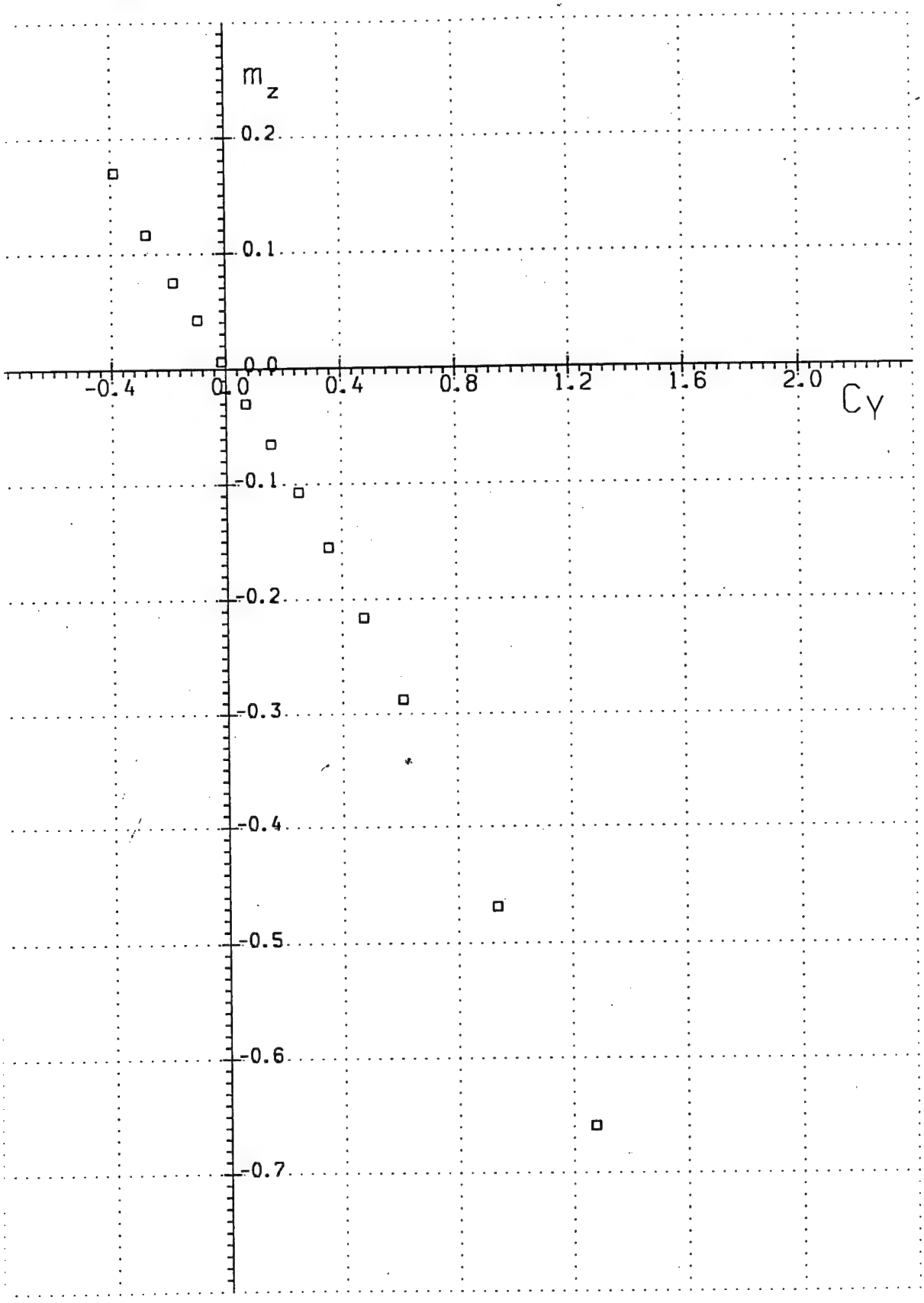

Run 20

Fig. 78

$M_\infty = 7.07$ $Re_x = 4.39 \cdot 10^6$

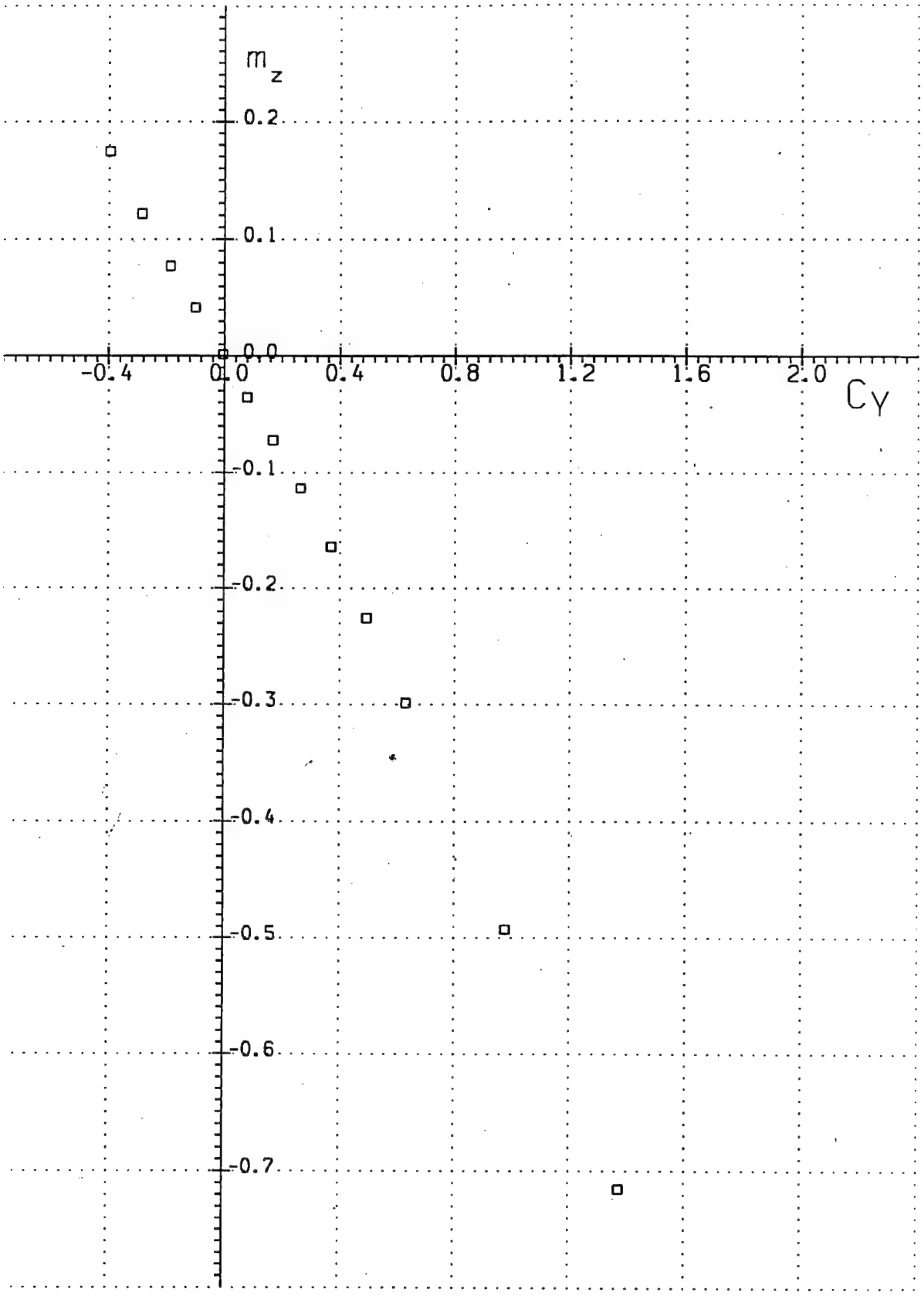

Run 21

Fig. 79

$M_\infty = 7.07$ $Re_x = 6.26 \cdot 10^6$

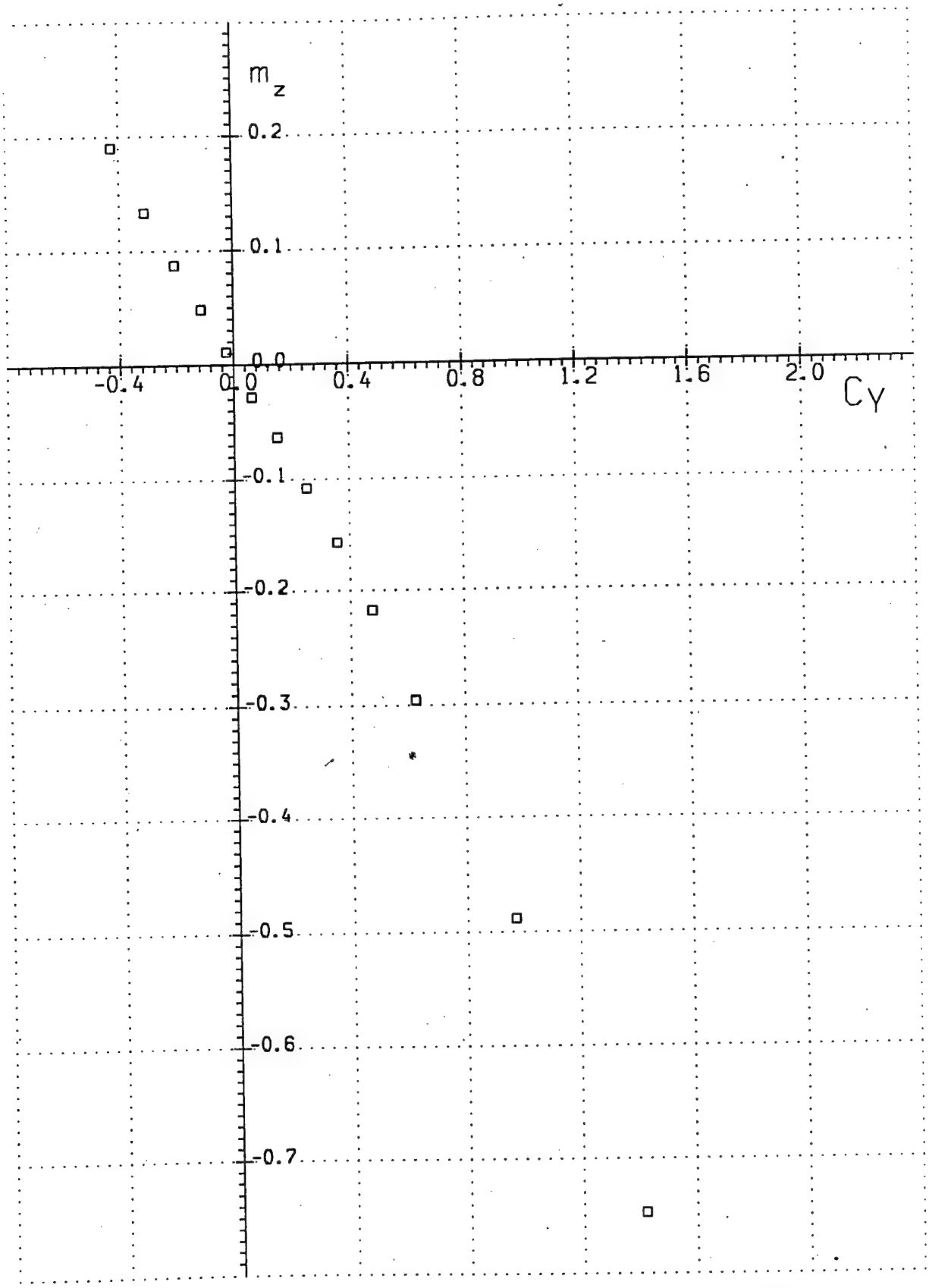

Run 22

Fig. 80

$M_\infty = 7.97$ $Re_x = 1.28 \cdot 10^6$

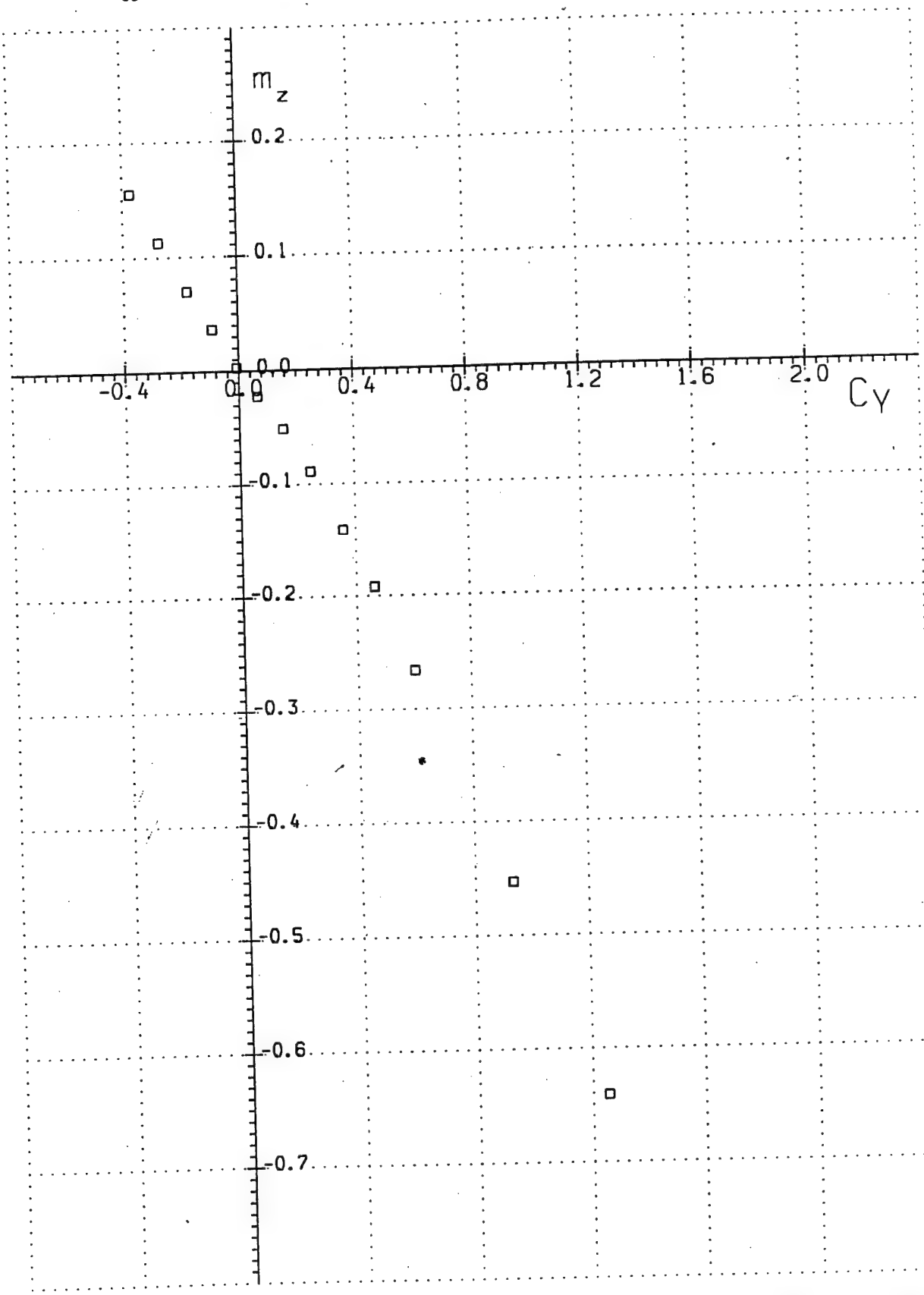

Run 23

Fig. 81

$M_\infty = 8.00$ $Re_x = 2.00 \cdot 10^6$

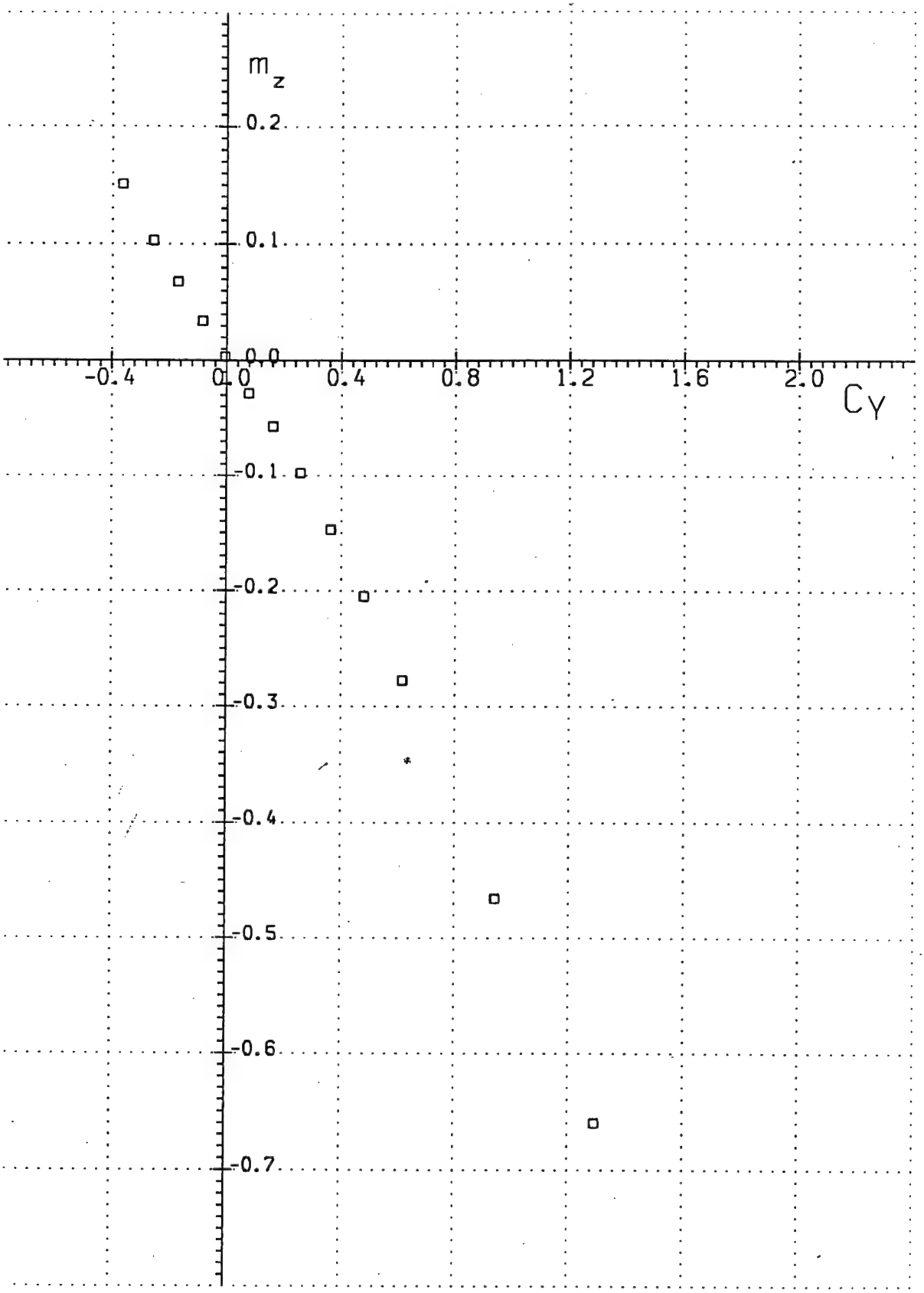

Run 24

Fig. 82

$M_\infty = 8.03$ $Re_x = 3.30 \cdot 10^6$

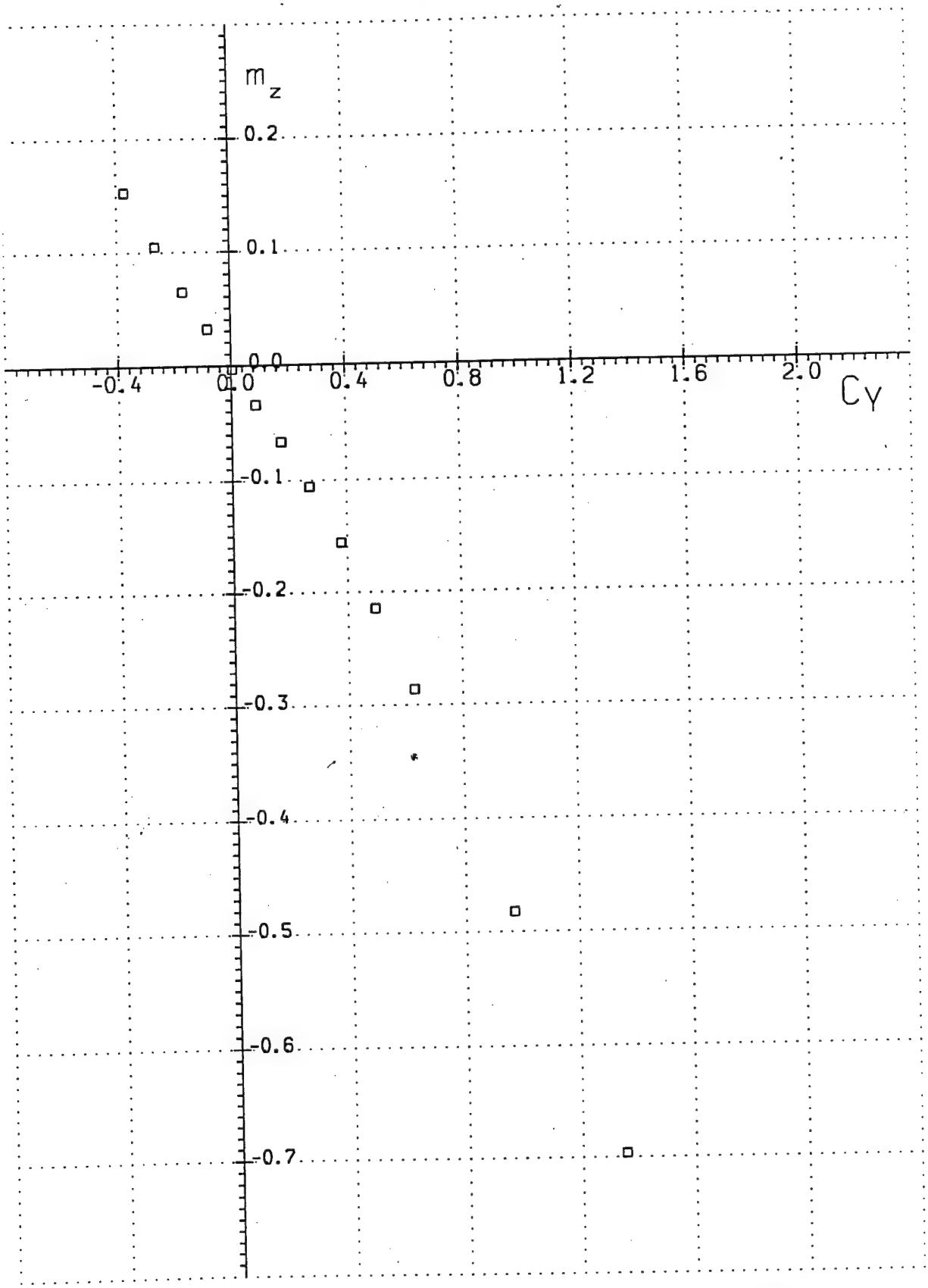

Run 25

Fig. 83

$M_\infty = 8.96$ $Re_\chi = 1.21 \cdot 10^6$

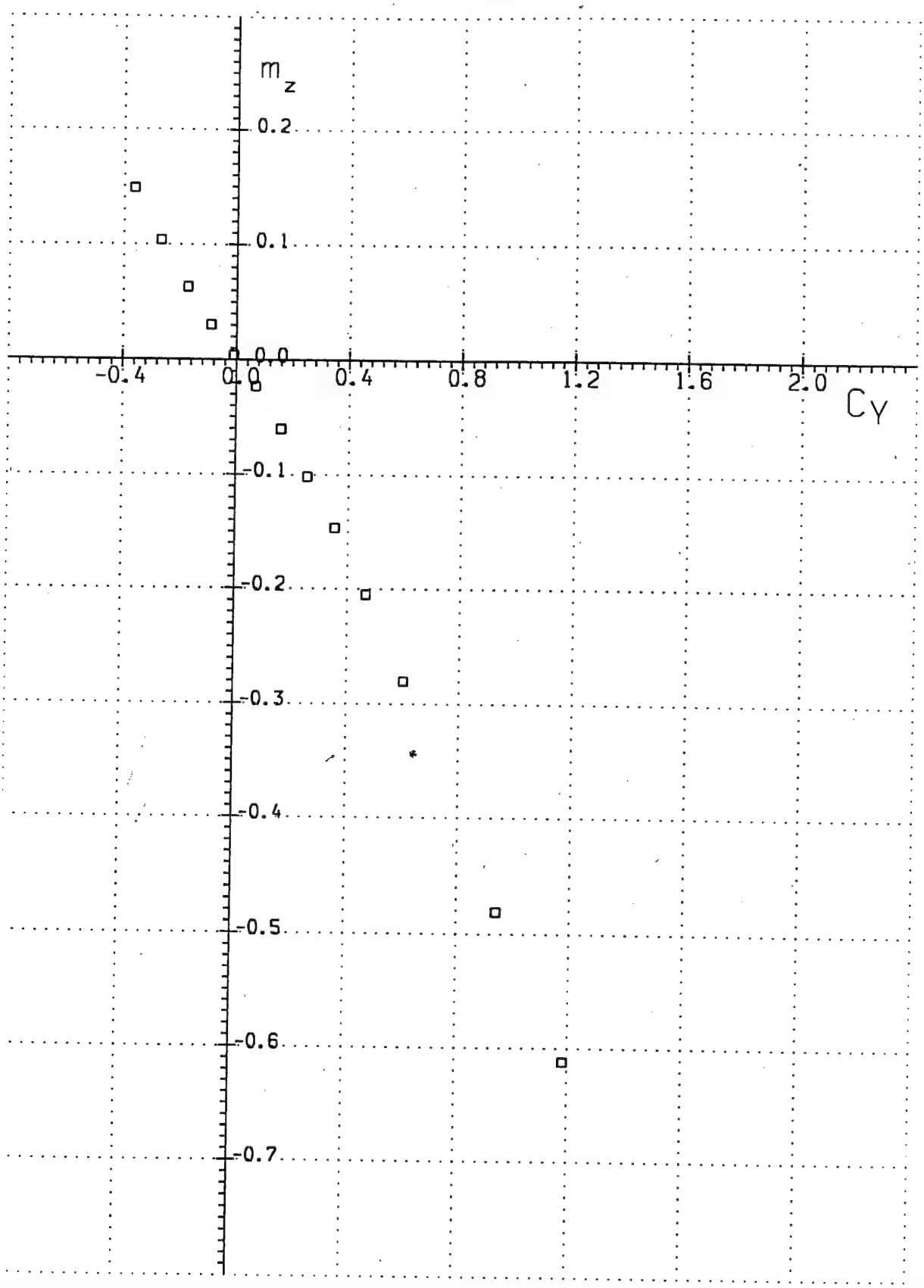

Run 26

Fig. 84

$M_\infty = 9.04$ $Re_x = 2.23 \cdot 10^6$

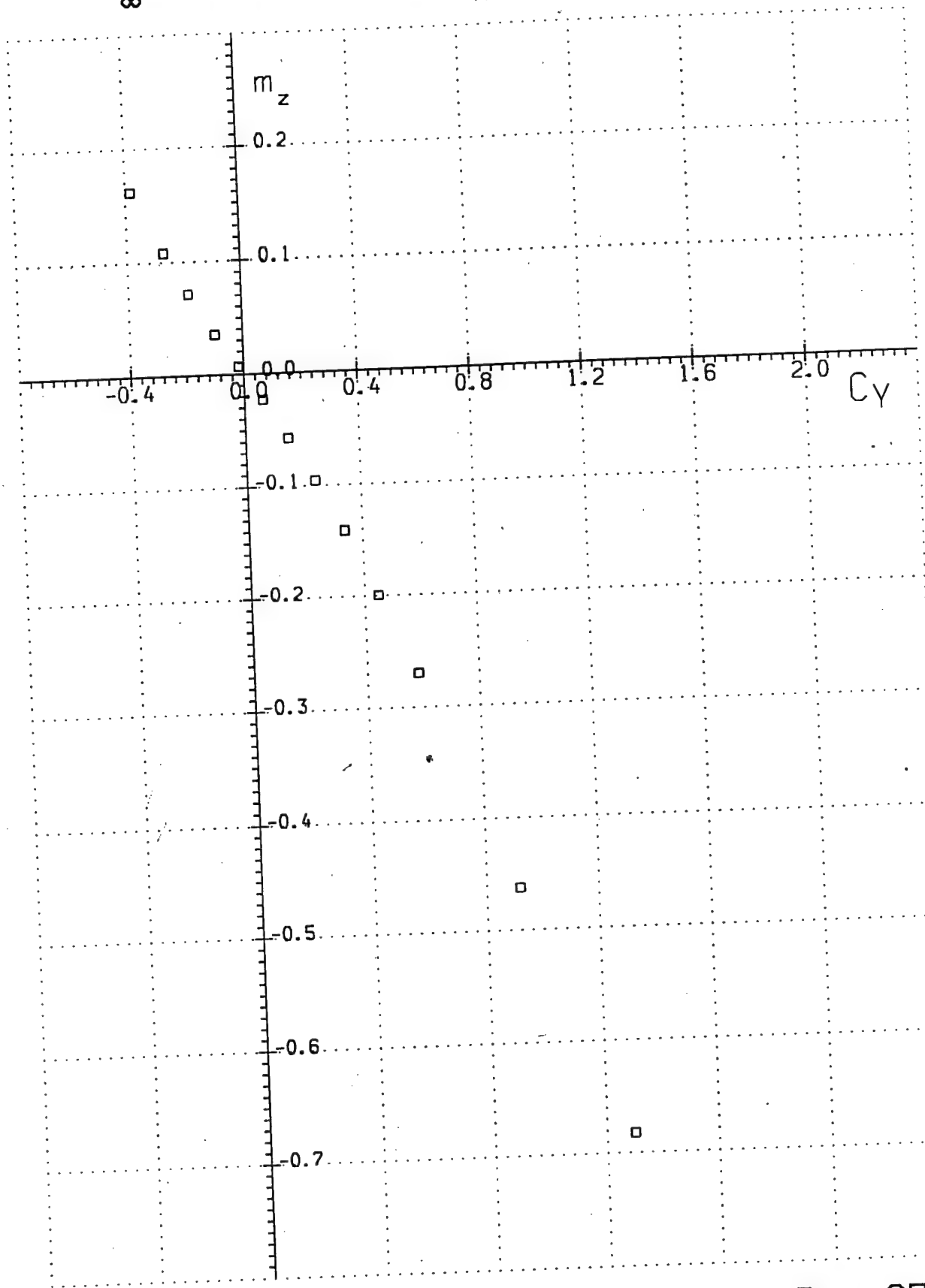

Run 27

Fig. 85

$M_\infty = 4.00$ $Re_x = 1.16 \cdot 10$

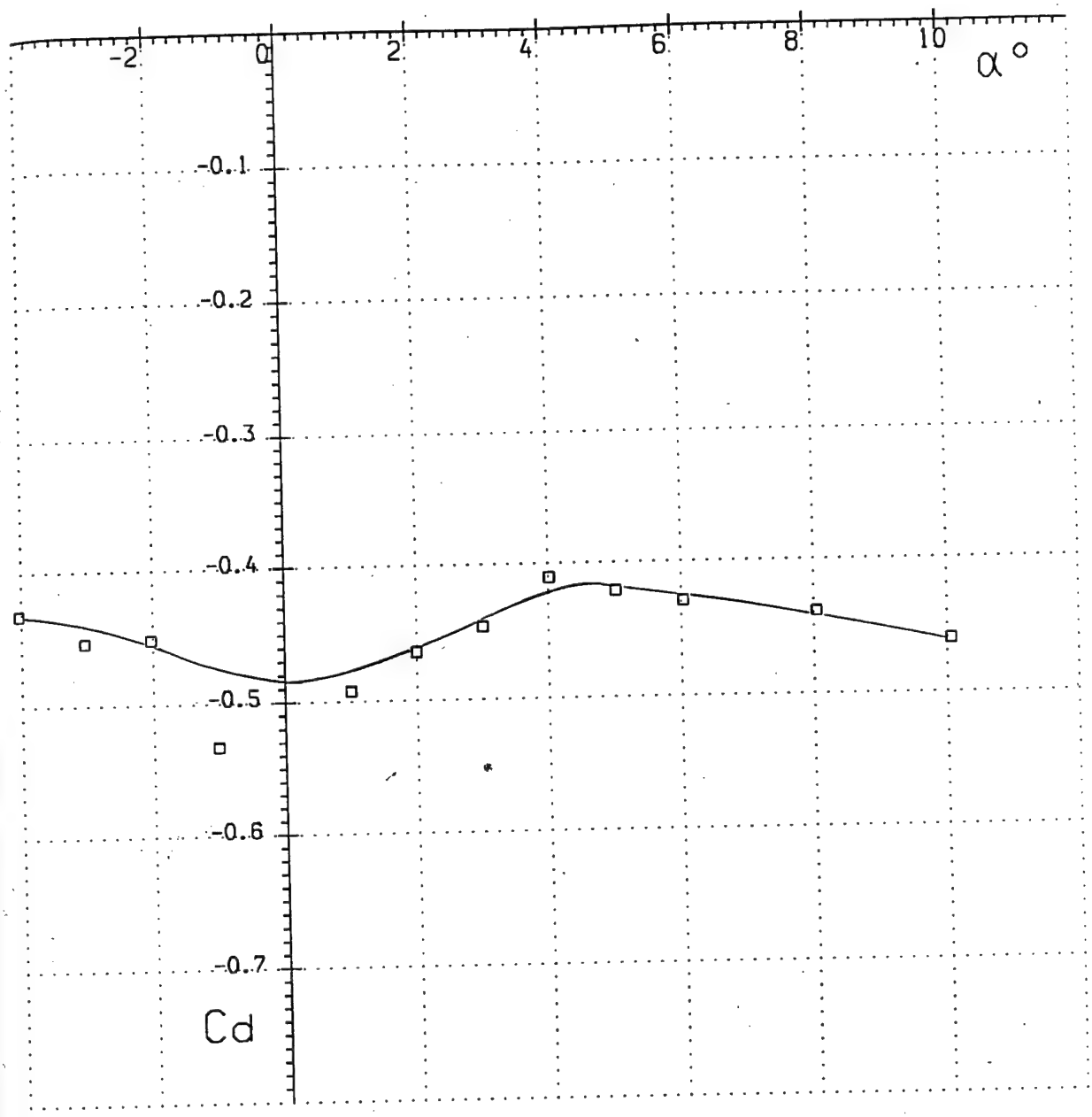

Run 1

Fig. 86

$M_\infty = 4.01$ $Re_x = 1.45 \cdot 10$

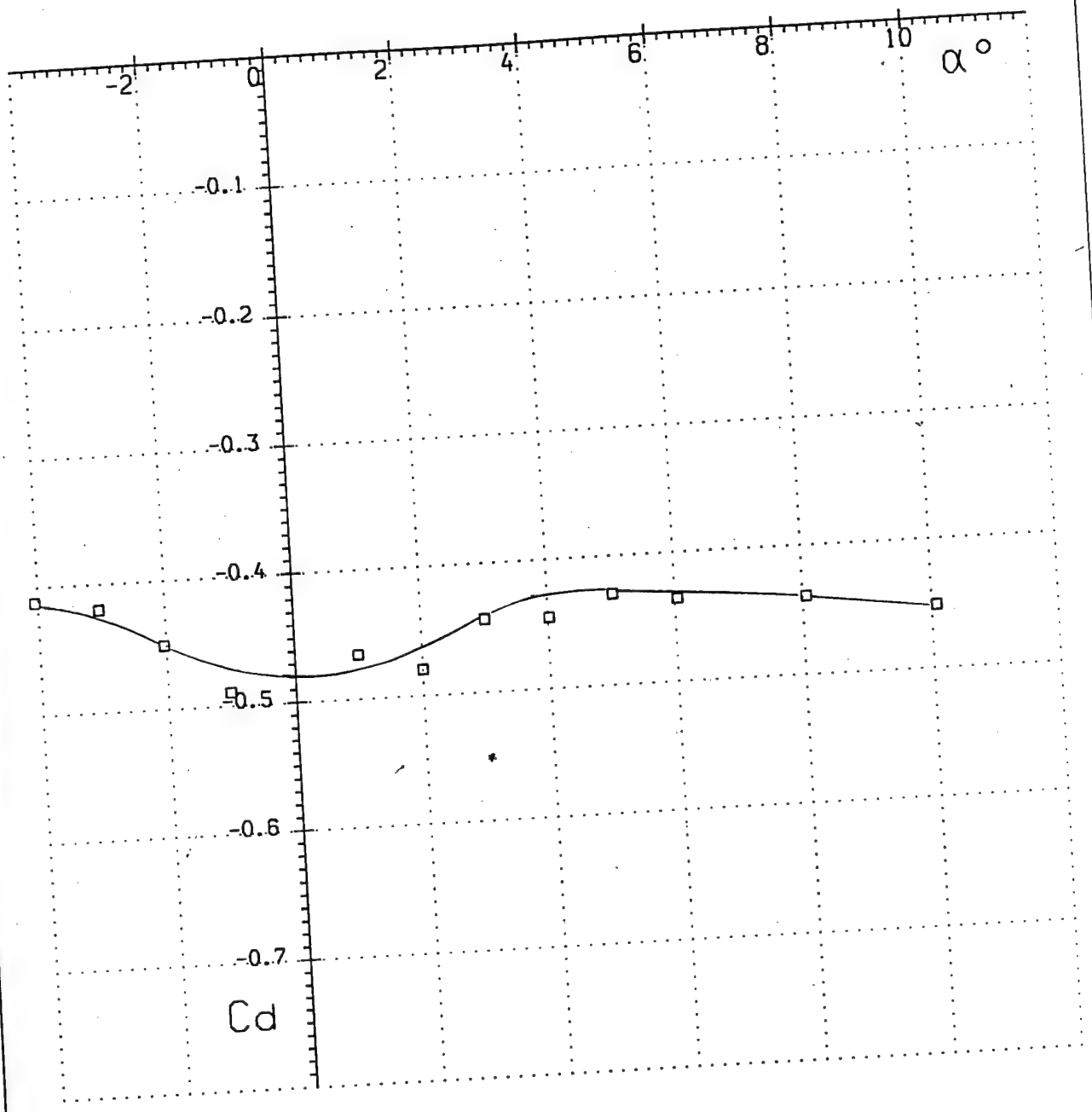

Run 2

Fig. 87

$M_\infty = 4.02$ $Re_x = 1.81 \cdot 10^6$

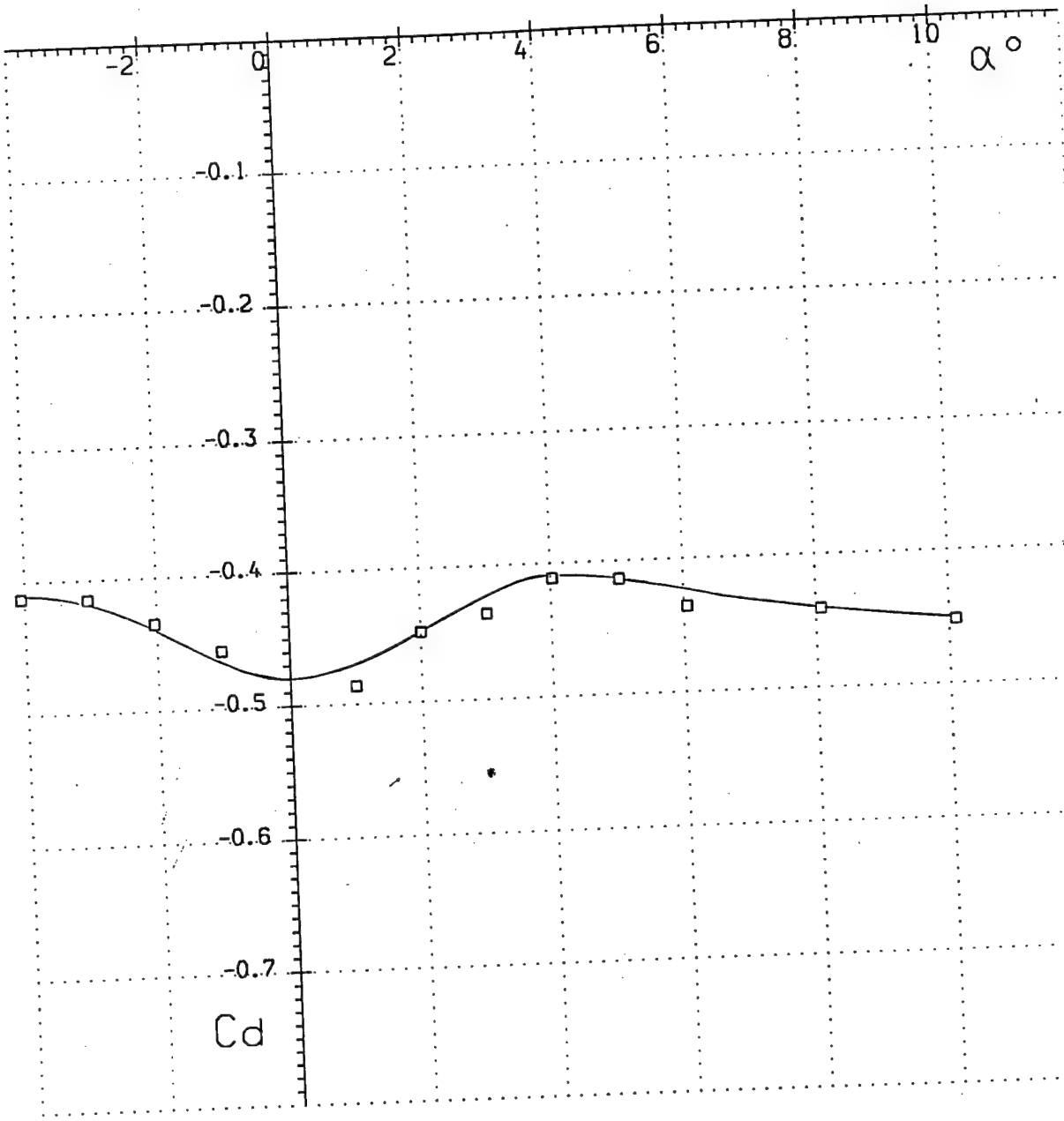

Run 3

Fig. 88

$M_\infty = 4.03$ $Re_x = 2.34 \cdot 10^6$

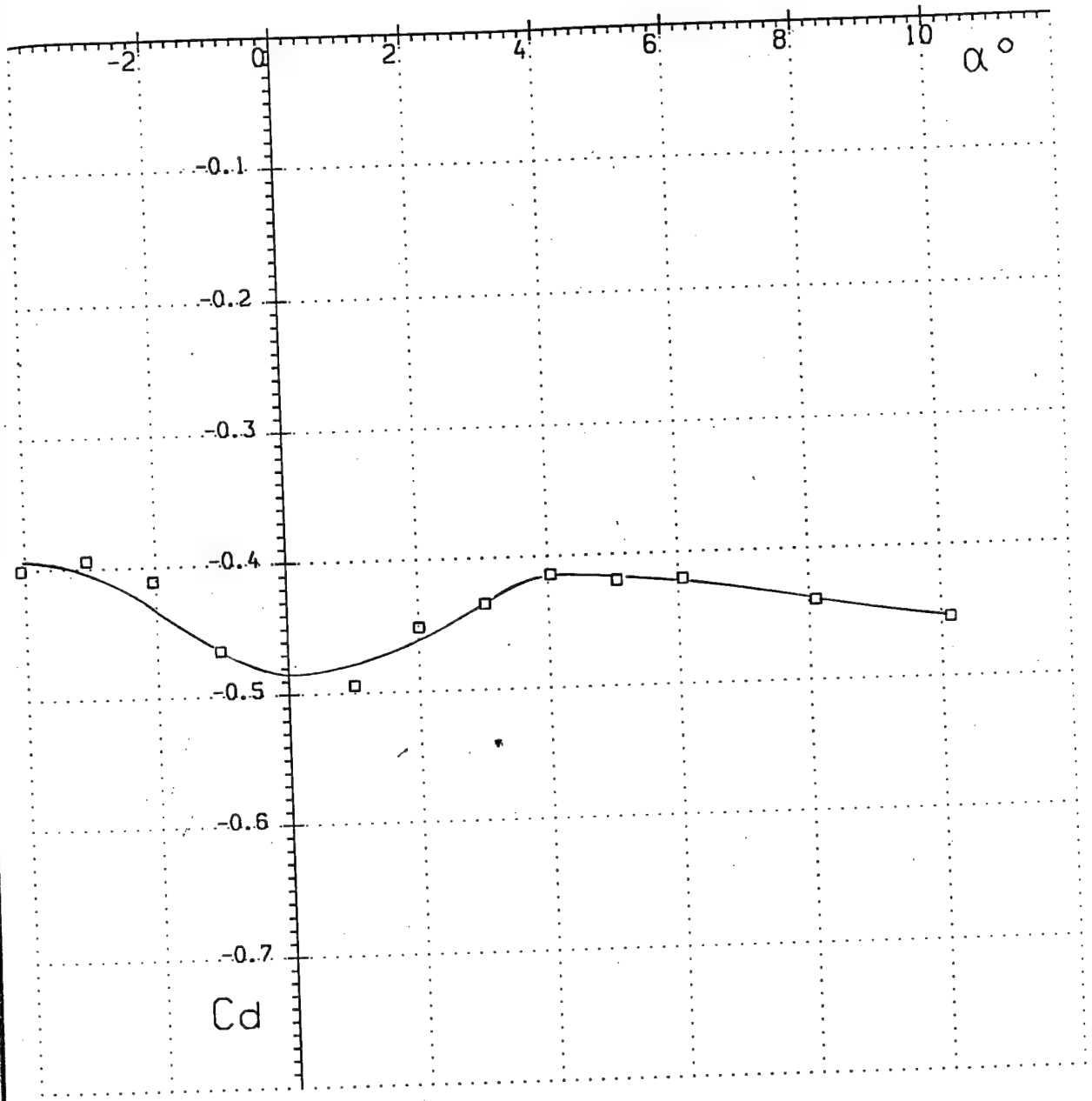

Run 4

Fig. 89

$M_\infty = 4.03$ $Re_x = 3.13 \cdot 10^6$

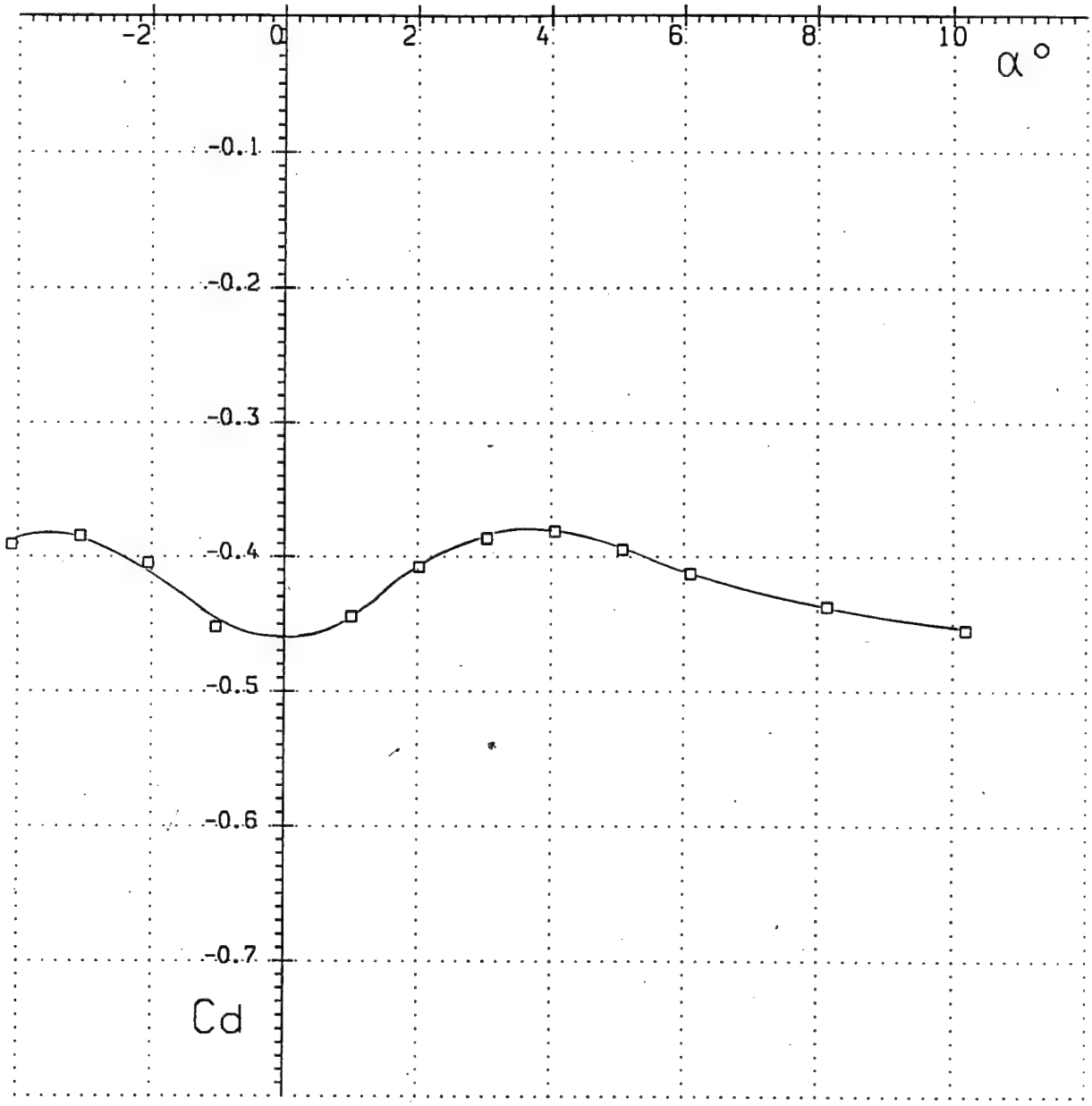

Run 5

$M_\infty = 4.04$ $Re_x = 3.91 \cdot 10^6$

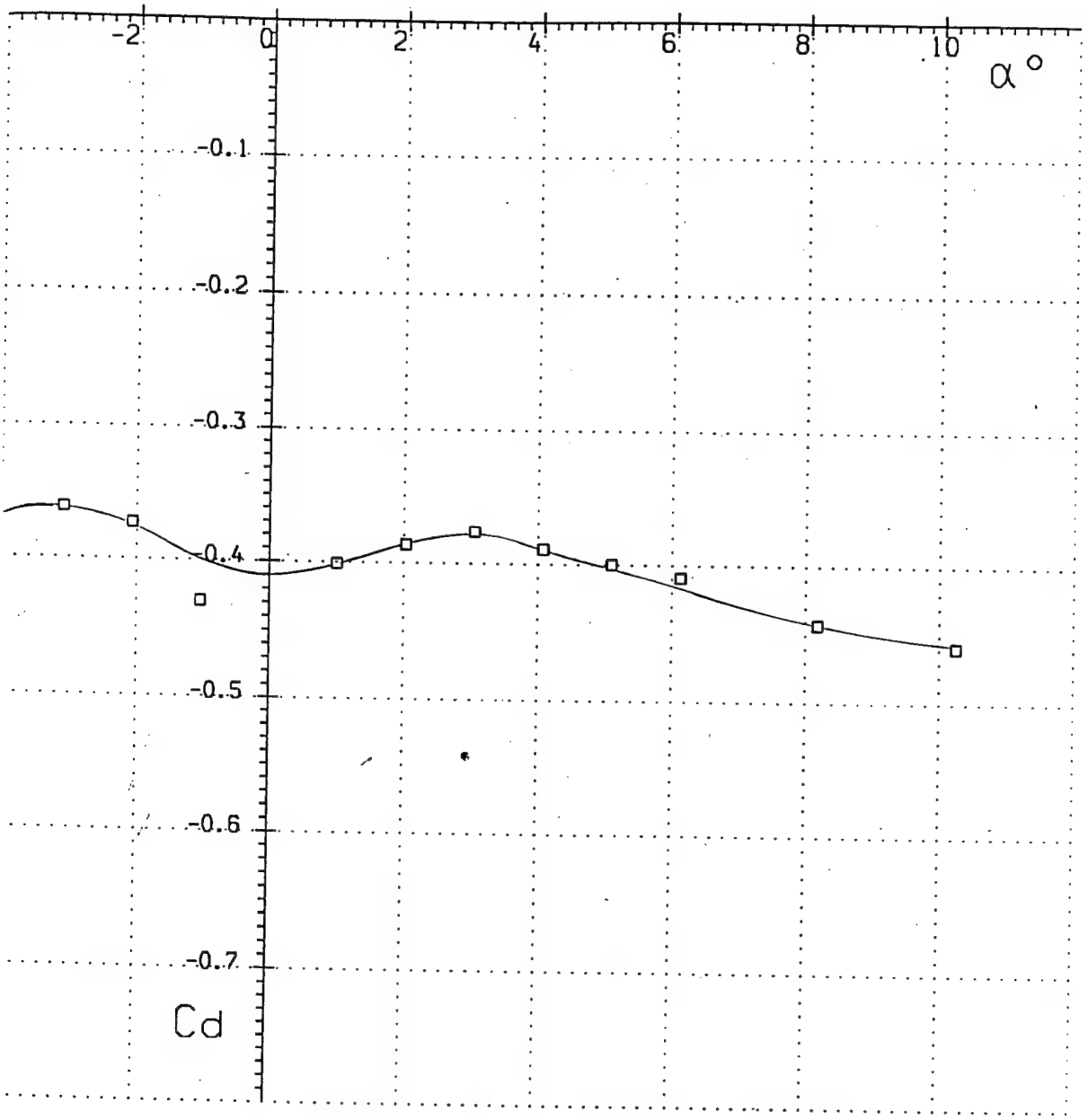

Run 6

Fig. 91

$M_\infty = 4.05$ $Re_x = 6.27 \cdot 10^6$

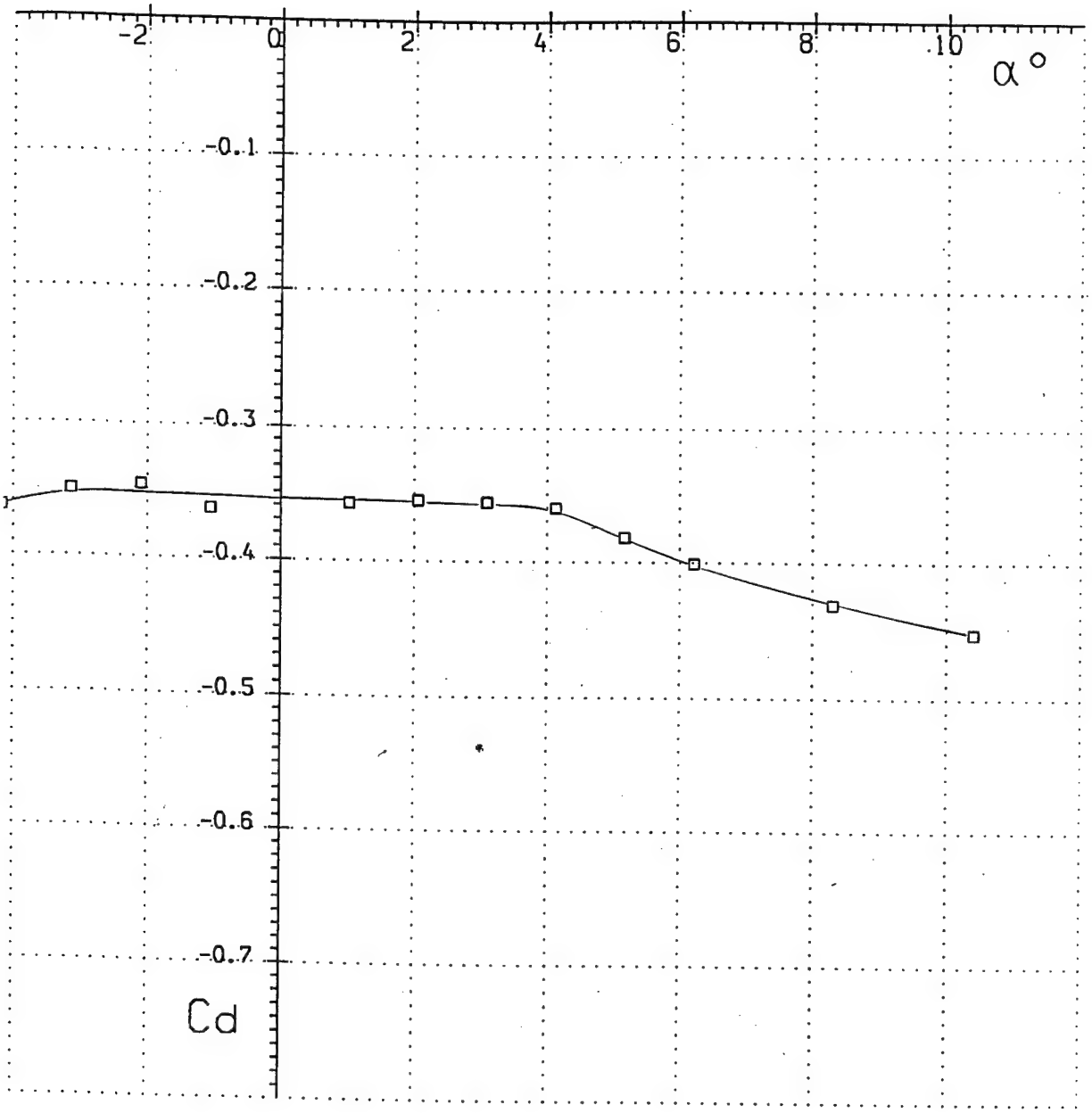

Run 7

Fig. 92

$M_\infty = 4.06$ $Re_x = 8.60 \cdot 10^6$

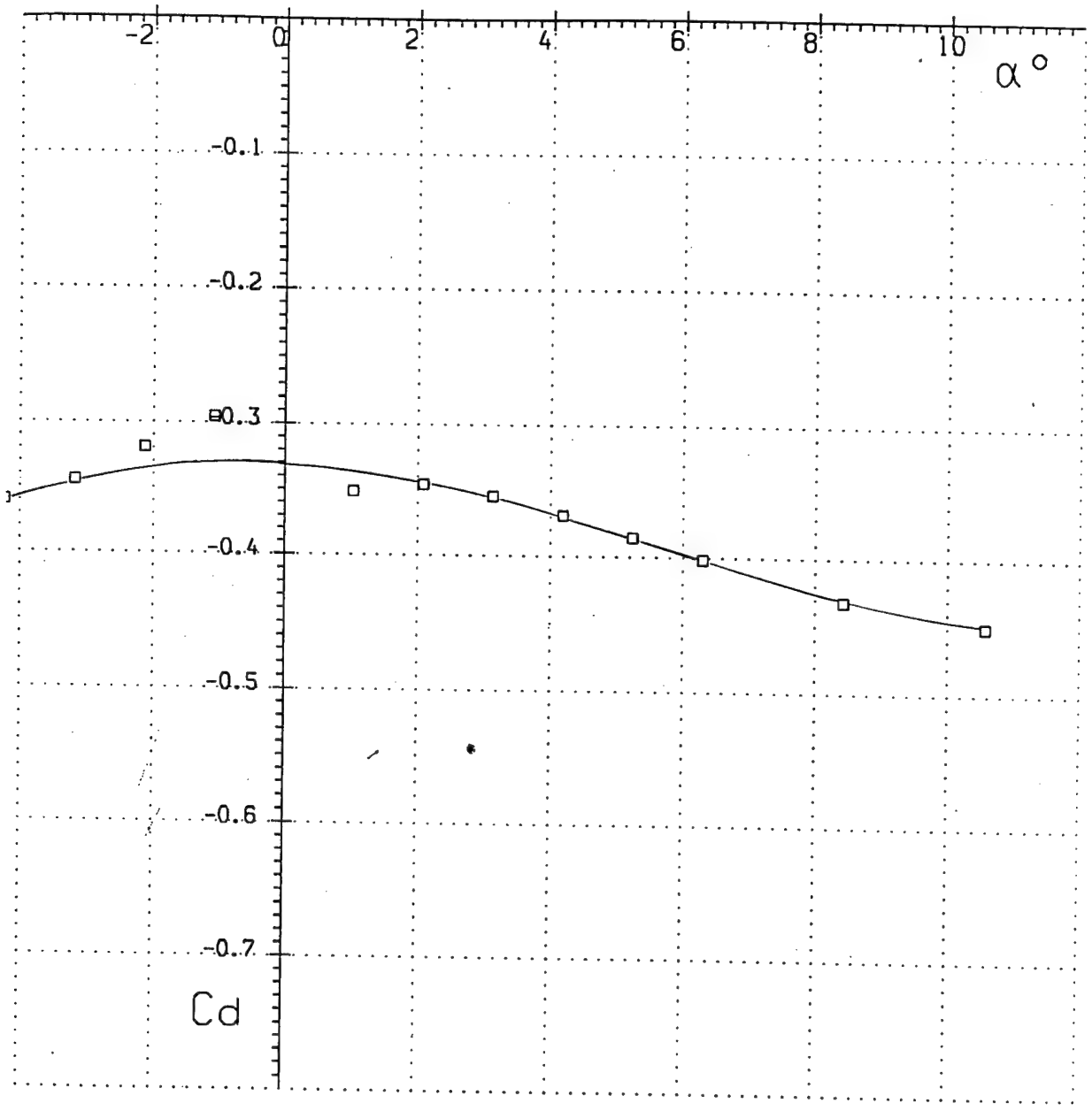

Run 8

Fig. 93

$M_\infty = 4.96$ $Re_x = .90 \cdot 10^6$

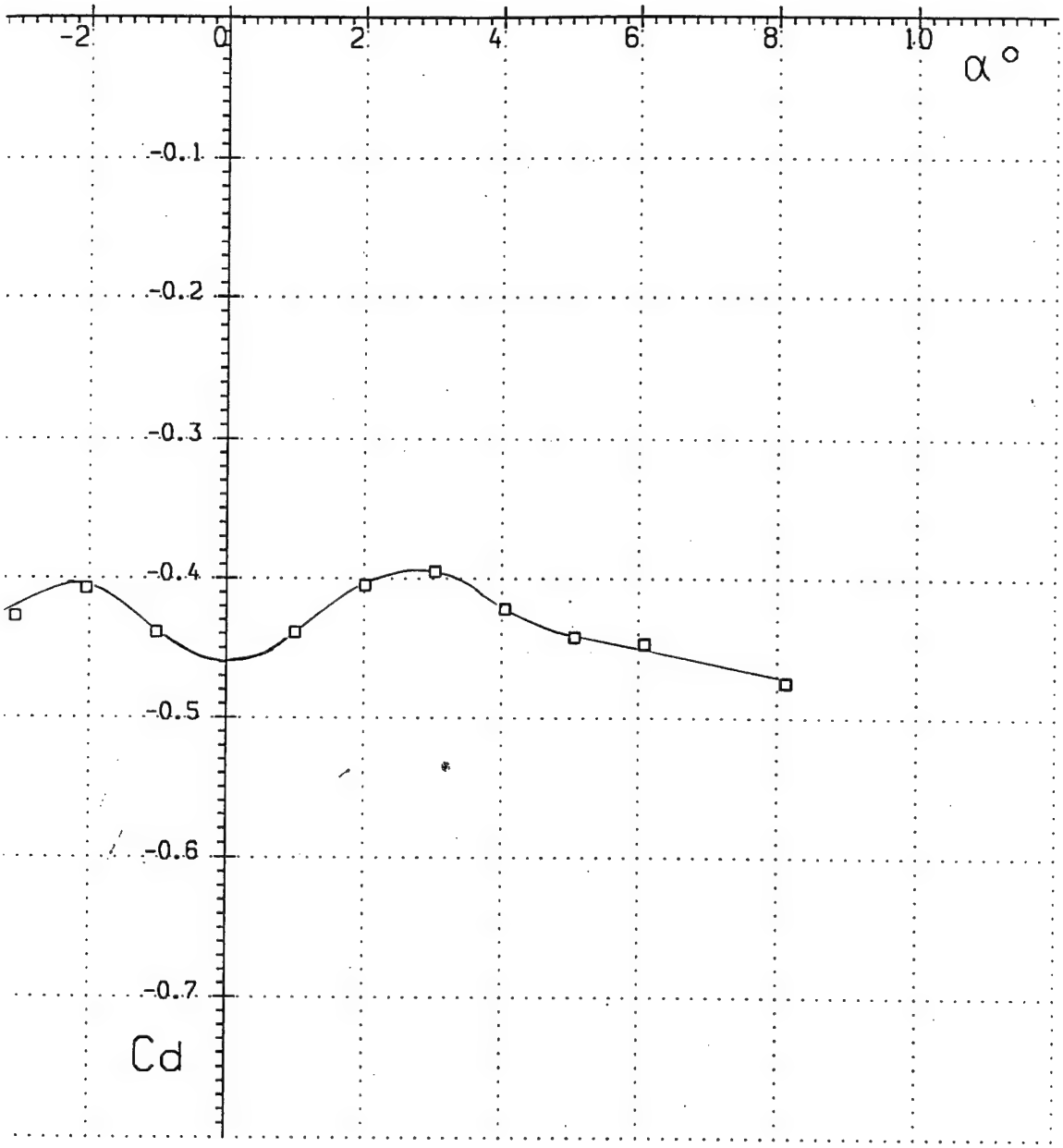

Run 9

Fig. 94

$M_\infty = 4.97$ $Re_x = 1.38 \cdot 10^6$

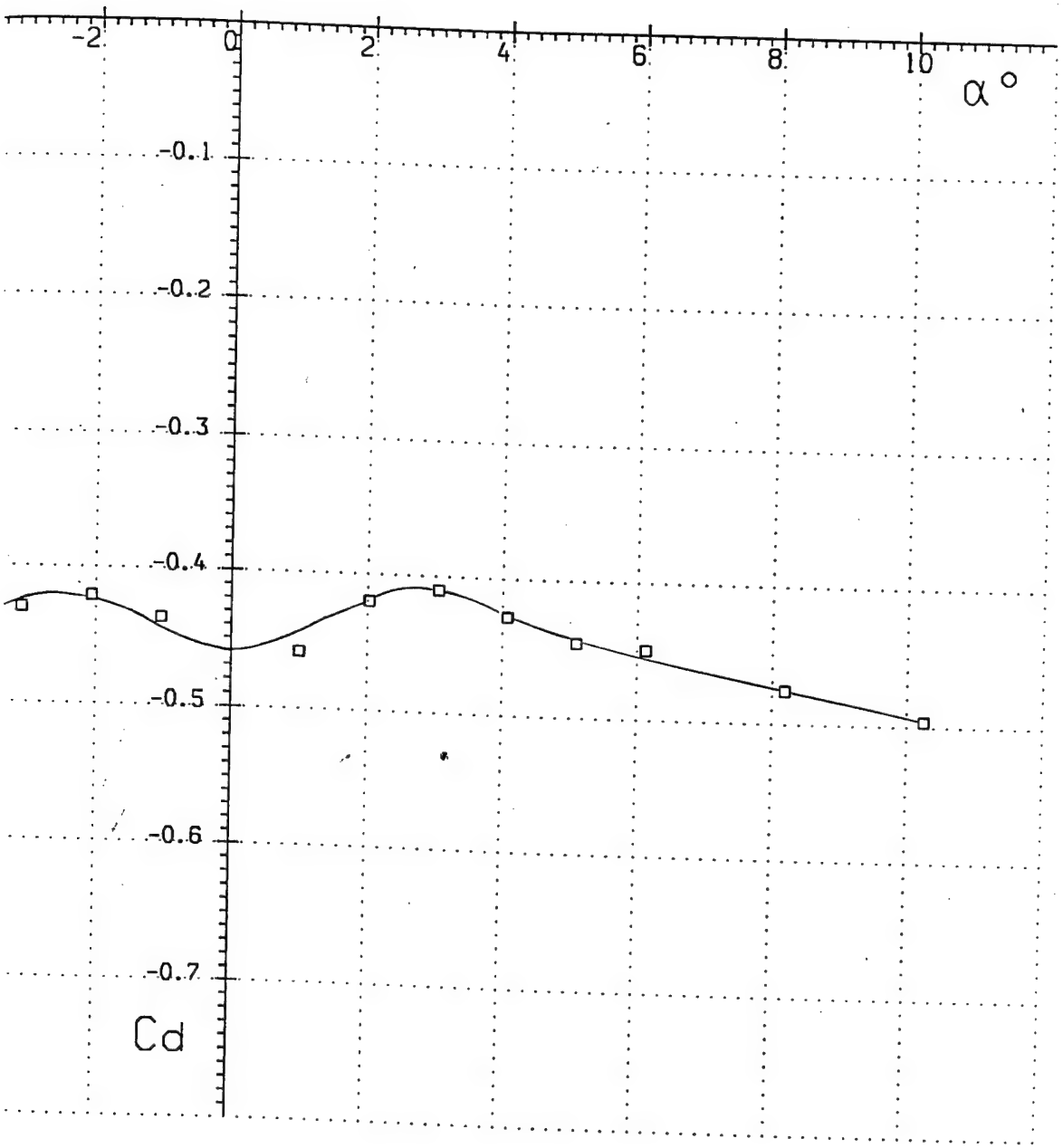

Run 10

Fig 95

$M_\infty = 4.98$ $Re_x = 1.82 \cdot 10^6$

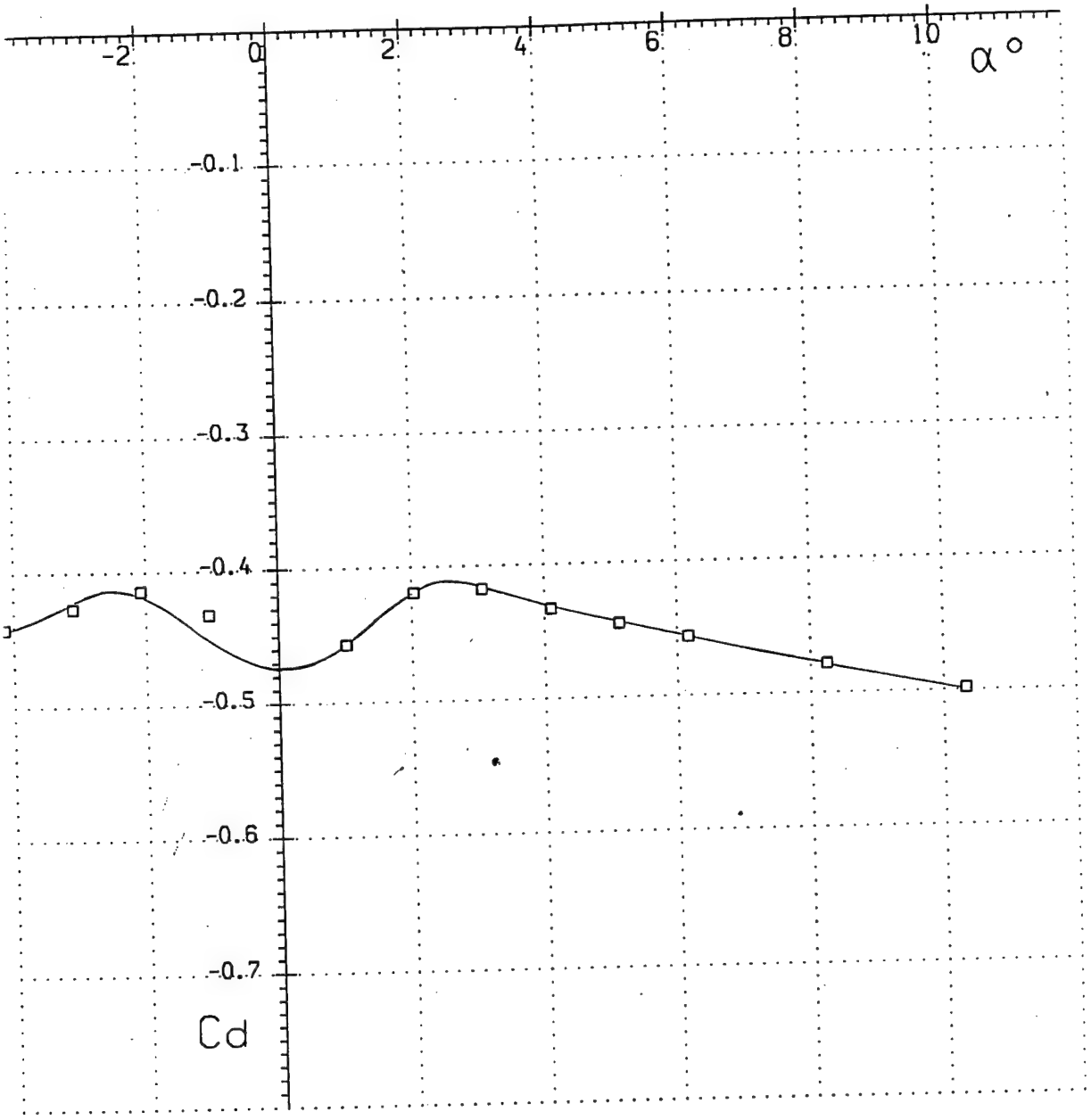

Run 11

Fig. 96

$M_\infty = 5.00$ $Re_x = 3.23 \cdot 10^6$

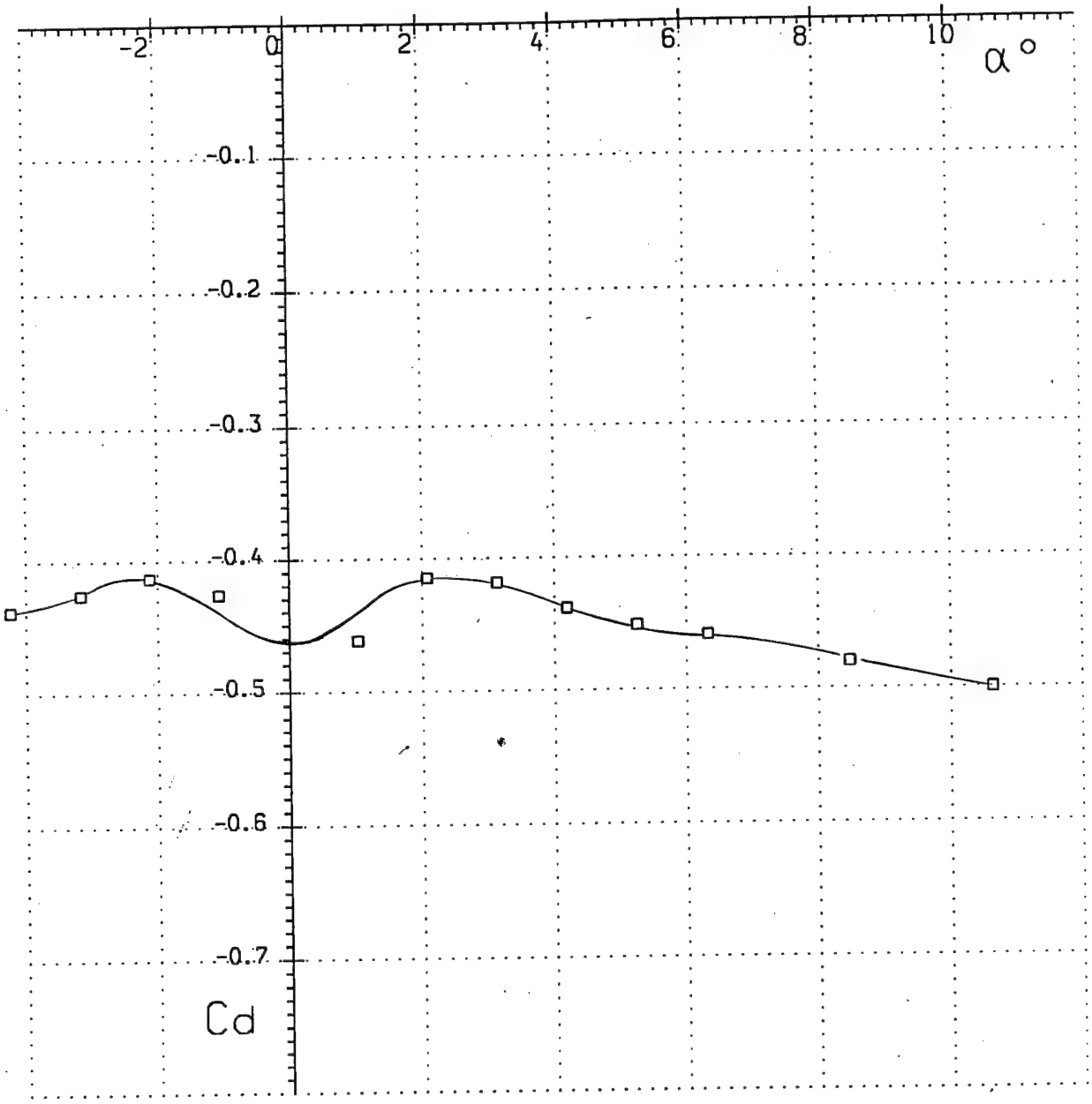

Run 12

Fig. 97

$M_\infty = 5.00$ $Re_x = 4.52 \cdot 10^6$

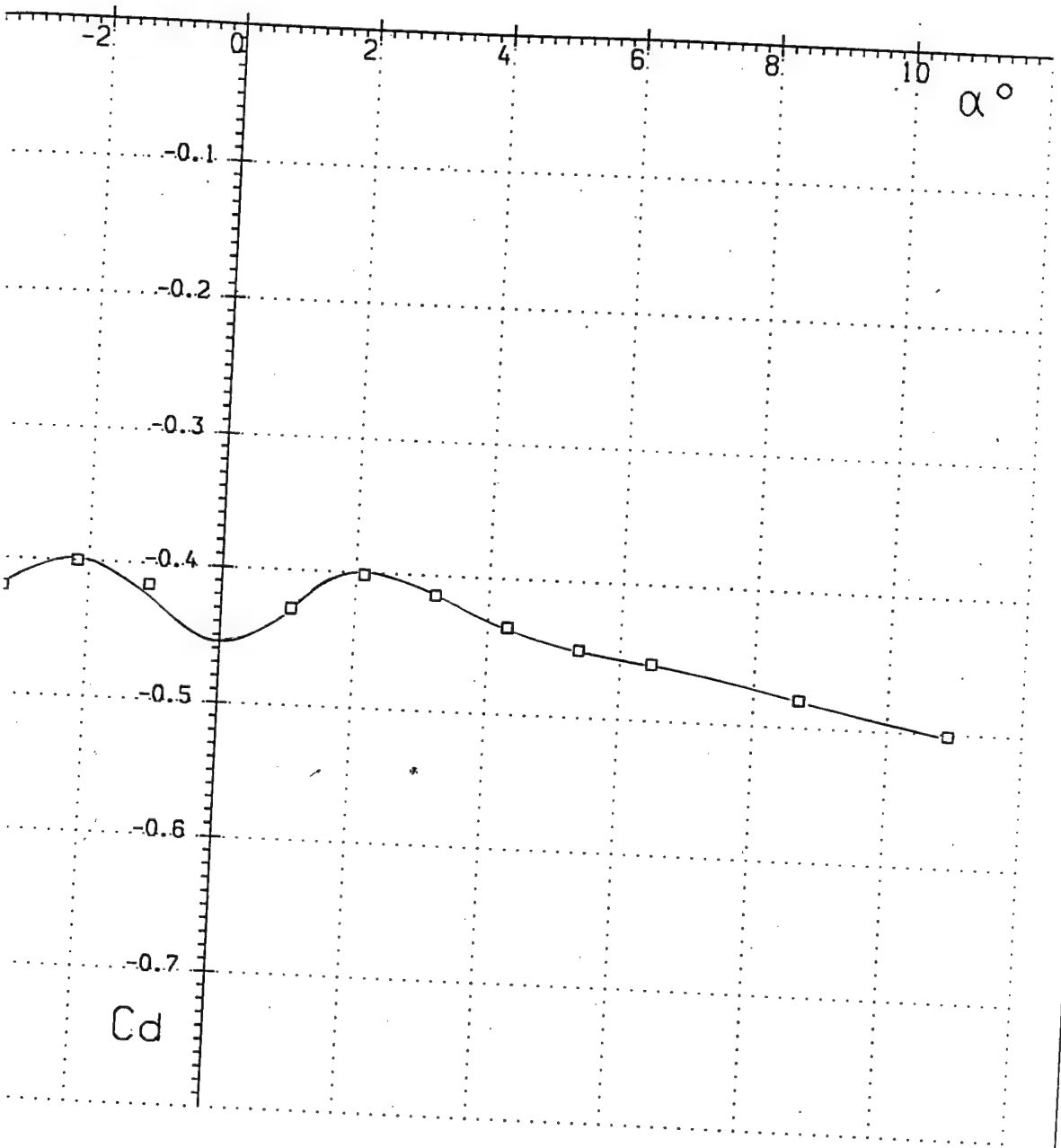

Run 13

Fig. 98

$M_\infty = 5.02$ $Re_x = 7.60 \cdot 10^6$

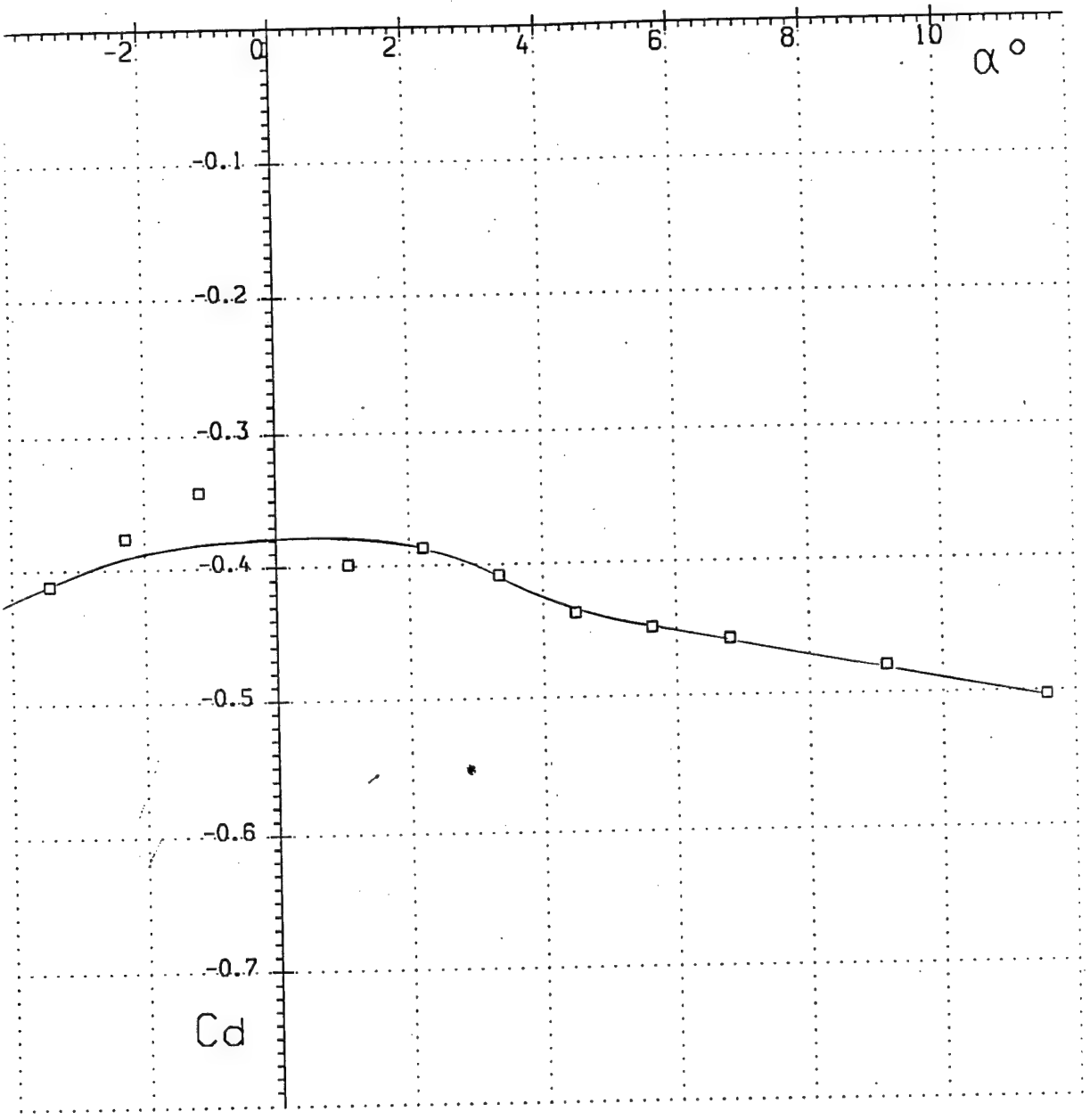

Run 14

Fig. 99

$M_\infty = 6.00$ $Re_x = .98 \cdot 10^6$

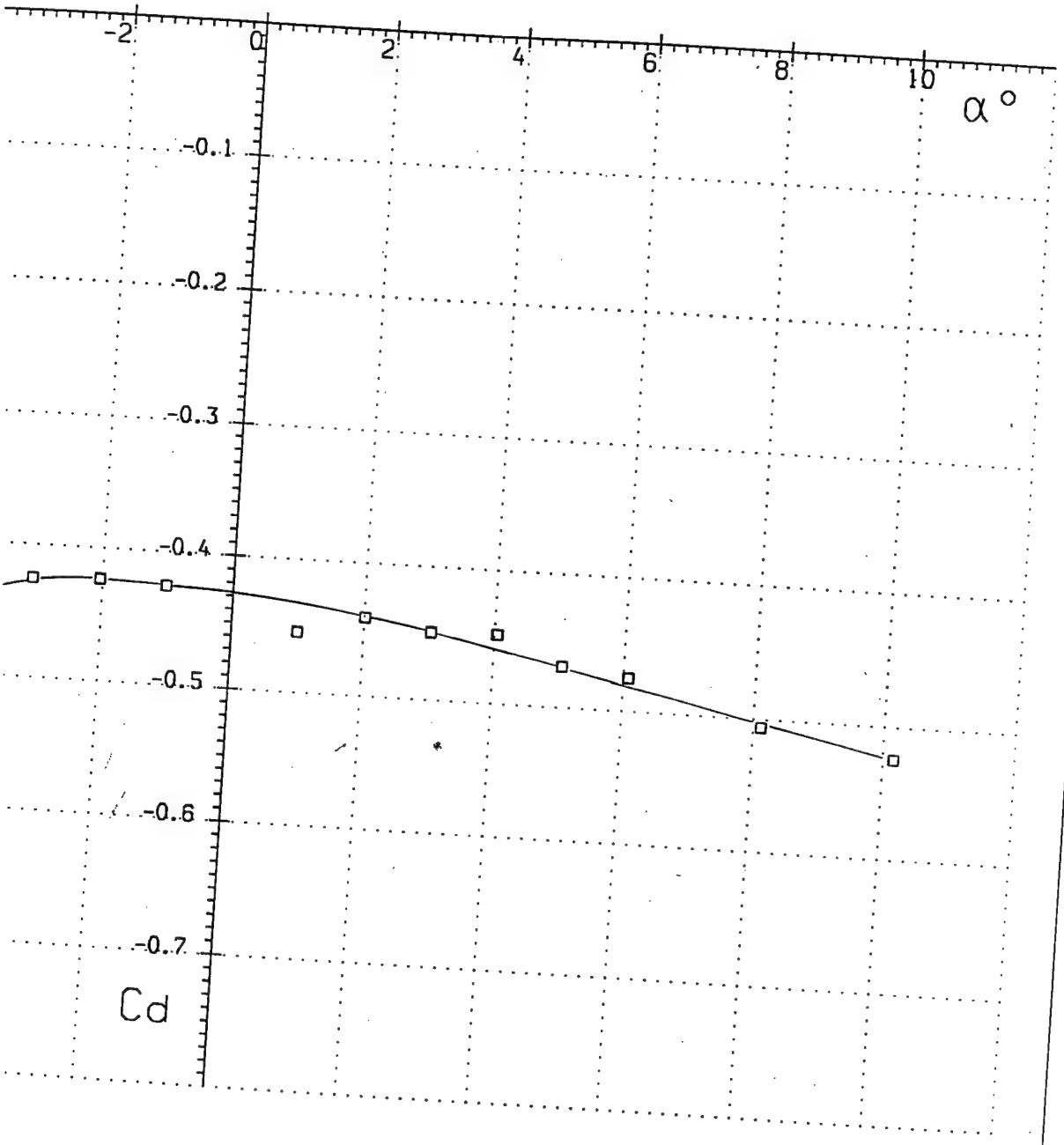

Run 15

$M_\infty = 6.05$ $Re_x = 1.85 \cdot 10^6$

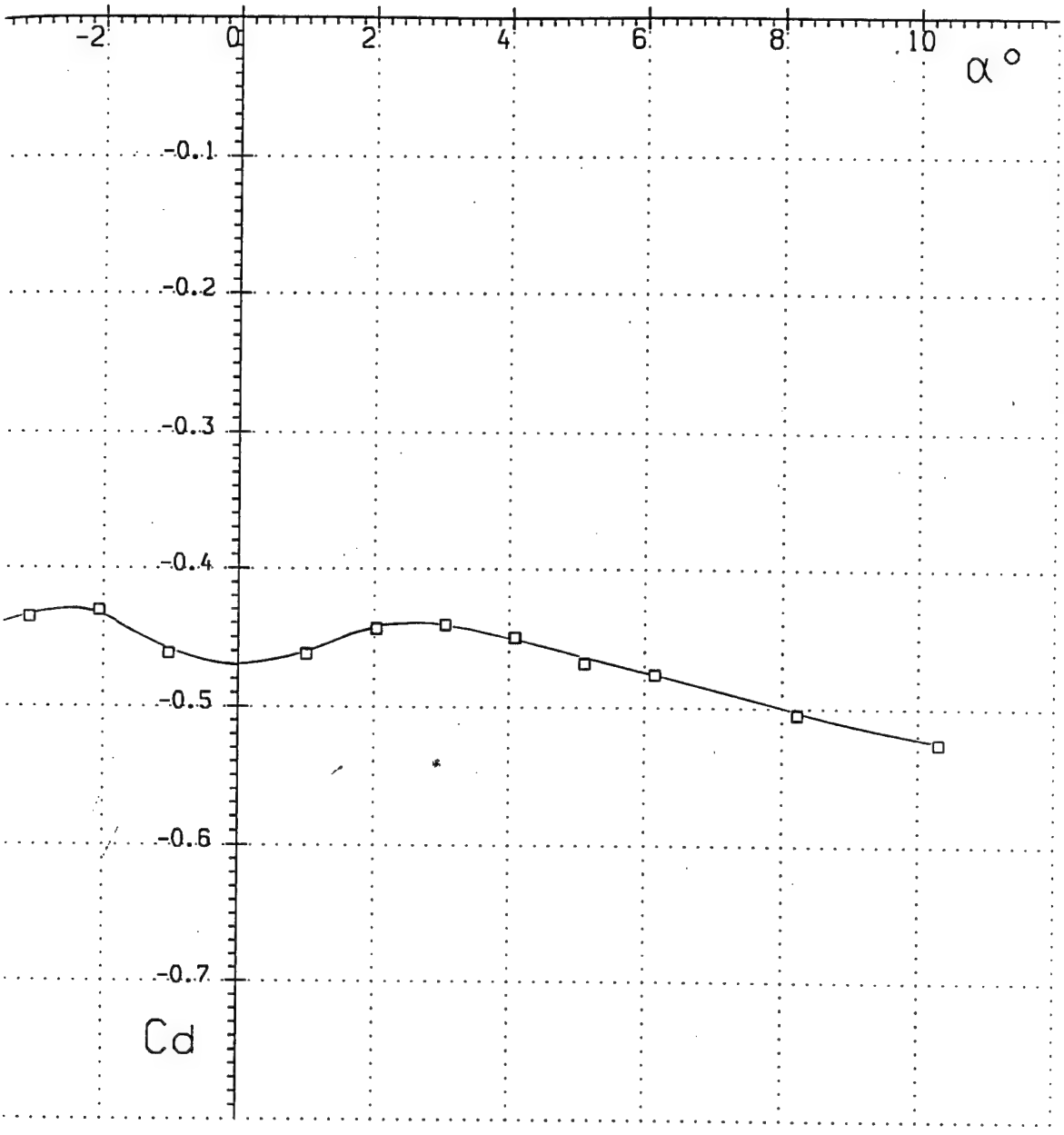

Run 16

Fig. 101

$M_\infty = 6.08$ $Re_x = 2.99 \cdot 10^6$

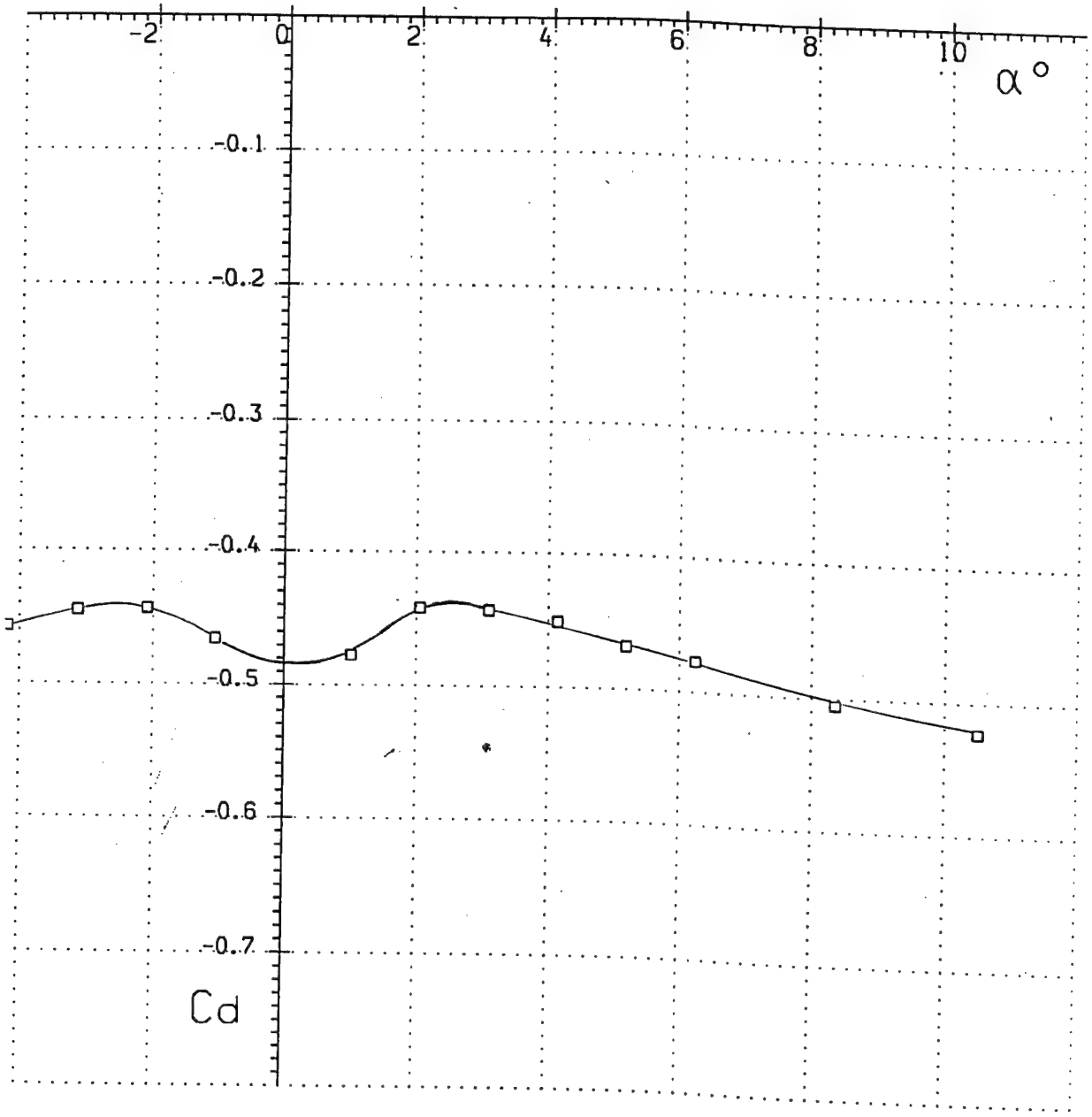

Run 17

Fig. 102

$M_\infty = 6.96$ $Re_x = 1.69 \cdot 10^6$

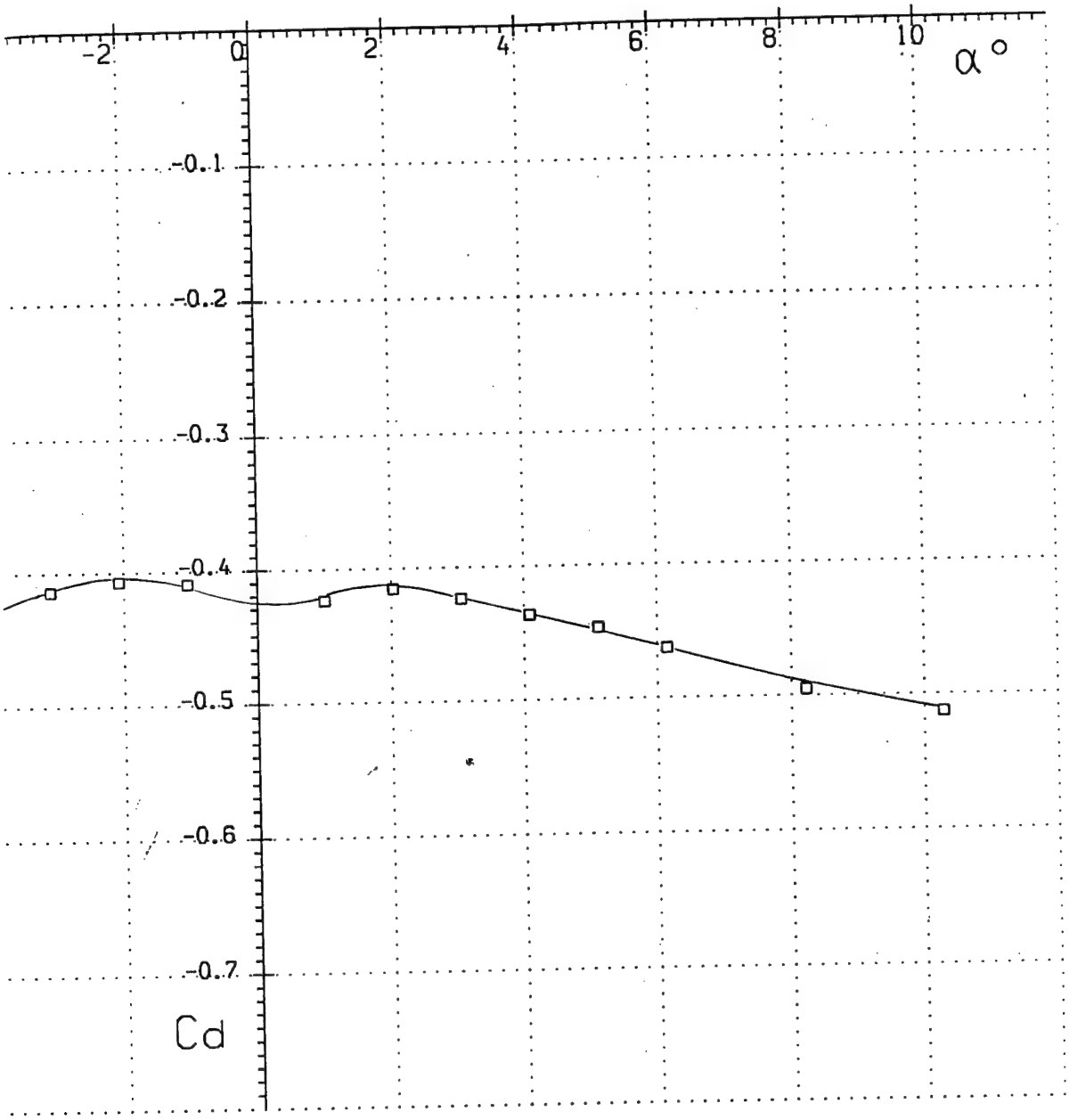

Run 18

Fig. 103

$M_\infty = 7.03$ $Re_x = 2.27 \cdot 10^6$

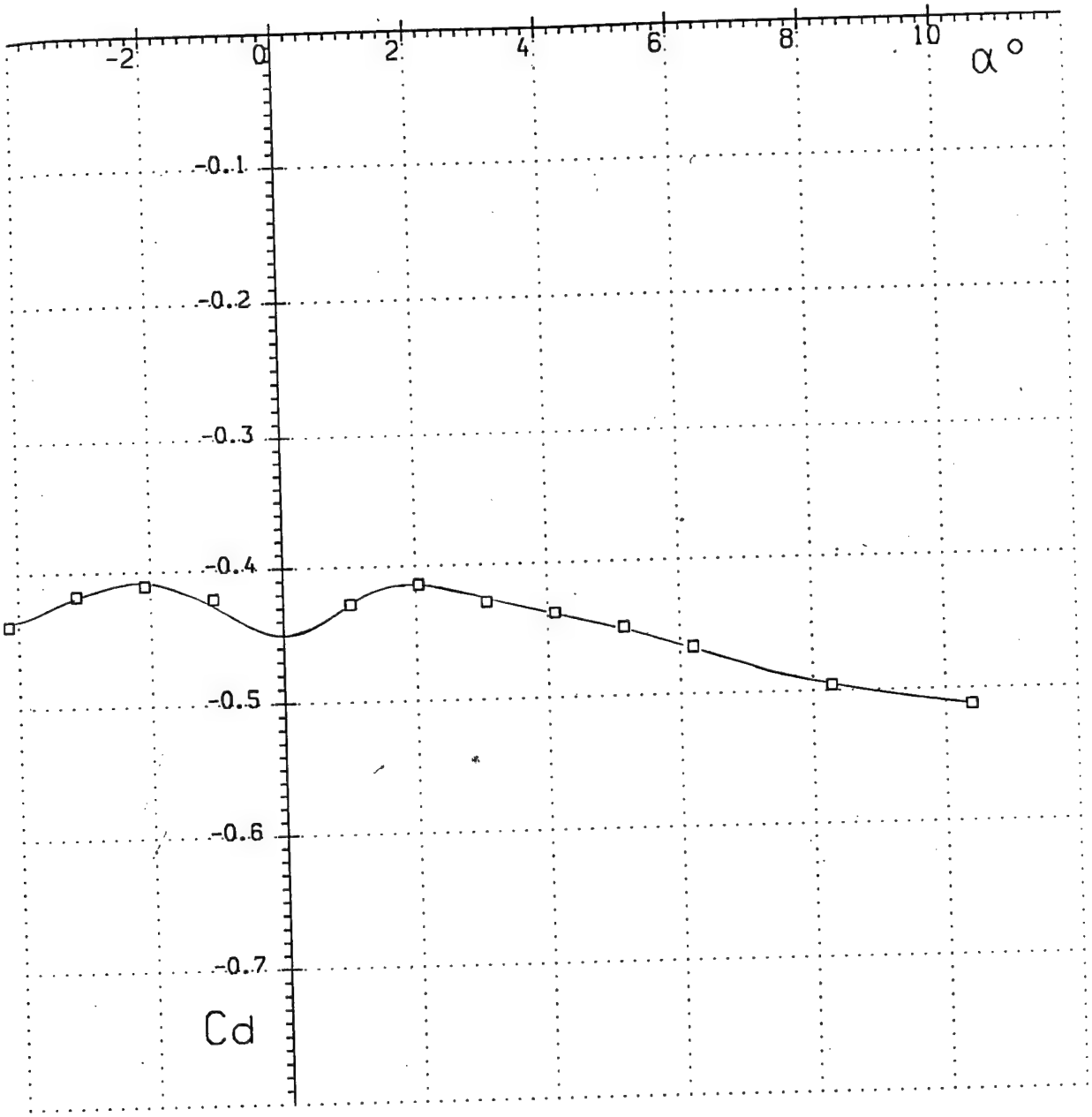

Run 19

Fig. 104

$M_\infty = 7.05$ $Re_x = 2.74 \cdot 10^6$

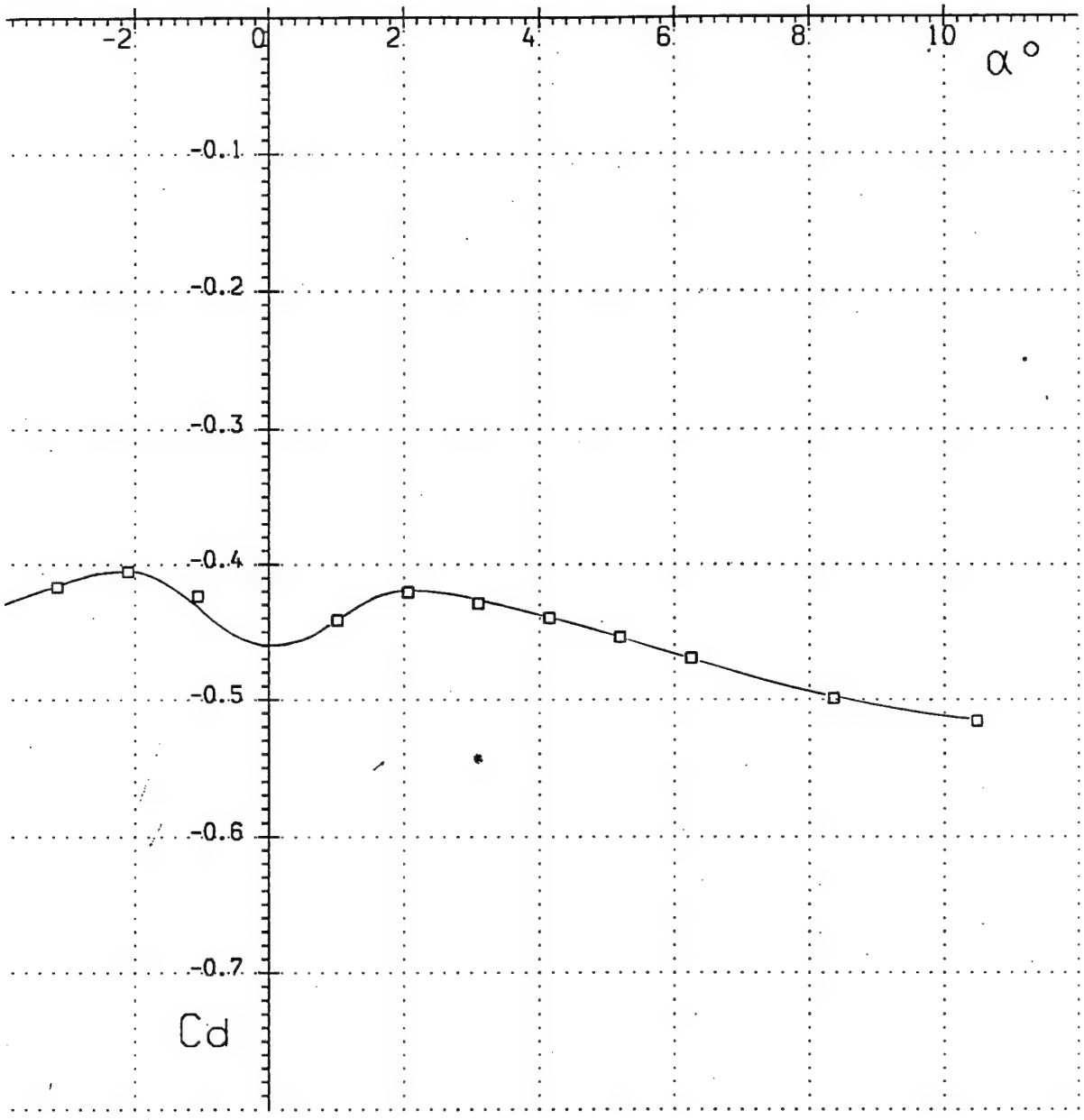

Run 20

Fig. 105

$M_\infty = 7.07$ $Re_x = 4.39 \cdot 10^6$

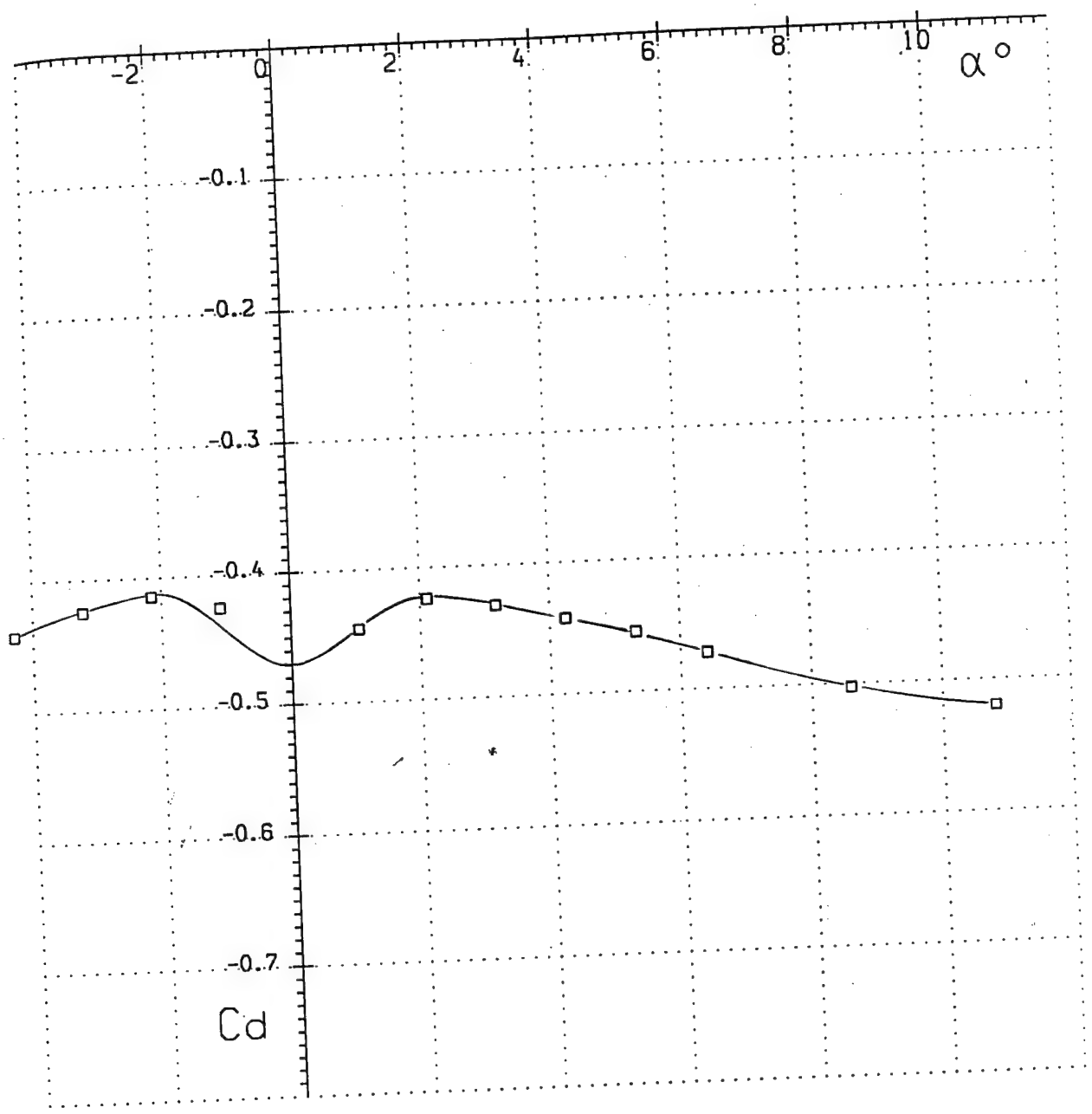

Run 21

Fig. 106

$M_\infty = 7.07$ $Re_x = 6.26 \cdot 10^6$

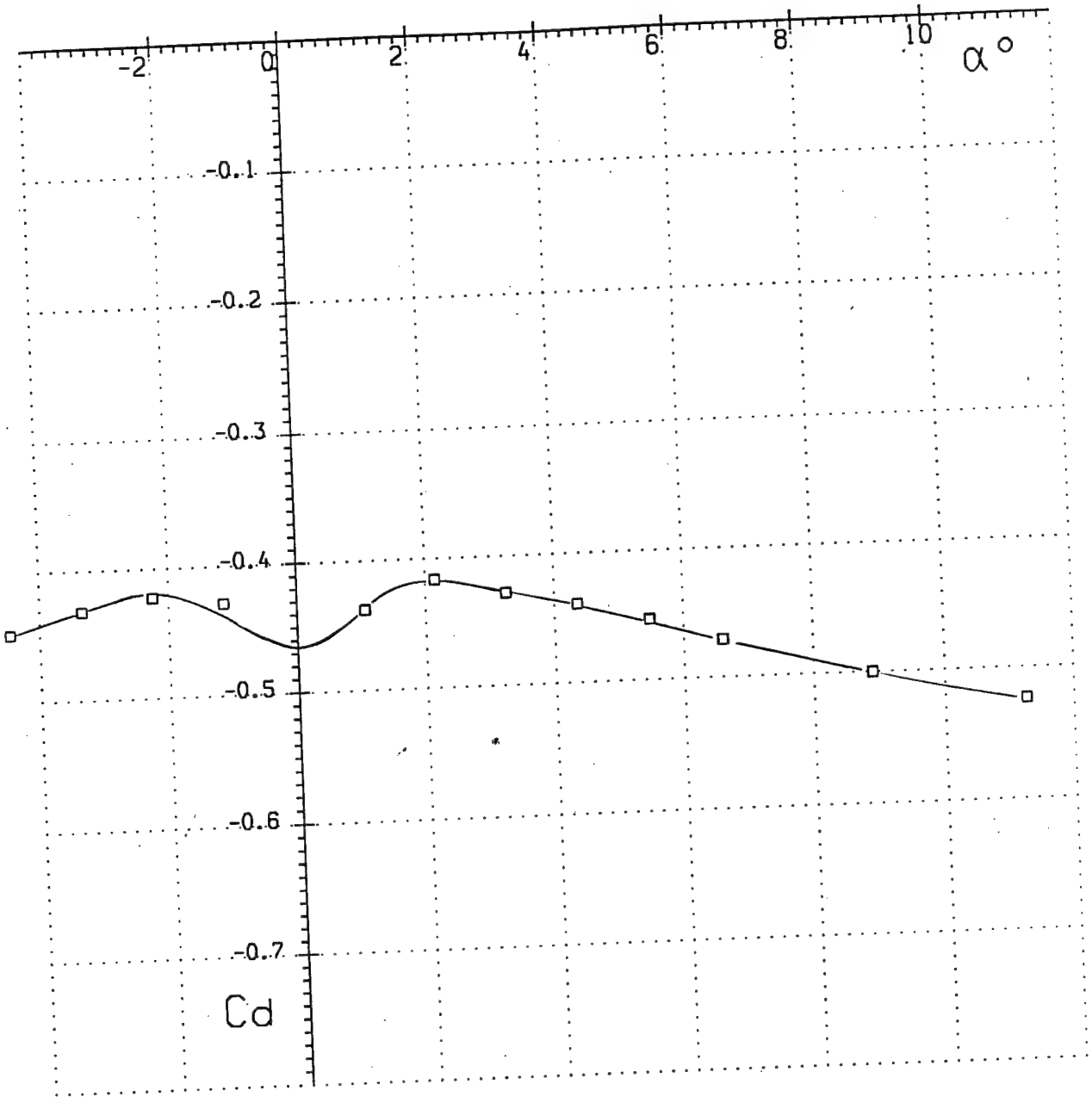

Run 22

Fig. 107

$M_\infty = 7.97$ $Re_x = 1.28 \cdot 10^6$

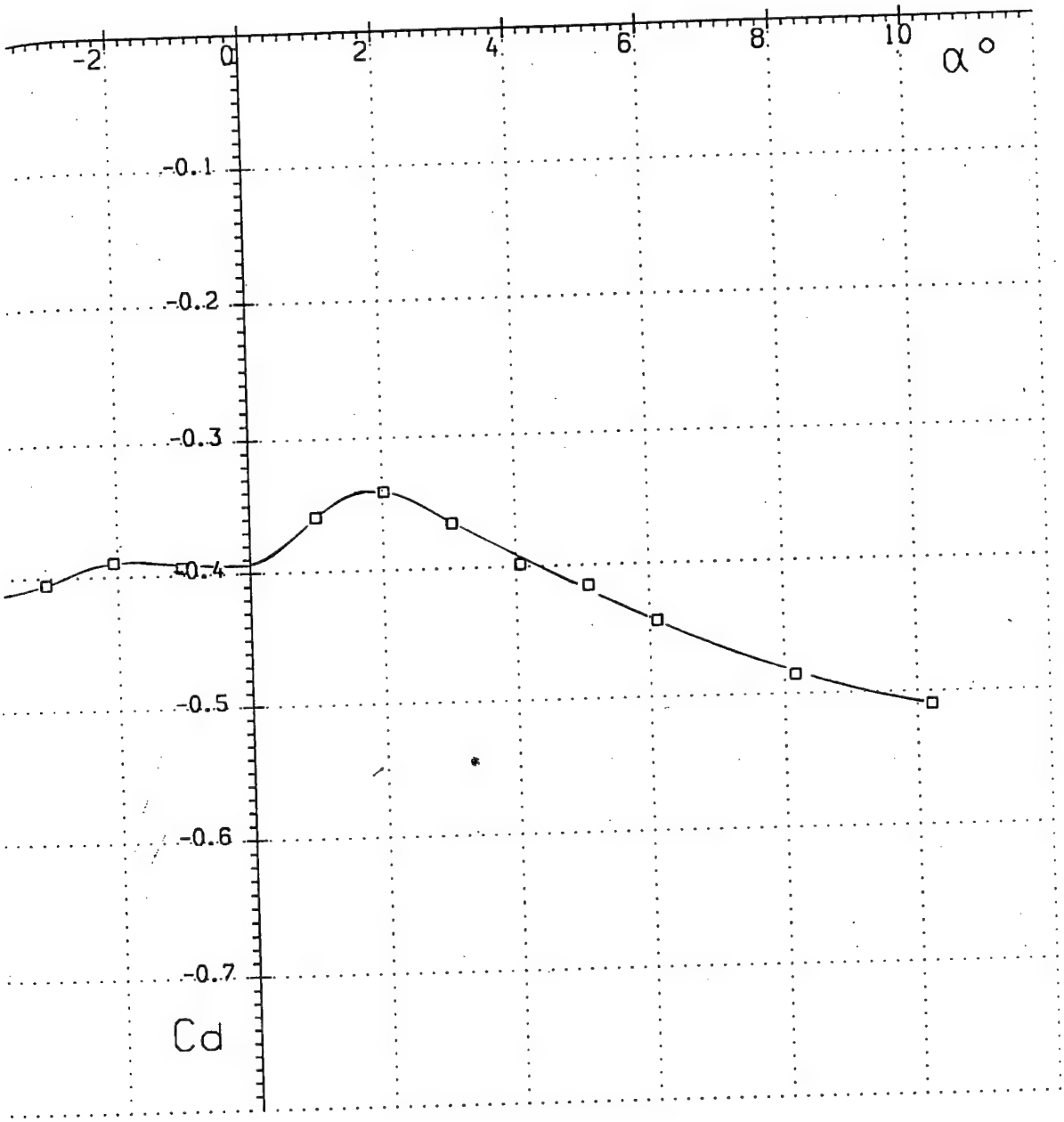

Run 23

Fig. 108

$M_\infty = 8.00$ $Re_x = 2.00 \cdot 10$

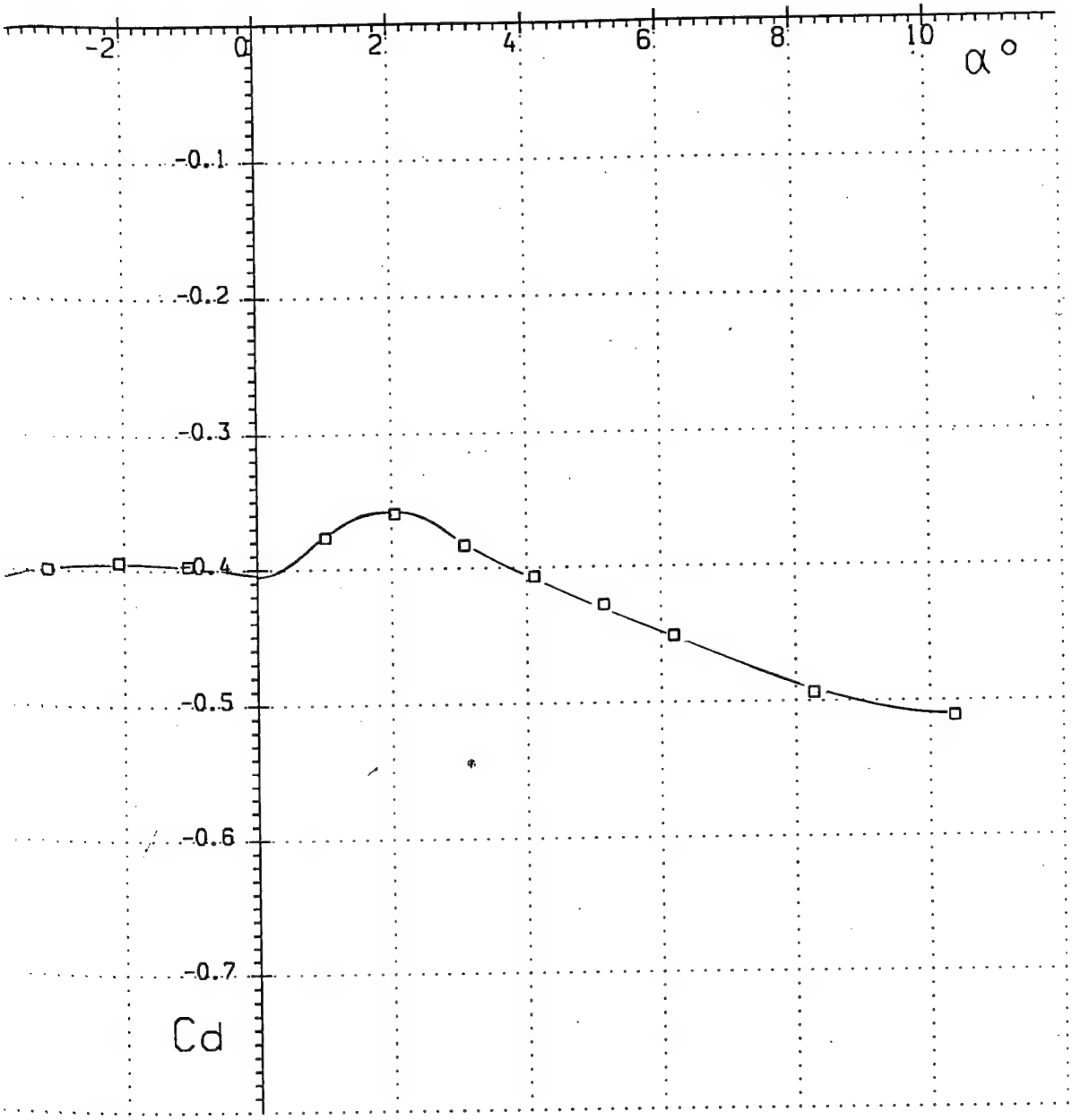

Run 24

Fig. 109

$M_\infty = 8.03$ $Re_x = 3.30 \cdot 10^6$

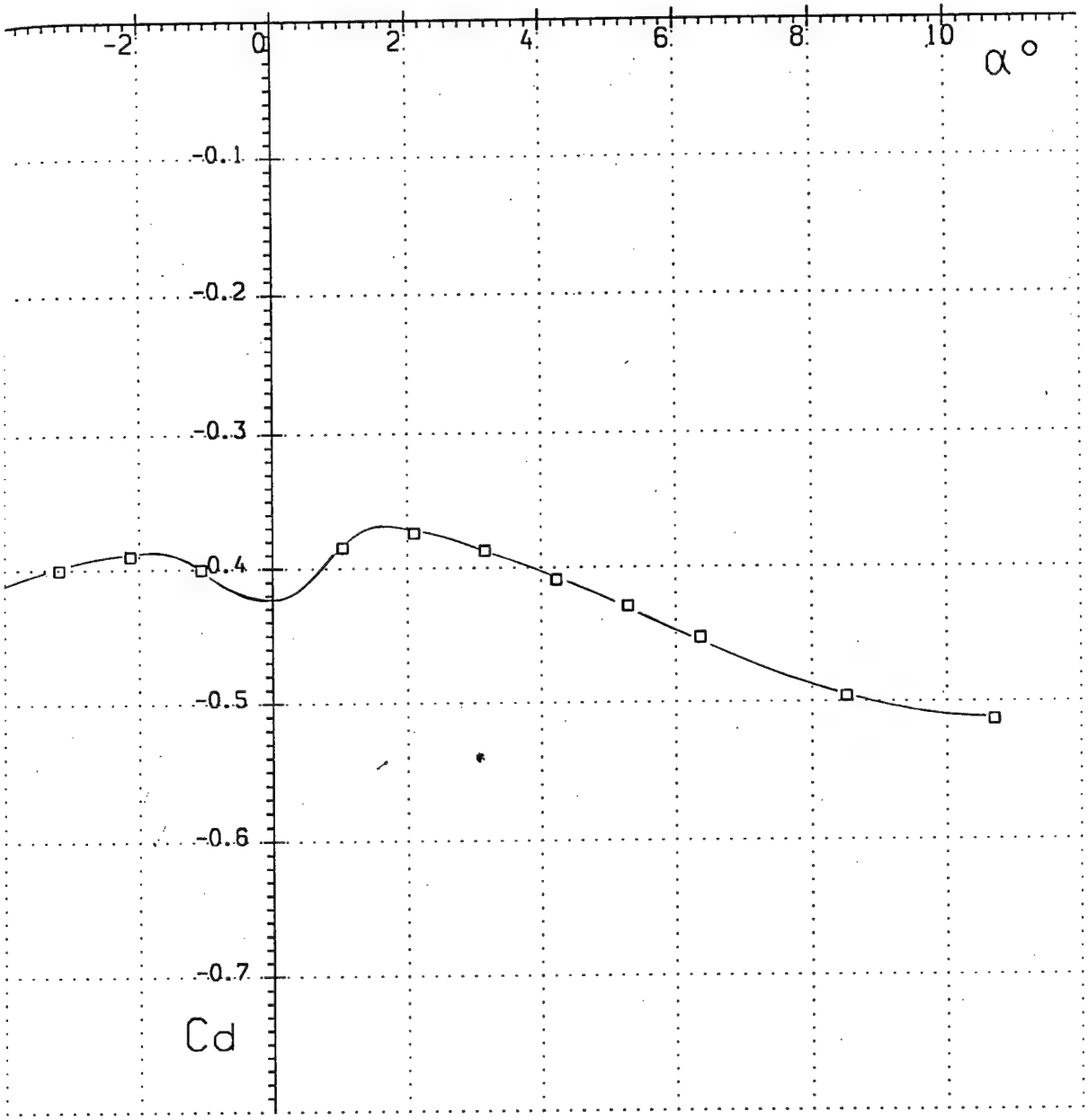

Run 25

Fig. 110

$M_\infty = 8.96$ $Re_x = 1.21 \cdot 10^6$

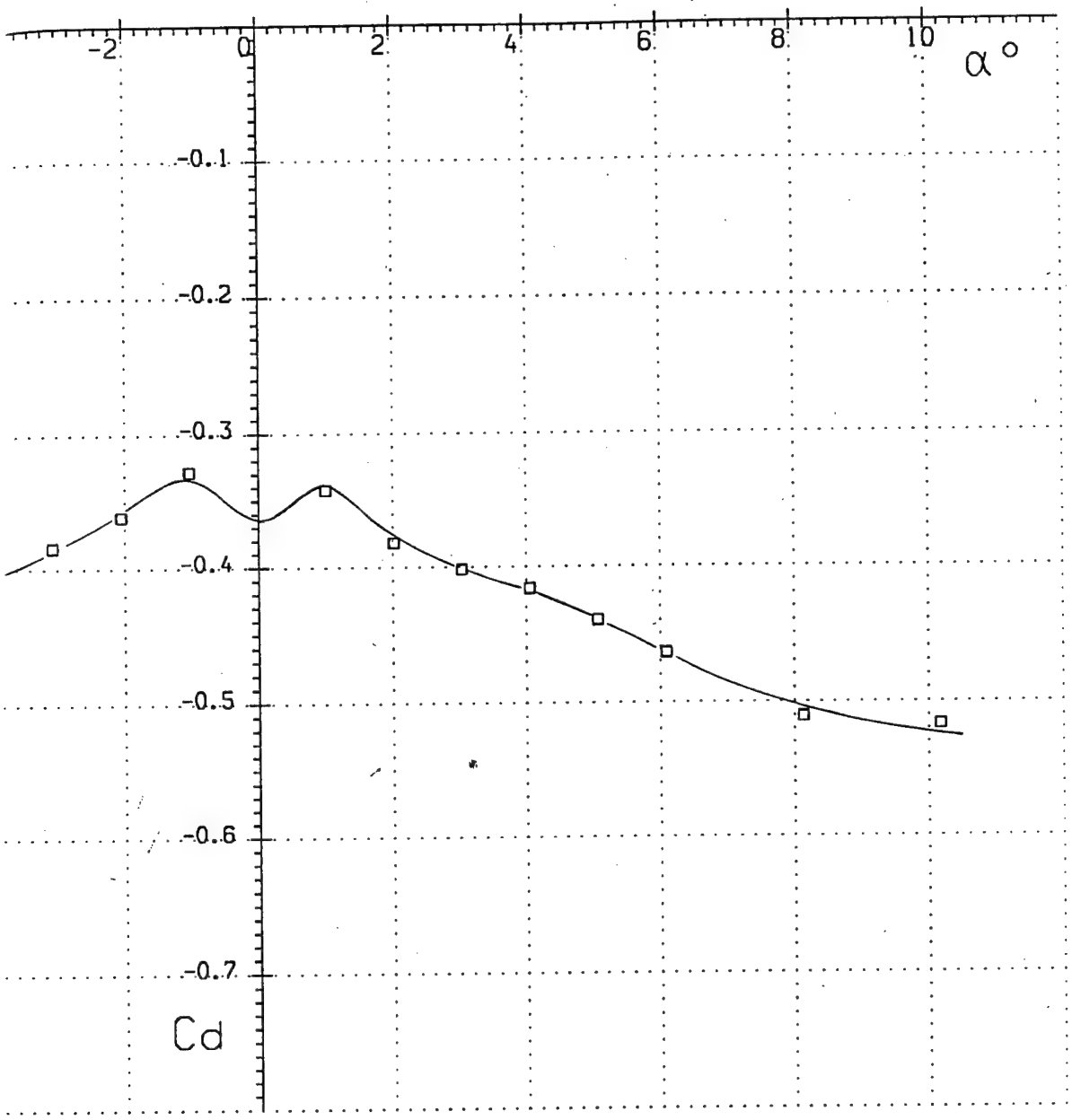

Run 26

Fig. 111

$M_\infty = 9.04$ $Re_x = 2.23 \cdot 10^6$

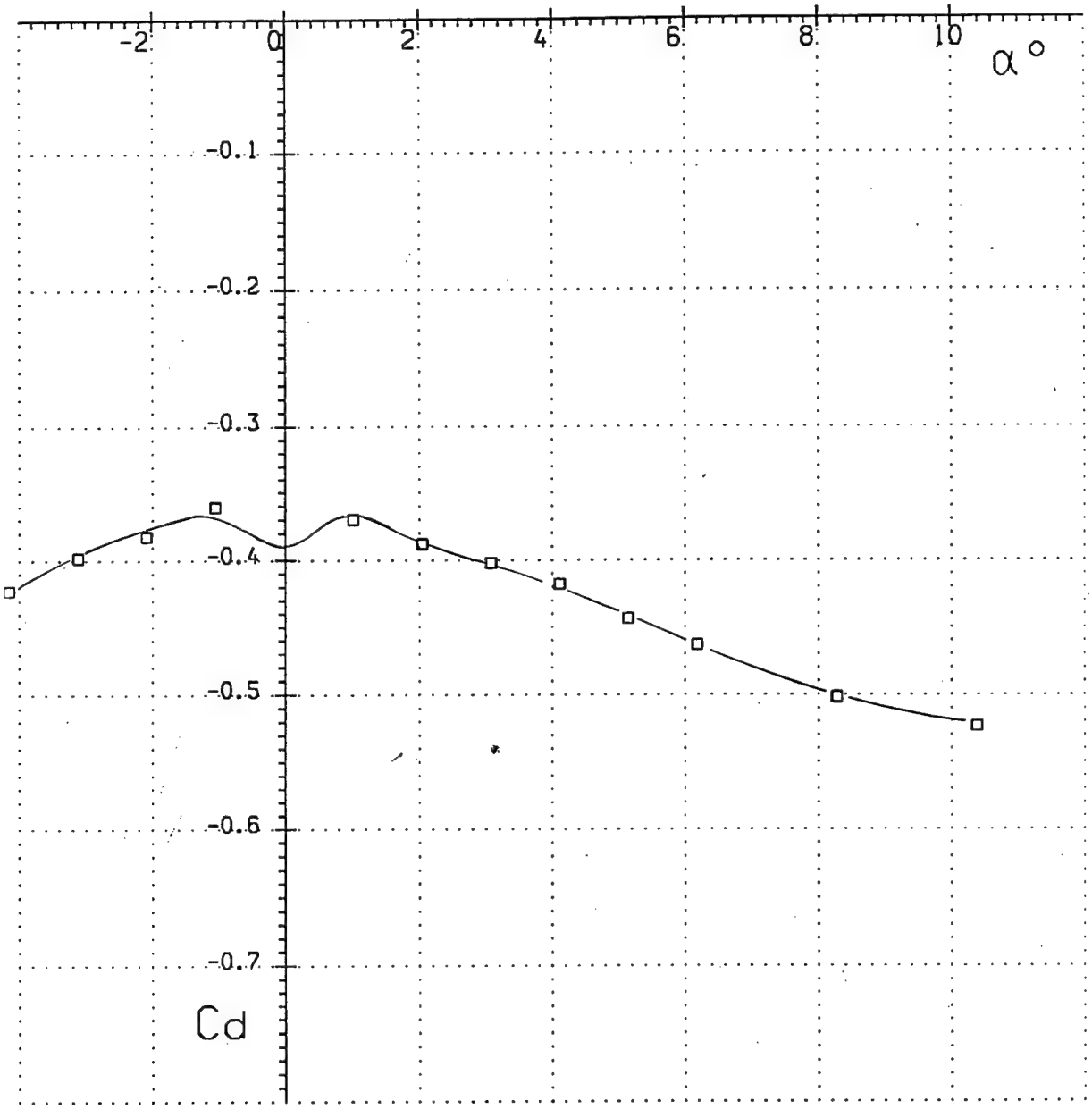

Run 27

Fig. 112

$\alpha = 0°$

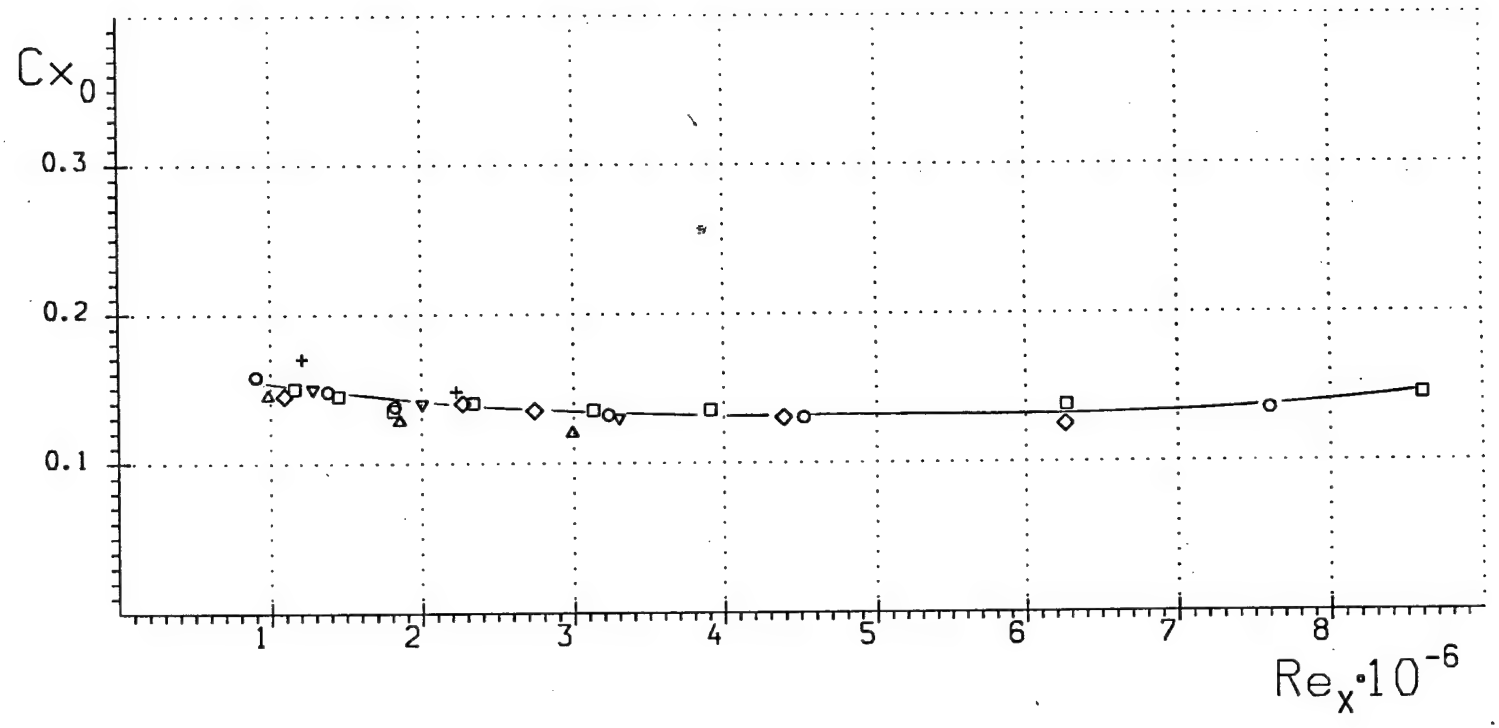

□ $M_\infty \approx$ 4.0 ◇ $M_\infty \approx$ 7.0

○ $M_\infty \approx$ 5.0 ▽ $M_\infty \approx$ 8.0

△ $M_\infty \approx$ 6.0 + $M_\infty \approx$ 9.0

Fig. 112

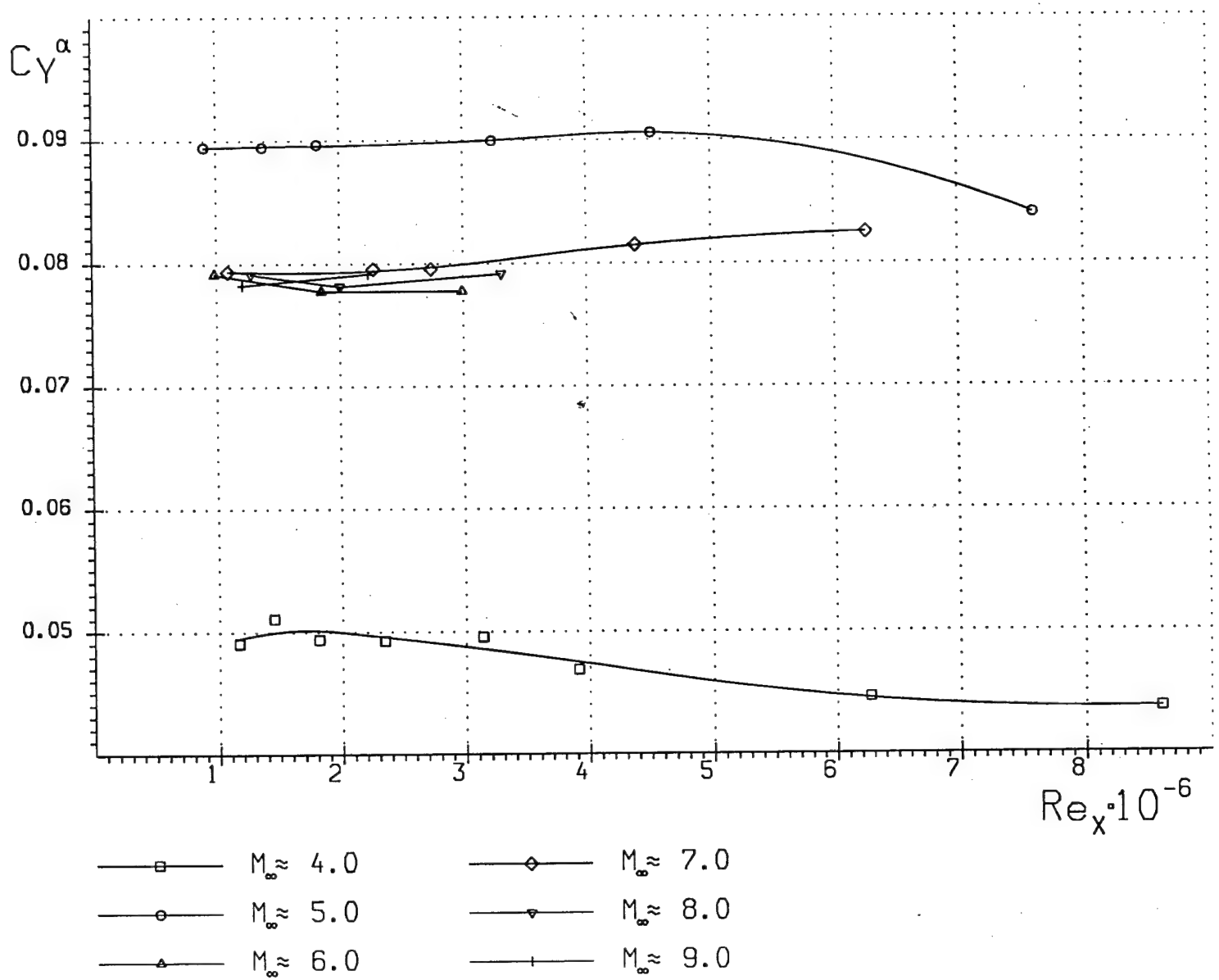
C_Y^α
0.09
0.08
0.07
0.06
0.05
1
2
3
4
5
6
7
8
$Re_x \cdot 10^{-6}$
$M_\infty \approx$ 4.0
$M_\infty \approx$ 5.0
$M_\infty \approx$ 6.0
$M_\infty \approx$ 7.0
$M_\infty \approx$ 8.0
$M_\infty \approx$ 9.0

Fig. 114

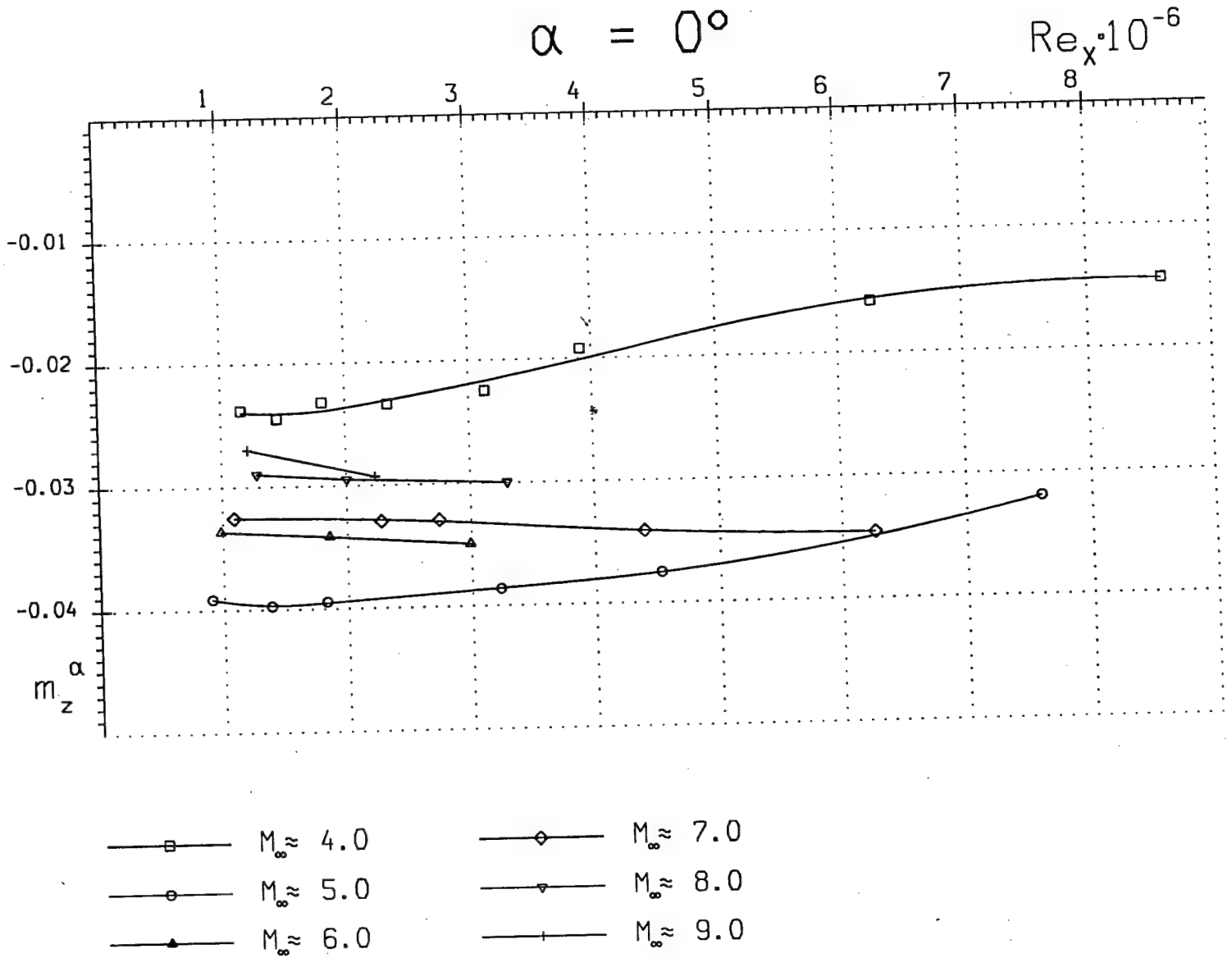
α = 0°
$Re_x \cdot 10^{-6}$
1
2
3
4
5
6
7
8
-0.01
-0.02
-0.03
-0.04
m_z^α
$M_\infty \approx$ 4.0
$M_\infty \approx$ 5.0
$M_\infty \approx$ 6.0
$M_\infty \approx$ 7.0
$M_\infty \approx$ 8.0
$M_\infty \approx$ 9.0

Fig. 115

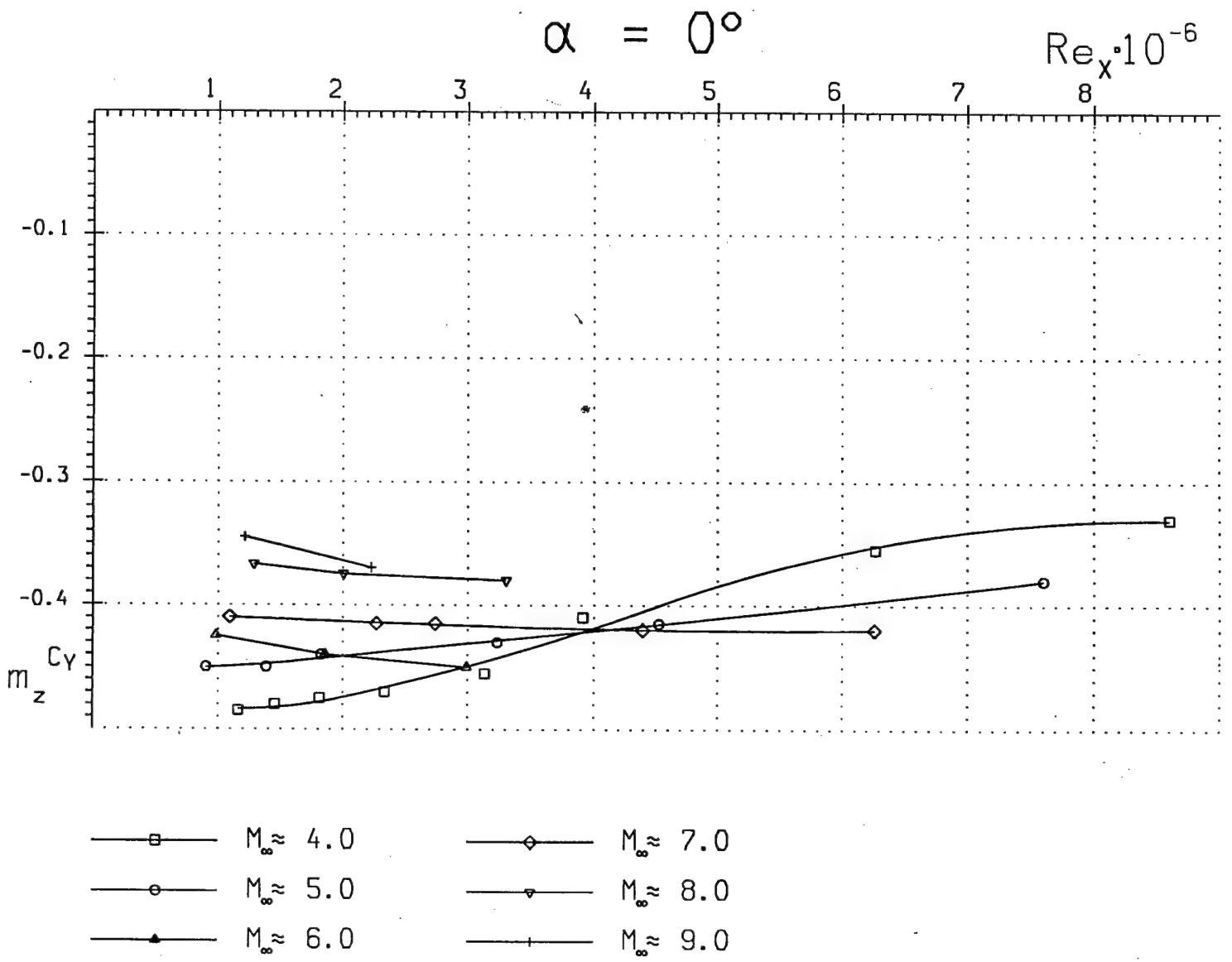

Fig. 116

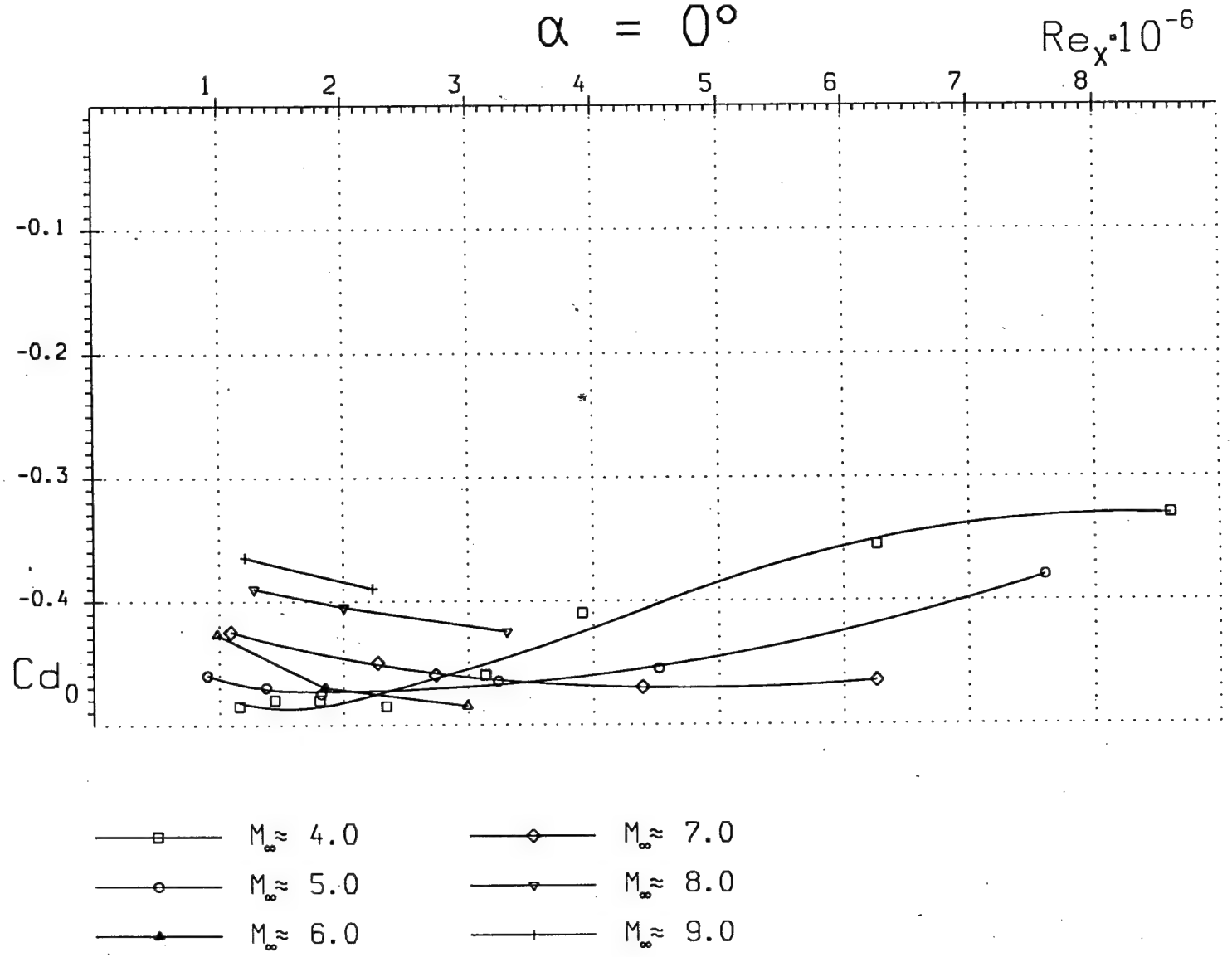
α = 0°
$Re_x \cdot 10^{-6}$
1
2
3
4
5
6
7
8
-0.1
-0.2
-0.3
-0.4
Cd_0
$M_\infty \approx$ 4.0
$M_\infty \approx$ 5.0
$M_\infty \approx$ 6.0
$M_\infty \approx$ 7.0
$M_\infty \approx$ 8.0
$M_\infty \approx$ 9.0

Fig. 117

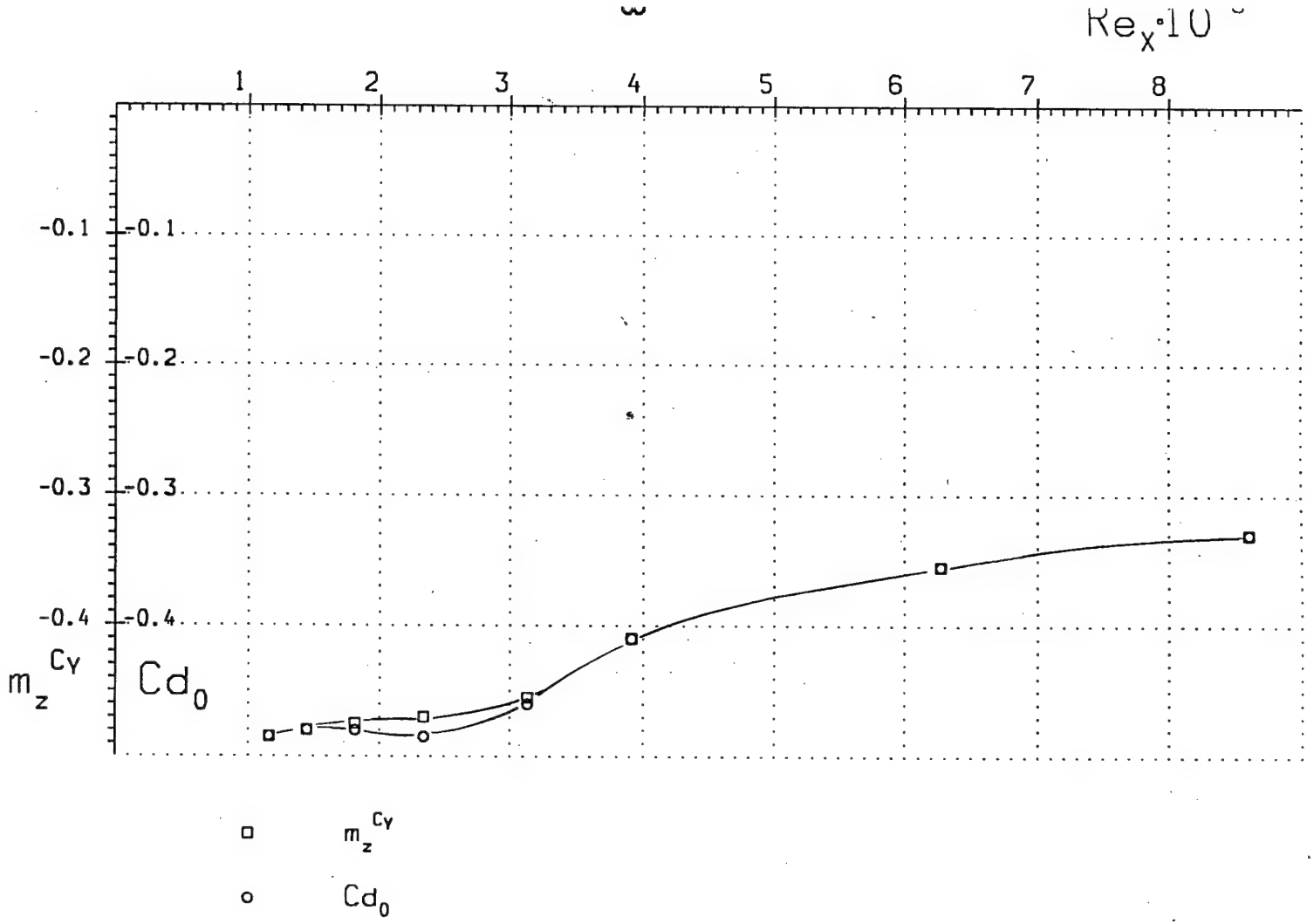

Fig. 118

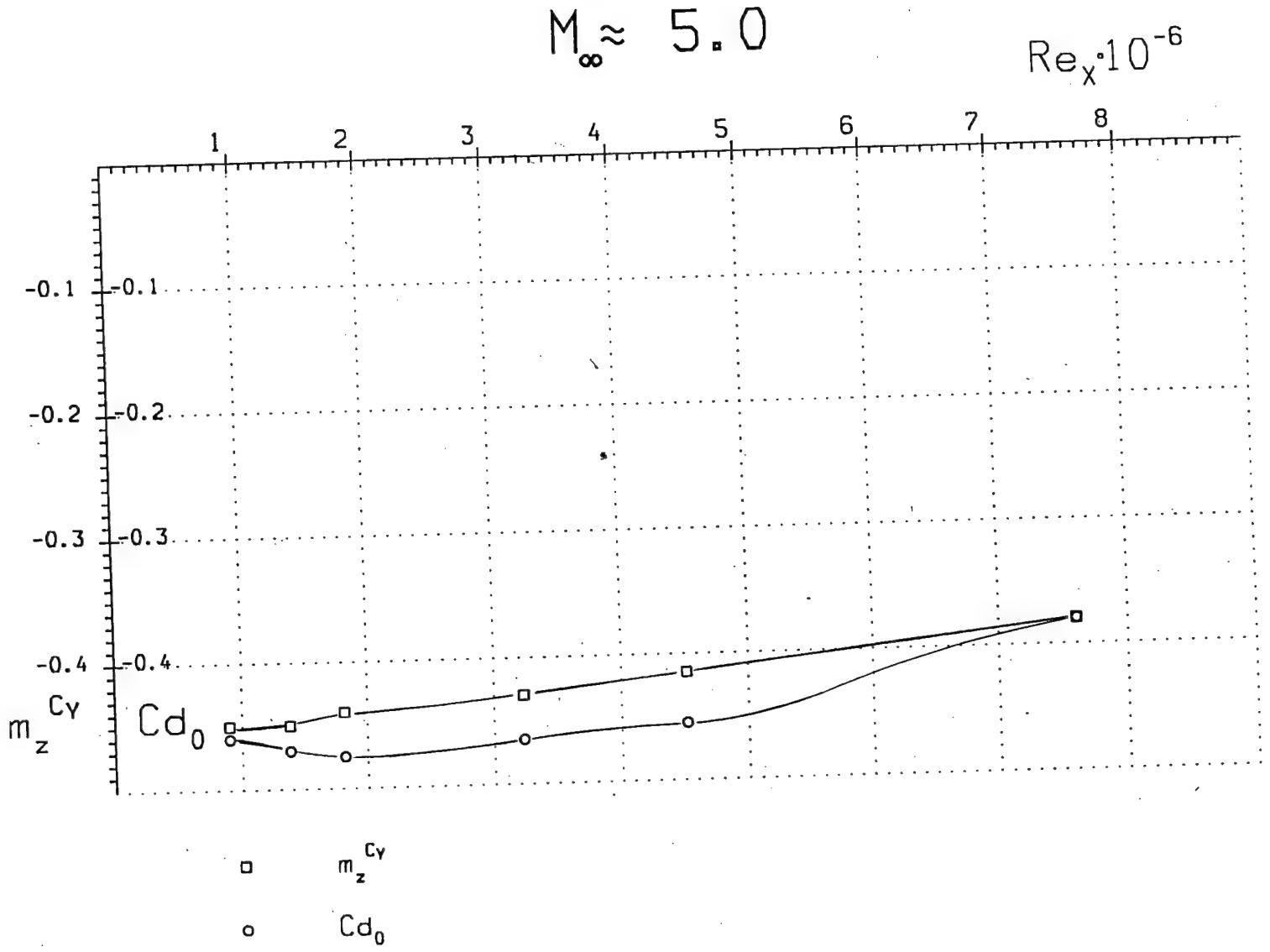
$M_\infty \approx 5.0$
$Re_x \cdot 10^{-6}$
1
2
3
4
5
6
7
8
-0.1
-0.2
-0.3
-0.4
m_z^{Cy}
Cd_0
m_z^{Cy}
Cd_0

Fig. 119

$M_\infty \approx 6.0$

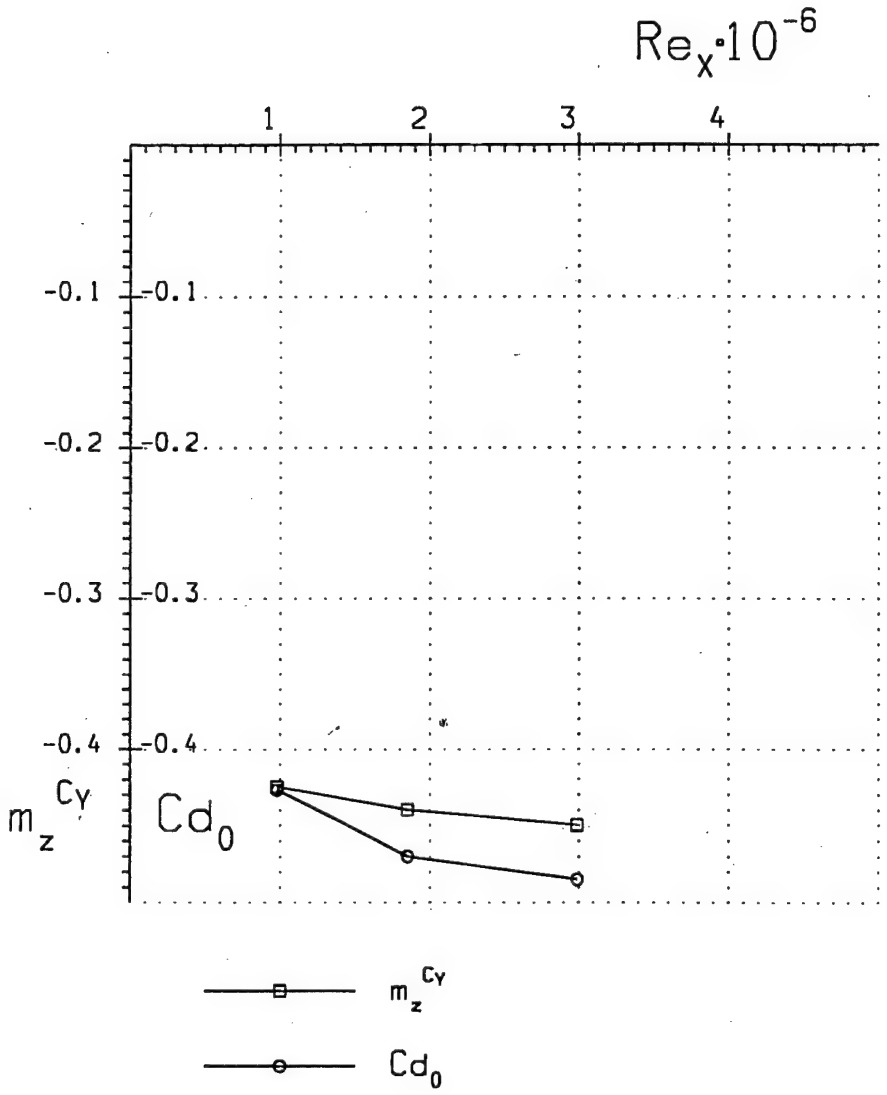

Fig. 120

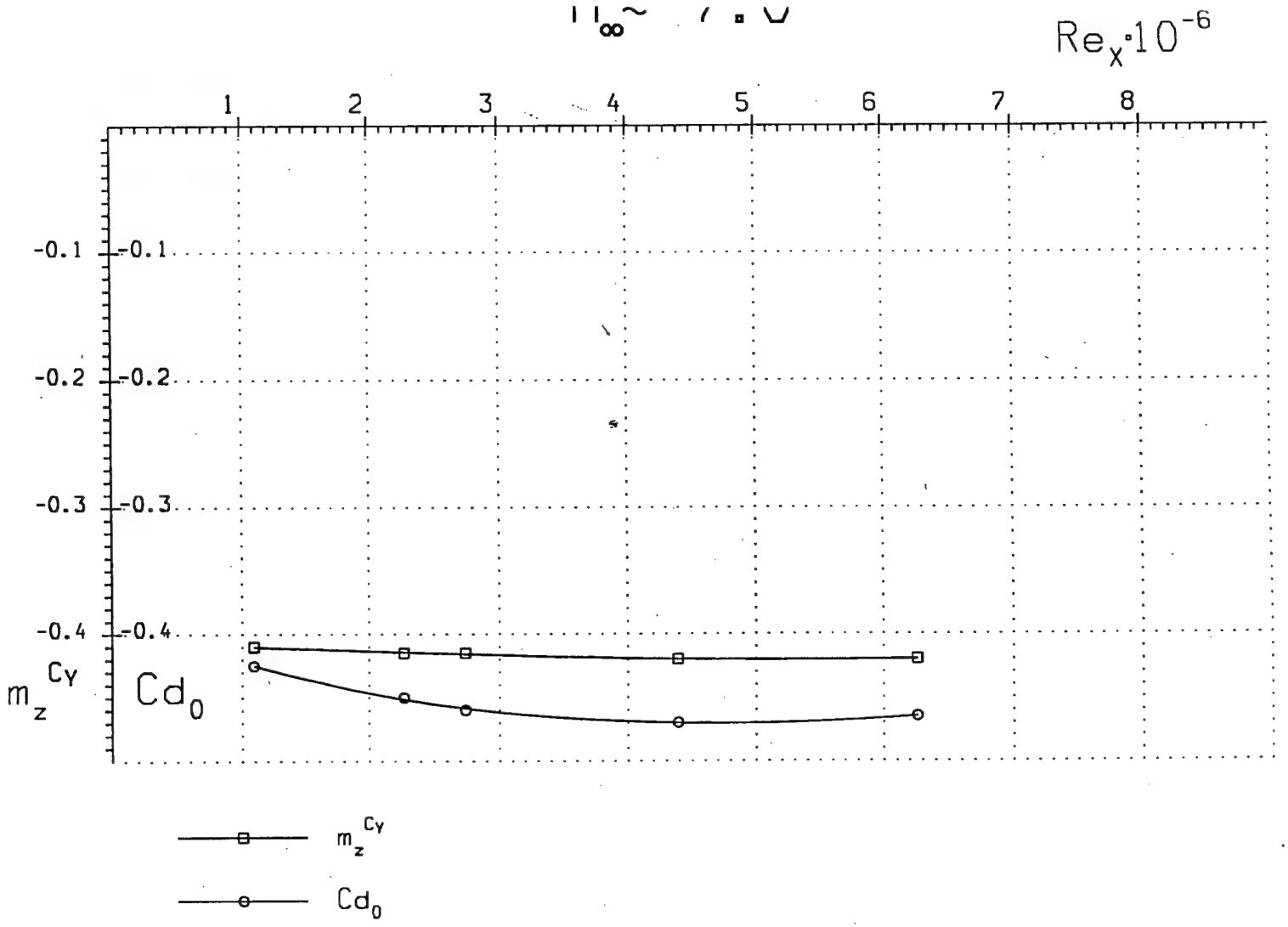

Fig. 121

$M_\infty \approx 8.0$

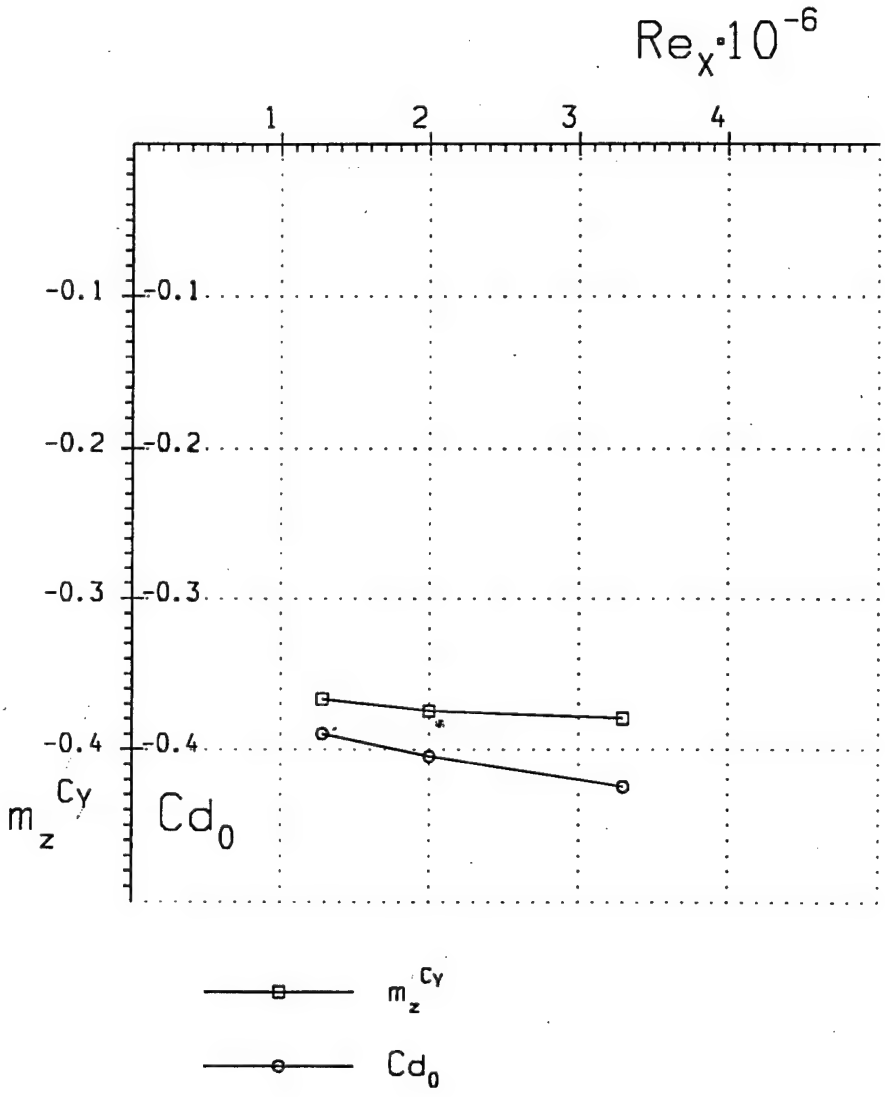

Fig. 122

$M_\infty \approx 9.0$

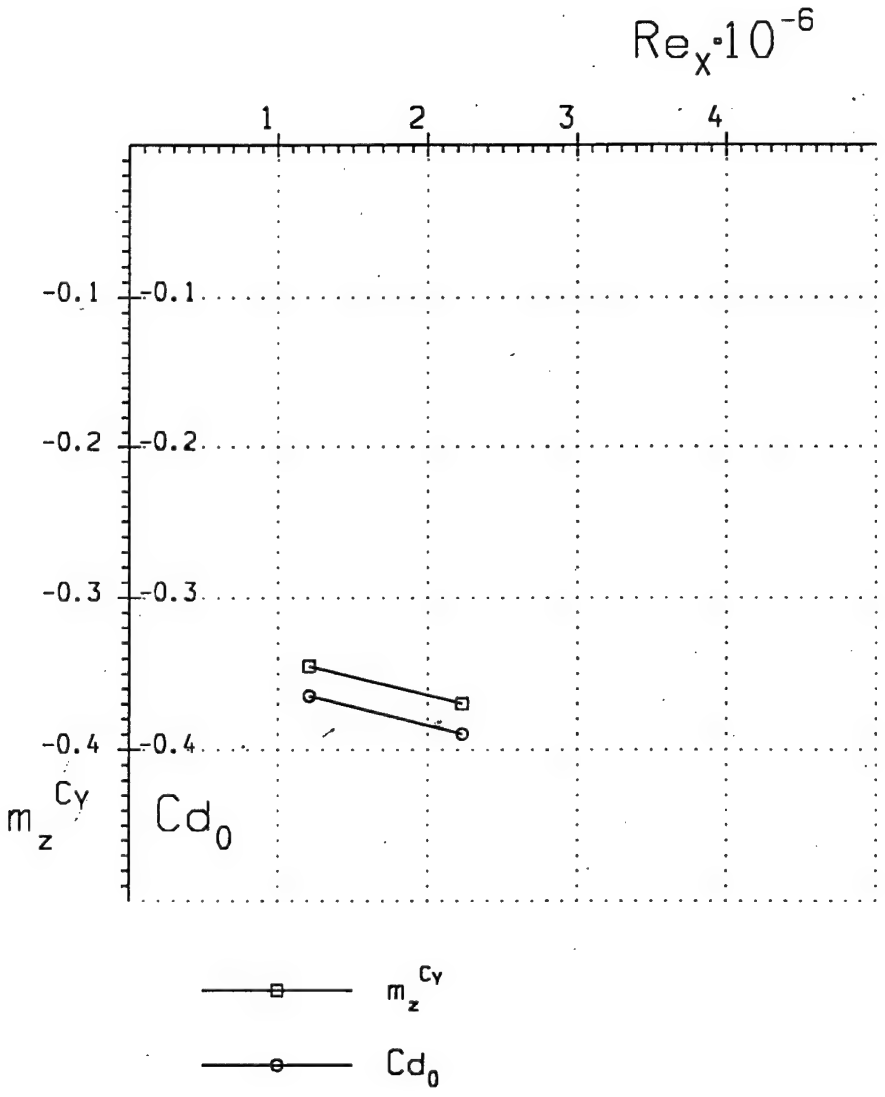

Fig. 123

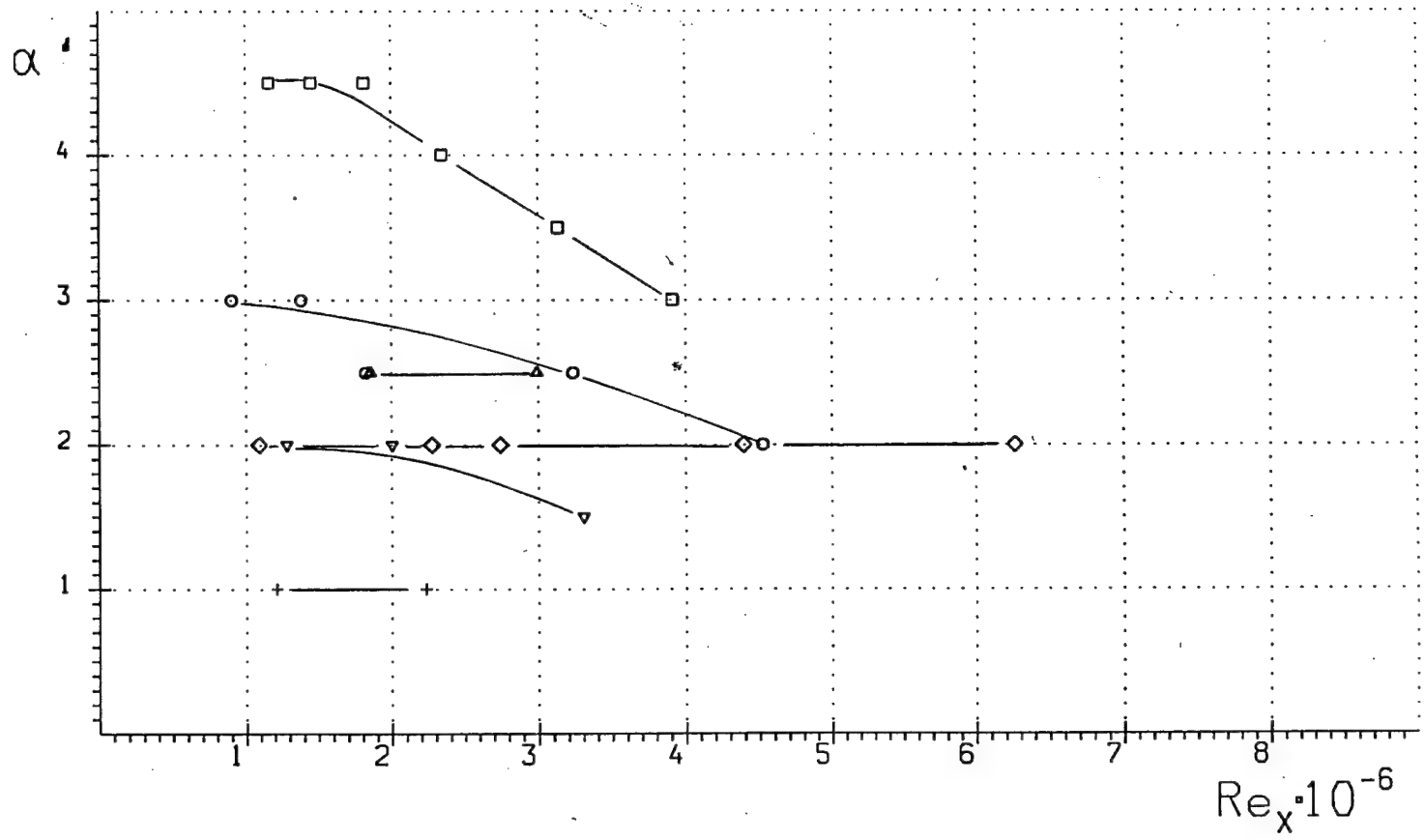
α
4
3
2
1
1
2
3
4
5
6
7
8
$Re_x \cdot 10^{-6}$
□ $M_\infty \approx$ 4.0
◇ $M_\infty \approx$ 7.0
○ $M_\infty \approx$ 5.0
▽ $M_\infty \approx$ 8.0
△ $M_\infty \approx$ 6.0
+ $M_\infty \approx$ 9.0

Fig. 124

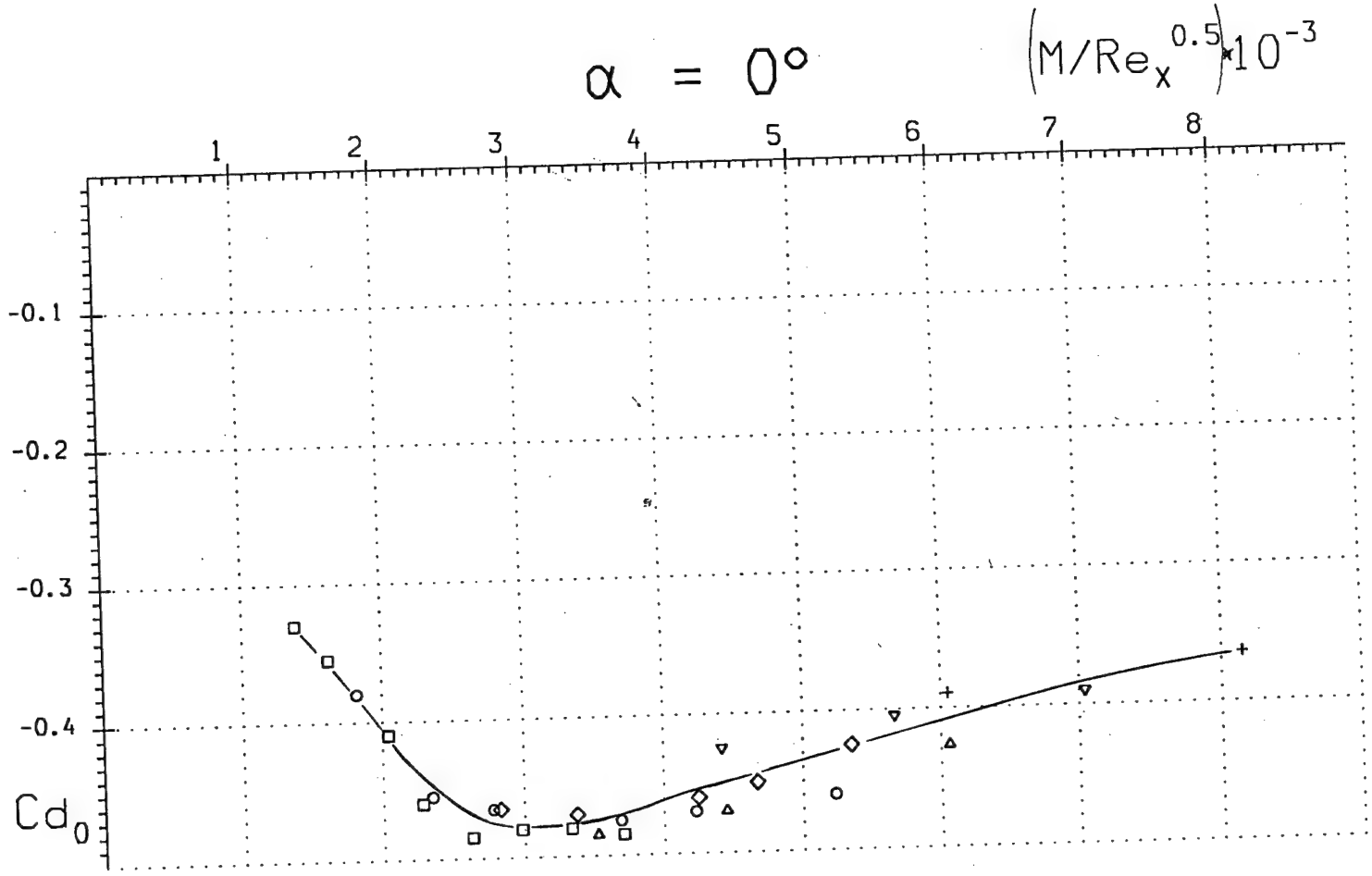
α = 0°
$\left(M/Re_x^{0.5}\right)\times 10^{-3}$
1
2
3
4
5
6
7
8
-0.1
-0.2
-0.3
-0.4
Cd_0
□ $M_\infty \approx$ 4.0
○ $M_\infty \approx$ 5.0
△ $M_\infty \approx$ 6.0
◇ $M_\infty \approx$ 7.0
▽ $M_\infty \approx$ 8.0
+ $M_\infty \approx$ 9.0

Fig. 125

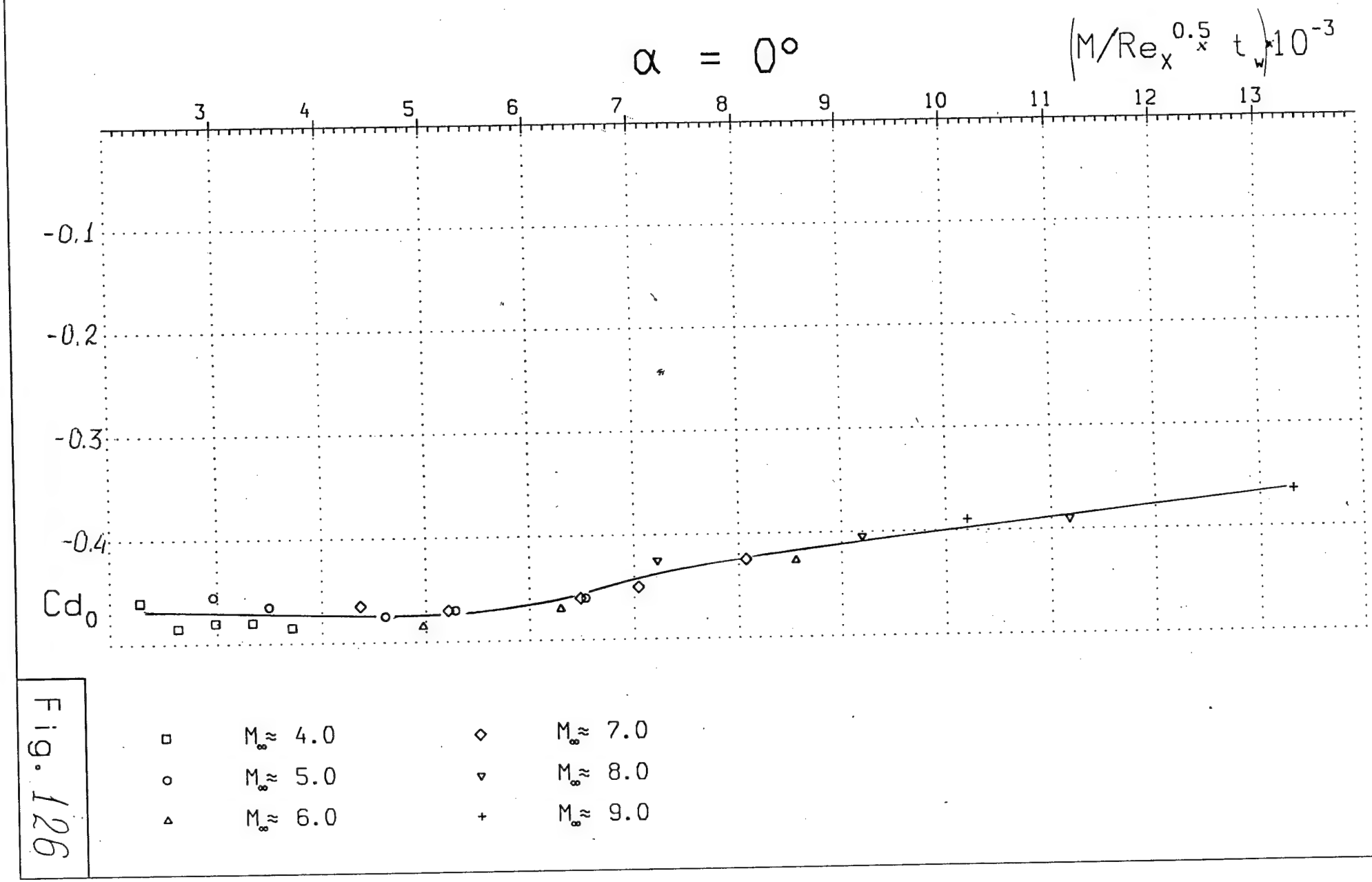
α = 0°
$(M/Re_x^{0.5} t_w) 10^{-3}$
3
4
5
6
7
8
9
10
11
12
13
-0.1
-0.2
-0.3
-0.4
Cd_0
$M_\infty \approx 4.0$
$M_\infty \approx 5.0$
$M_\infty \approx 6.0$
$M_\infty \approx 7.0$
$M_\infty \approx 8.0$
$M_\infty \approx 9.0$

Fig. 126

$M_\infty = 4.00$ $Re_x = 1.16 \cdot 10^6$

$M \cdot Re_x^{-0.5} = 3.71 \cdot 10^{-3}$

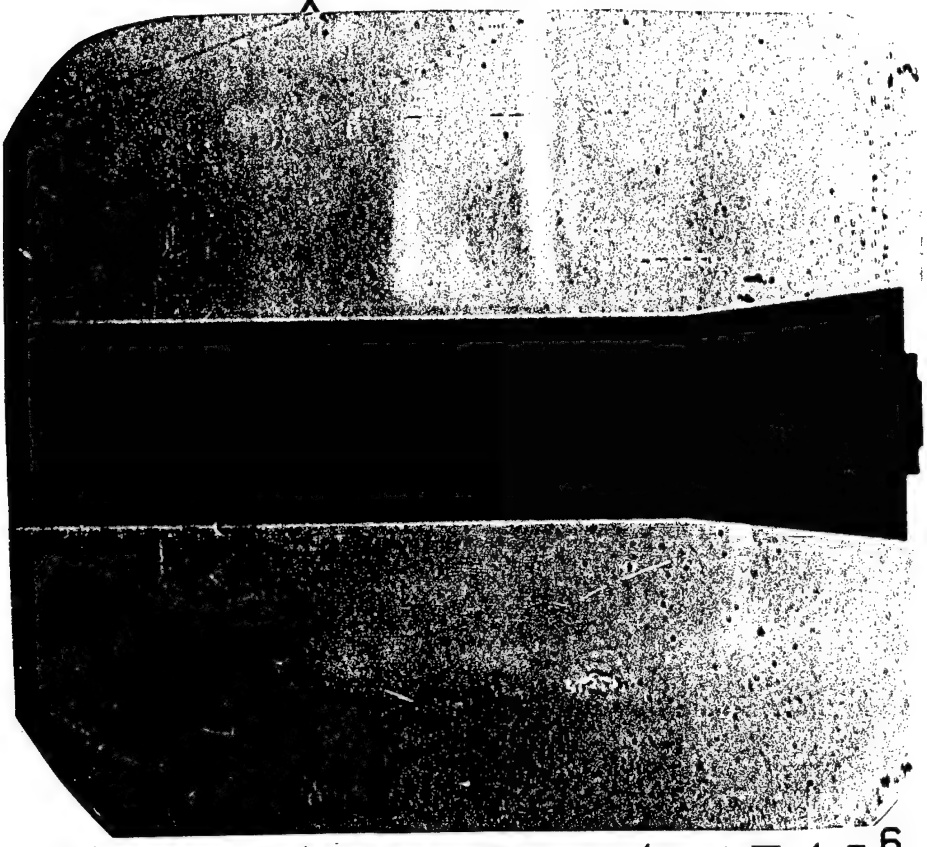

$M_\infty = 4.01$ $Re_x = 1.45 \cdot 10^6$

$M \cdot Re_x^{-0.5} = 3.33 \cdot 10^{-3}$

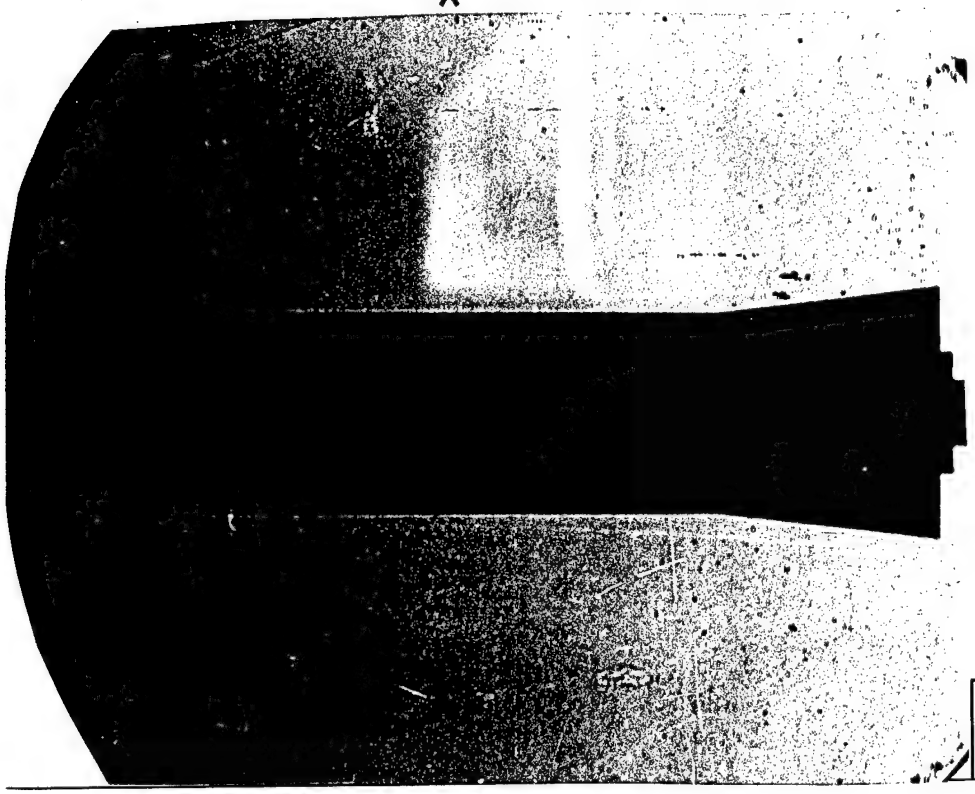

Fig. 127

$M_\infty = 4.02$ $Re_x = 1.81 \cdot 10^6$

$M \cdot Re_x^{-0.5} = 2.99 \cdot 10^{-3}$

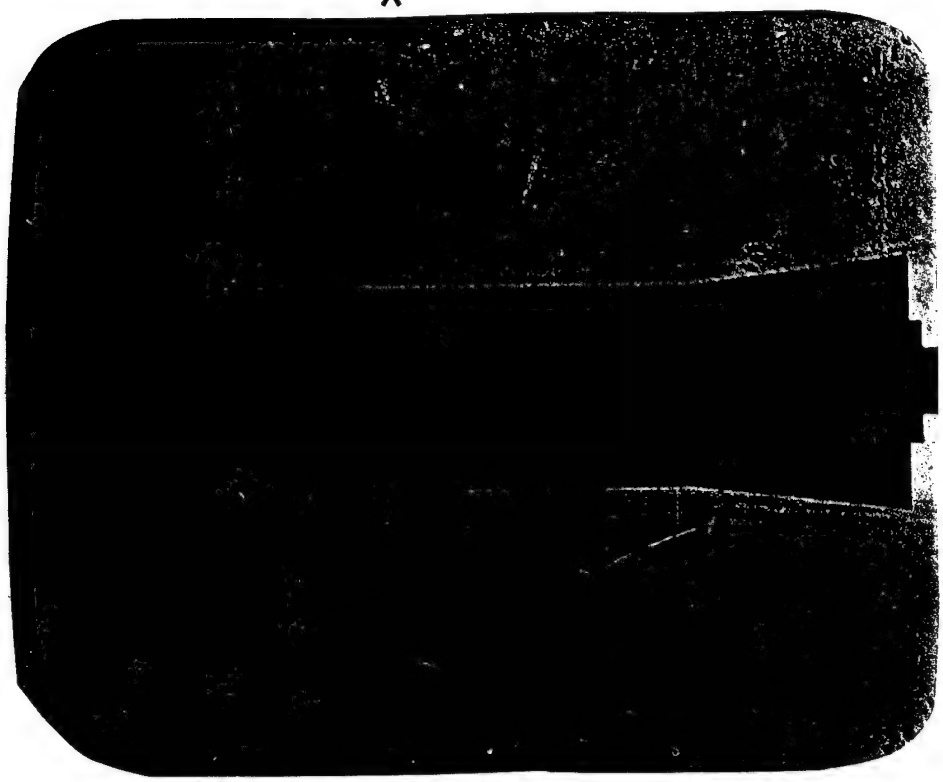

$M_\infty = 4.03$ $Re_x = 2.34 \cdot 10^6$

$M \cdot Re_x^{-0.5} = 2.63 \cdot 10^{-3}$

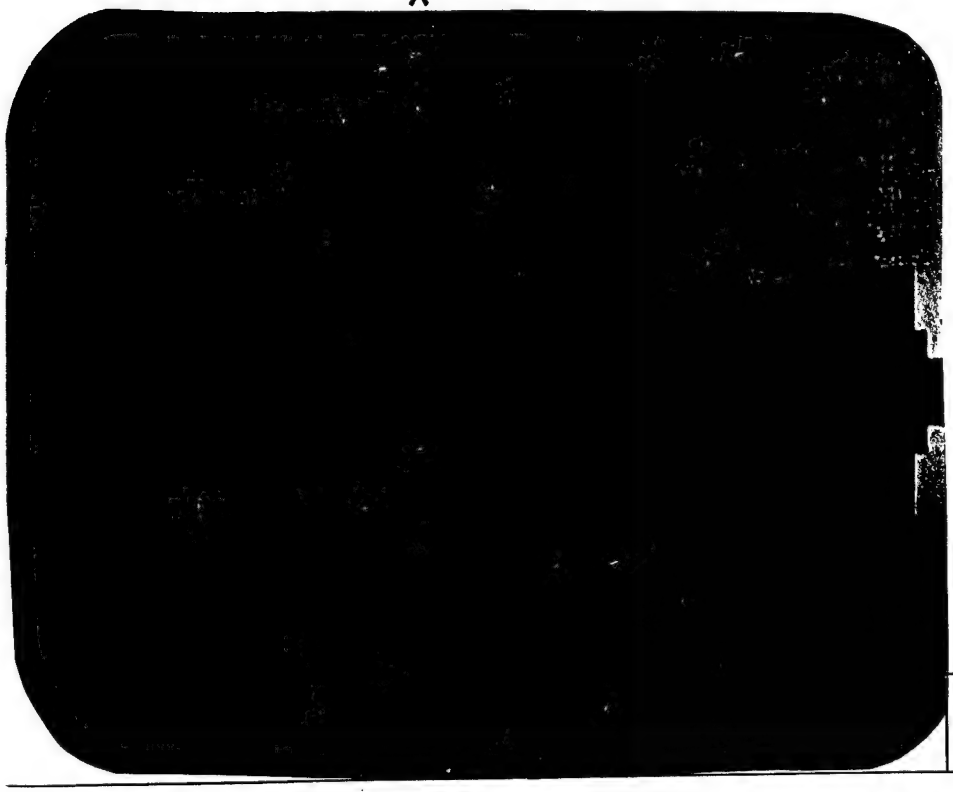

Fig. 128

$M_\infty = 4.03$ $Re_x = 3.13 \cdot 10^6$

$M \cdot Re_x^{-0.5} = 2.28 \cdot 10^{-3}$

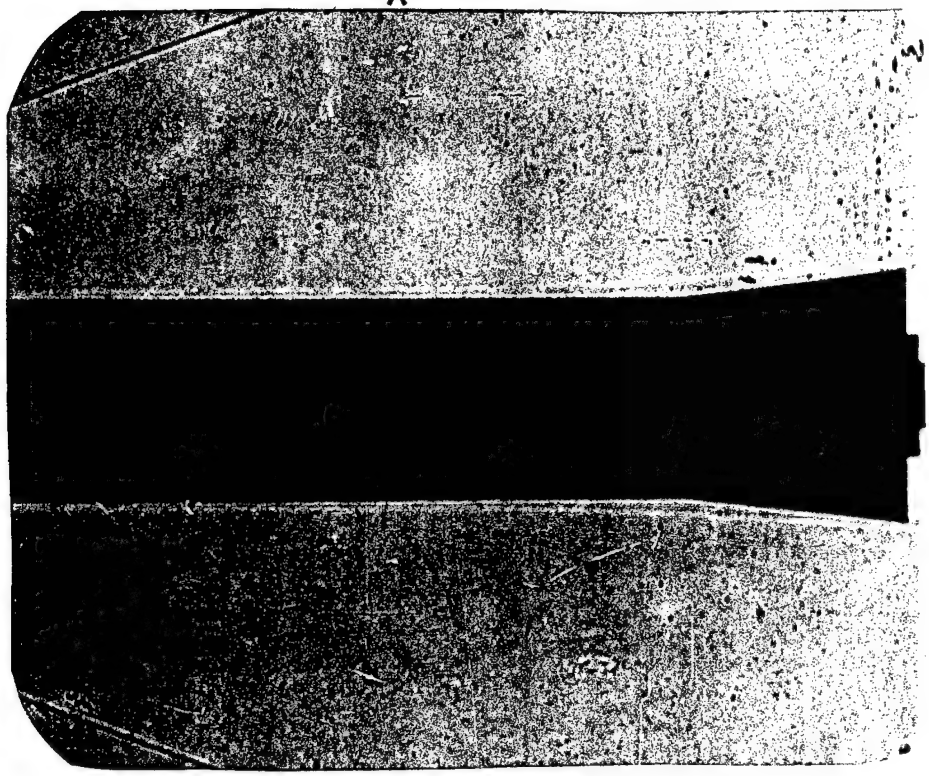

$M_\infty = 4.04$ $Re_x = 3.91 \cdot 10^6$

$M \cdot Re_x^{-0.5} = 2.04 \cdot 10^{-3}$

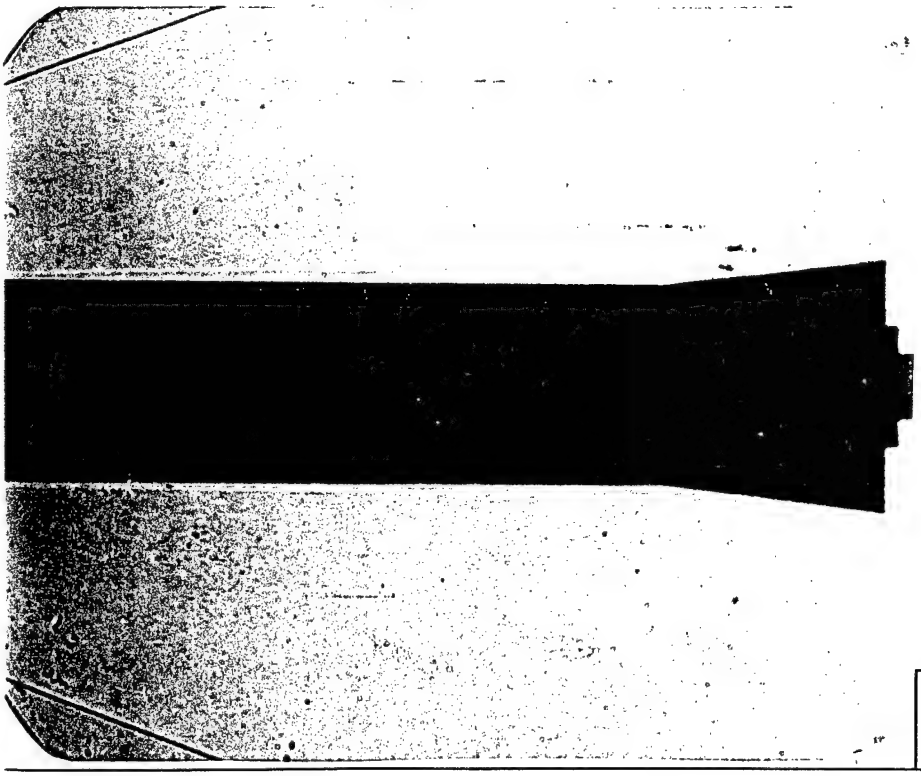

Fig. 129

$M_\infty = 4.05$ $Re_x = 6.27 \cdot 10^6$

$M \cdot Re_x^{-0.5} = 1.62 \cdot 10^{-3}$

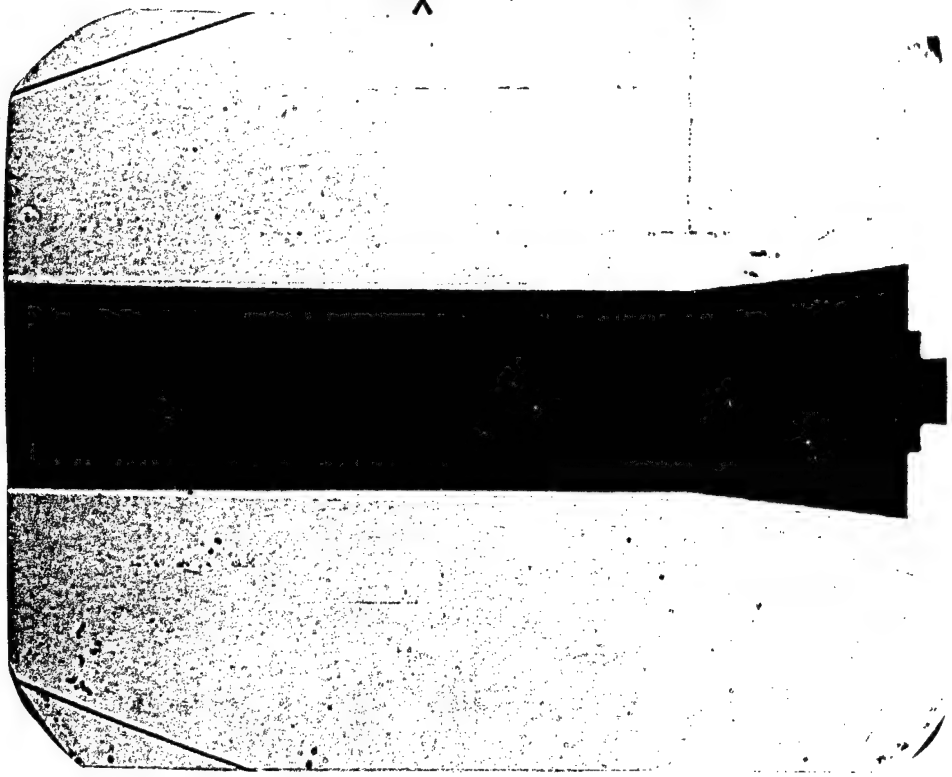

$M_\infty = 4.06$ $Re_x = 8.20 \cdot 10^6$

$M \cdot Re_x^{-0.5} = 1.42 \cdot 10^{-3}$

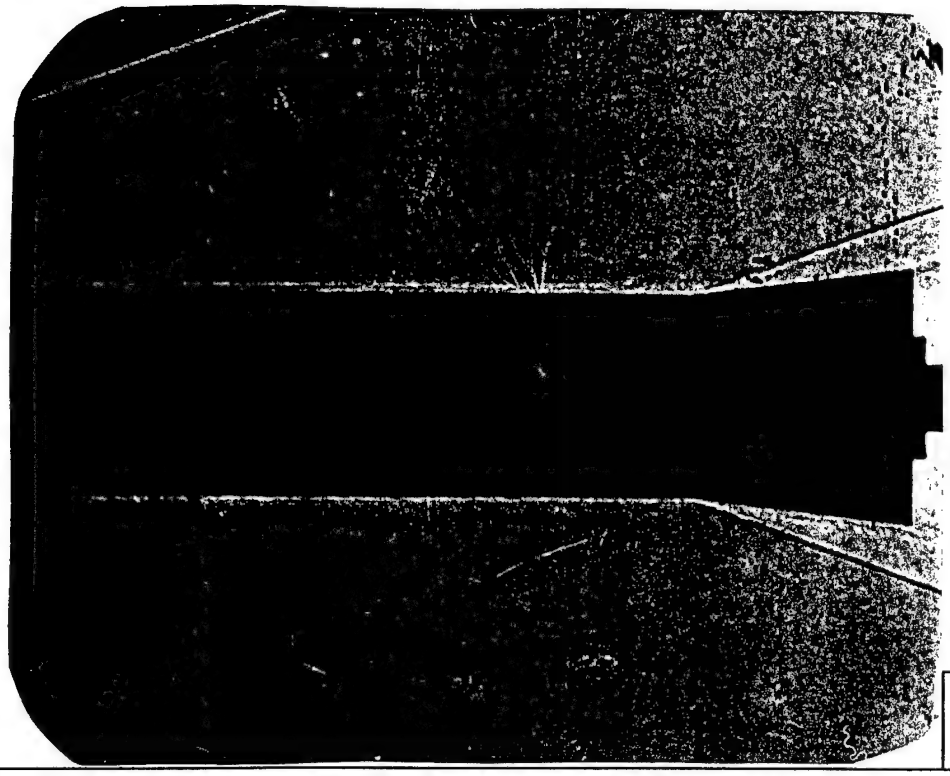

Fig. 130

$M_\infty = 4.96$ $Re_x = .90 \cdot 10^6$

$M \cdot Re_x^{-0.5} = 5.23 \cdot 10^{-3}$

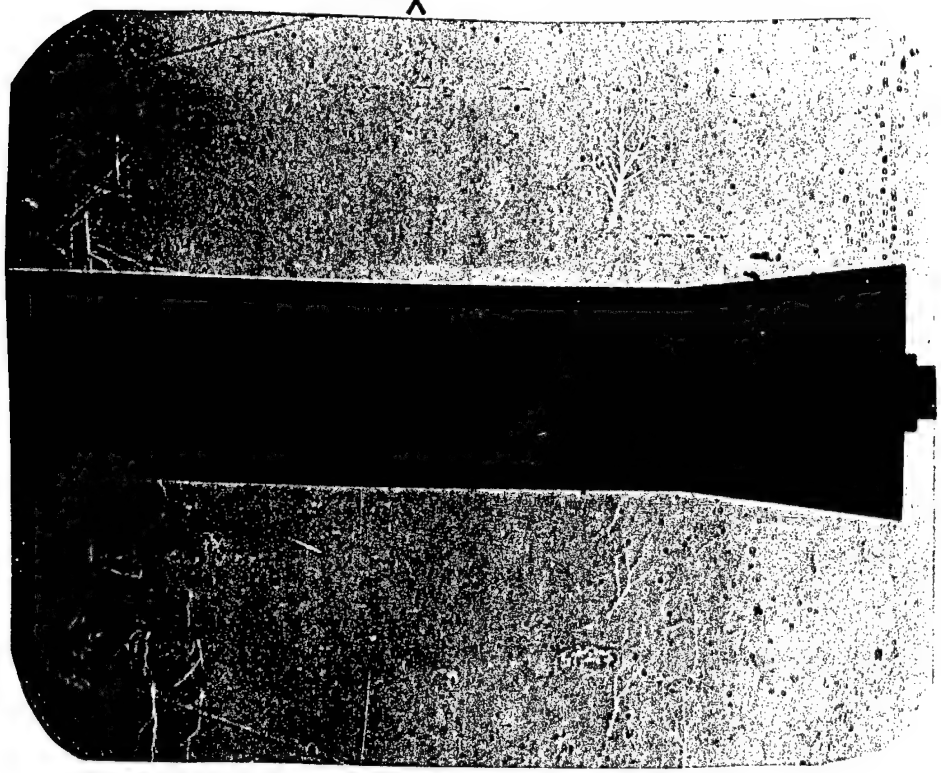

$M_\infty = 4.97$ $Re_x = 1.38 \cdot 10^6$

$M \cdot Re_x^{-0.5} = 4.23 \cdot 10^{-3}$

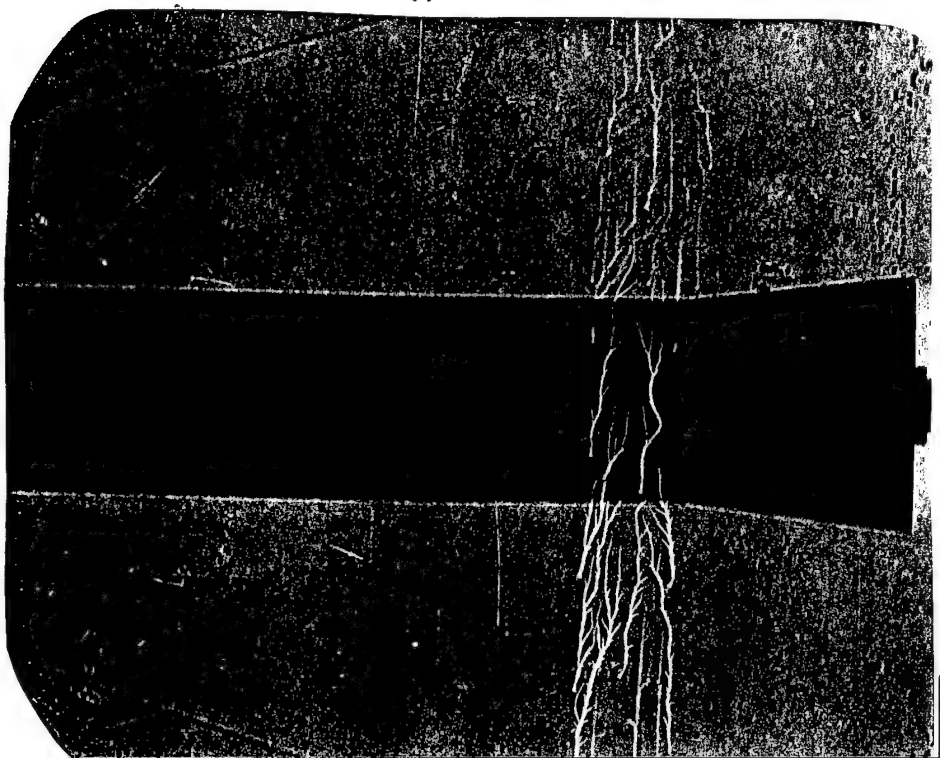

Fig. 131

$M_\infty = 4.98$ $Re_x = 1.82 \cdot 10^6$

$M \cdot Re_x^{-0.5} = 3.69 \cdot 10^{-3}$

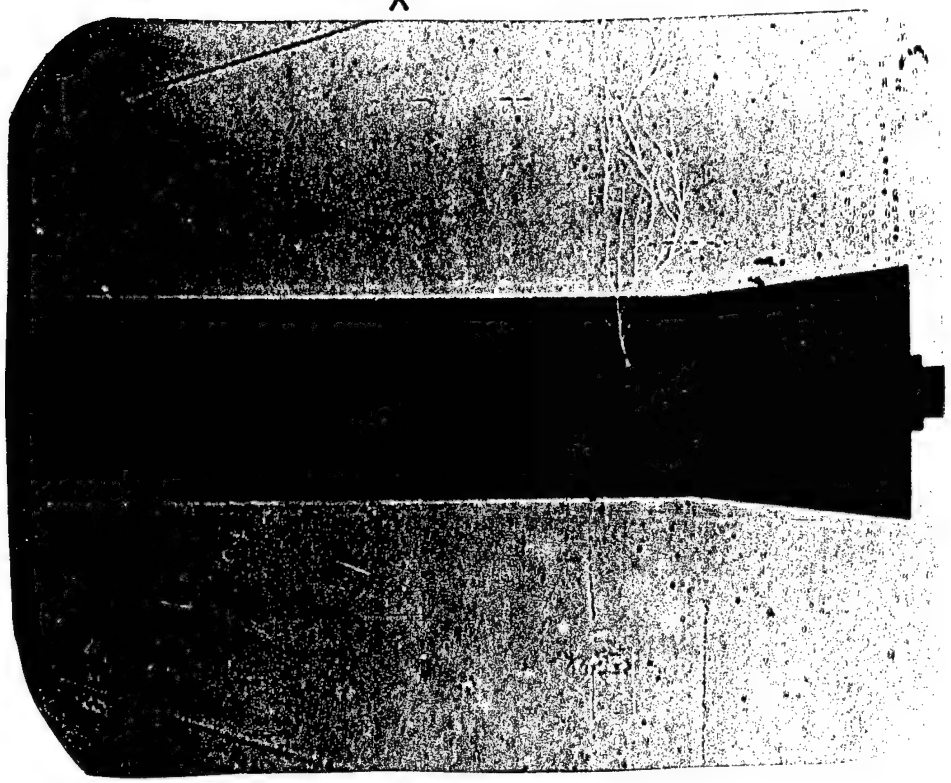

$M_\infty = 4.99$ $Re_x = 2.63 \cdot 10^6$

$M \cdot Re_x^{-0.5} = 3.08 \cdot 10^{-3}$

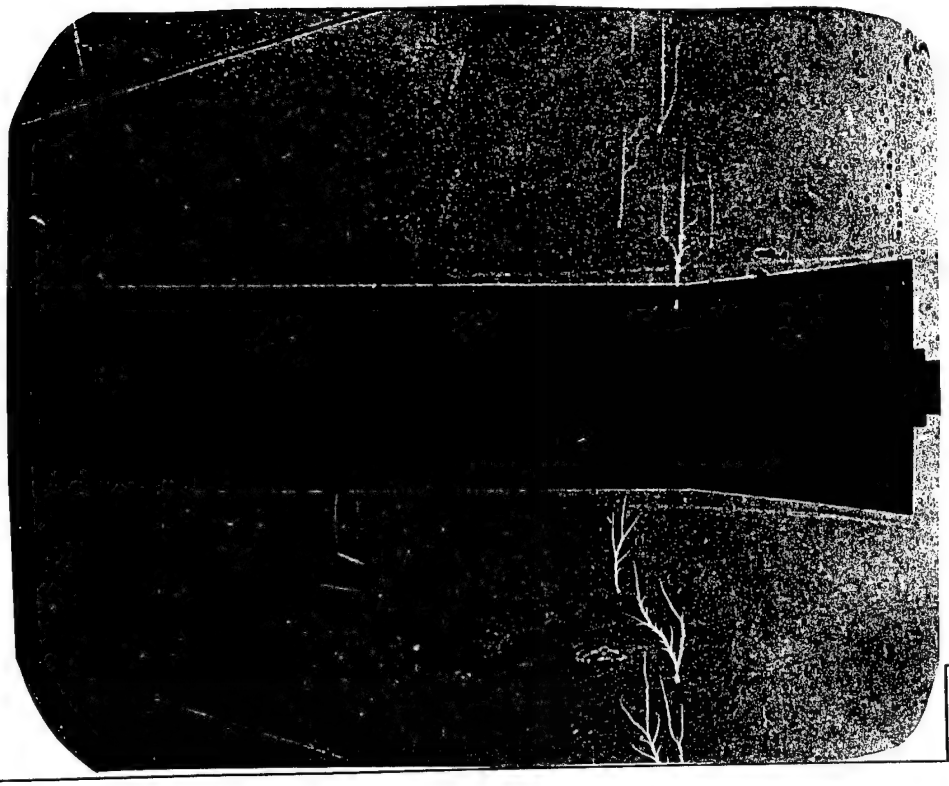

Fig. 132

$M_\infty = 5.00$ $Re_x = 3.23 \cdot 10^6$

$M \cdot Re_x^{-0.5} = 2.78 \cdot 10^{-3}$

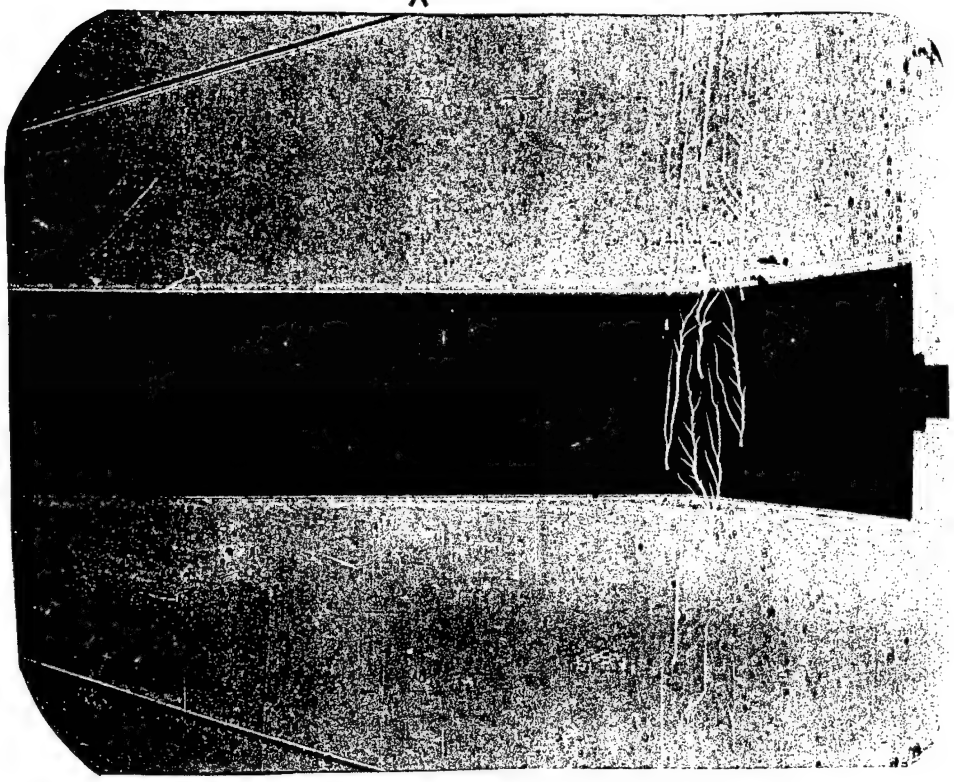

$M_\infty = 5.00$ $Re_x = 4.52 \cdot 10^6$

$M \cdot Re_x^{-0.5} = 2.35 \cdot 10^{-3}$

Fig. 133

$M_\infty = 5.01$ $Re_x = 6.31 \cdot 10^6$

$M \cdot Re_x^{-0.5} = 1.99 \cdot 10^{-3}$

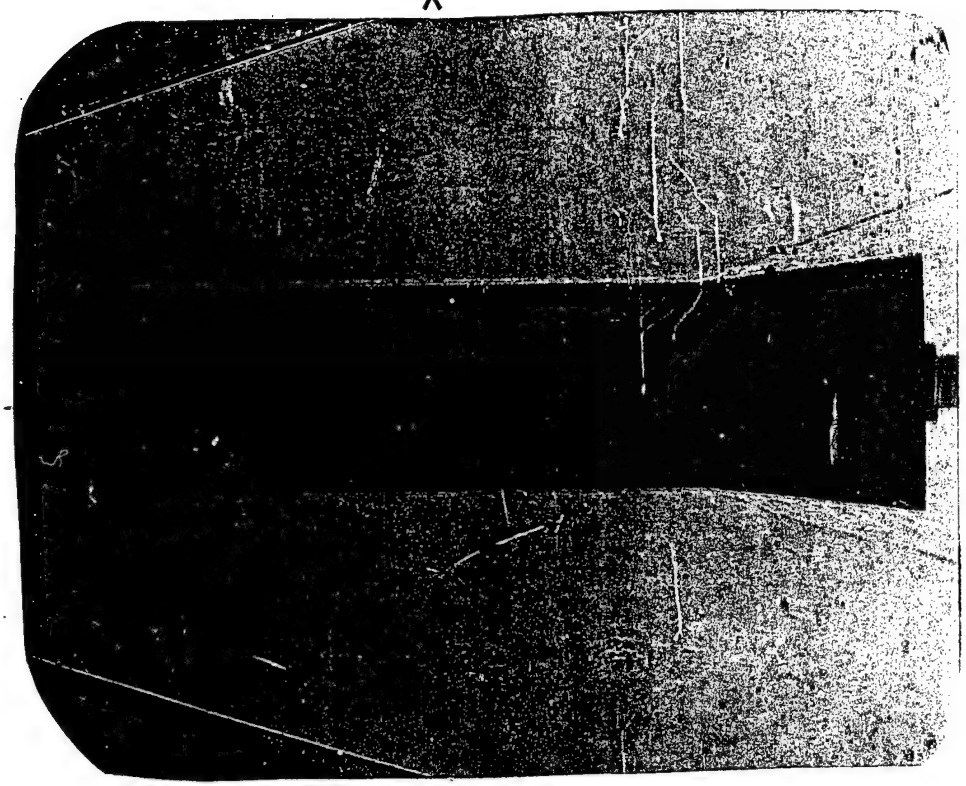

$M_\infty = 5.02$ $Re_x = 7.60 \cdot 10^6$

$M \cdot Re_x^{-0.5} = 1.82 \cdot 10^{-3}$

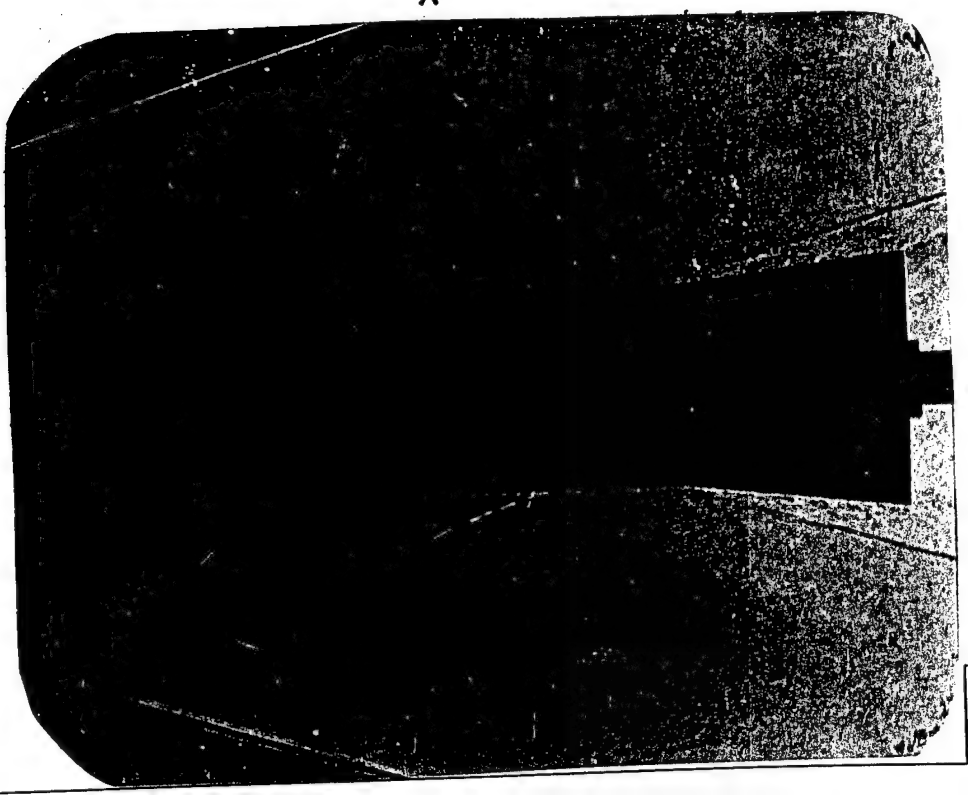

Fig. 134

$M_\infty = 6.00 \qquad Re_x = .98 \cdot 10^6$

$M \cdot Re_x^{-0.5} = 6.06 \cdot 10^{-3}$

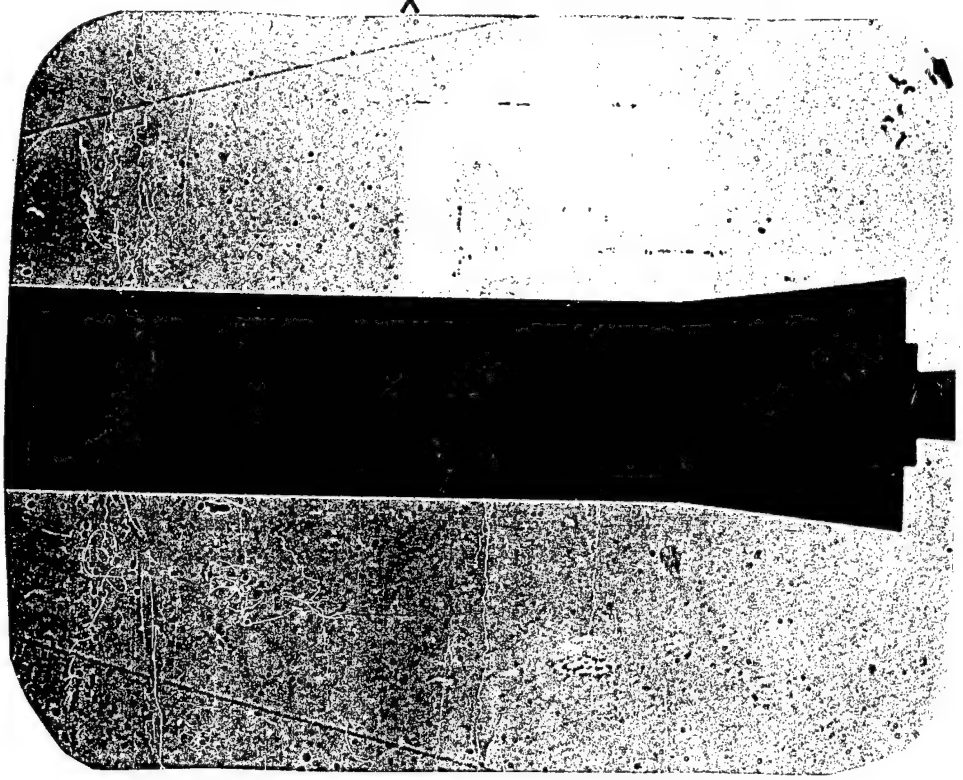

$M_\infty = 6.02 \qquad Re_x = 1.37 \cdot 10^6$

$M \cdot Re_x^{-0.5} = 5.14 \cdot 10^{-3}$

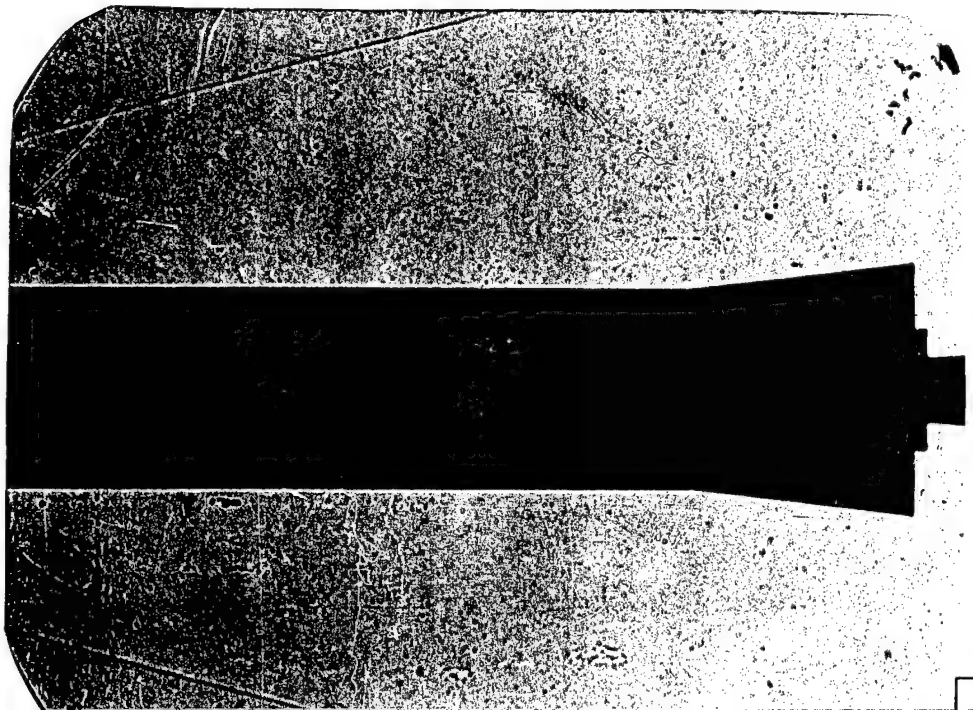

$M_\infty = 6.03$ $Re_x = 1.56 \cdot 10^6$

$M \cdot Re_x^{-0.5} = 4.83 \cdot 10^{-3}$

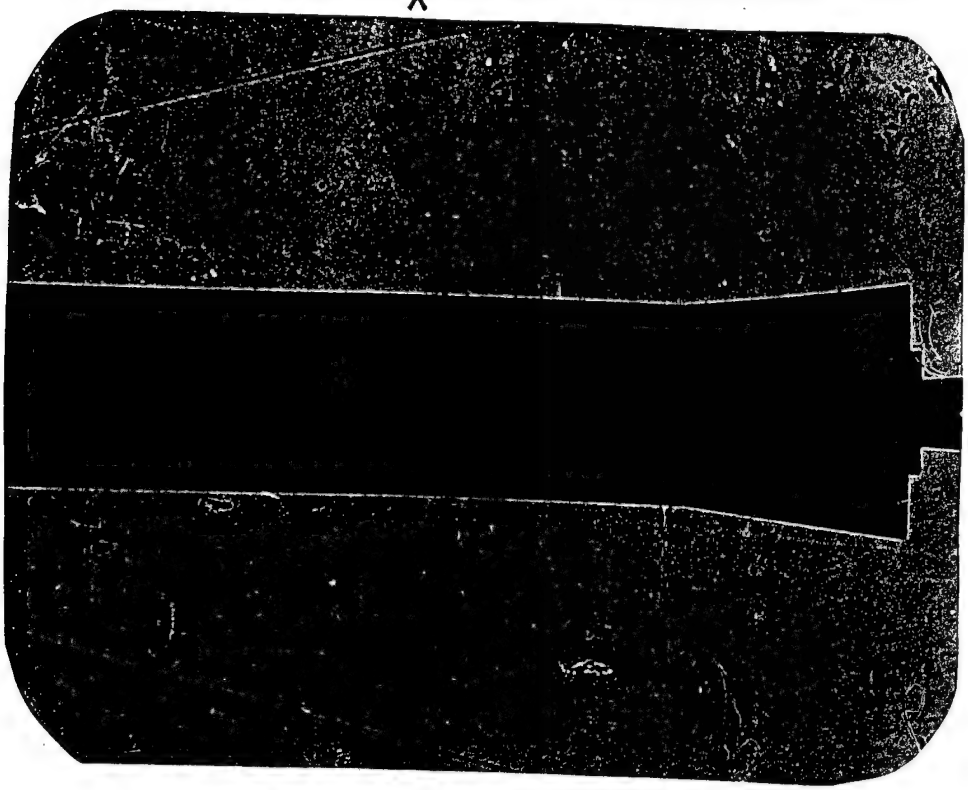

$M_\infty = 6.05$ $Re_x = 1.85 \cdot 10^6$

$M \cdot Re_x^{-0.5} = 4.45 \cdot 10^{-3}$

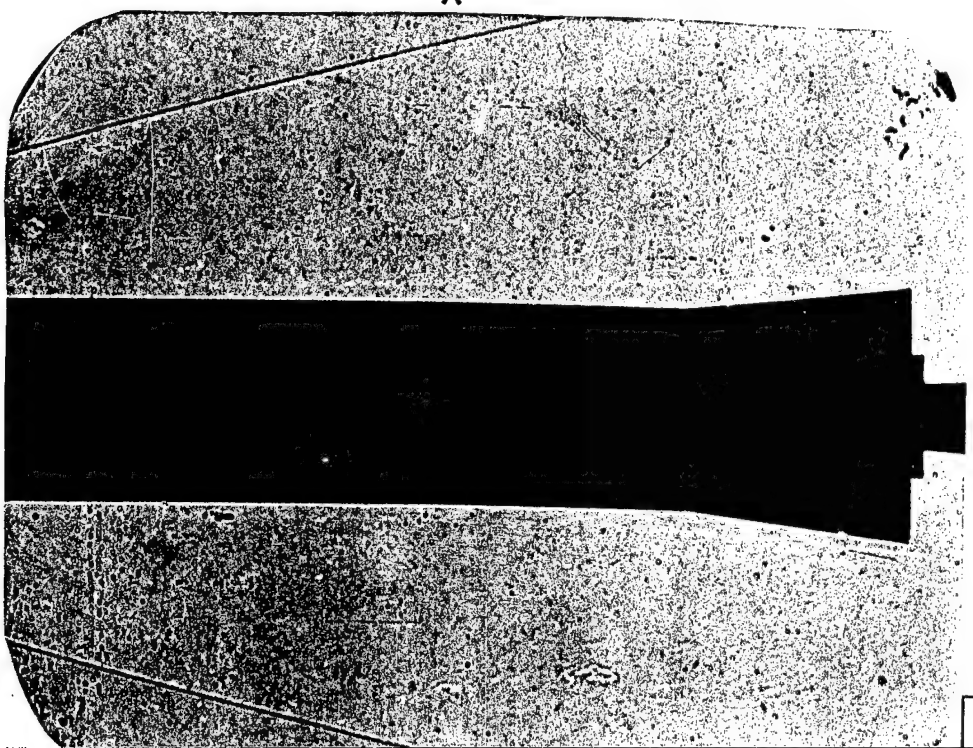

$M_\infty = 6.06$ $Re_x = 2.15 \cdot 10^6$

$M \cdot Re_x^{-0.5} = 4.13 \cdot 10^{-3}$

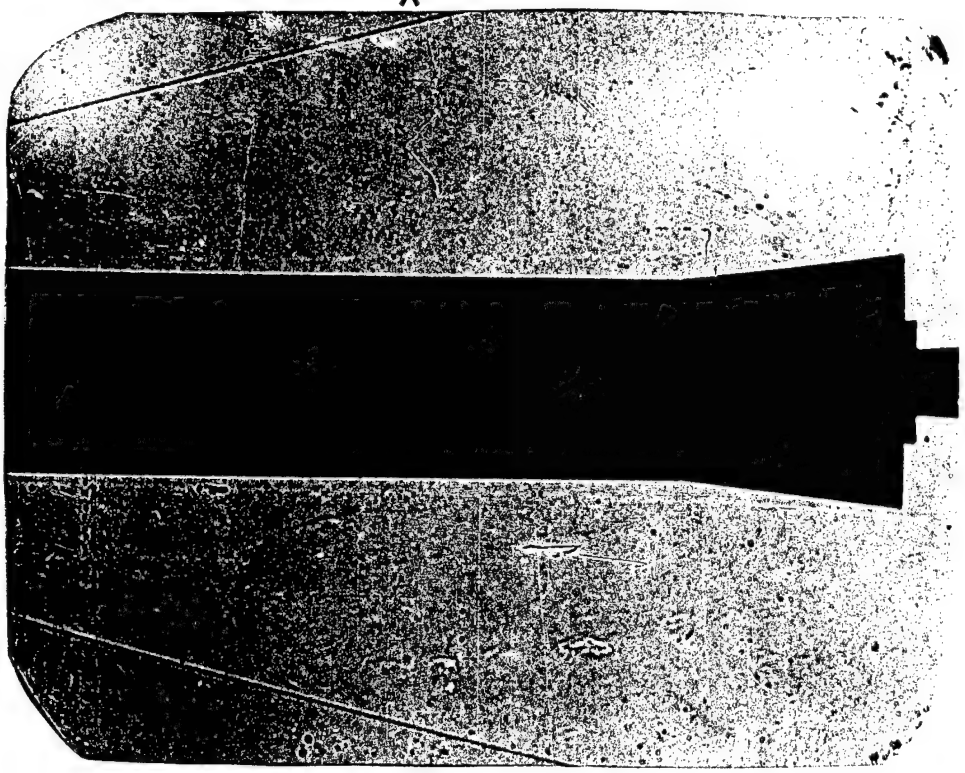

$M_\infty = 6.08$ $Re_x = 2.99 \cdot 10^6$

$M \cdot Re_x^{-0.5} = 3.52 \cdot 10^{-3}$

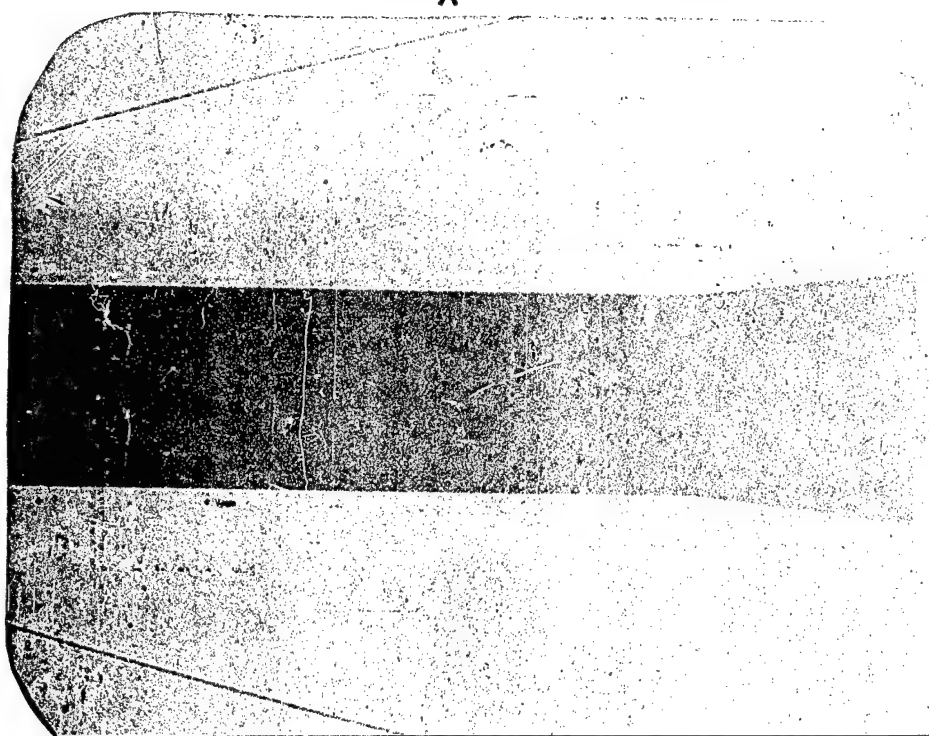

Fig. 13M

$M_\infty = 6.96$ $Re_x = 1.69 \cdot 10^6$

$M \cdot Re_x^{-0.5} = 5.35 \cdot 10^{-3}$

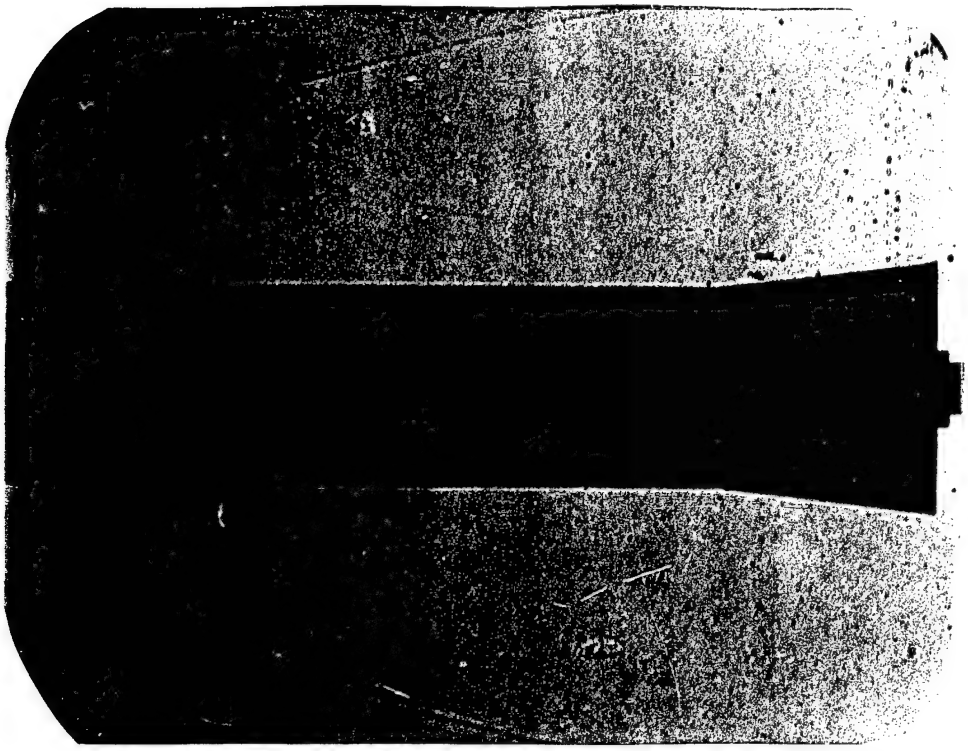

$M_\infty = 7.03$ $Re_x = 2.27 \cdot 10^6$

$M \cdot Re_x^{-0.5} = 4.67 \cdot 10^{-3}$

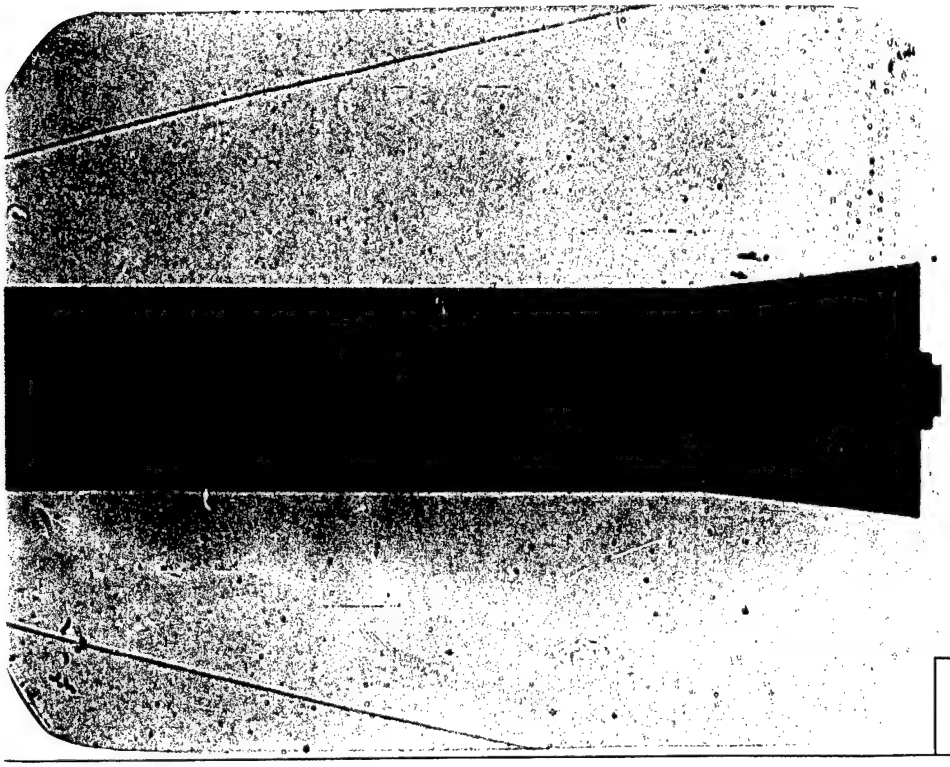

Fig. 138

M_∞=7.[illegible] $Re_x = 2.74 \cdot 10^6$

$M \cdot Re_x^{-0.5} = 4.26 \cdot 10^{-3}$

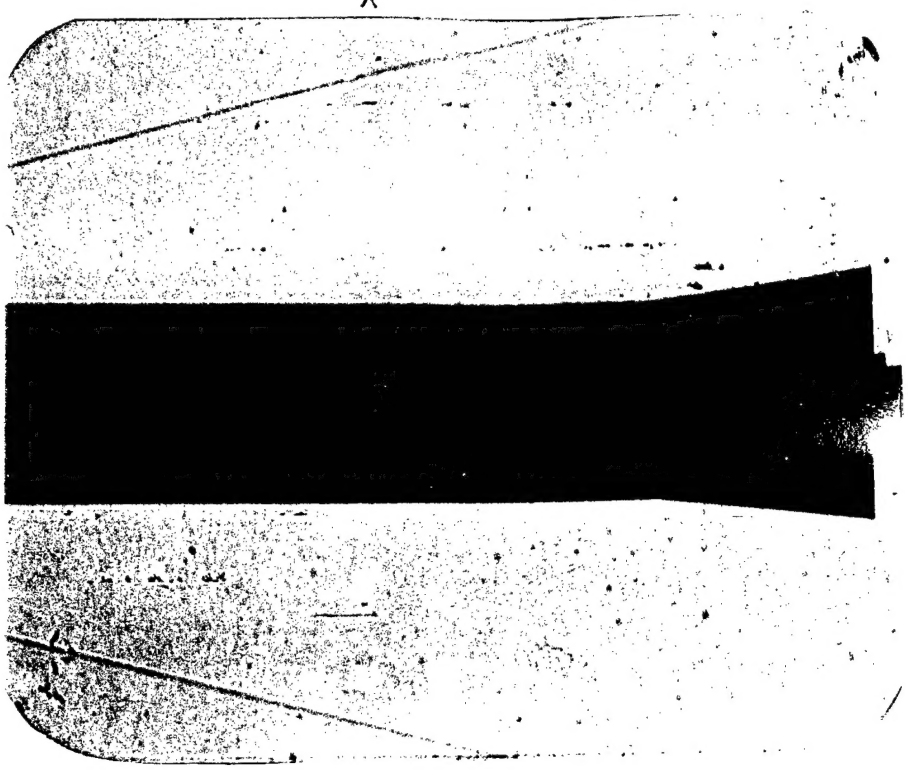

$M_\infty = 7.07$ $Re_x = 4.39 \cdot 10^6$

$M \cdot Re_x^{-0.5} = 3.37 \cdot 10^{-3}$

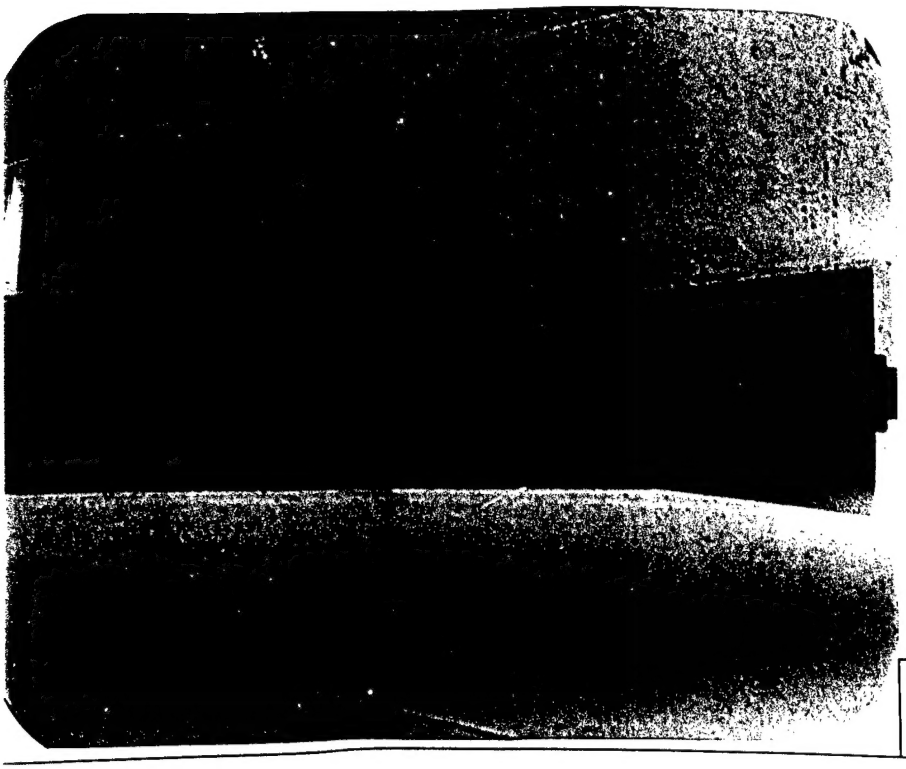

Fig. 139

$M_\infty = 7.07$ $Re_x = 5.09 \cdot 10^6$

$M \cdot Re_x^{-0.5} = 3.13 \cdot 10^{-3}$

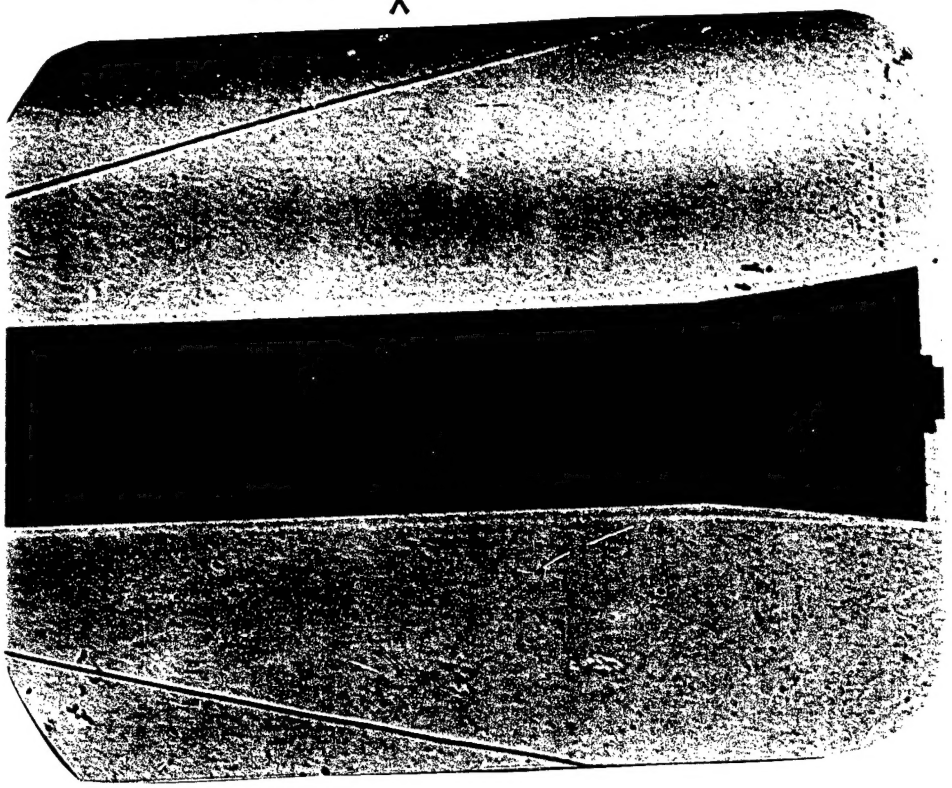

$M_\infty = 7.07$ $Re_x = 6.26 \cdot 10^6$

$M \cdot Re_x^{-0.5} = 2.83 \cdot 10^{-3}$

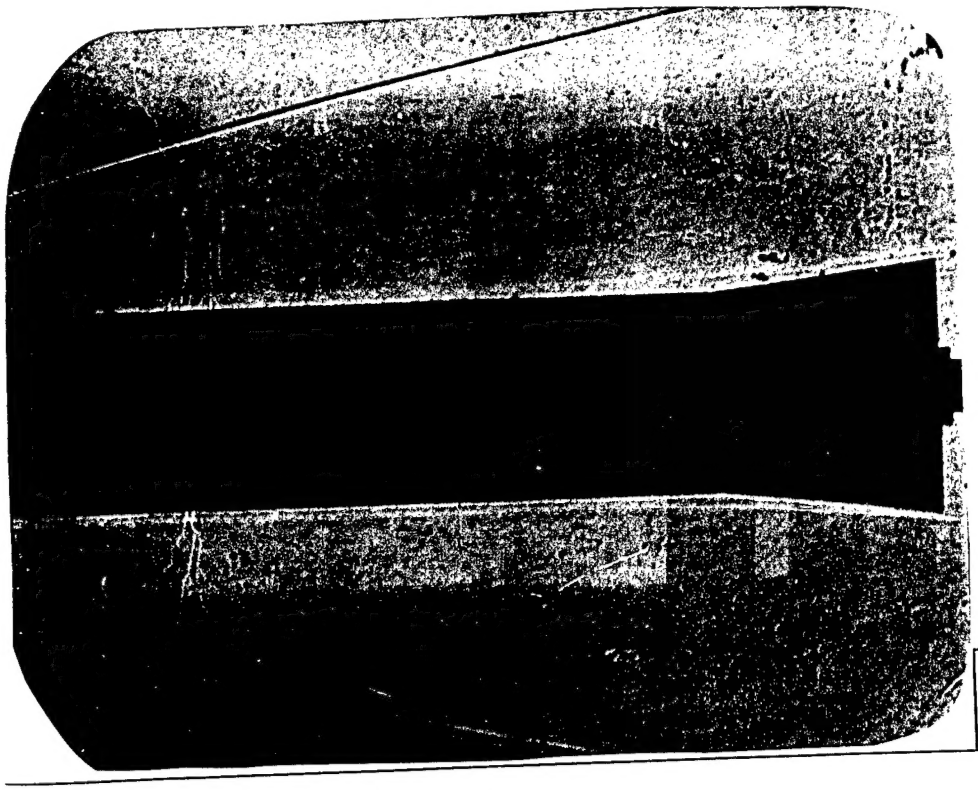

Fig. 140

$M_\infty = 7.97$ $Re_x = 1.28 \cdot 10^6$

$M \cdot Re_x^{-0.5} = 7.04 \cdot 10^{-3}$

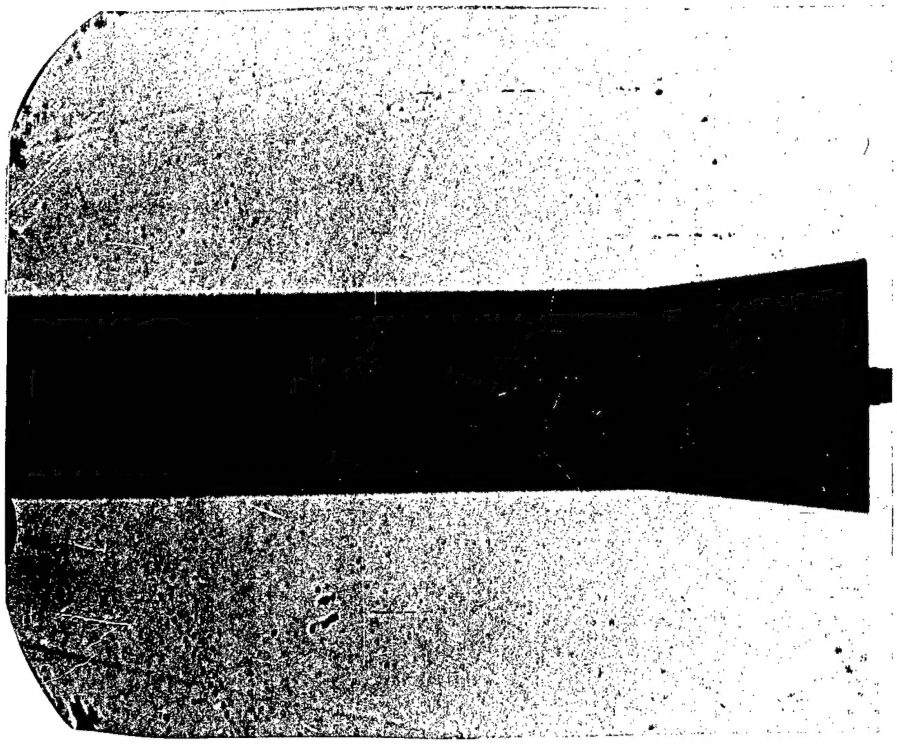

$M_\infty = 8.00$ $Re_x = 2.00 \cdot 10^6$

$M \cdot Re_x^{-0.5} = 5.66 \cdot 10^{-3}$

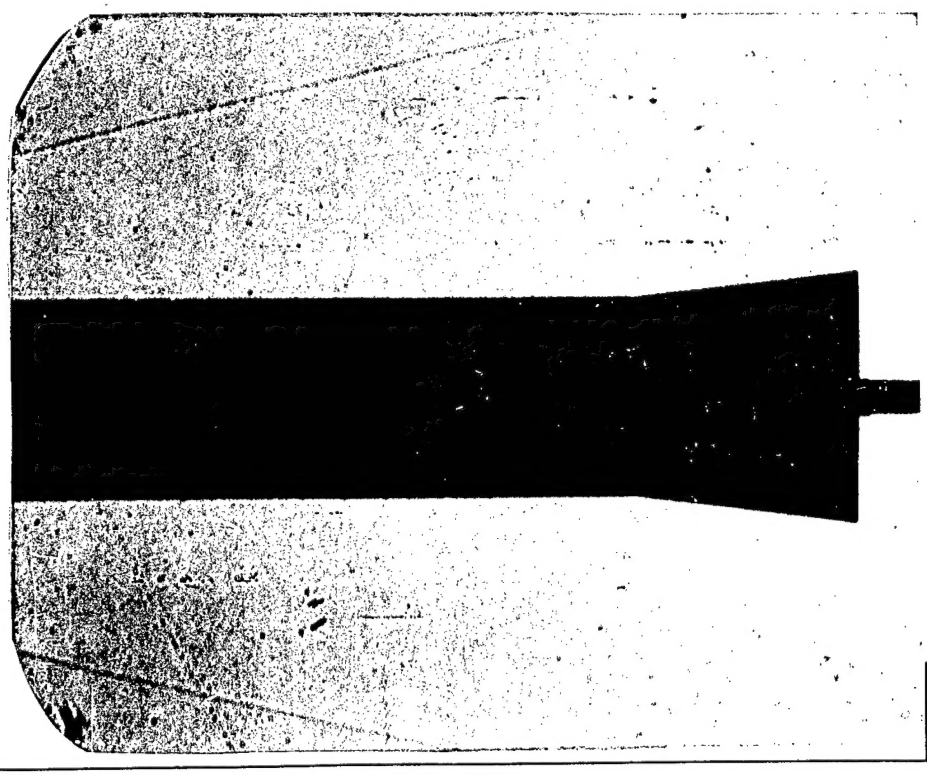

Fig. 141

$M_\infty = 8.02$ $Re_x = 2.95 \cdot 10^6$

$M \cdot Re_x^{-0.5} = 4.67 \cdot 10^{-3}$

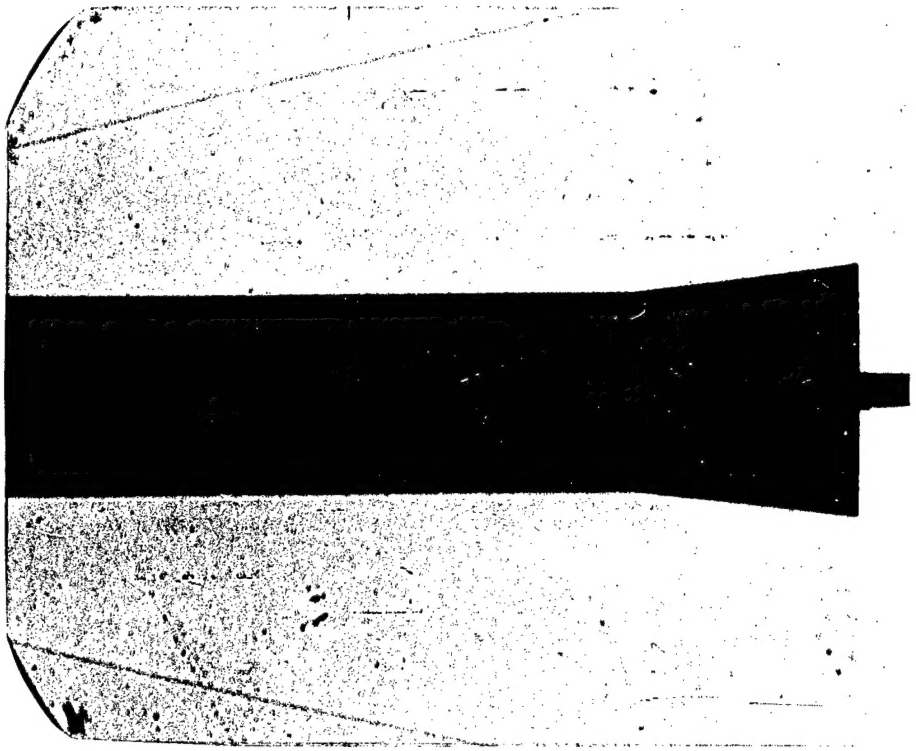

$M_\infty = 8.03$ $Re_x = 3.30 \cdot 10^6$

$M \cdot Re_x^{-0.5} = 4.42 \cdot 10^{-3}$

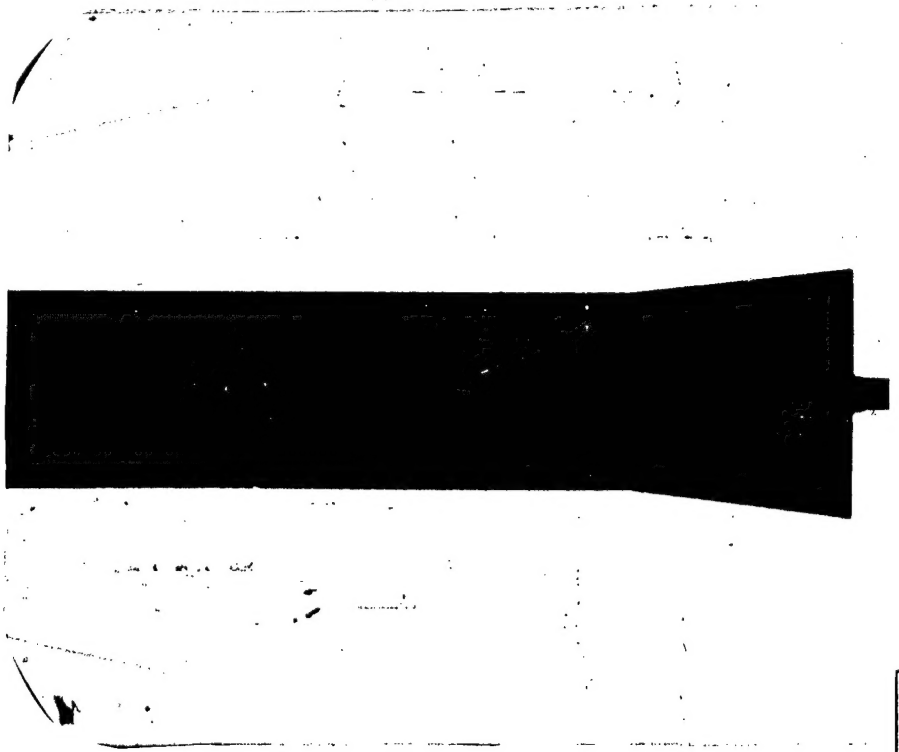

Fig. 142